Nonlinear Cardiovascular Oscillatory Dynamics in Malaria

Clinical, experimental and theoretical investigations

Yunus Abdulhameed Abdussalam, BSc.

Thesis submitted for the degree of

Doctor of Philosophy

Department of Physics
Lancaster University
Lancaster, UK

November 2019

Acknowledgements

All thanks are due to Almighty Allah, the lord of the world and creator of all creations for keeping me sane throughout my PhD studies. My profound gratitude goes to my supervisors Professor Aneta Stefanovska, and Professor Peter McClintock without whose insight and foresight this study would not have been accomplishable. I have been privileged to be able to closely work with them, particularly with my major supervisor Professor Aneta in such an interesting field. This project was viable through the understanding of life events, and the resilience and support that I have experienced from my major supervisor.

Without the funding from the Tertiary Education Trust Fund (TETFund), Nigeria (funded my 1st-2nd year) and Petroleum Development Trust Fund (PTDF), Nigeria (which funded mainly my final year living expenses), it would have been impossible to complete this work. I am very much grateful to them, may they benefit from the importance of the project.

I am especially thankful to Dr. Gemma Lancaster who introduced me to the physiological measurements equipment, including ECG, Laser Doppler flowmetry, TOSCA devices etc., alongside explicit explanation of some basic methods for analysing time series, and answering analysis questions in the early days that have benefited me throughout my studies. Many thanks to Professor Abdulrazaq G. Habib of the faculty of medicine, Bayero University Kano who facilitated my experiment on malaria patients in Murtala Muhammad Specialist Hospital, Kano Nigeria, and Matron Larai Alhamdu of the Intensive Care Unit of Murtala Muhammad Specialist Hospital who gave me helping hands during the measurement sessions. My appreciation also goes to the clinicians and microbiologists of the Murtala Muhammad Specialist Hospital and Bayero University (new site) clinic who were involved in my experiment in Nigeria, Dr. Hadiza, Dr. Remi, Mallam Isyaku Baba, Mallam Abdussalam, Mr. Sharafa, and Mallam Aliyu.

Thanks to Professor Sašo Džeroski of Jožef Stefan Institute, Ljubljana and Professor Martin Horvat of department of physics, University of Ljubljana for helping me with machine learning algorithms used to classify the results in chapter 6, which has given me much motivation in machine learning. Miroslav Barabash, Dr. Phil Clempson and Dr. Valentina Ticcinelli were helpful in answering programming and analysis questions, mostly in the early days of my studies. Many thanks to Rodney Gush and Brian Lock of Moor Instruments Ltd, Axminster, UK, for providing useful support and the equipment used for the experiments in chapter 5. The physiological measurements conducted throughout these studies would not have been possible without the participants who generously volunteered to be measured. I'm very grateful for this.

The atmosphere in the research group of Nonlinear and Biomedical Physics has been warm and friendly for all these years. I would also like to thank everybody that has made the department, especially my co-researchers in the office: Dr. Federico Devalle, Dr. Bastian Pietras, Dr. Mahmoud Eissa, Dr. Julian Newman, Dr. Yevhen Suprunenko, Dr. Maxime Lucas, Dr. William Gibby, Hala Siddiq, Alexandra Piddle, Sultan Alatawi, Mansour Alanazi and Joe Rowland Adams for providing a serene atmosphere throughout the years.

Finally, I express my deepest appreciation to my beloved son Eessa Abdulhameed and wife Dr. Maryam Imran Tijjani for patiently knowing when not to

query my long days at work (as well as when to make me come home) and for the sleepless nights, perseverance, and continuous support that kept me sane in the last stages of my PhD studies. In addition, my warmest thank to the members of my family who have always been there for me and for showing interest in my work, and the friends who understood why I could not always be around.

Declaration

This thesis is my original work and has not been submitted, in whole or in part, for a degree at this or any other university. Nor does it contain, to the best of my knowledge and belief, any material published or written by another person, except as acknowledged in the text.

Ethics Declaration

The data recorded and analysed within this work were collected in accordance with the appropriate permissions from their respective institutions or committees, as detailed below.

- The protocol used for data recorded from subjects with darkly and lightly pigmented skin, which are analysed in Chapter 4 was approved by the University of Lancaster Faculty of Science and Technology Ethics Committee. All volunteers gave their informed written consent.

- The blood flow, tissue oxygenation and other cardiovascular parameters recorded from black Africans and white Caucasians used in Chapter 5 were recorded in the Faraday cage in the Physics Department of Lancaster University. Approval of the research protocol was obtained from the Ethics Committee of Lancaster University Faculty of Science and Technology.

- The blood flow data and cardiovascular parameters analysed in Chapter 6 were recorded in the Murtala Muhammad Specialist Hospital of Kano State, Nigeria after obtaining written consent. The protocol was approved by the Ethical Committees of both the Kano State Ministry of Health, Nigeria and Bayero University Kano.

- The blood flow data analysed in Chapter 7 were separately recorded in the Faraday cage of Lancaster University Physics Department and the protocol was approved by the Ethics Committee of Lancaster University Faculty of Science and Technology.

List of publications

Parts of the work presented in this thesis have been published in the following papers and proceedings:

- Y. A. Abdulhameed, G. Lancaster, P. V. E. McClintock, and A. Stefanovska. On the suitability of laser Doppler flowmetry in capturing microvascular blood flow dynamics from darkly pigmented skin. *Physiol. Meas.,* 40:074005, 2019. (Work from Chapter 4).

- Y. A. Abdulhameed, P. V. E. McClintock, and A. Stefanovska. Race-specific differences in the coherence between microvascular blood flow and oxygenation dynamics: A simultaneous NIRS, white light spectroscopy and Doppler skin flow study. *J. Biophotonics*, 2019. (Work from Chapter 5).

The following manuscript has been drafted:

- Y. A. Abdulhameed, A. Habib, P. V. E. McClintock, and A. Stefanovska. Malaria causes changes in the wavelet phase coherence of microvascular blood flow. (Work from Chapter 6).

Parts of the work have also been presented at the following scientific meetings and workshops:

- Y. A. Abdulhameed, A. Habib, P. V. E. McClintock, and A. Stefanovska. Diagnosis of malaria based on phase coherence between oscillations of instantaneous heart frequency and respiration *Physics meets Biology conference, 9–11 September 2019. University of Oxford, United Kingdom.* Poster presentation.

- Y. A. Abdulhameed, and A. Stefanovska. Diagnosis of malaria based on alterations in microvascular blood flow oscillations. *The Digital Health Exchange. 4th December 2018. Lancaster University, UK.* Oral presentation.

- Y. A. Abdulhameed and A. Stefanovska. Diagnosis of malaria based on alterations in microvascular blood flow oscillations. *Physics of Biological Oscillators, Workshop. 27–30 November 2018. Chicheley Hall, Buckinghamshire, UK.* Poster presentation.

- Y. A. Abdulhameed, A. Habib, and A. Stefanovska. Cardio-respiratory coherence in malaria. *10th European Study Group on Cardiovascular Oscillations. 17-19 September 2018. Vienna, Austria.* Poster presentation.

- Y. A. Abdulhameed and A. Stefanovska. Racial disparities in coherence between the fluctuations in microvascular blood flow and oxygenation dynamics. *11th World Congress for Microcirculation. 9-13 September 2018. Vancouver, BC, Canada.* Poster presentation.

- Y. A. Abdulhameed, G. Lancaster, and A. Stefanovska. Evaluating laser Doppler flowmetry in capturing microvascular blood flow from high melanin skin. *World Congress on Medical Physics & Biomedical Engineering. 3-8 June 2018. Prague, Czech Republic.* Oral presentation.

- Y. A. Abdulhameed and A. Stefanovska. Microvascular dynamics in treated malaria. *Faculty of Science and Technology Christmas Conference. 12 December 2016. Lancaster, UK.* Poster presentation.

- Y. A. Abdulhameed and A. Stefanovska. Effects of malaria on the dynamics and rheological properties of blood flow in the microvasculature. *9th European Study Group on Cardiovascular Oscillations. 10-14 April 2016. Lancaster, UK.* Poster presentation.

Abstract

Erythrocyte deformability is known to be compromised due to the increased stiffness of the membrane of malaria-infected erythrocytes, and the latter also exhibit abnormal adherence to the endothelial cells that line all the blood vessels. This leads to alterations in the cells' shapes as well as in the viscosity, flow properties, and oxygenation of the blood, which are all altered by malaria in a specific pattern that is different from that in other diseases. As the red blood cells are the main particles of the blood flowing through the cardiovascular system, these changes result in impaired hemodynamics. The impairments are mostly because of the spatial distributions (arrangement) of red blood cells. A large number of earlier studies into the characteristics of erythrocytes have been invasive and conducted on animal models, and more recently performed with experimental *in vitro* optical assay models. However, recent technological and theoretical breakthroughs in biomedical research are enabling the application of non-invasive imaging techniques, yielding clinically relevant information on humans *in vivo*.

In this thesis, we first prove convincingly that the optical technique of laser-Doppler flowmetry (LDF) can be used to evaluate blood flow dynamics in dark-skinned individuals, a matter that has been subject to doubt and discussion since the introduction of the LDF technique. We then address the long-standing question as to whether malaria can be detected at an early stage by investigating the alterations in blood flow and cardiovascular dynamics in febrile and non-febrile malaria patients. The alterations were evaluated not only by optical methods, but also by use of several other sensors, and the resultant time series were analysed based on techniques specifically developed for non-strictly-periodic, but rather time-varying signals. Numerous investigations utilising optical methods have previously reported impaired oxygen delivery, reduced metabolic rate, ATP deficiency and respiratory distress in relation to metabolic acidosis in malaria. However, biological oscillations that manifest in the blood flow and cardiovascular dynamics,

and how they change over time, have not yet been utilised. Several measurements of human blood flow and oxygenation *in vivo* have demonstrated the manifestation of these oscillations in cardiovascular dynamics, and their physiological attribution have been established as being significant. These physiological oscillatory processes can in principle provide valuable information about the underlying dynamical properties of the system. Blood flow and cardiovascular dynamics were found to differ markedly in malaria and it is proposed to use such signatures in the development of a diagnostic test for the disease.

Besides characterizing the blood flow and cardiovascular dynamics in malaria, probable mechanisms in the causation of the observed alterations are explored. They are associated with two well-known characteristics of malaria: the effect of variant gene expression, race or environmental factors on vascular function; and the long-term effects of malaria recurrence. The former is investigated through the comparative measurements and analyses of microvascular blood flow and tissue oxygenation dynamics in white Caucasians and black Africans. The latter is explored by comparing the blood flow and cardiovascular data recorded from patients of black African origin who had suffered episodes of malaria in the past, and recovered from it, with that of subjects with no history of malaria.

Contents

List of Figures

List of Tables

Glossary

AAFT	Amplitude adjusted Fourier transform. A method used for building surrogates of a time series.
Aneurisms	A swelling that arises as a result of weakened blood vessel wall.
ATP	Adenosine triphosphate, the energy currency of the cell. ATP is used as an energy source for e.g., protein synthesis, signalling and cell division.
BF	Blood flow
Blood smear microscopy	A method for the noninvasive detection of malaria parasites in the blood, using a glass microscope slide.
Cytoadherence	The abnormal adherence of malaria infected red blood cells to vessel wall, mostly to the endothelium.
ECG	Electrocardiogram. It gives a measure of the electrical activities in the heart.
Diastole	A period during heartbeat, when the heart relaxes and enables the heart to be filled with blood.
Systole	A period during heartbeat, when the heart contracts and pumps blood into the arteries.
Erythrocyte	It is a cell that contains hemoglobin and transports oxygen to the body. It is also commonly called red blood cell.
Erythropoiesis	The process where new red blood cells are produced.
Febrile	Is a symptom of a fever, characterised by a very high temperature.

HbA1c	Glycated hemoglobin. It is formed when hemoglobin is exposed to glucose in the blood. Making the hemoglobin to be covalently bound to glucose.
Hemoglobin	An oxygen transport protein containing iron that exists within the red blood cells.
Hemostasis	The processes where blood is prevented from flowing within damaged vessel. It is the first stage of healing a wound.
Hypovolaemia	A decrease in amount of blood flow in the body.
IAAFT	Iterative amplitude adjusted Fourier transform. A method used for generating surrogates of a signal.
IHF	Instantaneous heart frequency
In vitro	In vitro (Latin: in glass) studies are conducted using components of an organism that have been isolated from their usual biological surroundings, such as microorganisms, cells, or biological molecules.
In vivo	Studies on living organisms or cells.
LDF	Laser Doppler flowmetry
Mechanotransduction	The process whereby cells sense and respond to mechanical stimuli by converting them to biochemical signals that trigger cellular responses.
NIRS	Near infrared spectroscopy. A method used to measure the changes in concentration of oxy- and deoxyhemoglobin in the blood.
NMD	Nonlinear mode decomposition. A technique that decomposes a time series into a set of components, or modes.
NO	Nitric oxide. It serves as vasodilator, causing the muscles of the blood vessels to relax, widening them, and enhancing circulation.
NO synthases	The nitric oxide syntheses belong to a group of enzymes that speeds up the production of NO from L-arginine.

Plasmodium falciparum	It is one of the deadliest of the protozoan parasite species that cause malaria.
Pyrexia	An increased body temperature.
RDT	Rapid diagnostic test. It is one of the standard methods used for diagnosing malaria.
Rhythms	In the context of human body, a biological rhythm is a natural process in the body that occurs/changes in a cyclic manner.
Rosetting	The processes whereby uninfected red blood cells bind to a malaria-infected red blood cell, which occurs after the parasites mature to become trophozoites.
RSA	Respiratory sinus arrhythmia. It refers to the modulation of heart rate by the respiratory frequency.
SpO2	Peripheral capillary oxygen saturation. It gives an estimate of the amount of oxygen in blood.
Stenosis	The abnormal narrowing of blood vessels.
Systemic	In the context of the human body, a process that affects the entire body is referred as a systemic process, for example the beating of the heart. The effects of systemic processes may be observed at large distances from where they originate.

1. Introduction

1.1 Background and rationale

1.1.1 Malaria

There are still more than 200 million cases of malaria annually. Of the resultant 600,000 deaths, about 90% are in Africa. Development of the infection evolves via two phases: one that involves the liver (exoerythrocytic phase), and one that involves red blood cells (erythrocytes). Typically, a bite from the Anopheles mosquito introduces the parasite Plasmodium (of which *P. falciparum* is the most dangerous species for humans) into the bloodstream as motile sporozoites, which travel to the liver. Following a possible dormant interval, the sporozoites differentiate to yield thousands of merozoites. After rupturing their hepatocyte host cells, most of these escape into the blood and infect erythrocytes. Other merozoites develop into male and female gametocytes in the mosquito's gut. After a blood meal from an infected person, these can fuse and eventually develop into new sporozoites ready to repeat the infective cycle.

According to WHO almost half the global population was at risk of infection in 2015. The "WHO Global Technical Strategy for Malaria 2016-2030" (2015), identifies 'ensuring universal access to malaria prevention, diagnosis and treatment' as a key pillar of the Strategy http://www.who.int/mediacentre/factsheets/fs094/en/. The present project, which aims to study the nonlinear dynamics of malaria, would contribute strongly to this aim. Diagnosis of malaria may be based on the overt symptoms (e.g. fever, enlarged spleen), by which time treatment may be ineffec-

tive. Earlier diagnosis is usually by the microscopic examination of blood films, but:

(a) There are many settings (especially rural) where the test is difficult to perform, especially in developing countries like Nigeria.

(b) Reliable results require skill and depend on the level of the parasites in the blood.

(c) The sensitivity is 75-90 % under optimal conditions, but can be as low as 50%.

Other diagnostic tests are discussed below in Section 1.1.2. Here we comment that commercially-available antigen-based rapid diagnostic tests (RDTs) can be more accurate in detecting malaria but, in addition to cost, they vary widely in diagnostic sensitivity and specificity. Early and accurate diagnosis of malaria is therefore uncommon. Where laboratory diagnostic tests cannot be afforded, use of the overt symptoms as an indication to treat for malaria can result in mistreatment of the common cold, thereby reducing the effectiveness of the malaria drugs in the future. There is an unmet need for a better and cheaper method of early diagnosis for malaria.

When a red blood cell becomes infected, its membrane becomes stiffer and develops knobs, making it more adhesive, so that it tends to stick to the inner linings of all the blood vessels. The increased stiffness and change in surface properties cause infected cells to pass less easily through the capillaries. The cell also changes shape, and its ability to transport oxygen is compromised. Consequently, the viscosity, flow properties, and oxygenation of blood are all changed by malaria. These effects show up most strongly in the microvasculature, i.e. in the capillary network. Hence the possibility of diagnosing malaria by examining characteristic changes in the microvasculature, though no purpose-designed device to perform this function yet exists.

This study therefore developed a real time technique based on noninvasive optical measurements of blood flow oxygenation, ECG, respiration and temperature,

with state-of-the-art nonlinear analyses to identify microvascular changes characteristic of malaria. The method was finally established following the experiments conducted on malaria patients in Kano, and on healthy control subjects in Kano and Lancaster. As we will see, a classification analysis based on an optimal set of discriminatory parameters distinguished with 90% success between the malaria and healthy states.

1.1.2 Existing non-invasive diagnostic methods for malaria

Almost any attempt to estimate the number of malaria cases globally is likely to be subject to dispute, and this is largely due to the lingering challenges accompanied with the existing diagnostic techniques for the disease. But such conjecture can be addressed with the introduction of a novel real time malaria diagnosis alongside an improved public health data reporting system and healthcare access.

Early and accurate diagnosis of malaria is essential for effective disease management and malaria surveillance. High-quality malaria diagnosis is important in all settings as misdiagnosis can result in significant morbidity and mortality. It is the first step in the WHO-recommended T3 (Test, Treat, Track) approach to malaria treatment. WHO recommends prompt malaria diagnosis either by microscopy or by RDT in all patients with suspected malaria before treatment is administered.

Diagnostic testing improves the management of all patients with febrile illnesses, and may also help to reduce the spread of drug resistance by reserving antimalarials for those who actually have the disease [1]. Furthermore, the requirement of more expensive drugs may be unaffordable to resource-poor countries [2]. Although clinical diagnosis is imprecise, it remains the basis of therapeutic care for the majority of febrile patients in malaria endemic areas, where laboratory support is often out of reach.

This section reviews briefly the microscopy and rapid diagnostic tests (RDTs), which are the two malaria diagnostics that are having the largest impact on malaria control today, but first we consider clinical diagnosis.

Clinical diagnosis

Clinical diagnosis, although expensive when carried out by professionals, remains the most commonly used method, and is the basis for self treatment. However, the overlapping of malaria symptoms with other tropical diseases impairs its specificity and therefore enhances the indiscriminate use of anti-malarials for managing febrile conditions in endemic areas. This led to a report that less than half of the malaria patients in Sri Lanka hospitals (see [3]) thought they had malaria [4], with many of them not actually having disease. The precision and accuracy of a clinical diagnosis varies with the level of endemicity, malaria season, and age group, so that no single clinical algorithm is a universal predictor [5, 6].

Microscopy

Microscopy examination of blood films remains the mainstay of malaria diagnosis in most large health clinics and hospitals. According to the WHO, however, the quality of microscopy-based diagnosis is frequently inadequate [1]. Diagnosis by microscopy has the disadvantages that –

- The distinction of *P. falciparum* from other human malarial species in causing sequestration of parasitized red blood cells in microvessels [7] (thought to result from the adhesion of the parasitized cells to vascular endothelium [8, 9]) only occurs in the second half of the intra-erythrocytic life cycle. Thus pigmented trophozoites are rarely seen in peripheral blood film, increasing the likelihood of false negative results.

- False positive result can sometimes be recorded, due to poor blood film preparation that generates artifacts commonly mistaken for malaria parasites, including bacteria, fungi, stain precipitation, dirt and cell debris [10]

- For the results to be reliable, some degree of skill is needed on the part of the person examining the blood film. Even in developed countries, expert

malaria microscopists are scarce [2, 11] and results will also depend on the level of the parasite in the blood.

- In comparison to expert microscopy, a wide range of poor specificity local microscopy is reported [12]; with blood films, the sensitivity is 75 to 90% under optimal conditions, but can be as low as 50%.

- In practice, there are many settings (especially rural) where the test is difficult to perform.

Rapid diagnostic tests (RDT)

The rapid diagnostic test relies on a device that requires no huge capital investment or electricity, is simple to perform, and easy to interpret. This method detects malaria antigen in a small amount of blood, usually 5 to 15 $\mu\ell$ by immunochromatographic assay with monoclonal antibodies directed against the target parasite antigen and impregnated on a test strip [2]. However, the RDTs vary widely in diagnostic sensitivity and specificity. Malaria rapid diagnostic tests have the potential to improve significantly the management of malaria infections, especially in remote areas with limited access to good quality microscopy services [1].

Other tests

Saliva and urine have been investigated as alternative, less invasive specimens. More recently, modern techniques utilizing antigen tests or polymerase chain reaction have been developed, but they are not widely implemented in regions where malaria is endemic. Where laboratory diagnostic tests cannot be afforded, the history of subjective fever is used as the indication to treat for malaria, whence the abuse of antimalarial drugs mentioned above.

1.1.3 Physiological oscillations and their potential in characterising cardiovascular dynamics in malaria

Measurements of blood flow and oxygenation in human subjects reveal several co-existing oscillatory processes, covering a very wide range of frequencies [13]. Use of the continuous wavelet transform reveals at least six such processes [14, 15]; with the same oscillations being seen at different sites and for different measured quantities, not only in blood flow and oxygenation. Their physiological attribution has been established (see Section 2.3.3). Briefly: hemodynamic oscillations near 1 Hz and 0.25 Hz are due to cardiac and respiratory activity respectively; the oscillation near 0.1 Hz is attributable to the natural properties of smooth muscle which oscillates at about 0.1 Hz even *in vitro*; that near 0.03 Hz is neurogenic, associated with autonomic nervous activity; and those near 0.007 Hz and 0.01 Hz arise [16] from NO-independent and NO-dependent endothelial activity. The physiological oscillatory processes giving rise to the signals suggested the introduction of a coupled-oscillator model of the cardiovascular system [17]. Understanding the nature of these oscillations in a healthy biological system allows the observation of transitions to pathological states. However, up to now, this approach has not been explored in gaining additional insights that are relevant to malaria therapy.

Malaria is a disease in which the oscillations in blood flow and cardiovascular dynamics may be expected to be substantially altered, due to the possibility of an infected red blood cell's membrane sticking to the endothelial cells that line all the blood vessels in a processes known as cytoadherence, thereby impairing the cell's deformation and passage through the capillaries. On this account, the viscosity, flow properties, and wall shear stress in blood vessel are all altered by malaria in distinctive ways. Premised on these unique effects of malaria, the disease provides an opportunity to observe noninvasively the characteristic changes in blood flow and cardiovascular dynamics using optically-based equipments, such as laser Doppler flowmetry.

1.2 Aim and objectives of the study

The overarching objective is to exploit the intuition of physics of the cardiovascular system to create a robust, reliable and effective method for the noninvasive diagnosis of malaria based on characterization of the oscillations in physiological data such as blood flow, ECG, respiration, skin temperature and oxygenation signals, using optimized nonlinear methods developed for treating time series from non-autonomous oscillators. The specific objectives are:

(a) To investigate whether the technique of laser-Doppler flowmetry (LDF) can be used to evaluate blood flow dynamics regardless of skin colour, i.e. in dark-skinned as well as light-skinned individuals.

(b) Using nonlinear time–series analyses methods to evaluate and characterize sets of blood flow and oxygenation data from subjects of different race, in-order to unravel the racial differences in cardiovascular dynamics.

(c) To evaluate the long-term effects of malaria on the microvasculature.

(d) Development of a novel non-invasive measurement/analysis system to measure simultaneously instantaneous microvascular oxygenation and blood flow, and to determine the phase coherence of these two parameters and other nonlinear characteristics of their oscillations.

(e) Following ethical approval, to use (d) on malaria patients, and healthy controls, in Murtala Muhammad specialist Hospital, Kano, Nigeria.

(f) Using the results from (d), to identify the analyses that provide the best discrimination between the disturbed microvascular dynamics of malaria patients and those of healthy subjects.

(g) Applying a machine-learning algorithm to the results from (f), to perform a classification analysis based on an optimal set of discriminatory parameters

that can distinguish with high precision between the malarial and healthy states.

1.3 Thesis layout

As discussed above, the main goal of this thesis is to describe the use of oscillations in microvascular blood flow and cardiovascular dynamics to investigate malaria, for the purpose of testing the hypothesis that cardiovascular dynamics are altered in febrile and non-febrile malaria when compared with healthy control subjects. Furthermore, these oscillations are also explored in treated malaria and in terms of their relationship to race-specific disparity.

Chapter 2 presents background information on the physiology and biophysics of the cardiovascular system alongside oscillations in cardiovascular flow in the context of malaria. Chapter 3 discusses the methods of measurement that were used in the data acquisition. This chapter also describes dynamical systems, draws attention to the significance of considering living systems as thermodynamically open and nonautonomous, and describes the nonlinear time series analysis techniques used to extract the results.

Chapter 4 evaluates the efficiency of using LDF to capture information about the dynamical changes in microvascular skin blood flow from darkly pigmented skin. The findings of this study reveal that with illumination derived from a laser diode of 780 nm wavelength, the blood flow dynamics can be investigated effectively using LDF, with the dynamics being uninfluenced by pigmentation, even in darkly pigmented skin. Effects of race-specific disparities in microvascular blood flow and oxygenation dynamics are investigated in Chapter 5. These promise to illuminate race-specific differences in cardiovascular dynamics, particularly in relation to cardiovascular diseases such as diabetes and malaria. The aim of this Chapter is to investigate how cardiovascular and microvascular dynamical processes differ between black Africans and Caucasians, using only resting-state recordings obtained from combined LDF and white light spectroscopy, alongside

near-infrared reflectance spectroscopy.

Chapter 6 investigates the blood flow and cardiovascular dynamics in febrile and nonfebrile malaria, as compared to healthy controls. The results of the study provide insights into the pathophysiology of cytoadherence of the infected red blood cells to the vascular endothelium, and are also used in the development of a diagnostic test.

Finally Chapter 7 presents analyses of physiological parameters measured from patients who had suffered episodes of malaria and recovered from it. This chapter aims to investigate the long-term effect of malaria on microvascular blood flow dynamics.

2. Physiological and biophysical background

2.1 Nutrient and oxygen transport

Note that for several billion years only bacteria were evolving, i.e. single-celled organisms evolved, individual cells structured into multi-cellular systems of increasing complexity and, as living organisms evolved further, they differentiated into specially designed tissues arranged to form organs. At this stage of development, individual cells could no longer sustain independent life. Hence, a unified system to supply and disseminate oxygen and nutrients to each cell and remove the products of their metabolism became an absolute necessity. Cells must exchange these substances with their environment for them to survive and this is accomplished by the cardiovascular system.

2.1.1 The circulatory system

The circulatory system, which is part of the cardiovascular system, sustains the life of all cells in the living organism on a continuous time scale. It achieves this task by maintaining the instantaneous chemical environment of the individual cells present in the body (i.e., the interstitial fluid) in a state suitable for the cellular function.

The essence of the human cardiovascular system can best be understood from a brief review of how the circulation of blood around the body was discovered.

From the earliest perception, blood was identified as a life providing fluid. Until the early seventeenth century, however, it had been believed that [18] the veins contained blood which is prepared and purified in the liver from chyle and then moved through the veins into organs, where it was consumed [18–20]. Galen viewed that [19] blood vessels carried blood and identified venous (dark red) and arterial (brighter and thinner) blood, each with distinct and separate functions [19]. He also proposed that blood is produced in the liver, flowed from the heart through arteries. Subsequently the blood moves to all parts of the body, where it was consumed and supposed that there was no return of blood to the heart or liver. The heart did not pump blood around, the heart's motion sucked blood in during diastole and the blood moved by the pulsation of the arteries themselves. A small amount of blood entering the vena cava is diverted to the right ventricle where it is divided into two streams, one supplying the lungs via the pulmonary artery to the left side of the heart and other organs from the left ventricle to the right through "pores", moving to the left heart [18, 21]. According to [20], the flaws in this view are striking, and one can only wonder how these concepts, established as dogma, were able to prevail for centuries. The first criticism of Galen's view was proposed by Ibn el-Nafis who became the first person to describe accurately the process of pulmonary circulation [22]. He was of the view that blood flows from the right chamber of the heart, passes to the lungs, and spreads in the pulmonary substance to mix with the air and that it must return to the left chamber of the heart; however he denied the presence of pores [23, 24] and that there was any direct path between the two chambers [18].

Finally it was to William Harvey that we owe the conception and proof of the idea that blood indeed circulates, after he had gone through a sequence of experiments. Fabricius had earlier described the valves of the veins without recognizing their function. But the role of the valves in the heart was first described by Andrea Casalpino [18]. Harvey was able to show that the valves in the heart they are arranged so as to allow the passage of blood in one direction only. He described his

experimental analysis of the movements of the heart and blood, establishing the phase of emptying the ventricles, known as systole. He concluded that the heart actively contracts in all dimensions, expelling its contained blood as a muscular pump to the lungs via the pulmonary artery and to the rest of the body. He also found that cardiac diastole or dilatation was passive and not active as Galen had hypothesised. Having demonstrated that the right ventricle is responsible for the pulmonary circulation, Harvey showed that the left ventricle supplied the rest of the body through its arteries. He observed that blood flows towards the heart in the veins and he demonstrated this experimentally by cutting them. By obstructing them with ligatures, he observed the action of their valves in preventing blood from moving to the periphery [24, 25]. Here again he contradicted Galen. In 1628, Harvey formulated his results, where he concluded that the circulation of the blood is the primary purpose of the motion and contraction of the heart [18]. However he was not able to identify the capillary system connecting arteries and veins; these were later discovered by Marcello Malpighi in 1661 after the microscope was introduced by Van Leeuwenhoek [18, 26].

The vascular bed is comprised of pre-stressed, curved vessels with numerous branches, and more or less divergent (arteries which carry blood from the cardiac pump to the tissues and capillaries) and convergent (veins which drains out blood back to the heart). The nerve-controlled muscular layer on the walls of the vessels adjusts their bore to control the flow (mechanotransduction). There are pressure and flow variations within the arterial tree which are linked to their corresponding wave propagations. The waves propagate with a speed of 5 to 30 m/s and therefore change their shapes.

The arteries carry blood from the cardiac pump to the tissue capillaries, which are loci of gas and substance exchanges. However the artery wall can be injured, thus leading to mortal consequences which include dilations of the lumen (aneurisms) or its narrowing (stenosis) [28**?**].

Today, Harvey's theory of blood circulation is widely recognized as the foun-

dation of medicine which opened the door to modern physiology. It is believed, however, that [19] Harvey rejected the mechanical explanations that were emerging as part of the Scientific Revolution, led by such contemporaries as Galileo, Rene Descartes and Francis Bacon, which ushered in a new era of mathematics, mechanization and an atomic theory. The world was no longer seen in qualitative terms but rather in mathematical terms. For example, the terms 'hot' and 'cold' were represented by numbers on a temperature scale. According to the atomic theory, matter could be broken up into discrete entities, which were not cold, hot, dry or wet, but rather possessed quantities of length, breadth, depth and motion [19]. These elements interacted with one another in a mechanical manner. Particles interacted and reacted according to the laws of physics, not according to a final cause. Premised on the continuous interaction and exchange of matter (particularly with the surrounding environment) within the human system, therefore, the human body came to be seen as complex machine [19].

The sections that follow trace the development of the understanding of the physics involved in blood circulation, by discussing topics of the human cardiovascular system in the light of physics grounded on Harvey's observations.

2.1.2 The cardiovascular system

The cardiovascular system supplies adequate blood to various organs of the body, responding to sudden changes in need for nutrients [28], which is essential to maintain life. About 5.5 litres of blood is propelled per minute in a typical human body for a stoke volume of 80 ml and at a cardiac frequency of 70 beats per minutes [28]. The non-autonomous nature of cells within the body ensures that the time taken for oxygen to be delivered between the right atrium and peripheral tissues has a magnitude of 0 (s) [28].

Cardiac functioning is dependent on several factors [28] which include: (1) cardiac loads; (2) sarcomere activity, mostly the cross bridge cycling rate; (3) ion carriers, which determine the rate of ion fluxes and the intracellular concentrations;

(4) the extra-cellular matrix; and (5) wall perfusion, which is solely responsible for exchange of nutrients.

Ventricular systole and diastole are strongly coupled. Moreover the re-expansion of the ventricle helps in refilling blood in the atrium. Hence, the recoiling force which arises from the downward motion of the beating heart alongside the stretch applied on the vessels helps the atrium to fill.

The function of respiration is to utilize homoeostasis within the human body [29]. The neural network which is mainly the autonomous nervous system (which has two subsets, the sympathetic and parasympathetic systems) controls the cardiovascular system. It also adapts its output to the body's needs depending on its activity and the environmental stimuli. Hence, the cardiovascular system plays a vital role in the interaction of respiration (the respiratory system is exposed outside through ventilation and alveoli) and circulatory system as described in Figure 2.1 [28, 29]. Furthermore, it is reported that an interaction between respiratory and circulatory system results in an oscillation that manifest in the sympathetic nerves, thereby synchronizing the latter with respiratory rhythm [29, 30].

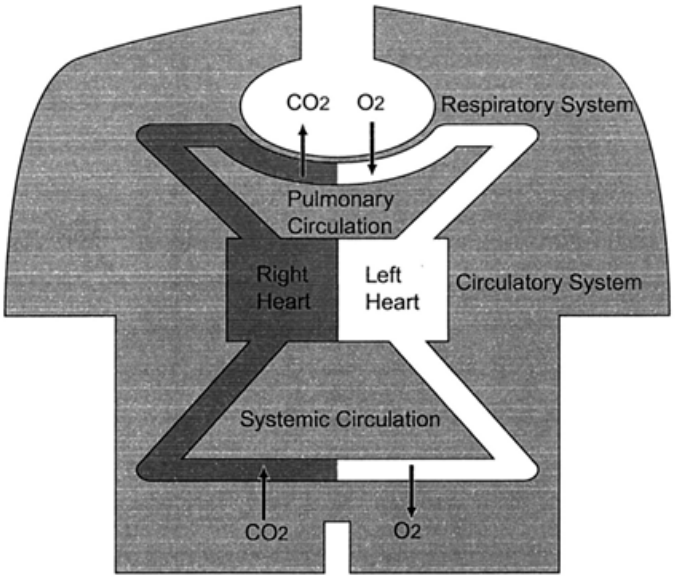

Figure 2.1: Respiratory and circulatory systems. The respiratory system is open to the exterior of the human body through ventilation and to its interior via the alveoli, while the circulatory system consists of two closed loops of pulmonary and systemic circulation. Pulmonary circulation originates in the right ventricle and terminates in the left atrium. Systemic circulation originates in the left ventricle and terminates in the right atrium. Extracted with permission from [29]).

2.1.3 The heart

The heart consists of two synchronized pumps in parallel, composed of two chambers. These two pumps propel blood into the pulmonary and systemic systems (Figure2.1). They merge into a single and muscular organ, that can beat synchronously [28]. The blood flow is not driven by absolute pressure, but rather the differences in pressure between the vasculature entry and exit.

The atria serve as auxiliary pumps that enable rapid ventricular filling particularly at rest when the cardiac frequency is low. Electrical excitations, originating from a region in the right atrium called the sinoatrial node (SAN), trigger the contractions of the heart. The SAN works relentlessly as an oscillator in generating heart rhythms, while its rate of oscillation is adaptive to changes in the energy demand of the body and to environmental factors [31]. However, due to the occurrence of electrical turbulence in the ventricles or to SAN malfunction, the

heart may spontaneously lose its ability to pump blood effectively thus leading to sudden cardiac death (SCD). SCD accounts for 300,000 – 400,000 deaths annually in the United States and it is a major cause of death, particularly in industrialized countries [31–33].

The average oxygen required by the heart is 6 to 8 ml/min per 100 g at rest, and so approximately 80 percent of oxygen consumption is related to its mechanical work while 20 percent is for the basal metabolism and myocardial blood flow. Arthur Winfree [31, 34] noted that SCD is not a problem confined to biology and medicine alone, but also a phenomenon that arises in physics and mathematics. This is due to the fact that the heart is not only a biological organ but also a mechanical pump and electrical conductor [31], and therefore could only be fully explored through a multidisciplinary approach. This realisation generated intensive research into understanding the nonlinear dynamics of the electrical and mechanical properties of the heart [31, 35–39].

The cardiac output (CO) represents the quantity of blood pumped by each ventricle per unit time that crosses any point in the circulatory system. It is determined by multiplying the stroke volume (SV is the volume of blood pumped by the ventricle in each beat, usually about 70 ml) by the heart rate (HR) in beats per minute [40]. The difference between the end-diastole volume (EDV) (the maximum volume achieved at the end of the ventricular filling) and the end-systole volume (ESV) is referred as stroke volume [28, 40]. The ratios of blood volume to SV in the serial compartments of both systemic and pulmonary circulations are shown in table 2.1.

There are a variety of factors that determine the cardiac output including the preload and the afterload. The dilatation force exerted on the myocardium at the end of the diastole (imposed by the ventricular volume) corresponds to the preload; meanwhile the resistance force to ejection corresponds to the afterload. The increase in HR results in an increase of the cardiac output until a critical HR is attained. However, these two factors can be related to two other factors. First,

the ratio between the rate of blood flow and body surface area, which is commonly referred as the cardiac index. Secondly, the ability of the heart to rapidly adjust to immediate demands which is described as the cardiac reserve [28].

Pulmonary circulation 16.3	
Arteries	5
Capillaries	0.8
Veins	10.5
Systemic circulation 38.7	
Aorta	1.3
Arteries	5.6
Capillaries	3.7
Veins	28.1

Table 2.1: An estimate of blood compartment volume relative to the SV (%), with SV of 80 ml and total volume 4.41. Extracted from [28]

The aperiodic behaviour of the heart describes its ability to respond rapidly to changes within the body's environment. It may therefore be characterised by behaviour and thus the normal heartbeat manifests itself with complex nonlinear dynamics [28, 41]. Correspondingly, stable and periodic cardiac dynamics can be interpreted as implying an unhealthy state and a bad prognosis. The work of [41] shows that a decay in random variability over time is associated with a weaker form of chaos, and it is an indication of congestive heart failure. It is believed that the changes in diastole duration lead to most of this variability [28].

2.1.4 The relationship between electrocardiogram and cardiac cycle.

The human heart generates electrical voltages which can be recorded from the surface of the skin as an electrocardiogram (ECG). The ECG contains *P, Q, R, S* and *T* waves, reflecting different activities associated with the heart. The spread

of depolarization through the atria mediates the P wave, and is accompanied by an atrial contraction, which results in a small rise in the atrial pressure curve immediately after the P wave. The ventricular depolarization ensues about 0.16 s after the P wave emerges, leading to the appearance of QRS waves at the same time initiating the ventricles' contraction and causing the ventricular pressure to start rising. Hence the QRS complex emerges shortly before the commencement of ventricular systole.

Consequently, the ventricular T wave can then be observed in the ECG indicating the period of repolarization of the ventricles in which the ventricle starts to relax. Finally, the T wave appears shortly before the ventricular contractions finishes.

The existing relationship between the ECG and cardiac cycle is critical for clinical investigation, as this can provide us with information about pathological cases (such as malaria) that directly or indirectly have an adverse effect on the heart.

2.2 Vascular architecture and organization

One of the features which governs blood flow dynamics is the arrangement of the vascular network (Figure 2.2). It is through the vasculature (blood vessels) that the ions, proteins and other nutrients carried by the blood are supplied to every tissue and organ of the human body. As the blood vessels (arteries and arterioles) take blood away from the heart, the vessels' diameters decrease as one moves further away from the heart towards the capillary beds, whilst increasing on returning back towards the heart (venules and veins). Of these vessels, the aorta and venae cavae are the largest artery and vein in the body respectively.

The artery has a three-layer thick wall (the endothelial lining, middle smooth muscle and elastic connective tissue layer, and outer connective tissue layer), and carries relatively high-pressure blood from the heart to the arterioles. The arteriole has a three-layer wall (smaller arterioles have an endothelial lining, some smooth

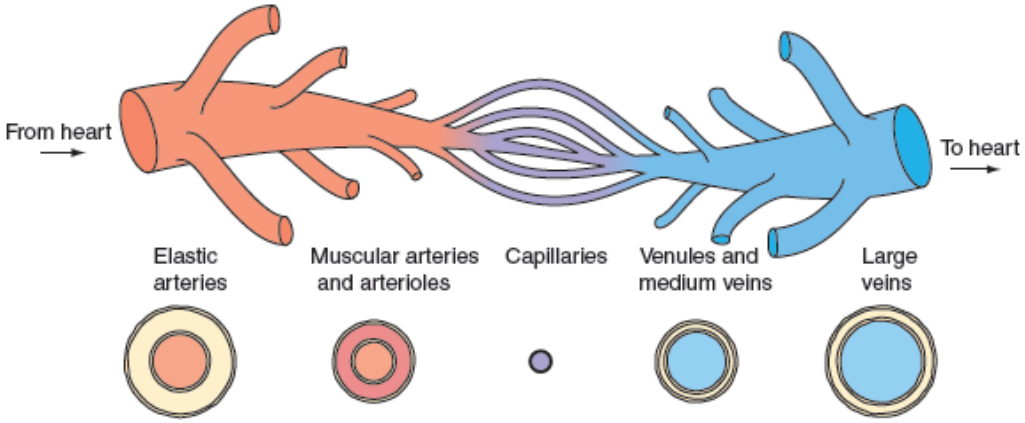

Figure 2.2: Structure and diameter of blood vessel walls. Extracted with permission from [40].

muscle tissue, and a small amount of connective tissue), but it is thinner than that of the artery, and it helps in controlling blood flow from arteries to capillaries by vasoconstriction or vasodilation. The capillary has a single layer of squamous epithelium, and contains a membrane that allows nutrients, gases and wastes to be exchanged between the blood and tissue fluid. The venule has a thinner wall than an arteriole, with less muscle and elastic connective tissue, but it also connects capillaries to veins. Veins have thinner walls than arteries, although they share similar layers. Veins carry relatively low-pressure blood from venules to the heart, and also serve as blood reservoirs.

The blood vessels play another vital role in addition to facilitating blood flow and exchange. The endothelial lining of blood vessels produces several substances (e.g. nitric oxide [NO], endothelin-1 [ET-1], and prostacylin [PGI^2) which modulate cardiac and vascular function, hemostasis (blood clotting), and inflammatory responses [40].

The functional and structural features of each blood vessels vary with consecutive bifurcation. Yet the whole cardiovascular system has one structure in common, and that is a smooth, single-celled layer of endothelium or endothelial cells that line the inner surface of all blood vessels. Capillaries are comprised only of endothelium, whereas every other vessel also has additional layers including smooth muscle and connective tissue.

Arteries The aorta and other systemic arteries have of thick walls comprising considerable amounts of elastic and connective tissues. Because they are also made of smooth muscle, arteries are commonly seen as elastic tubes. Given that the radii of arteries are mostly large, they act as low-resistance tubes that carry blood to different organs of the body. The other major function of the arteries associated with their elasticity is to serve as pressure reservoir for sustaining flow of blood across the tissue during diastole.

Arterial blood pressure Arterial pressure is commonly measured as systolic or diastolic, typically in the form, 126/76 mmHg. The systolic pressure is the maximum arterial pressure attained during ventricular ejection, while diastolic pressure is the minimum arterial pressure just prior to the beginning of ventricular ejection.

Moreover, the pulse pressure can be obtained from the arterial pressure. It is the difference between the systolic and diastolic pressures. By touching the arteries of the wrist or neck and noticing the pulsation with each heartbeat, the pulse pressure can be detected. If the volume of blood ejected increases, then the pulse pressure produced as a result of ventricular ejection becomes greater. More so, if the blood is ejected with a very high speed, then the pulse pressure also gets increased.

Arterial pressure changes continuously throughout the cardiac cycle. But the average between sytolic and dystolic pressures does not in fact represent the mean arterial pressure, because the diastole lasts longer than systole: the true mean arterial pressure is approximately the sum of the diastolic pressure and one-third of the pulse pressure. The mean arterial pressure is a good measure that describes the pressure at which blood is moving into the tissues in an average cardiac cycle.

Arterioles Two major important roles are known for the arterioles. First, at any given mean arterial pressure, the arterioles in each organ ensure the regulation of blood flow across every organ. Secondly the arterioles are major elements in deter-

mining mean arterial pressure. Since the latter is identical throughout the body, changes in relative blood flow between organs depend solely on the corresponding resistances produced by the arterioles of each organ.

Arterioles are composed of smooth muscle that can either increase the radius of the blood vessels by making them to relax via the vasodilation process, or decrease the radius of the vessels via vasoconstriction. Therefore, the level of arteriolar smooth muscle contraction in every tissue determines the manner of the blood flow distribution. The arteriolar smooth muscle also has spontaneous activity known as intrinsic tone. External signals such as neurotransmitters could increase or decrease the level of vessel contraction and this effect is controlled by the intrinsic tone.

Vasodilation in the arterioles occurs when the contractile force is lower than the vessel's intrinsic tone, whereas vasoconstriction occurs due to an increase in the contractile force. The direct response of arteriolar smooth muscle to dilation and constriction is known as the myogenic response. Both vasodilation and vasoconstriction in arterioles are controlled locally – by mechanisms that are independent on nerves or hormones, and extrinsically – by mechanisms that are dependent of nerves (sympathetic and parasympathetic nerves).

Endothelial cells and vascular smooth muscle As mentioned previously, several mechanisms can mediate the contraction or relaxation of vascular smooth muscle through the release of biochemical substances including nitric oxide. While most of the effects caused by these substances are through direct action on the arteriolar smooth muscle, others act indirectly through the endothelial cells adjoining the smooth muscle. The endothelial cells responds to these substances in addition to other specific mechanical stimuli, by secreting several paracrine agents that spread to the vascular smooth muscle.

Nitric oxide, also known as endothelium-derived relaxing factor, is one of the major paracrine vasodilatory substance released by the endothelial cells. It is continuously released by the endothelial cells in the arterioles and contributes

to relaxation of the arteriole. Furthermore, its production is fast and increases significantly in response to a sizeable number of the chemical inducers.

Endothelin-1 is one of the major paracrine vasoconstrictor substance released by endothelial cells in response to mechanical and chemical stimuli. It belongs to the endothelin family of peptide paracrine substances produced by a number of cells in the different organs. Apart from serving as a paracrine substance, the endothelin-1 could under certain circumstances serve as a hormone, leading to an extensive vasoconstriction of the arterioles.

Not only do the endothelial cells in the arteriole secrete substances, but the endothelial cells in the arteries also produce various paracrine substances by extension that affect the arteries' smooth muscle and thus modify their radii and resistances to blood flow. As the blood flows, it exerts force on the endothelial cells (the inner surface of the arterial wall) and this is referred as shear stress. When the blood flowing through the vessels increases, so also does the shear stress. The arterial wall responds to an increase in shear stress by releasing greater amounts of nitric oxide and some endothelin-1. It is these changes that bring about the relaxation of arterial vascular smooth muscle and correspondingly dilation of the artery.

Capillaries Approximately less than 90 percent of the entire circulating blood in the body flows through the capillaries. The main function of the whole cardiovascular system - the supply of nutrients and removal of metabolic end products, is performed by the 5 percent of blood flowing in the capillaries. The venules are often regarded as extension of capillaries as some supply and removal of nutrients and metabolic end products happens there.

Cells present in the microvasculature are usually not greater than 0.1 mm from a capillary, thereby making the capillaries pervade almost all the body's tissue. This also ensures the exchange of nutrients and metabolic end products highly efficient. About 25,000 miles of capillaries have been estimated in a adult, with the length and inner diameter of each capillary being 1 mm and 5 μ respectively. This allows the erythrocytes to squeeze its way through the capillary.

The organization of the capillaries differs considerably from organ to organ. A typical capillary has no smooth muscle and is comprised of a thin tube with one layer resting on a basement membrane, whose inner wall is linned with endothelial cells. In some organs of the body, the capillaries contain additional cells surrounding the basement membrane and this impacts on the way substances penetrate the capillary wall.

The condition of other vessels within the microvasculature influence flow of blood in the capillaries. For example, an increased flow in the capillaries result from vasodilation of the arterioles that supply the capillaries with blood, whereas a reduction of flow in the capillaries results from arteriolar vasoconstriction.

The blood moves through the aorta with a very high velocity, but at a lower speed in the arteries and arterioles. Subsequently the velocity significantly decreases as the blood flows through the capillary network. The slow motion of blood through the capillaries maximizes the period required for the exchange of substances between the blood and interstitial fluid. Afterwards, the velocity at which blood flows gradually increases in the venules and veins due to the decrease in their net cross-sectional area.

Veins After leaving the capillaries, blood flows into venules and subsequently moves to the veins. In a similar manner as with the capillaries, exchange of substances between the interstitial fluid and the venules occurs as blood flows through the venules.

The last set of vessels that takes blood back to the heart are the veins. The pressure differences between the peripheral veins and right artrium provides the force that drives the flow of returning blood. The pressure exerted by the heart as blood flows through the arterioles, capillaries and venules is lost due to the resistance of these vessels, therefore causing the pressure in the peripheral veins to be lower, usually between 10-15 mmHg. Normally, the pressure in the right artrium is zero, thereby making the pressure that drives blood from the peripheral veins to the right atrium stand between 10 and 15 mmHg – since the veins' diameters

are large and offer low resistance to flow of blood. The veins serve mainly as low resistance channels for the blood returning from the tissue to the heart.

Besides serving as low resistance channels, the veins also maintain peripheral venous pressure for the flow returning from venous side to the heart. This is because the veins' diameters are spontaneously changed in response to variations in blood volume.

Vasomotion and flow motion

The maintenance of adequate local tissue perfusion is the result of control mechanisms which reside at the level of the microscopic blood vessels, and is aided by mechanical events: the constriction and relaxation of the vessels whose walls are endowed with smooth muscle. The final outcome of the combination of these processes is the setting of vascular tone which is associated with the rheological properties of blood and determines vascular resistance.

Based on studies of the bat wing circulation in 1852 [42], Jones described the oscillations in tone of blood vessels that result in flow motion as vasomotion – which reflects the oscillations of flow within an organ. Both *in vivo* [43–45] and *in vitro* [46–50] studies have reported vasomotion in the vascular beds of different species.

Evidence that significant temporal variability may underlie local regulatory controls was reported in a number of studies conducted in single microvessels of the intact tissue, where it was shown that both blood flow motion and vessel diameter undergo rhythmic changes [51]. These two phenomena were christened flow motion and vasomotion respectively. The rhythmic oscillations in a blood vessel's diameter reflect vasomotion *in vivo* [52, 53]. Consequently, these rhythmic oscillations of vessel diameter influence blood flow, resulting in the periodic fluctuations referred to as flow motion [54]. Flow motion is a phenomenon that is synchronous with the activity of terminal arterioles and is readily obvious in direct observation of the capillaries. Hence, flow motion represents an oscillatory phenomenon, which is a

consequence of vasomotion [55].

Although vasomotion is considered a local phenomenon, it is not easily observed *in vivo* in subjects; but in contrast, flow motion is easier to monitor through laser Doppler flowmetry measurements, as well as other techniques, such as near infrared and white light spectroscopy methods. One has to be careful with these measurements particularly the laser Doppler flowmetry, as they could be influenced by neighbouring bigger vessels and central circulatory factors including blood pressure oscillations. However, this could be overcome by trying to target the smaller vessels that reflect the local activities in the microcirculation.

A broad spectrum of oscillation frequencies [14] has been identified in the analyses of flow motion recorded *in vivo* using laser Doppler flowmetry [15, 17, 56], using recordings of oxygen tension [57], and in measurements of oxygenation using near infrared and white light spectroscopy [58–60]. The frequencies of oscillation identified have been characterized into several bands, where oscillations at high frequency originating from the cardiac and respiratory activities are accompanied by other oscillations at lower frequencies. Flow motions within the 0.005-2 Hz frequency intervals has been observed in an analysis of laser Doppler flowmetry recordings in the human skin [16, 61].

Vasomotion appears to be a natural property of the vascular network, occurring at frequencies determined by both local and systemic effects. These effects can be directly observed in skin microvascular blood flow oscillations, with each having a distinct frequency and representing different physiological processes. These activities and their frequency bands spanning from 0.005-2 Hz have been widely studied in both the healthy and pathological states [15, 62, 63]. The conclusion reached was that 0.6-2 Hz reflects the cardiac activity, 0.145-0.6 Hz the respiration, 0.052-0.145 Hz the intrinsic myogenic activity, 0.021-0.052 Hz neurogenic activity (sympathetic nerve), 0.005-0.0095 Hz endothelial activity [15–17]. Hence, by analysing the components of vasomotion in health one can explore how their behaviour is changed in pathological states.

Furthermore, the intermediate frequencies of vasomotion reflect local effects that vary along the length of the vessel and are due to signals originating from locations of well defined activity, and perhaps in pathological state such as malaria may therefore significantly affect these manifested activities of vasomotion in blood flow. Hence, these phenomena will be investigated in this study alongside the oxygen dynamics, which is connected with the vasomotion, as will be described in the next section.

Alterations of vasomotion in disease states

There are significant differences in vasomotion between the healthy state and many pathological states [15, 63–70].

For example, there is clear proof that diabetes in both human [71, 72] and experimental animal models [73, 74] is associated with an altered pattern and reduced effectiveness of vasomotion. Knowing that vasomotion is strongly modulated by sympathetic innervation [75], it was therefore proposed that altered vasomotion in diabetes arises partly from the associated neuropathy [71, 76]. This interpretation was further supported by the finding that the vasomotion impaired by diabetes has a frequency of 0.1 Hz [77], which is the frequency interval associated with myogenic activity. Furthermore, the alteration of vasomotion in type 2 diabetes is arguably to promote arterial hypertension [78]. Temperature, which is known as a major experimental parameter of skin perfusion, has been demonstrated to impair vasomotion. It is found that heat stress attenuates vasomotion [79, 80]. Earlier studies on laser Doppler flowmetry measurements also demonstrated that, at high temperature, flow motion was increased, whilst during the pre-heating, α- and β-oscillations disappeared [75]. This could further suggest that an increase in temperature is likely to influence the central nervous system, and consequently the widening of the blood vessels (vasodilatation) alongside its elasticity. Note that, previous studies [56] have suggested that the β-oscillations are a vascular reaction of purely neurogenic origin.

Using the wavelet transform and wavelet phase coherence analysis, more recent studies [81] have investigated the effect of high temperature on simultaneously recorded skin and muscle sympathetic nerve activities and haemodynamic fluctuations. It was found that an increase in temperature could markedly augment oscillations in skin blood flow and skin sympathetic nerve activity, over a wide range of low frequencies. In addition, the coordination between skin and muscle sympathetic oscillations was reduced (although not significantly) by an increase in temperature.

The pattern and effectiveness of vasomotion is reportedly altered in hypertension [70]. Whilst vasomotion appears exactly alike in the skin of humans with crucial hypertension, investigation has indicated impaired vasomotion following ischemia in the same group [67]. This investigation *in vivo* has yet to be confirmed *in vitro* as the extraction of vasomotion from arteries isolated from the skin requires biopsies of subjects with hypertension which is challenging [82]. More recently, evidence has revealed that impaired vasomotion in hypertension is not fully restored by current anti-hypertension medications, as some impairment is still found in treated hypertensive patients [70]. The level of coherence in vasomotion at the 0.1 Hz frequency range in laser Doppler flowmetry recordings was markedly attenuated in treated hypertension as compared to healthy subjects.

Furthermore, laser Doppler flowmetry signals have shown that the vasomotion rhythm is modified by general anesthesia. This effect was uncovered by Landsverk *et al.* [68] in their study on eleven patients undergoing faciomaxillary surgery. With the transdermal delivery (known as iontophoresis) of acetylcholine and sodium nitroprusside by use of a voltage gradient on the skin, they were able to measure skin microcirculation before and during general anesthesia with propofol, fentanyl, and midazolam. The analyses of the laser Doppler flowmetry signals revealed that general anesthesia attenuates the vasomotion in the frequency intervals associated with the sympathetic and myogenic activities and with the component modulated by the endothelium.

Cancer has also been discovered to alter the pattern of vasomotion. Lancaster *et al.* have demonstrated that vasomotion is markedly impaired in melanoma through the analyses of laser Doppler flowmetry measurements of humans with skin melanocytic lesions [63]. It was reported that vasomotion at lower frequencies was significantly attenuated in melanoma. Similarly, ageing has also been shown in several studies [83–86] to have a significant effect on vasomotion, as evidenced by the analyses of complex and nonlinear dynamics of blood flow signals recorded with laser Doppler flowmetry [15]. These studies found a significant reduction in vasomotion with increasing age, particularly in the frequency interval associated with endothelial-dependent vasodilation.

Therefore, it is undoubtedly clear that a better understanding of the fundamental mechanisms underlying vasomotion will advance our knowledge of its physiological and pathophysiological consequences. Furthermore, the reverse may also hold true, meaning that the impaired effectiveness of vasomotion in pathological states may provide useful information about the underlying pathology, e.g. the incomplete restoration of the key mechanisms central to vasomotion by the current anti-hypertension medications [87].

Effect of vasomotion on tissue oxygenation

Terminal arteriole vasomotion produces a continuous interdependent adjustment of the capillary hematocrit and erythrocytic velocity, such that the red blood cells may travel through the capillaries in concentrated waves at a relatively high velocity. The aforementioned influence of vasomotion on capillary hematocrit indicates the potential effect of vasomotion on oxygen delivery to the microvasculature. The effects of vasomotion on oxygen transport to the capillary networks have been studied and strong evidence suggests that vasomotion helps in facilitating tissue oxygenation, although this has not been universally demonstrated [88]. It was found that patients with mild peripheral arterial occulusive disease exhibiting flow motion displayed a significantly higher measure of tissue oxygenation when compared

to those patients with no flow motion [54, 89]. The same findings were observed in other studies [90, 91] on laser Doppler flow motion in peripheral arterial occlusive disease.

Besides the experimental studies reporting the effects of flow motion on the oxygenation level, a number of studies based on mathematical modelling have also affirmed the influence of vasomotion on oxygen delivery [58, 92–95]. Their findings collectively propound the idea that the activity of vasomotion has the potential for changing the supply of oxygen to tissues by a factor of up to eight [96], with a more recent investigation suggesting an additional complex effect of vasomotion on oxygenation.

Furthermore, an association between vasomotion and oxygen extraction has been observed while studying the influence of vasomotion on oxygen extraction, by investigating its consequences for blood flux derived from LDF and the concentration of oxy- and deoxyhemoglobin in the tissue using optical reflectance spectroscopy [88]. Blood flow and oxygen transport have been investigated for varying tissue oxygen consumption rates, in which the importance of the frequency and amplitude of vasomotion-induced blood flow oscillations was studied. The effect of myoglobin on oxygen delivery during vasomotion has also been examined. In these investigations [93], in the absence of myoglobin, it was found that when consumption is high enough to produce regions of hypoxia under steady flow conditions, vasomotion-induced flow oscillations can significantly increase tissue oxygenation and decrease oxygen transport heterogeneity. The largest effect observed was for low-frequency, high amplitude oscillations. In contrast, at physiological tissue myoglobin concentrations, it was reported that vasomotion only improved oxygen supply to the skeletal muscle bed when the myoglobin concentration was low [93]. This unpredicted observation was thought to stem from the buffering effect of myoglobin, suggesting that, in highly aerobic muscles, short-term storage of oxygen is more important than the possibility of increasing transport through vasomotion [93].

2.3 Perfusion in skin

Physiologically, the process of supplying nutrients such as oxygen through blood delivery to the microvascular capillary bed is referred as perfusion. Usually, it is considered as the volume of blood moving through the aorta to the capillary bed in tissue per unit time. Inadequate perfusion (i.e. malperfusion) is associated with serious cardiovascular impairment. A detailed understanding of the anatomy and physiology of the human skin structures is crucial when studying perfusion in the skin. Numerous studies of skin perfusion have been used in the evaluation of microvascular dynamics under pathological and normal conditions, with some of the studies proposing skin microvasculature as a model for generalized microvascular function [97]. Skin perfusion is mostly studied using noninvasive optical techniques, as they allow signals to be recorded easily by exploiting the optical properties of the skin. These include near infrared spectroscopy, laser Doppler flowmetry, and optical coherence tomography, among others.

2.3.1 Anatomical structure of the skin

The body's largest organ is the human skin. It performs numerous important functions, and about 15 % of the total body's weight is accumulated by the skin. Key functions include aiding in thermoregulation and protecting the body against external attacks.

The skin is comprised of three layers with each of them exercising distinct functions: the epidermis, the dermis and the subcutaneous tissue (called hypodermis) [98], as shown in Figure 2.3. The epidermis is situated in the outermost layer and is composed of a specific arrangement of cells known as keratinocytes, which are responsible for the synthesis of keratin protein for the purpose of protection. The dermis layer which lies on the subcutaneous tissue essentially consists of the col-

lagen composed of a fibrillar structural protein. The thickness of each layer differs substantially, depending on the anatomical position in the body. For example, the thickness of the epidermis layer of the eyelid differs considerably from that of the sole of the foot, with each measuring about 0.1 mm and 1.5 mm respectively [98].

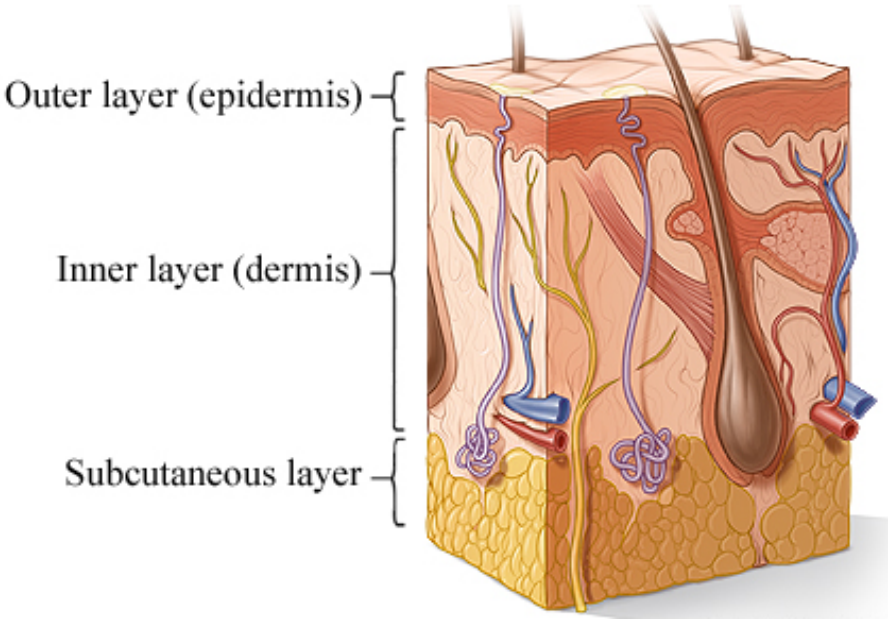

Figure 2.3: Cross-Section of the skin. Extracted from `https://www.healthlinkbc.ca/health-topics/tp10137`

Epidermis The epidermis is the stratified complex outermost layer of the skin, made of squamous epithelium. Several other cells such as the melanocytes are also contained within the epidermis. The stratum corneum forms part of the epidermis layer and it emerges following the differentiation of the keratinocyte into horny cells [99]. The epidermis is a repeatedly renewed layer that is mechanically exhausted by friction thereby producing derivative structures, such as sweat glands etc. The outer epidermis is renewed as soon as the basal cells go through some series of proliferations. In the innermost layer of the epidermis, skin cells mature and migrate from the basal layer to the skin surface and keratinization begins – a process in which the keratinocyte first passes through a synthetic and then a degradative phase [100]. These cells are present in the inner layer they accumulate and are subsequently moved to the epidermis. During this process they become

larger and acquire keratin filaments in their cytoplasm. This kills skin cells at the surface of the skin which in turn produces stratus corneum that serves as a substantial skin barrier to prevent water loss. As previously highlighted, the thickness of the epidermis varies in different parts of the body, due to the stratum corneum.

Dermis After the epidermis, the dermis is the second-thickest skin layer situated between the epidermis and subcutaneous tissues. It is a combined system of fibrous, filamentous and amorphous connective tissue which provides elasticity and support to the skin. The main role of dermis is to produce sweat and thus to help regulate the body's temperature as well as providing the epidermis with blood. In the dermis layer, there resides a combination of hair follicles, nerves endings and vascular networks. The follicle is connected to tiny muscles and is responsible for contractions in response to cold or anxiety. The nerve endings are responsible for signalling to the brain in response to stimuli from the body. The dermis is divided into two parts – the papillary dermis which is the thin, upper part and the reticular dermis which is the thick, lower part. The principal part of the dermis is the papillary dermis, and it is critical to dermis function. Nutrient delivery from dermis to the epidermis comes from the papillary dermis, while the strength, flexibility and elasticity of the skin are mostly provided by the reticular dermis. Similar to the epidermis, the thickness of the dermis layer differs depending on the anatomical position of the skin.

2.3.2 Optical properties of the skin

At any time the human skin is considered as a site of photobiological reactions such that can be investigated through spectroscopic imaging. Hence, the features of the skin's optics have some effect, and usually a critical effect, in influencing the reactions and the observations. The thickness, and morphological structure of, particularly, the stratum corneum is invariably a contributing factor, whenever ra-

diation propagates through the stratum corneum down to the capillary tissue bed. When the radiation reaches the capillary tissue bed, it is scattered and absorbed by the structures and chromophores of the skin which differ between subjects. Hence an understanding of skin photobiological reactions partly depends on how well the propagation of electromagnetic radiation within the skin is understood.

Almost all photobiological reactions depend on the wavelength of the electromagnetic radiation, because light of different wavelengths penetrates to different depths within the capillary tissue bed. Since the spectra of light-skin interactions and the fundamental frequencies of the electromagnetic radiation that are scattered or absorbed by the viable tissue are modified by the optics of the skin, a special consideration should be given to the scattering and propagation of the radiation within the tissue when analysing such spectra.

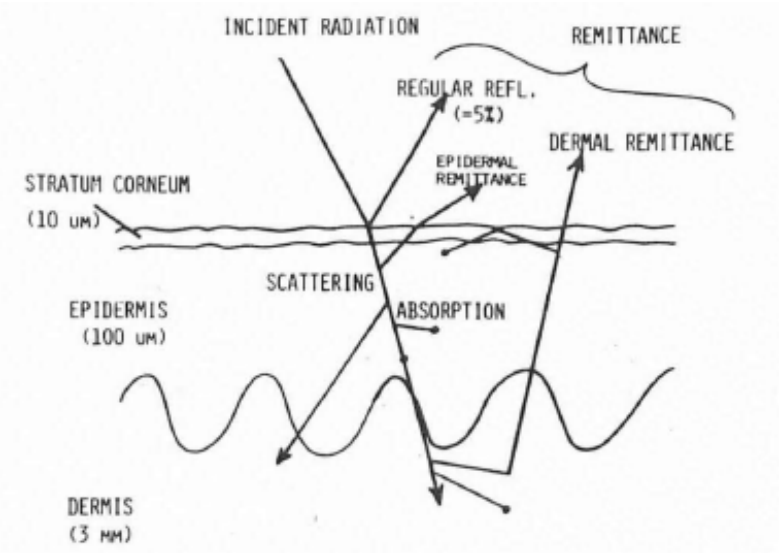

Figure 2.4: Schematic diagram illustrating the optical routes in normal human skin. Extracted with permission from [101].

The optical routes in normal human skin are shown in Figure 2.4. When a beam of light is shone on skin (either white or black skin) perpendicularly (i.e normal incidence), about 4-7% of the incident light is reflected (i.e regular reflectance) due to the change in refractive index between air and the stratum corneum [102]. For nearly perpendicular incident light, a small fraction of it undergoes this regular reflectance [103, 104]. Similarly, some light is internally back-scattered from the

target capillary tissue bed due to interference between the air and tissue. Given that the stratum corneum layer of the skin is rough in nature, light is not specularly reflected from it – that is to say the light reflected does not retain its direction, and also the incident light gets refracted after propagating from the stratum corneum further into the skin.

As mentioned above, only 4-7% of the incident radiation is reflected as a result of regular reflection at the stratum corneum. The remaining 93-96% of the incident light can be scattered or absorbed at any of the other layers of the skin. The reflected back-scattered light returned from the skin, as well as the penetration depth of the light incident on the skin, can be measured. The inhomogeneities between the refractive index of the medium relative to the physical inhomogeneities leads to scattering. The magnitude of these inhomogeneities relative to the wavelength, alongside the variation in the refractive index of the medium and the inhomogeneities, determine the intensity and spatial distribution of light scattered. Normally, scattering is relatively low and is equally-distributed spatially. It changes inversely with the 4th power of wavelength, for particles whose dimensions are less than 10% of the wavelength (i.e. subject to the Rayleigh scattering). In contrast scattering is much higher when the particle is of similar size to the wavelength. Scattering is very weak when the particle's dimension substantially exceeds the wavelength (known as Mie scattering). All these types of scattering take place within the skin. The penetration depth of light in the dermis is thought to be mostly determined by the scattering from collagen fibers [104].

Optics of the stratum corneum and epidermis Numerous investigations of the propagation of optical radiation, and especially of ultraviolet light through excised human epidermis and stratum corneum, have been described dating back to the study by Hasselbalch [105]. The diffuse manner of propagation through skin layers could not, however, be precisely elucidated in most of the early work. In the epidermis or stratum corneum of a fair-skinned Caucasian, the ultraviolet light propagates through the skin mainly at a low wavelength around 275 nm due

to absorption by chromophores, such as melanin [101].

Melanin chromophores often play a critical role in determining the propagation of optical radiation through the epidermis and stratum corneum. The inherited degree of pigmentation makes a huge difference to optical propagation. Peptide bonds are predominantly responsible for the high absorption of the epidermis and stratum corneum at wavelengths of < 240 nm. Figure 2.5 illustrates the absorption spectra of a few epidermal pigments. The diagram clearly shows that propagation of light through the epidermis and stratum corneum is influenced by rate at which melanin chromophores, urocanic acid and other substances absorb the light. Generally, spectral propagation in the epidermis depends on the epidermal thickness, as well as on the density and distribution of these chromophores. For example, melanin and urocanic acid have different densities and distributions, which may be attributable to the fact that their main function is to protect human skin from ultraviolet radiation, by absorbing most of it. However, melanin is the only pigment that significantly attenuates ultraviolet radiation in the epidermis.

The absorption rate of melanin across spectral interval of 250-1200 nm increases continuously as it approaches shorter wavelengths. Correspondingly, the absorption of radiation by melanin substantially declines in the near infrared spectrum (above 1100 nm or even beyond 780 nm). The total transmission and reflection of light of wavelength ≥ 1100 nm is not significantly affected by melanin pigmentation [106–108], see Figure 2.6.

Typically, dark-skinned skin contain a greater density of melanin granules, while Caucasians have less melanin. Investigations based on the comparisons of diffuse versus direct (i.e the proportion of total scattering to scattering across an optical direction in alignment with the incident light) transmission of either ultraviolet or visible light onto the epidermis or stratum corneum are completely independent of wavelength [109]. This implies that transmission of ultraviolet or visible light at the epidermis results from the rough nature of the skin layer, and rather than from how the particle scatters in the epidermis. Therefore, the

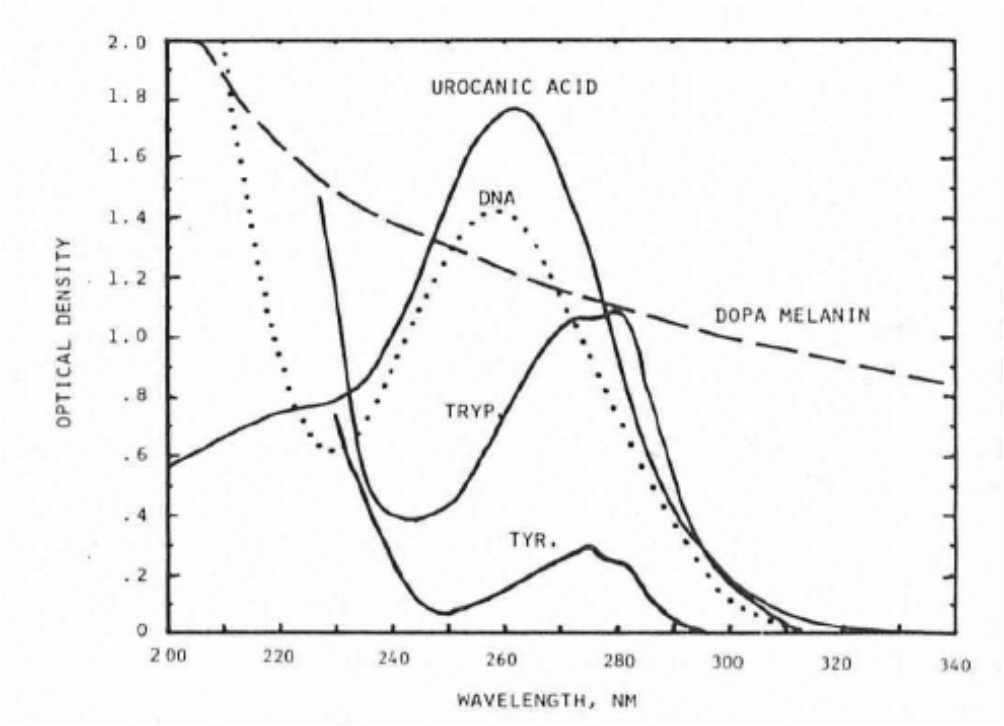

Figure 2.5: Ultraviolet radiation absorption spectra of considerable epidermal chromophores. The protein, urocanic acid, nucleic acids, and other aromatic chromphores absorbs the radiation which leads to the wide epidermal absorption spectrum close to 275 nm. Tryptophane (TRYP) is an amino acid, and deoxyribonucleic acid (DNA), and are both crucial for the physiology of the skin. DOPA and Tyrosine (TYR) are also an amino acid present in human body, they help in producing melenin in the skin. Extracted from [101].

epidermis is seen as being a layer where radiation including ultraviolet, visible and near infrared light radiation is mostly transmitted [104].

Optics of the dermis The optics of the dermis layer has different characteristics from those of the epidermis, and is associated with differences in structures and composition. It could be the reason that the epidermis can be separated and constitutes the foremost optical element of the skin. Hardy, Hammell, and Murgatroyd studied [108] skin optics by considering several parts of the dermis. They geometrically measured the fraction of visible and near infrared light that propagates across skin sections *in vitro*. Their investigation showed that the Beer-Lambert relation does hold when the dermis is considered as the material through which the light travels, and that radiation of longer wavelength exhibits higher transmission. In another study on the pig dermis [110], it was also found that

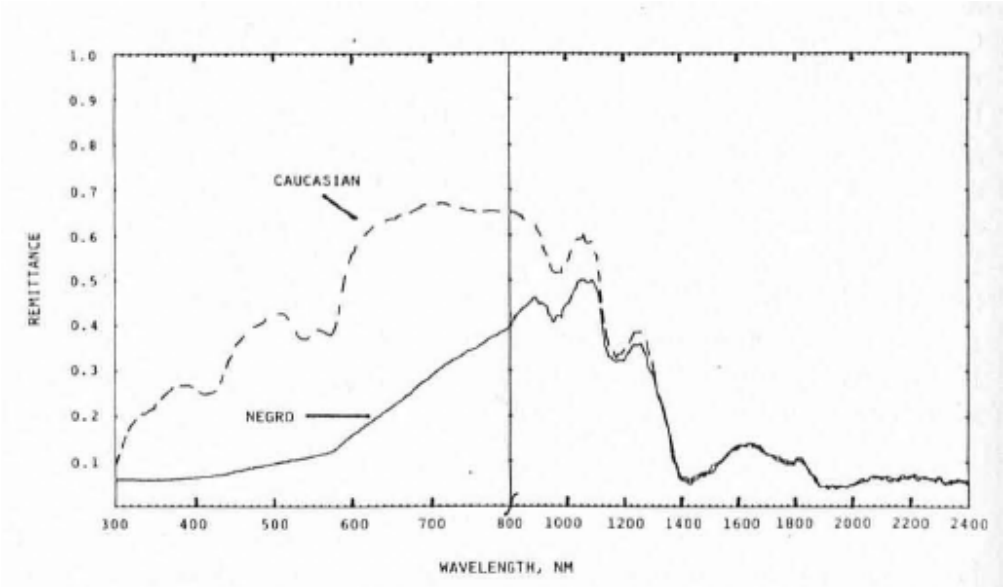

Figure 2.6: Spectral remitttance of dark-skinned and Caucasian skin obtained from the flexor surface of forearm. The significant increase in the absorption by melanin across shorter wavelengths and the significant reduction in absorption at longer wavelengths, is clearly obvious. Extracted with permission from [101]

light has higher transmission through the dermis at longer wavelengths, with a correspondingly higher remittance at shorter wavelengths.

Accordingly, the skin dermal layer has a significant impact on the depth to which light penetrates, and mainly explains the finding [108, 111] that generally, light (either ultraviolet, visible or near infrared lights) at longer wavelengths has higher penetration of the dermis than that at with shorter wavelengths.

2.3.3 Dynamical properties of skin microcirculation

The dynamical properties of blood flow which manifest as oscillations reflect both vasomotion and flow motion. These dynamical characteristics include the dilation and constriction of the muscular component of the small blood vessel's walls, which results in rhythmic variations of the vessels' diameters, popularly known as vasomotion (see above). In addition, the dynamical properties of blood also encompass the motion of the blood cells (particularly the red blood cells) and their interface with the blood vessel walls.

Oscillations in skin Doppler perfusion and their physiological origin

Based on careful interpretation of Doppler frequency shifted light, Cummins *et al.* [112] demonstrated the possibility of measuring the velocities of particles in solution. This came four years after Maiman [113] introduced the first working laser. The approach of Cummins *et al.* was used by Riva *et al.* [114] to measure the velocities of red blood cells in the glass tube model. However, the measurement of blood perfusion *in vivo* in an undisturbed microcirculation using a laser Doppler technique was first demonstrated by Stern [115], and has remained the most widely used method for evaluating microvascular blood flow. Watkins and Holloway [116] as well as Nilson [117] pioneered the equipment for measuring blood perfusion. A successful comparison between measurements made by instruments and microvascular blood flow was reported by Fischer *et al.* [118]. Despite the promising results obtained from clinical trials, application of the method is yet to become widespread clinically. This is because the instrument does not output signals in absolute units, thus making the interpretation of data more challenging. Nonetheless the technique still remains the most widely used for noninvasive recording of skin microvascular blood flow.

Several physiological measurements have revealed that the blood flow fluctuates in an oscillatory manner [64, 119, 120]. The absence of absolute units does not influence the observed oscillations in the blood flow, as it can be calibrated by a reference value. The physiological perturbations that result from the openness of the living system make the periods of oscillations continuously varying (aperiodic). Therefore, to properly discern such a signal, it has to be analysed in the time-frequency domain. Even in this domain, equilibrium between time and frequency resolution becomes challenging as the oscillations in blood flow occur on multiple varying time scales. Mostly, the dynamic properties of blood flow were assessed by evaluating its Fourier transform. Usually, the blood flow signal is windowed either to reduce the leakage or to obtain time localization. Selection of a window length to determine the time and frequency resolution can be

a difficult task. However, Stefanovska *et al.* [17] introduced a way of avoiding the explicit choice of a window length by applying the *wavelet transform* (details about wavelet transform are provided in Chapter 3) to blood flow signals. This allows the simultaneous observation of the oscillations in time and frequency.

Using the wavelet transform Stefanovska *et al.* investigated the oscillations that occur in the frequency range between 0.005 and 2 Hz in the peripheral blood circulations measured by the laser Doppler technique. The upper frequency limit was chosen because no physiological rhythm higher than the heart beat frequency is known. Only higher harmonics were detected above 2 Hz.

The choice of the lower frequency limit related to a number of physiological oscillations that were detected over a continuous time variation [121]. Longer recordings were required to study the lower frequencies in order to capture the slow oscillations. On average the volume of blood pumped by the heart (in its resting state) every minute equates to the whole amount of blood in the body [17]. It therefore suffices to set a low frequency limit of 0.005 Hz when analysing the dynamics of blood distribution. This reasoning led to many studies which investigated microvascular blood flow dynamics between similar frequency intervals of 0.005 to 2 Hz.

From the wavelet transform of the blood flow signals averaged over time alongside *a priori* physiological understanding, six characteristic frequency intervals were establish [15, 17, 18]. These frequency intervals manifest in blood flow dynamics, thereby reflecting various physiological activities within the microvascular system:

Interval	Frequency (Hz)	Physiological origin
I	0.6–2 Hz	Cardiac activity
II	0.145–0.6 Hz	Respiration
III	0.052–0.145 Hz	Myogenic activity
IV	0.021–0.052 Hz	Neurogenic activity
V	0.0095–0.021 Hz	Endothelial metabolic activity
VI	0.005-0.0095 Hz	Endothelial activity

Table 2.2: The frequency intervals of oscillations observed in blood flow dynamics, and their physiological origins [15].

These same frequency intervals have been applied in the analysis of heart rate variability/instantaneous heart frequency and blood pressure signals [122]. The physiological attributions of these intervals are summarised in Table 2.2 and we now discuss these in more detail:

Frequency interval I (0.6–2 Hz) reflecting the heart beat It is well-established that, in a healthy, resting state, the human heart beats at around 1 Hz, and can be as low as 0.6 Hz in those who partake in physical exercise or as high as 1.6 Hz in individuals with a weak cardiovascular system. Cardiac activity is reflected in all arterial blood vessels, meaning that it is detectable around all parts of the body and also evident in the microvascular skin perfusion signal. Simultaneous recordings of the respiration, ECG, and blood flow recorded with LDF have demonstrated the physiological origin of the cardiac frequency peak in the peripheral blood flow signal [123, 124]. Both the heart and lungs produce pressure differences which cause the blood to flow in the peripheral vessels. Generally, the overall contribution of the cardiac activity in the blood flow signal depends on the proximity of the LDF probe to bigger or smaller vessels during recordings. To capture the dynamical activities occurring at the lower frequencies, it is important to avoid placing the LDF probe in the proximity of bigger vessels and better to aim at smaller vessels. Other peripheral mechanisms also bring about the oscillations

seen in the blood flow.

Frequency interval II (0.145-0.6 Hz) reflecting the respiratory activity In 1993, Bolinger *et al.* [125, 126] found that HF waves were induced by respiratory changes, corresponding to oscillations around 0.3 Hz [127]. Unlike the cardiac oscillation, respiratory activity is not strongly manifested in the microvascular blood flow signal [125].

Frequency interval III (0.052-0.145 Hz) reflecting the myogenic activity The oscillations associated with myogenic activity of vascular smooth muscle cells have previously been highlighted in the context of vasomotion. Several studies have demonstrated the presence of oscillations at around 0.1 Hz in blood flow, blood pressure and even instantaneous heart frequency signals, and these are related to blood pressure regulation [128–130]. An earlier study, suggested that changes in the intravascular pressure constantly stimulate the vascular smooth muscle cells in the vessel's wall, which in turn is referred to as the myogenic response [113]. More to the point the work of Folkow in 1963, indicated that myogenic control induces rhythmic changes in vessel diameter [131]. After some years, it was illustrated that constriction and dilation of a blood vessel occurs in response to the rise and fall in transmural pressure. This action was described as myogenic response, it being argued that it is inherent to smooth muscle and is not influenced by neural, metabolic or hormonal agents.

A number of studies proposed that the spontaneous oscillations measured in vascular smooth muscle found within the 0.007-0.1 Hz interval are locally generated: they reflect the intrinsic myogenic activity of vascular smooth muscle cells in resistance vessels [43, 120, 132, 133]. Taube [134] similarly observed the presence of rythmic oscillations within the same frequency interval in a recorded blood pressure signal, and was substantiated by Hering in 1869 [135].

Furthermore, a study on small arteries in rats revealed that myogenic response is not altered by the effect of the vessels transmitter which is aided through the

blockade of adrenoceptors [136]. Similar observations have been documented on cat cerebral [137], rat cerbral [138] and rat saphenous arteries [139], by using tetrodotoxin to inhibit the nerve action potentials. Convincing evidence has been presented in these studies, finding that the myogenic response is as a result of the reaction of transmural pressure on vascular smooth muscle cells only. This finding agrees with an investigation done in humans where blood flow recorded in intact skin was compared with that measured from microvascular flaps deprived of sympathetic nerve activity [140].

Frequency interval IV (0.021–0.052 Hz) reflecting the neurogenic (sympathetic) activity Several studies have shown that oscillations in this frequency interval is where the neurogenic (sympathetic) activity lies. An oscillation with a fundamental frequency peak at 0.04 Hz associated with metabolic [130] or neurogenic activity [141] has been discovered in blood flow, blood pressure and instantaneous heart frequency signals. The activity is thought to be superimposed on myogenic activity in the control of blood pressure through changes in vessel's diameter.

These rhythmic adjustments were referred as β-oscillations by Kastrup *et al.* [75]. In a similar investigation, Golenhenhofen and Hildebrant [142], found that after local and ganglionic nerve inhibition, these β oscillations suddenly vanish, agreeing with the findings of Kastrup *et al* [75]. Another study also showed that slow oscillations measured in rabbit skeletal muscle tissue that occur around 0.02-0.05 Hz suddenly vanish following pharmacological nerve inhibition, thereby indicating that these slow oscillations are under neurogenic regulation [143].

The involvement of sympathetic nerve activity in this frequency interval has been confirmed by the work of Söderström *et al.*, where LDF blood flow was recorded from free microvascular flaps whose sympathetic nerve activity is inhibited and compared with LDF blood flow recorded from intact skin [140]. A significant reduction was observed in the spectral amplitude of blood captured from skin flap between 0.02-0.05 Hz frequency interval, and were therefore attributed

to sympathetic nerve activity. The latter influences blood flow oscillations in normal tissues with repetition times of 20–50 s (equivalent to 0.02-0.05 Hz). Malpas [144] further explained that the sympathetic nerve activity essentially contributes to the processes that regulate blood flow by rhythmically mediating the dilation and constriction of the blood vessels [140]. Additional proof for the origin of the neurogenic oscillations was reported by Landsverk *et al.* [145] in their work on the effects of brachial plexus block on the skin perfusion, which is widely believed to instigate sympathetic impairment [146]. Using wavelet analysis on the LDF signal with a logarithmic frequency resolution the study revealed a significant reduction in the relative amplitude of the oscillations in 0.0095-0.021 Hz and 0.021-0.052 Hz frequency intervals, suggesting a blockade in both endothelial and sympathetic activity.

Frequency interval V (0.0095–0.021 Hz) reflecting the endothelial activity, nitric oxide (NO) dependent Oscillations in this frequency interval emanate from endothelial activity as proven using different vasoactive substances, in active endothlial cells and after their inhibition [13, 147]. An experimental study on rabbit has shown that the vasodilation of a vessel can be instigated by acetylcholine (ACh) through the action of endothelial cells [148], and that ACh induces release of a substance. It was later discovered that the substance released was a nitric oxide (NO). Skin microvascular endothelial activity was first investigated using the endothelial-dependent vasodilator ACh and the endothelial-independent vasodilator sodium nitroprusside (SNP), through iontophoresis of these two substances [147, 149, 150]. Moncada later suggested that endothelial dysfunction could be checked by examining and comparing an impaired ACh-inducued vasodilation with SNP-induced vasodilation [151].

Following several investigations into the role of the endothelial-dependent vasodilator ACh in rhythmic activities, Kvernmo *et al.* hypothesised that the dynamical properties of blood flow are regulated by the endothelium [61]. Based on the wavelet analysis of LDF blood flow recorded for 20 minutes, they noticed

that the ACh and SNP responses manifested around the 0.01 Hz. The oscillation observed at 0.01 Hz was linked to the endothelium mediated vasodilation, although its physiological origin is yet to be fully explored. A few years later, the same dose-response protocol was used in a different study that compared healthy athletes with control subjects and the findings reported earlier was substantiated [152].

The identification of low frequency oscillatory activity near 0.007 Hz brought about 30-minute recordings of blood flow alongside the iontophoresis protocol. The protocol was chosen in order to demonstrate that the observed low-frequency oscillatory component arose as a result of endothelial-related activity and was not due to the induced iontophoretic current and transdermal potential difference [153, 154]. It was thus confirmed that the oscillations observed at the low frequency interval V did not emanate from the iontophoretic current or transdermal potential difference. Furthermore, the contribution of endothelium to low frequency oscillatory activities seen around 0.0095–0.021 Hz interval has been explored in the literature [16, 68, 145, 155]. These oscillations were demonstrated to be slightly mediated by NO, as the infusion of L-NMMA diminished the oscillations but were observed to have suddenly re-appeared with the infusion of L-arginine and not endogenous prostaglandins [155]. This discovery that low frequency oscillation around 0.0095–0.021 Hz are NO-dependent was substantiated in a separate study, which demonstrated that endothelial activity was reduced in congestive heart failure and was partially restored following β1-blockade treatment [156].

Frequency interval VI (0.005–0.0095 Hz) reflecting the endothelial activity, nitric oxide (NO) independent In contrast to frequency interval V, the oscillations around 0.005–0.0095 Hz were demonstrated to be significantly higher in response to ACh compared with SNP, whose origin is believed to arose from endothelium related mechanisms such as endothelium-derived hyperpolarizing factor (EDHF) [16, 56]. Using the same protocol as Kvandal *et al.* [155] but substituting ACh and SNP with deionised water (a low conductance electrolyte) and

NaCl solution (a high conductance solution), Veber *et al.* [153] tested whether the observed oscillations around 0.005–0.0095 Hz emanate from endothelial activity or are due to iontophoretic current induced blood flow. They observed an increased oscillatory spectral power in all frequency bands after conducting a cathodal iontophoresis of deionized water, and the comparison between oscillations around each of the frequency intervals showed that they were not differently affected. In addition, they also found that an iontophoresis of NaCl did not significantly influence the oscillations in blood flow, and therefore corroborating the findings that was observed in an earlier study that used the iontophoresis of ACh and SNP [153].

In summary, all of these physiological oscillatory processes interact with one another, thereby resulting in complex blood flow signals due to their coupling. Locally, the exhibition of these complex interactions occurs through the adjustment of vasomotion by the physiological interplays, particularly those that manifest in the blood flow dynamics (shown in Table 2.2) discussed above in section 2.3.3. Stefanovska and Bračič in 1999 [14, 18] introduced a coupled oscillator model inspired by the observation of these six oscillatory frequencies, which demonstrated the value of skin microvascular blood flow recordings. The aim was to understand the underlying mechanistic processes involved in microvascular dynamics of the healthy state and to investigate how it becomes modified in a pathological state. To do this they evaluated the influences of these oscillations in each frequency interval, using appropriate time-frequency analysis methods. The procedure has been used in characterising blood flow dynamics at rest, and proven to be methodologically good and reproducible [157]. This approach has been widely used to inspect the skin microvascular blood flow dynamics in athletes [152] and several pathological states, which include hypertension [67, 69, 70], the effect of anethesia [68], congestive heart failure [56], obesity [158], diabetes [159], critical lamb ischemia [160], ageing [15, 87] and cancer [63]. Subsequently, the method has also been extended to the study of microvascular blood flow in malaria, and biracial groups

which will be discussed in detail below in Chapters 6 and 5 respectively.

2.4 Microvascular blood flow model based on the microvasculature and biophysics of blood flow

The microvasculature of a perfused tissue facilitates transport and exchange of materials, and ensures the delivery of blood to each point in the tissue. The structure of the microvasculature and biophysical behaviour of the blood flowing through it are important factors in influencing material transport and exchange [161]. There have been extensive researches in the field of microcirculation [162–164].

The microcirculation uses the smallest vessels in the body and consists of the capillary network: arterioles, capillaries, venules, and terminal lymphatic vessels regulate blood flow within organs, transcapillary exchanges, and the removal of cellular waste [28, 161]. These duties of microcirculation are what differentiates it from the larger vessels of the macrocirculation, which serve as conduits to and from the heart and peripheral organs. Another interesting distinction is that the microvasculature is mostly embedded within organs whereas most of the macrocirculatory vessels are not.

Diseases such as sickle cell anaemia, hypertension, diabetes and malaria, manifest themselves mainly through deleterious effects on the microvasculature. Significant blood loss due to injury or other causes, if not quickly replenished can lead to irreversible malfunction, circulatory shock and ultimately death. Disruptions or disorderliness in the microvasculature are widely regarded as the prime contributors to morbidity and mortality around the world. For example, the importance of blood replenishment, irrespective of the cause of the loss, has led to tremendous efforts towards establishing blood substitutes for the past two decades. As loss in blood could result in maldistribution of red blood cell, which in turn could negatively influence capillary viscosity and consequently lead to microvas-

cular dysfunction. Despite enormous research, there are not yet any substitutes enabling recovery from the loss of function caused by loss of blood from the circulatory system. So it is still of paramount importance to better explore how the fundamental features of blood and its flow behaviours makes it such an efficacious means for delivery and exchange in the microvasculature.

Blood is a suspension of discrete elements comprising red blood cells (RBCs) or erythrocytes, white blood cells (WBCs) or leukocytes, and platelets. The blood plasma is an aqueous solution comprising different types of chemical species, which include ions, mainly Ca^{2+}, Na^{+}, Cl^{-}, K^{+} and macromolecules, ranging up to 500-kilodalton molecular weight. RBCs are a bioconcave discoid shape, typically with a diameter and thickness of 6-8 and 2 μm respectively. The cells are found to be non-nucleated in mammals and consist of a solution of concentrated hemoglobin wrapped in a highly flexible membrane. WBCs are classified into two main groups, the agranulocytes and the granulocytes which include, lymphocytes, monocytes, basophils, phagocytes, macrophages, eosinophils and neutrophils. The WBCs differ in size and properties, e.g., a typically inactivated neutrophil is approximately spherical in shape with a diameter of 8 μm. Discoid shaped particles with a diameter of approximately μm are referred to platelets. The distribution of blood flow within the networks of microvessels and the overall resistance are significantly affected due to the mechanical interactions between the blood cells and the microvasculature [161, 163].

The science of the blood flow, including the deformation of its constituents elements led to the field of hemorheology, due to the crucial necessity for detailed understanding of the flow properties of blood. This includes the interactions between the cellular components of blood and the endothelial cells that line the blood vessels. However, the shear rate, dimensions, time history and geometry of the system are also essential factors.

The rheological properties of blood include its non-Newtonian behaviour, which was realised from viscometric studies of RBCs in suspension [165]. It yielded useful

details on the properties and behaviours of blood flow under standard conditions. However, Aleksander and Paul [163] hold the view that, for numerous pedagogical reasons this detail is insufficient to understand the behaviour of blood flow in the microvasculature. For example, the viscometric studies cannot adequately predict the rheological properties of blood in a network, e.g., the microvasculature with its myriad vessels branches of various length, diameter, and flow rates [163]. Moreover, in the venules, the endothelial cells that line within its walls are provided with receptors that communicate with the ligands on the WBCs. The interactions between the ligand-receptor play a pivotal role in RBCs under pathological conditions such as diabetes mellitus, sickle cell diseases and malaria.

It is of great significance that the blood vessel wall interface has a sensor mechanism that monitors the shear, forming part of the blood flow regulation mechanism that also involves the microvasculature. The contractile elements in the vessel wall require an input that will respond in order to keep these forces constant, therefore making it an important sensor mechanism. However, the adaptive changes that occur within the organization of the microvascular network and the vessel wall (angiogenesis and vascular remodelling) are more or less due to chronic or persistent changes in these forces. The forces are generated by the blood in the vessel lumen and therefore, the rheological behaviours of blood will strongly influence the mechanics of this coupling [163].

The biophysics of blood flow in microvessels has been studied for many years, leading to considerable progress based on a variety of different approaches and techniques. These include *in vivo* and *in vitro* experimental studies, theoretical and mathematical models [166, 167]. In the attempt to better understand the characteristics that determine blood flow in the vessels, a French physicist and physician in 1830, Poiseuille, conducted a classic experiment on the study of the hydrodynamics of tube flow [163, 168]. The foundation for subsequent research on microvascular flow and the unique behaviours of blood flow in small glass tubes was conducted by the Swedish physiologist, Fahraeus in 1930. Fresh interest in

the area occurred from 1960 onwards and has led to significant advances in the understanding of the mechanics of microcirculation [163, 169–172]. A description of theoretical and experimental achievements in the field of microvascular hemorheology flow mechanics was provided, and mathematical models were proposed in [161, 163, 173, 174].

2.4.1 Rheological behaviours of the blood components

Blood can be defined as a non-Newtonian, shear thinning fluid which is composed of more than 90% of cellular elements [174]. As proposed from this physical definition, the blood viscosity decreases with increasing shear force corresponding to an increase in the flow rate in blood vessels as shown in Figure 2.7. Blood viscosity at high and low shear rates differs because of the characteristic behaviours of RBCs. The determinant of blood viscosity at high shear rates is connected to RBC deformability, while it is RBC aggregation that determines blood viscosity at low shear rates [173].

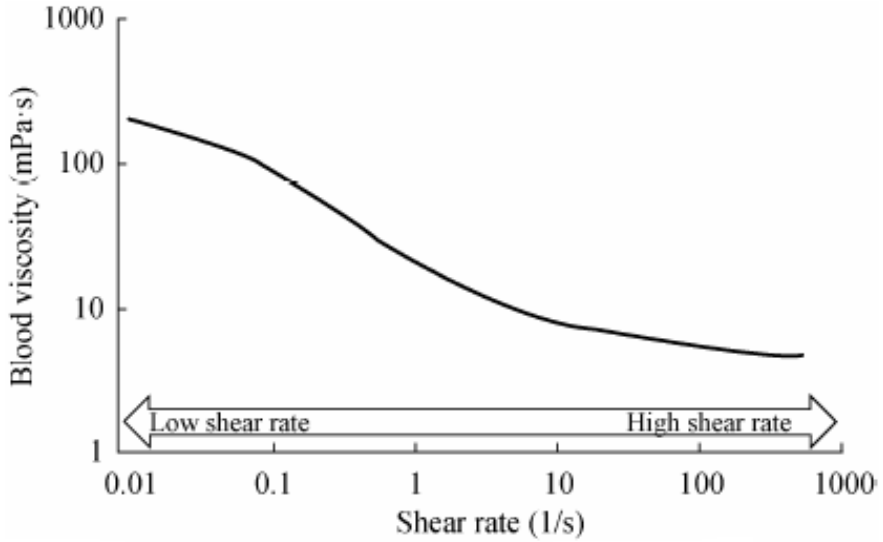

Figure 2.7: The effect of shear rate on whole blood viscosity. Shear rate is the velocity gradient between adjacent layers of blood, is expressed as 1/s and is proportional to flow rate in a tube (e.g., blood vessel). The lower shear rates correspond to the circulatory conditions in the venous circulation while higher shear rates characterize the arterial vessels. The unit of viscosity is mPa.s, numerically equal to centiPoise (cP); water has a viscosity of about 1 mPa.s at 25°C and is independent of shear rate. Figure modified from [174].

The rheological behaviours of the constituent elements of blood were recently reviewed [174]. The main role of RBCs is to carry oxygen from the lungs to the tissues and to carry carbon dioxide from the tissues to the lungs. It is widely considered that the solution is Newtonian under physiological conditions and has a viscosity of ∼6 centipoise (cPs). It is believed that, in the healthy state, the endothelium does not interact with the RBCs through specific receptors: but that receptor-ligand interaction may be present under pathological conditions. This view perhaps originated from the experimental studies that reported the involvement of various types of receptors in RCB-EC interaction. For example, in sickle RBC, the receptors involved in the RBC-endothelium interaction include VCAM-1 [175], P-selectin [176] and $\alpha_v\beta_3^b$ [177]. Similarly, other investigations [178, 179] on malaria have also reported the involvement of different receptors in the interaction between malaria infected RBC and endothelium. Therefore, receptor-ligand interactions are present under pathological conditions [180]. Furthermore, the mechanical behaviour of RBCs (e.g., cellular deformability) can be significantly affected by disease processes.

WBCs belong to the immune system. Some get activated by foreign particles or molecules as they circulate in the blood stream, e.g., in the presence of an antigen, their shape, cytoskeletal structure, and mechanical properties change dramatically. Others exist in the interstitial space between the tissue cells. The WBCs are comprised of a plasma membrane and a three-dimensional cytoskeleton as part of the cytoplasm, and a nucleus. The rheological properties of WBCs have been interestingly explained in terms of viscoelastic models and a model of a compound drop which has a viscous nucleus enveloped by two layers of less viscous fluid denoting the plasma membrane and the cytoplasm [181]. WBCs also interact with other cells, especially the endothelial cells, via their adhesion molecules and cell surface receptors. Several experimental studies in the last decades have revealed and elaborated the nanomechanics of the interactions of the WBCs as described in [182–184].

2.4.2 Red cells deformation

The most flexible cells of the mammalian organism are the RBCs: this is due to their ability to change their structure to an ellipsoidal shape under the influence of an external force, to a much greater extent than other cells [169]. This behaviour applies to the RBCs of all mammalian species. The RBC shape alterations facilitate their orientation to flow motion in blood vessel, resulting in decreased blood viscosity. At high shear rates, the changes in orientation and shape are optimized [173]. The major determinants of RBC deformation are its biconcave-discoid shape and lack of organelles and nucleus which are the key features of RBCs [174].

Alterations of RBC deformability

Pathophysiological changes of RBC cytoplasmic and membrane behaviours seldom accompany significant alterations of RBC deformability. A typical example in cytoplasmic viscosity, is sickle cell disease. This is due to a genetic disorder producing a single amino acid change in the β - globin chain, whereby hemoglobin S is formed [185]. The deformability of an RBC is also affected by disease, including infections, circulations, circulatory disorders (e.g., ischemia and reperfusion), and metabolic diseases (e.g., diabetes), etc [186]. However, alterations during disease processes may signify one of the following changes [186]: (1) cytoplasmic hemoglobin concentration and viscosity alterations; (2) changing of shape from biconcave-discoid to spherical structure, thus reducing the relatively high surface area of a biconcave disc.

Moreover, it is important to note that part of the hemorheological vicious cycle involves alterations of RBC deformability. The disturbed tissue perfusion leads to enhanced formation of oxygen free radical, resulting in impaired deformability, thus leading to further reduction in blood fluidity [187].

RBC aggregation

Unlike the case of high shear rates, the biconcave-discoid shape of the RBC is retained under low-shear conditions, or at stasis where it aggregates into unique shaped structures resembling stacks of coins. This is a reversible process and is referred to as rouleaux formation [174]. Frictional resistance between the flow streamlines is increased as a result of the aggregation, thus magnifying blood viscosity under low-shear conditions [173]. Large macromolecules are believed to induce the RBC aggregation, while the efficiency of the concentration of such macromolecules is determined by the cellular properties [174]. Altogether, the aggregability of the RBC is defined by the contribution of cellular properties to rouleaux formation [188].

Alterations of RBC aggregation

Enhancement of RBC aggregation is mainly caused by an inflammatory response. The physical factor that affects sedimentation of erythrocyte is RBC aggregation [189]. However, instead of measuring the erythrocyte sedimentation rate (ESR), an alternative and more appropriate method of evaluating the rationale behind inflammation has been proposed in [190]. During malignant diseases, chronic inflammatory conditions, infections and circulatory disorders, the aggregation of RBC was found to be increased [191]. Therefore, it was proposed that acute phase reactants under such clinical conditions are particularly influenced by aggregation [174]. Likewise, it has been suggested that the RBC aggregation index could serve as a prognostic quantity for ischemic diseases [192].

RBC aggregation is a complex phenomenon, and its influence on hemodynamics is still not completely understood. Contradictory studies report an increase [193–196], as well as a decrease [197–199] or no effect on apparent viscosity [198–200]. Enhanced aggregation is associated with a wide range of pathologies [201], but were reportedly observed in human subjects who were athletes [201]. It is therefore still unclear whether RBC aggregation is a deleterious or beneficial phenomenon [201].

2.4.3 Influence of blood rheology on blood flow and tissue perfusion

It has became clear in earlier experimental studies that there is a distinction between *in vivo* blood flow behaviour and that studied *in vitro* [202]. Blood viscosity was found to have limited effect as recorded from measurements based on *in vivo* flow resistance, therefore creating more questions regarding the significance of blood rheology alteration in terms of tissue perfusion. However, whole blood viscosity was reported to be increased with human ageing [174], in which the reported relationship indicates the influence of RBC deformation instead of the influence of RBC aggregation [203, 204]. Numerous physiological mechanisms are available to describe the lower apparent viscosity of blood *in vivo*, such as reduced microvascular hematocrit, in addition to other related biophysical phenomena such as the plasma skimming, Fahraeus effect and Fahraeus-Lindqvist effect, all of which are related to the flow of RBC suspensions in a narrow tubes. Elaborated discussion on these hemodynamic factors will be made in the sections that follow, and can also be found in [205–207].

2.4.4 Biophysical description of blood flow in microvessels

Rheological behaviours of blood in microvessels can be inferred from *in vitro* studies of blood in rotational viscometers and small glass tubes. A segment of reduced hematocrit and increased concentration of RBCs adjacent to the wall and near the center of the tube, respectively, result from the mechanical interactions between the RBCs and tube walls. The effects of the overall behaviour of blood flow in narrow tubes include the dynamic reduction of intravascular hematocrit (Fahraeus effect), and the reduction of resistance of flow below the level expected, given the bulk viscosity (Fahraeus-Lindqvist effect). These effects are highly significant and can result in what is termed as axial migration [161, 208, 209]. Though the significance of these phenomena for blood flow in living tissue is not fully understood, they

have been studied extensively *in vitro* and have also been modelled theoretically. They will be discussed in next section.

Flow of RBC in narrow tubes – Fahraeus effects

From the foregoing discussion, it can be clearly understood that RBCs in many living organisms undergo deformation due to the influence of local forces. They also go through aggregation, although the RBCs can reversibly disaggregate under the action of shear forces. These characteristic features of the RBC can account for the shear thinning property of blood. Across the tube's radius the velocity of fluid varies from zero at the wall to a maximum near the center of the tube. This creates a strong correlation between the concentrations and velocity of RBCs over the cross-section of the tube but the average RBC velocity (V_{c}) is higher than the mean of the whole blood velocity (V_{b}) [161], thereby decreasing the time required by the RBC to transit through a segment of the tube. This in turn reduces the percentage of hematocrit in that particular segment of the tube (i.e., tube hematocrit, H_{T}) with respect to the hematocrit of blood entering or leaving the tube (discharge hematocrit, H_{D}), which is expressed in equation (2.1) [161, 210].

$$\frac{H_{\mathrm{T}}}{H_{\mathrm{D}}} = \frac{V_{\mathrm{b}}}{V_{\mathrm{c}}} \tag{2.1}$$

This phenomena in which the dynamic or tube hematocrit, which is measured by pausing the flow and emptying the tube content, is consistently smaller than the ejected hematocrit measured in the discharge reservoir, is generally known as the Fahraeus effect. [163]

Fahreaus – Lindqvist effect

Fahraeus and Lindqvist [211] conducted an experimental investigation on blood flow in long glass tubes. They proposed that the resistance of blood flowing in a tube cannot be predicted from the blood viscosity as measured in large viscometers and the hydraulic resistance of the tube. Their experiment took account of

Poiseuille's law in estimating the blood's viscosity on the basis that the volume flow rate decreases with a decreasing tube diameter. The material properties of the blood are not well described by this measure of blood viscosity, but better by the blood/tube property in a particular instance of flow, and this is known as the apparent or effective viscosity μ_a.

Several studies have elaborated the dependence of apparent viscosity of blood on tube diameter, velocity of flow and hematocrit. A parametric description of apparent viscosity of blood relative to the viscosity of plasma, as a function of tube diameter and hematocrit, was merged with results from 18 different studies on flow velocities ranging from medium to high velocities. This comparison showed that, in long tubes of $\leq$ 300 μm diameters, the measured apparent viscosity of blood decreases dramatically with a decrease in tube diameter. The viscosity of blood attained a minimum when the tube's diameter was approximately 5-7 μm, which corresponds to the diameters of capillary blood vessels [163]. The foregoing phenomenon is described as the Lindqvist-Fahraeus effect

$$\mu_{\mathrm{a}} = \pi \Delta p D^4 / 128 Q L, \tag{2.2}$$

$$\eta_{\mathrm{vitro}} = 1 + (\eta_{0.45} - 1) \cdot \frac{(1 - H_{\mathrm{D}})^{\mathrm{C}} - 1}{(1 - 0.45)^{\mathrm{C}} - 1}. \tag{2.3}$$

Equation (2.2) defines the effective viscosity [161, 163], where Δp is the pressure drop, D is the tube internal diameter, L is tube length, and Q is the volume flow rate. Equation (2.2) reduces to Poiseuille law in the case of Newtonian fluid.

Based on the assumption for blood flow velocities $>$ 50 tube diameters/s, a parametric description apparent blood viscosity was obtained from a combination of data from 18 studies. Equation 2.3 describes the dependence of apparent blood viscosity (relative to the viscosity of plasma, i.e. relative apparent viscosity) on tube diameter (μm), hematocrit and velocity. For a constant discharge hematocrit (H_D) of 0.45, the relative apparent viscosity $\eta_{0.45}$, is expressed as

$$\eta_{0.45} = 220 \cdot \exp^{-1.3\ \mathrm{D}} + 3.2 - 2.44 \cdot \exp -0.06 D^{0.645}, \tag{2.4}$$

where C is a constant denoting the shape of viscosity dependence on hematocrit and D remains the diameter. Note that, the value 0.45 was estimated from [161].

$$C = (0.8 + \exp^{-0.075\mathrm{D}}) \cdot \left(\frac{1}{1 + 10^{-11} \cdot D^{12}} - 1 \right) + \frac{1}{1 + 10^{-11} \cdot D^{12}}. \tag{2.5}$$

However, within the range of this diameter (i.e, 5-7 μm), the apparent viscosity of blood having a discharge hematocrit of 0.45 was found to be 25 % higher than that of the cell-free plasma, signifying a very low hematocrit dependence. But the apparent viscosity does increase beyond the level observed in large vessels at diameters less than $\sim$ 3.5 μm [161].

2.5 Biophysics of the cardiovascular dynamics in the malarial state

Circulating malarial infected blood cells are usually destroyed in the spleen, however, to avoid this fate, the *Plasmodium falciparum* parasite displays adhesive proteins on the surface of the infected blood cells, causing the blood cells to stick to the walls of small blood vessels, thereby sequestering the parasite from passage through the general circulation and the spleen.

At the onset of malaria, it can be understood from the foregoing that the *Plasmodium* parasite invades the RBCs right from the erythrocytic stage and strongly influences the mechanical behaviour of the RBC. However, the consequences of the pathophysiology of malaria from the mechanistic point of view is believed to be the significant increase in rigidity and cytoadherence of parasitized RBCs onto the inner linings of the blood vessels and capillaries, causing them to sequestrate in the microvascular bed [212]. This sequestration is likely to hinder the action of vasoac-

tive substances. It also affects the blood viscosity which is strongly dependent on RBC deformability [213], perhaps impairing the combined effects (i.e. the cardiac, respiratory, myogenic, neurogenic and endothelial activities) that manifest as oscillations in the dynamics of blood. It is widely known that high deformability is a prerequisite for healthy RBCs, the reason being that in order to facilitate adequate transport of oxygen to the various parts of the body the RBCs must squeeze their way through narrow capillaries where cells exchange nutrients, thanks to their ability to deform and flow in the microvascular network. As discussed above, the capillary vessel is made of a thin monolayer of endothelial cells (ECs) which interact directly with the blood, thus strongly contributing to the dynamics of blood flow. Therefore, since the deformability and adhesiveness of RBCs are markedly affected in this disease, it is reasonable to anticipate that the blood flow dynamics, especially the oscillatory processes associated with microvascular dynamics as discussed earlier are likely to be impaired in the malarial state.

Exactly how the *Plasmodium falciparum* erythrocyte membrane protein-3 (PfEMP) and the knob-associated histidine rich protein (KAHRP) in the development of enhanced rigidity in the malaria infected RBCs lead to changes in the mechanical behaviour of the RBCs still remains unclear. However, Glenister *et al.* have identified [214] a significant effect of these proteins on the rigidity of cells in malaria.

It has also been reported [215] that almost all cytoadherence is mediated by the parasite protein PfEMP as well as various endothelial receptor molecules, including intracellular adhesion molecule-1, E-selecting and vascular cell adhesion.

2.5.1 Distinctive effect of malaria on blood flow and oxygenation

The increased stiffness of the membrane of an infected erythrocyte (red blood cell), [212] and its tendency to stick to the endothelial cells that line all the blood vessels, cause infected cells to pass less easily through the capillaries. The cell also changes shape, and its ability to transport/release oxygen is compromised. Consequently,

the viscosity, flow properties, and oxygenation of blood are all changed by malaria in ways that do not occur in other diseases. Hemodynamics is altered [216] on account of the spatial distributions of erythrocytes [217] and merozoites, and it is reasonable to infer that endothelial reactivity is affected too. Erythrocytes are an important factor determining the hemorheological properties of blood and the shear-thinning of blood is mainly attributable to their characteristics. Variations in the hemorheological properties alter the flow resistance and wall shear stress in blood vessels [213] so a detailed understanding of the relationship between the hemorheological and hemodynamic properties is of great importance. Experimentally [213], it has been shown that increased blood viscosity is associated with a blunt velocity profile and a high velocity component at the wall of a microchannel.

2.5.2 Interactions between malarial (*Plasmodium falciparum*) infected erythrocyte and endothelium cells

Many published articles have shown that sickle red blood cells and diabetic red blood cells can threaten metabolism, upregulate the expression of vasoactivators in endothelial cells (ECs) and enhance RBC-EC adhesion [180]. The severity in the features of malaria is believed to be in connection with the extreme systemic inflammation and magnification of the RBC-EC adhesion leading to the local accumulation of infected RBCs [180, 218, 219]. It is commonly believed that the functional effects of infected RBC-EC adhesion is not restricted to blood flow impairment alone. Nonetheless, only discerning and gaining an excellent understanding of the underlying mechanism hindering the flow of blood can lead to ways of ameliorating other consequences of the blood flow impairment.

The study of the effects of the endothelin-1 (ET-1) (a potent vasoconstrictor produced by vascular endothelial cells) in the microvascular ECs due to interactions between abnormal RBCs and ECs has produced controversial results. The endothelins (ETs) are involved in the regulation of vascular tone, in the amplifi-

cation of the inflammatory response, as well as in normal cell proliferation, repair and tissue development, thus ET-1 can in turn modulate the endothelial expression of adhesion molecules and cytokines production [215]. Basilico and colleagues used static coincubation assays to conclude that the production of both stimulated and constitutive endothelin-1 in the microvascular ECs decreases with infected *P. falciparum* parasitized RBCs as compared with healthy RBCs [180, 215]. This result seems to contrast with clinical findings that reported an increased plasma level of endothelin-1 in eighteen patients with severe malaria [180, 220].

2.5.3 Possible mechanism underlying endothelial cell modulation by red blood cells in the malaria state

Activities in the microvasculature are modulated by the action of both biochemical and mechanical factors. The ligand-receptor mediated process that results in cytoadherence of RBCs - ECs may activate signal transduction in the ECs, thus threatening protein production/activation. The biochemical events are reported to include the release of lipids and free radicals from unstable sickle RBCs (sickle cells have altered and abnormal organization of lipids [180]). The EC phenotype is influenced by the circulation of RBCs due to their influence on mechanical contact and the non-physical mechanisms (Figure 2.8), and this implies that both mechanism are apparently modulated by flow of blood as well.

Moreover, convective mass transfer and mechanical forces induced by blood flow may contribute to both mechanisms. First, this is because the mechanical contact between the RBCs and ECs could be influenced by the fluid shearing forces, which often result in cytoadhesion/cytoadherence – that is the processes whereby the malarial *Plasmodium* parasite adheres/sticks to the endothelial cell receptor. The cytoadherence occurs when the dispersive fluid force is resisted by the interactions between the cells (cell-cell contact). Secondly, the presence of agonist on the EC may also affect blood flow due to the obstructions in mass transport [180, 221, 222]. It can be understood from the foregoing that the role of

ECs is directly affected by the hemodynamic forces.

Therefore, an approach that employs dynamical measurements of blood flow followed by appropriate data analyses and interpretation could reveal a great deal of information about the endothelial reactivity in the microvasculature, particularly in the malarial state.

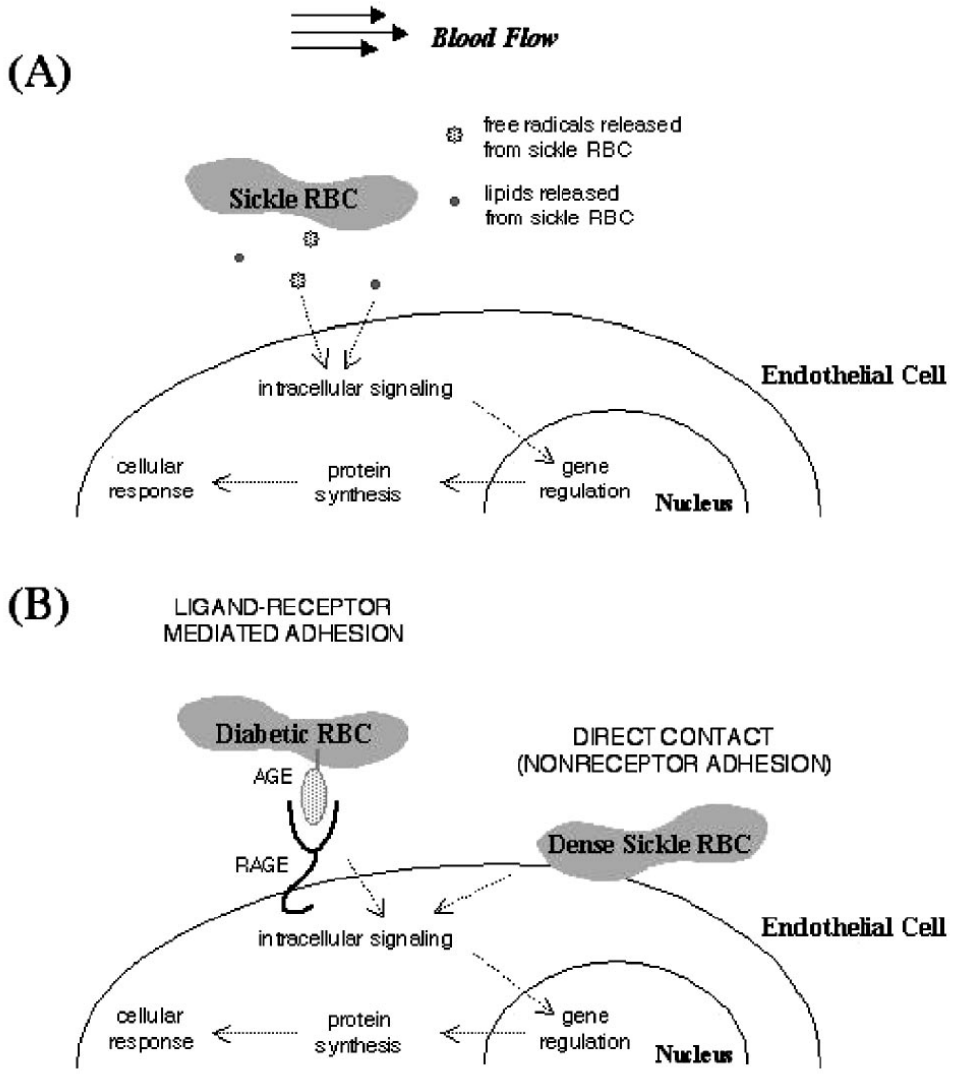

Figure 2.8: An illustration of how blood flow could influence the mechanisms involved in the endothelial cell modulation by diseased RBCs: (A) example of the biochemical factors involved include the release of lipids and free radical from sickle RBC and (B) mechanical contact, including ligand-receptor mediated adhesion and direct/non-specific contact, (extracted with permission from [180]).

2.6 Effects of racial disparity on the cardiovascular system

Awareness of ethnic health disparities in cardiovascular and many other diseases is increasing, due to the increase in heterogeneity among the world's population. Extensive data collected from both clinical and epidemiological studies have demonstrated racial disparity as a health issue [223–225]. This means that it is more important than ever to address racial effects on many physiological processes.

Differences in race significantly influence the physiology of many cardiovascular parameters including the blood pressure [226]. By extension, this may manifest as differences in the blood flow, as well as the layer of cells that form the inner lining of all blood vessels, the endothelium, which, as discussed above, play an important role in the regulation of blood flow.

It is known that African Americans (AA) and Africans are more affected by cardiovascular disease [227], with AAs reported to have higher incidence of hypertension and a higher rate of target organ damage, such as stroke and myocardial infarction as compared to non-African Americans [228]. The prevalence of hypertension in AA is believed to be related to a decrease in vasodilatation dependent on nitric oxide (NO) [223], a vascular endothelial cell derived factor which relaxes the underlying smooth muscle (see above) [229]. Besides more prevalent cardiovascular diseases, racial effects also cause higher incidence of other diseases in which NO plays a critical role such as type II diabetes mellitus linked with insulin resistance [230, 231].

Despite the significant contributions being made to decipher the effects of race on the pathophysiology of diseases, most of the studies that provide information about these effects investigate vascular responses in subjects of different races as well as employing in-vitro techniques to investigate the functionality of endothelium through recording the kinetics of NO/O_2 release.

2.6.1 Racial disparity in the resting heart rate

Racial disparities in cardiovascular dynamics could be associated with quality of life and lifestyle [232]. One of the fundamental mechanisms behind cardiovascular disease and associated consequences such as malaria, hypertension and diabetes may be attributed to impairment of the autonomic nervous system [233].

Several investigations have shown mortality from a number of diseases and other conditions results from autonomic instability in relation to an increased sympathetic activity together with decreased parasympathetic activity [234]. This viewpoint is that parasympathetic cardiac activity, (that is the vagal activity) gets attenuated over time, while the peripheral and central sympathetic activities become higher [235–237]. It has recently been evinced in the literature that heart rate variabilty – the dynamical change between consecutive heart beats, is connected with all-cause mortality and an inreased rate of disease from a plethora of risk factors including: family hsitory of cardiovascular disease, age and socio-economic life style [233, 234, 238, 239]. Clinically, heart rate variability has been used for medical examinations and for prediction of risk of cardiac shock or sudden death, following hypertension and myocardial infarction [240, 241].

A malfunctional autonomic nervous system has been associated with subjects that are highly susceptible to cardiovascular diseases [242, 243]. Thus it is argued that white and black individuals exhibit different cardiovascular autonomic modulation [244, 245]. Furthermore, disparity in the heart rate variability of white and black subjects has been reported, with some data demonstrating a higher heart rate variabilty in whites in the resting state compared to blacks and some studies revealed a contrary result[244–249], although this contradiction could partly result from the differences in the experimental protocols adopted in each study.

Considering the fact that attenuation of vagally mediated heart rate variabilty is linked with a greater cardiovascular risk in African Americans (AAs), one would expect a decreased vagally-mediated heart rate variability in AAs compared to European Americans. However, findings from several investigations reveal a higher

heart rate variability in AAs than EAs [246, 250–253]. For example, Lio *et al.* [246] investigated the heart rate variability which was recorded for 2 mins in supine and resting state, from subjects with atherosclerotic risk. They observed that the high and low frequency components of the heart rate variability were increased and decreased respectively in AAs compared to EAs. Although with 2 min recordings one cannot talk about the low frequencies as a longer recording is needed to properly capture low frequency information. Likewise, findings from different studies demonstrated not only an increased heart rate variability in AAs [247, 254] but also evinced the stability of this effect longitudinally [255]. While a preponderance of data has reported higher heart rate variability in AAs, anthropometric characteristics of the subjects recruited and other possible confounding effects require extensive analyses in order to evaluate their influence on the detected differences.

2.6.2 Racial disparity in endothelial function

Diseases such as hypertension, diabetes mellitus and malaria have associated endothelial dysfunction and the cardiovascular impediments are significantly higher in blacks than the whites. It has been proposed [223, 256] that the endothelium-derived nitric oxide (NO), which is a critical in vascular pathophysiology, is influenced by racial disparity. Physiologically, NO mostly mediates activities within the cells and organs of the body, and thus protects the cardiovascular system from pathological impairments or endothelial dysfunction. In addition NO inhibits smooth muscle cell proliferation, and the sticking of white blood cells to the endothelium. One of the primary processes in the onset of vascular diseases is a the destruction of the path through which NO communicates, and that is simply the endothelial impairment.

The increase in the production of O_2^- and decrease in the synthesis of NO is thought to be the cause of the decreased NO bioavailability seen in vascular pathophysiology. The reduction of NO bioactivity and generation of $ONOO^-$, arise from the swift reaction between O_2^- and NO. The substantial reduction of

NO in the pathogenesis of vascular diseases such as hypertension and diabetes is a consequence of the raised production of O_2^- within the endothelium. In most situations, however, the origin of the excessive production of O_2^- is not clear. However, several studies have argued that NAD(P)H-dependent oxidases, xanthine oxidase, cyclooxygenase, mitochondrial oxidases, and endothelial nitric oxide synthase (eNOS) and neuronal NOS participate in the processes that lead to the generation of O_2^- [257–260]. The differences in endothelial NO/O_2^-/ $ONOO^-$ metabolism is widely believed to occur differently among biracial subjects [228, 261].

Several independent studies have examined the effect of racial disparities in NO production/bioavailability. It has been demonstrated that endothelial cells in black individuals produce markedly higher O_2^-, whose origin is essentially from NAD(P)H-oxidase and endothelial NO synthase (eNOS) [261]. A different study attributed the reduction of NO bioavailability within the endothelium of black individuals to the dulled response of the vasodilator to acetylcholine [223, 256]. Multiple mechanisms including genetic factors, socio-economic status and environmental factors predispose the effects of these racial differences. The influence of these race-specific mechanisms on the pathogenesis of vascular diseases is crucial for deciphering the complexity of the diseases.

2.7 Experimental models of the erythrocyte and vascular endothelium interactions

Cells are continuously open to mechanical forces (sticking together), as blood flows in the cardiovascular system. Local fluid mechanical forces modulate several cell – plasma and cell – cell interactions in blood vessels. For example, the equilibrium between the dispersive forces due to blood flow and adhesive forces resulting from the interactions of ligands and counter-receptors conveyed on the cell surface is what determines the ability of the blood cell and vessel wall to stick together. For these cells to be properly anchored against shear forces, the sticking strength most

be strong enough. Moreover, for the successful capture of blood cells from the blood stream within a very short ligand/receptor interaction time, the kinetics of this sticking must be rapid [180].

The adhesive interactions between blood and vascular endothelial cells (ECs) lining the vessel wall are needed to allow diverse biological processes, e.g., hemostasis (platelet-EC or platelet – extracellular matrix adhesion) and inflammation (leukocyte-EC adhesion) [180]. However, the abnormal or improper adhesion of blood elements to ECs can be deleterious because it may hinder blood flow, diminish oxygen supply and therefore cause tissue damage or death. As is clear from the foregoing, normal RBCs are readily deformable and are not adherent to inactive ECs. Many studies have revealed that RBCs from patients with sickle cell anemia, diabetes mellitus, β-thalassaemia, hereditary hydrocytosis, chronic uremia, and malaria, have abnormally increased adhesiveness to ECs [180, 262–269]. The vaso-occlusive pathology and vascular damage identified in these diseases are argued to have led to the increased RBC-EC adhesion. However, the molecular mechanism by which the ECs recognize abnormal RBCs and the phenomena that lead to pathological responses are yet to be understood.

It is of paramount importance to discern the complex interactions between blood flow, RBCs, and ECs at the molecular level in order to come up with therapeutics that can tackle this abnormal RBC interaction with ECs. Therefore this section compares various *in vitro* experimental models on RBC-EC interactions, including the static assay, (gravity sedimentation method), the human umbilical vein model, the micro-pipette technique, the rat mesentric vascular model, the parallel-plate flow chamber, and the cone- and -plate viscometer. In addition, we then review recent understanding of the molecular bases of RBC-EC adhesion, RBCs modulated alterations and the functions of ECs. Even though *in vivo* models provide the optimum approach, it is still challenging to unveil the effects of specific molecular mechanisms due to the complexity of the processes.

2.7.1 Static assay (gravity sedimentation method)

The static coincubation of washed RBCs and cultured ECs was the pioneer *in vitro* attempt to study RBC-EC interactions. The abnormally high adhesiveness of sickle RBCs to ECs from calf aortas and human umbilical veins (HUVECs) was described by both Hoover and Hebbel respectively using static assay method. They found a strong correlation between the enhanced RBC-EC adhesion and the acuteness of microvascular occlusion in sickle cell patients [180, 264]. The same method was similarly used to describe the enhanced endothelial adhesion of RBCs from patients with hereditary hydrocytosis, diabetes mellitus, chronic uremia and malaria [180, 262, 263, 267–269].

In conducting a typical experiment on static assays; washed RBCs are allowed to settle on and adhere to EC monolayers at 37° for a time duration ranging from minutes to a few hours. After the RBC-EC coincubation is completed, the RBCs that are unattached are separated by repeated washes; the RBCs that remained are calculated for obtaining the adherence of RBCs, and ECs are collected for analyzing their functional changes or altered gene expression. Static assays provide a speedy and simple method to investigate RBC-EC interactions, and have produced sufficient information on the molecular mechanisms underlying abnormal cytoadhesion (e.g., the ability of the parasite to adhere to endothelial cell receptors) and RBC-induced EC dysfunction. But static assay produces almost zero flow in the blood vessels, thus prolonged static incubation may result in RBC sedimentation. This can cause an oxygen and nutrient deprived interface between ECs and RBCs, and thus threaten the EC metabolism. In addition, the static incubation lacks the dynamic variables present in the physiological vascular environment, such as the very short contact time for adhesive bond formation [180]. Therefore, the details obtained from the method may not be reliable for predicting the consequences of RBC-EC interactions under flow conditions.

2.7.2 Human umbilical vein model

The perfusion of human umbilical veins by RBC suspensions at a regulated flow rate is a dynamic environment closer to *in vivo* criteria than the static assays. In the standard approach of this model, RBC suspensions are pumped through cannulated umbilical veins, followed by cell-free medium washing. The number of RBCs that adhere to the vessel wall can be obtained, and the EC products released into the flow can also be collected in the effluent for analysis [180]. Kucukcelebi *et al.* were the first to use this approach in studying the interactions between sickle RBCs and ECs [270], where they observed that enhanced adhesiveness of the sickle RBCs to ECs lining umbilical veins can withstand wall shear stress at the arterial level [180]. However, the inherent limitation of this approach is that the flow type and local wall shear stress are not properly regulated, because the geometry of the flow channel is only approximately known.

2.7.3 Micropipette assay

The micropipette method was initially developed by Mohandas *et al.* in order to determine a quantitative measure of sickle cell adhesiveness to ECs cultured on micro-carrier beads [180, 271, 272]. This technique involves the removal of a single RBC adherent from the EC surface: the strength of the adhesion can be obtained and the characteristic of adhesive contact can be analysed on a cell-by-cell basis.

In summary, a small suction with the aid of micropipette is used to aspirate a single RBC and bring it closer to the EC surface. Then, the RBC is gently pushed against the EC from the pipette by zeroing the suction pressure, and the pipette is removed: the RBC either sticks to the EC or is repelled away from the EC surface. The adhesive strength between the adherent RBC and EC is therefore deduced from the re-aspiration of RBC into the micropipette at increasing pressures followed by the removal of the pipette until the RBC is pulled away from the EC [180].

This method reveals that the interaction between sickle RBCs and bovine aortic ECs (BAECs) is stronger than that between normal RBCs and BAECs. The quantitative result of the adhesion strength for the detachment of these cells in the direction normal to the EC surface is 2.19 ± 1.36 e^{-10} dyn and 3.08 ± 1.14 e^{-10} dyn, obtained for normal and sickle RBCs to BAECs respectively [180, 271]. This same technique was later used by Nash and colleagues to measure the strength of adhesion between malaria-infected RBCs and HUVECs, and it was found to lie within the range of 10^{-5} dyn in the direction normal to the EC surface.

2.7.4 *Ex vivo* mesentric vascular model

The approach of this model is similar to that of the *in vivo* vascular architecture, as well as that of the shear force encountered as a result of the blood flow. The RBC perfusion was investigated in an isolated, acutely denervated, and artificially perfused rat mesocecum vasculature using the methods of Baez and colleagues [180, 273] as modified for RBC infusion [180, 274]. The perfusion fluid, which is driven by a peristaltic pump constantly perfuses the isolated tissue; arterial perfusion pressure (P_{A}), venous outflow pressure (P_{v}), and the venous outflow rate (F_{v}) are observed throughout the experiment. After observing the measurements of (P_{A}) and (F_{v}), the variations in each of them was also recorded when a bolus of RBC suspension is supplied through an injection to the site of arterial cannulation [180]. However, it was found that at constant (P_{v}) the peripheral resistance units (PRUs) and pressure-flow recovery time (T_{pf}) are the two common hydrodynamic parameters indicating changes after delivery of the sample. The arteriovenous pressure difference divided by (F_{v}) per gram of tissue weight is defined as the PRU, whereas (T_{pf}) is the time taken for (P_{A}) and (F_{v}) to return to their baseline after sample delivery.

The adhesion of malarial infected RBCs to ECs was investigated by Raventous-Suarez and colleagues via this method, showing that the adhesion is limited to venules in the malarial state [180, 275].

2.7.5 Parallel-plate flow chamber

The parallel-plate flow chamber (which is comprised of a silicon gasket, polycarbonate base, glass slide or a tissue culture dish where the ECs are cultured) is an excellent approach for studying RBC-EC interactions, by simulating the fluid mechanical properties inside the vasculature. In this approach, a syringe pump is used to perfuse an RBC suspension through the chamber over ECs. By assuming Newtonian fluid behaviour, the momentum balance equation (shown in equation 2.6) was used to obtain the wall shear stress (τ_w) on the cell monolayer,

$$\tau_w = \frac{6\mu Q}{wh^2}, \tag{2.6}$$

where the volumetric flow rate is Q, the viscosity of perfusing fluid (RBC suspensions) is μ, and h is the flow channel height with width w [180].

This technique was used for characterizing the enhanced endothelial adhesion of RBCs from malaria patients [269, 276]. A simplified version of the parallel-plate flow chamber in which ECs can also be cultured inside a micro-slide, and a syringe pump is used to perfuse an RBC suspension, is known as a micro-slide; this was introduced by Cooke and colleagues. It utilizes a flat, open-ended glass microcapillary tube of rectangular cross-section of 0.03 cm $\times$ 0.3 cm [180, 277]. The adhesive behaviours of malarial infected RBCs have been exhaustively studied by using the micro-slide method.

2.8 Early methods of blood flow measurement

The technique of blood flow measurement came into being around the mid 19^{th} century in an attempt to measure the rate of arterial blood flow for comparison with Poiseuille's equation [278]. These techniques were used in estimating the volumetric flow rates of blood in the head, limbs, kidneys and abdominal viscera of average size laboratory animals; cannulation of the blood vessel and the resis-

tance offered to the actual blood flow were considered to be disadvantages [278]. Thus the literature [279] contains detailed modifications performed on these direct flowmeters. Another method used to estimate blood flow was through the process of collecting venous blood into a graduated cylinder over a known period, and this was automated in its successive modifications [280]. Measurement of flow rates lower than 2 ml/min using a drop recorders was also introduced [278]. The use of a photoelectric method and the establishment of a closed circulatory system for the measurement of blood were used to overcome the disadvantages of drop recorders like blood loss and the reaction that occurs at the electrodes.

In another attempt, a measure of flow velocity was obtained by estimating the time taken by a bubble to move a known distance along a glass tube having the same diameter as the bubble through which blood is enabled to flow [278, 281]. Characteristics of the bubble flowmeters include their simplicity, reliability, and low resistance together with disadvantages like the need for anticoagulants and cannulation [278, 281]. Measurements of blood flow based on the electric conductivity of blood using permanent/DC magnets have been performed [282], but had some disadvantages such as difficulty in the choice of potentials and electrode polarization interference. Alternatively, AC magnets were used with various excitation waveform shapes e.g., sinusoidal, square, trapezoidal etc. although they all have their pros and cons as well the disadvantage of the transformer effect at the electrodes [283].

As another possible substitute, thermal convection was introduced to to blood flow studies, based on the use of thermal sensors such as thermistors and thermocouples [142, 278, 284]. The technique behind this method is solely based on the phenomenon of thermal convection (where a hot object placed in a colder flowing medium gets cooled) and the rate of cooling is proportional to the rate of flow in the medium. Thus the blood flow is estimated from the electrical energy required to maintain the constant temperature of the sensor inserted into the stream [278].

Direct plethysmography techniques have been used in observing the volumetric

changes in blood flow, by confining the interested part of the body to a constant pressure chamber and observing the changes in volume occurring in the chamber due to changes in blood flow. The capacitance plethysmograph uses the variations in capacitance of the transducer due to the volumetric changes in blood flow; and the small changes in electrical resistance of the interested body segment can be measured with the aid of an impedance plethysmograph [285].

2.9 Recent blood flow measurement techniques

The limitations of the conventional methods highlighted above have led to more developed techniques for blood flow measurement. They include Doppler ultrasound techniques, magnetic resonance imaging, positron emission tomography and laser based techniques used for flow measurement such as laser speckle and laser Doppler.

2.9.1 Ultrasound technique

Ultrasound waves have a frequency of at least 20 kHz. They have led to major accomplishments in various fields of medicine such as imaging and flow measurements. The propagation of ultrasound waves in the tissue is the phenomenon which this technique employs in measuring blood flow.

2.9.2 Doppler Ultrasound

Doppler ultrasound is a non-invasive method of measuring blood flow. It is based on the frequency shift that occurs in the reflection of sound from a moving source. Ultrasound of a specific frequency is transmitted into a blood vessel as described in Figure 2.9. The reflected sound (from the blood vessel) is observed and thus gives a measure of blood flow velocity. The Doppler frequency shift due to flow (movement) of blood is described by equation 2.7.

$$V_{\mathrm{D}} = \frac{c f_{\mathrm{D}}}{2 f_0 \cos\theta}, \tag{2.7}$$

where the velocity of sound in test tissue is denoted by $c = 1540$ m/s, V_{D} is the velocity of blood flow and f_0 is the irradiated ultrasound frequency. The Doppler shift frequency of the received sound signal is denoted by f_{D} and θ is the angle at which the transducer is placed relative to the blood vessel [278, 285]. The form of the transmitted sound signal could be as a continuous wave (CW) or pulse wave (PW).

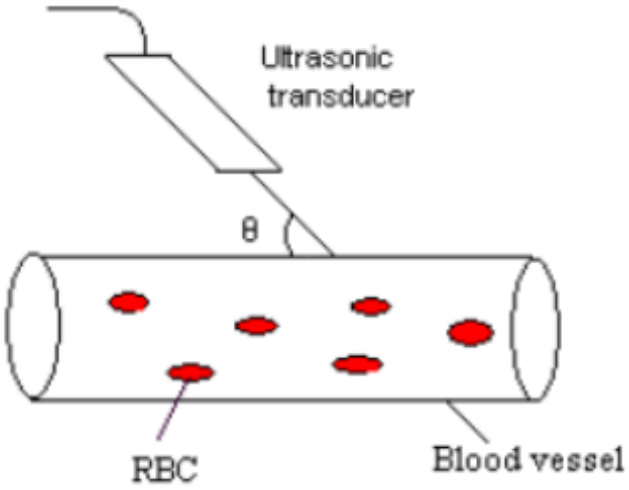

Figure 2.9: An illustration of the Doppler ultrasound method, extracted with permission from [278].

Continuous wave Doppler ultrasonic flow meter

Doppler signals are generated from all moving obstacles in the path of the ultrasound beam during its propagation. A number of studies were performed using the method. An example of such studies is the investigation of changes in the velocity of blood flow in the carotid artery during various stages of physical exercise based on ultrasound by use of a 2 MHz CW Doppler ultrasonic probe and a Doppler discriminator circuit [286]. Figure 2.10 presents a schematic of the measurement. The Doppler signal and the 2MHz fundamental frequency were observed synchronously in the Doppler signal discriminator. Low-frequency and harmonic

noise are removed in order to take out the Doppler signal and digitized with the aid of an analog/digital converter interfaced to the computer. Equation 2.10 is used in estimating the velocity of blood flow.

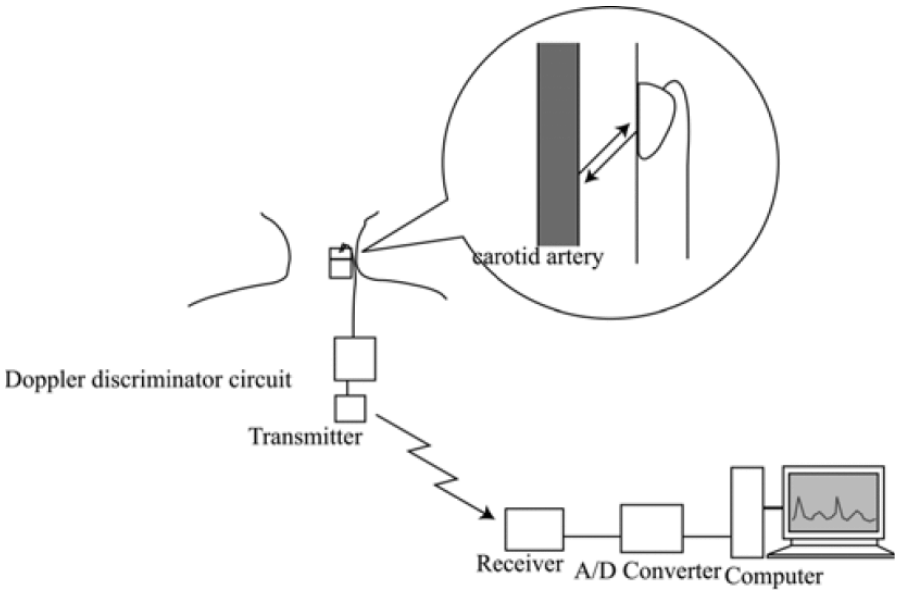

Figure 2.10: Doppler ultrasound method, extracted from [278].

Analysis of the dynamics and distribution of blood in human subjects during exercise was studied [287], by changing the postures of exercise to supine, seating, standing, and by carrying out analysis on the generated power spectra; flow velocity was measured in carotid, brachial and femoral arteries. Blood flow measurements during physical exercise also yielded important results for the monitoring and early detection of cardiovascular diseases [286].

Ultrasound for measuring perfusion

The velocities of flows in major blood vessels can be estimated using ultrasound techniques. However, the measurement of flow in capillaries, otherwise known as perfusion or tissue blood flow, seems challenging because separation of the reflected spectrum from the noise spectrum becomes difficult due to the reduced flow velocity. In an attempt to address this limitation, low blood velocity within microcirculation in the thumb of a subject was studied with the use of a CW Doppler ultrasound device utilizing a frequency of 8.1 MHz [288]. The ultrasound

probe with and without the target (to give the noise spectrum) was used to take the measurements and the results were compared with the measurements obtained from the disk phantom rotating at low velocity. Note that the disk phantom is useful for investigating low frequency Doppler, such that the tangential velocity of the disk within the ultrasound beam is used determine the Doppler velocity. Noise spikes at low frequencies (below 20 Hz) were observed in the spectrum resulting from the tremor in the operator's hand, in the case of the free probe [278, 288].

Although, CW Doppler ultra-sound is a good technique, one of its limitations is that the device cannot fathom target positions along the direction of sound wave through the tissue. It also cannot distinguish Doppler shifted signals that arise from various points along the transmitted ultrasound beam.

Pulsed wave Doppler ultrasound technique

The technique of pulsed wave (PW) Doppler is based on a transducer that alternates the transmission and reception of ultrasound to and from human tissue. In this approach, the ultrasound pulse is transmitted into the tissue travels for a certain period time until it is reflected back by a moving red blood cell. It then returns to the transducer over the same time interval but at a shifted frequency (Doppler shift); thus the blood flow velocity can then be estimated by measuring the Doppler shift in frequency and using equation 2.7.

Blood flow velocity in the superior mesenteric artery (SMA) in 25 healthy newborn infants was measured using the transcutaneous pulsed Doppler ultrasound technique to study the response of intestinal blood flow due to feeding [289]. A fast Fourier transform was used to analyze the Doppler flow signal and the peak blood velocity (V_{p}), the pulsatility index (PI) and the mean velocity (V_{m}) were estimated. An increase in V_{p} and V_{m} with a corresponding decrease in the PI was observed before and after feeding. This pulsed-wave ultra-sound technique is rapidly becoming a common clinical procedure in non-invasive neonatal diagnosis.

2.9.3 Role of optics in measuring blood flow

A number of Doppler ultrasound techniques have been discussed in the foregoing section. While ultrasound methods of measuring blood flow are non-invasive, they are incapable of measuring blood flow in the microvasculature. Table 2.3 compares the various techniques used to measure skin blood flow.

Optical techniques used for monitoring the blood flow are based on frequency shift lasers (Doppler effect) which have the ability to measure the microcirculation flux of the tissue, fast changes of perfusion during provocations and temporal statistics of time-varying laser speckle. They are referred to as laser Doppler and laser speckle methods respectively.

Table 2.3: A summary of various approaches suggested for measuring skin microvascular blood flow

Technique	Non-invasive?	Measured quantity	Principle	Disadvantages
Radioactive microsphere technique [290]	No	Mean blood flow	Radioactive microsphere are injected into the blood stream; recovered isotope count from the tissue is used to estimate the mean blood flow	No real time measurement possible
^{133}Xe wash out technique [291]	No	Absolute blood flow	^{133}Xe is injected subdermally and the rate of clearance is a measure of blood flow	Point measurement. Does not measure all capillaries. No information provided about regional flow.

Table 2.3 – continued from previous page

Technique	Non-invasive?	Measured quantity	Principle	Disadvantages
Capillary microscope [125]	Yes	Blood velocity and capillary distribution	Distance covered by the erythrocytes in the successive frames gives a measure of blood velocity	Capillary perpendicular to the skin surface cannot be visualized
Thermography [292]	Yes	Temperature map on skin	Skin temperature radiation is imaged and its associated with the blood flow	No direct relationship between blood flow and skin temperature
Doppler ultrasound [293]	Yes	Spatially resolved velocity	It is based on Doppler shift imparted by moving cells to the probing sound waves	Resolution insufficient for smallest vessels; sensitive to only one component
Speckle techniques [294, 295]	Yes	De-correlation time and speckle contrast, related to blood flow	No spectral information; quantitative measurement is impossible	Speckles generated by back scattered photons from the tissue analyzed in spatial and temporal domain to estimate blood flow

Table 2.3 – continued from previous page

Technique	Non-invasive?	Measured quantity	Principle	Disadvantages
Laser Doppler flowmetry [296]	Yes	Relative concentration and velocity of moving red blood cells	It is based on the Doppler shift imparted by the moving red blood cells to the probing light	No absolute measurement
Doppler Optical Coherence Tomography [297]	Yes	Spatially resolved velocity of moving red blood cells	Combination of Doppler velocimetry with low-coherence optical interferometry	Limited probing depth 1-2mm

2.9.4 Laser speckle contrast imaging

It is believed that the laser speckle technique offers more advantages than the laser Doppler technique. These include the fact that it is a real time, non-scanning whole field method with higher resolution. Figure 2.11 describes the experimental set-up [278]. In this approach, the light from the laser source is shone on the object of interest. The illuminated area is imaged with a CCD (Charge coupled device) camera and a frame grabber captures and digitizes the speckle pattern, it is then processed and displayed on the PC monitor [278]. A speckle pattern is described as the random intensity distribution pattern formed as a result of the fairly coherent light reflected from a rough surface (or propagated through a medium) with a random refractive index fluctuations. This laser speckle pattern can only be explained statistically [298]. However, both the coherence of the incident light and the detailed properties of the random surface or medium determines the statistical

properties of the speckle patterns.

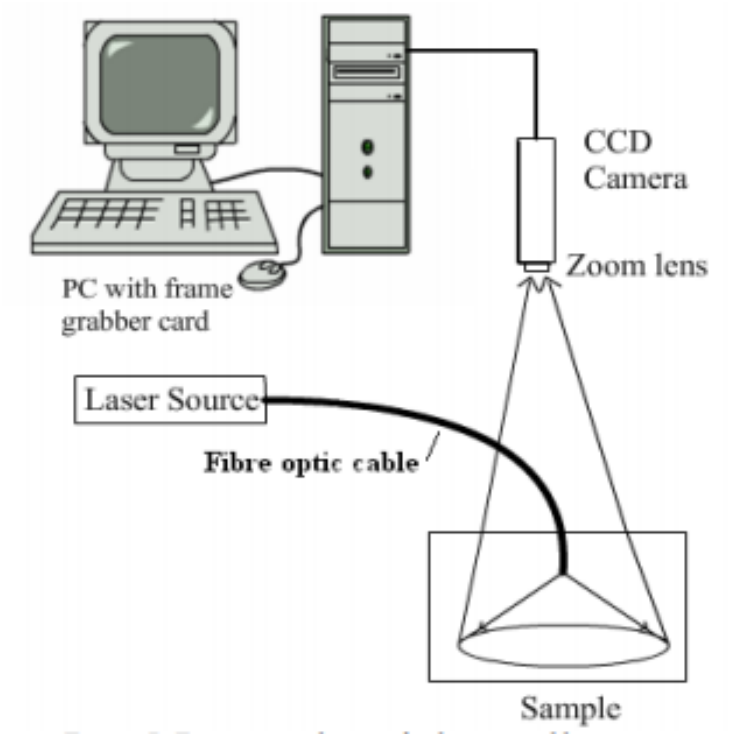

Figure 2.11: Experimental setup for laser speckle imaging, extracted from [278].

Moreover, the intensity of the speckle can only be explained by statistics because of its non-deterministic nature [294, 295, 299]. In practice, the standard deviation of the speckle pattern is less than the mean intensity, therefore leading to a corresponding reduction in the contrast of the speckle pattern which is presented as,

$$K_{\mathrm{s}} = \frac{\sigma_{\mathrm{s}}}{< I >}, \tag{2.8}$$

where K_{s} is the speckle contrast, σ_{s} is the standard deviation of the spatial intensity variations in the speckle pattern and $< I >$ is the spatial average of the intensity fluctuations. Therefore, the speckle contrast is defined to be unity for a fully developed speckle pattern and can be less than unity for a partially developed speckle pattern. In the literature [298, 299], the variance of the spatial fluctuations is related to the time average of the auto-covariance, $C_{\tau}(\tau)$ of the intensity

of fluctuations described as

$$\sigma_s{}^2(T) = \frac{1}{T}\int_0^T C_\tau(\tau)d\tau. \tag{2.9}$$

However, due to the convoluted nature of the capillary network it was assumed that it has no multiple scattering, a Lorentzian velocity distribution and a perfect speckle formation; hence equation 2.10 describes the speckle contrast, where τ_c is the correlation time of the intensity fluctuations (i.e the time taken for the intensity to fall to $1/e$ the original value) and T is the exposure time,

$$K_s = \sqrt{\frac{\tau_c}{2T}\left(1 - \exp\left(\frac{-2T}{\tau_c}\right)\right)} \tag{2.10}$$

$$v_c = \frac{\lambda}{2\pi\tau_c} \tag{2.11}$$

$$F = v_c \times A. \tag{2.12}$$

By knowing the area of illumination and thus relating the blood flow in the vessel to the velocity, the blood flow can be estimated using equation 2.12, where F is the blood flow, v_c is the mean flow and A is the cross-sectional area of the blood vessel.

2.9.5 Laser Doppler Flowmetry

The Doppler effect in which there is a shift in frequency of the light that is scattered by moving red blood cells and the light scattered back from laser irradiated skin provides information on the blood flow in the skin. The blood flow in the skin can be inferred and evaluated from the Doppler frequency. In this working technique, a fibre optic cable is used to deliver the light from a laser source to the skin surface and the back-scattered light is collected from the skin using the same or second fibre optic cable and returned to detector. As the incident laser beam becomes normal to the velocity of flow, then equation (2.13) gives the Doppler shifted frequency (f), where v is the velocity of flow, λ is the wavelength of the laser beam and the

angle between the incident and scattered beam is θ [300]. The velocity of flow can be estimated once the Doppler shift frequency is measured.

$$f = \frac{v \sin \theta}{\lambda}. \tag{2.13}$$

Laser Doppler velocimeter was first used to measure the blood velocity in retinal arteries of albino rabbits, in which the magnitude of the Doppler shifted frequency was measured by optical heterodyne using a photo multiplier tube and the velocities of blood were in the range of 1.1 to 1.8 cm/sec [300]. Moreover the advantages of laser Doppler technique compared to the methods laser speckle imaging includes being a non-invasive and simple-to-apply technique, which provides continuous or nearly-continuous records but it arguable believed to suffers from the disadvantages of limited laser penetration depth [301].

2.10 Summary

Biophysical models of blood flow in the microvasculature remain daunting, due to the challenges faced with the true representation of some physiological activities such as the rhythmic variation of a small vessel's wall over time. However, by characterizing the oscillatory processes that manifest in the skin microvascular blood flow, one can efficiently examine and gain useful insight into microvascular dynamics in both pathological and healthy states. One example of such a pathological state is malaria, which is envisioned to alter the dynamical properties of blood flow due to various simultaneous influences: the stiffness of the red blood cell membrane, its propensity to stick to the inner linings of all the blood vessels, the increased stiffness and change in surface properties that makes the infected cells to pass less easily through the capillaries, and the subsequent effect of all these factors on the microvasculature, i.e. in the capillary network resulting in changes in the viscosity, flow properties, and oxygenation of blood and high vascular resistance due to hostile condition.

3. Measurements, non-linear dynamics and time series analysis methods

This Chapter present the methodologies used for measuring and analysing the physiological signals that are discussed in Chapters 4, 5, 6 and 7. The rational for choosing the methodologies discussed here (particularly for the analysis) is highlighted in Chapter 8.

3.1 Experimental protocol

Before measurements are taken, in order to ensure that the subject has fulfilled the appropriate inclusion criteria of the study, the researcher will go through the consent form, patient information sheet, participant details sheet, answer any questions and then obtain the written informed consent.

3.1.1 Measurement setup

A series of probes were attached to the subject (in all the studies presented in the thesis, except stated otherwise) as follows:

- LDF(Moor Instruments Ltd) sensors. These are small sensors that measure the blood flow. They are attached on the left and right wrists, or left and right ankles, depending the study.

- ECG sensors. One sensor on each shoulder and a sensor on the lowest left rib. These measure the electrical activity of the heart. The position of the sensors were the same in all the studies presented in the thesis.

- VMS-NIRS sensor. The channel was placed on the forearm . It measures the deep tissue oxygenation. This was used only in the work presented in Chapter 5.

- VMS–OXY sensors. One channel was placed on the right forearm. The sensor measures superficial tissue oxygenation. This was also used in the work presented in Chapter 5.

- Respiration belt. A Velcro belt was fastened loosely around the chest, to mechanically measure the breathing rate.

- Temperature sensors at the left ankle and left wrist. These measures the temperature of the skin at the point where blood is measured.

- Arterial oxygen saturation was meaured using a small sensor attached to the left ear. This was only used in Chapter 6

Before the measurements begin volunteers were asked to abstain from food, coffee, and alcohol for 3 hours prior to the experimental measurements. Recordings occurred in the morning and evening with subjects lying in the room (Faraday cage for experiments done in Lancaster and in a quiet room for experiments conducted in Nigeria) with a stable room temperature. Measurements presented in Chapters 4, 5, 6 and 7 were made in a temperature controlled room of 23.0-23.5^{o}C. In all the experiments, subjects were acclimatized and relaxed for a period of about 20 minutes prior to the measurements A photograph of the measurement setup is shown in Figure 3.1. The blood pressure of the subjects was recorded before starting the measurement – measured with a Digital Automatic Blood Pressure Monitor (Omron, M10-IT), by wrapping a cuff on the subjects' upper right arm.

Subjects were requested to refrain from leaning forward, moving or talking and were ensured to be in a correct posture during the blood pressure measurements.

The above protocol was used for all the experimental studies discussed in this thesis, although the sample size for each experiment differs. The inclusion and exclusion criteria in some cases also differ.

Figure 3.1: Illustration of measurement setup. Typical illustration of an experimental session, with the subject lying down in a supine position and a set of cardiovascular signals being simultaneously measured.

3.1.2 Sampling frequency used for measurements

The skin blood flow was simultaneously measured at two or more different sites of the body (depending on the study's measurement setup) at a sampling frequency of 40 Hz. All the blood flow recordings analysed in this thesis were sampled at

40 Hz. The ECG, respiration, and skin temperature were recorded at a sampling frequency of 12000 Hz, but were later downsampled to 40 Hz. The measurement setup for respiration and ECG recordings was the same for all experiments. The oxygenation recordings were sampled at 40 Hz.

These cardiovascular signals/time series were pre-processed and recorded simultaneously (with voltage output digitized with a 16-bit A/D converter) using a signal conditioning system (Cardiosignals, Institute Jožef Stefan, Slovenia). All recordings discussed in this thesis lasted for 30 minutes with the volunteers lying relaxed in a supine state, except in the pilot study where the recordings were done whilst the subjects were sitting.

3.1.3 Recruitment of subjects

Generally, the subjects considered for the studies in Chapters 4 5 and 7 were all healthy and recruited within Lancaster University Campus and Lancaster City, by distribution of information sheets. They were monitored at Lancaster University in a purpose built lab in the physics building. Subjects were ensured to be healthy, as assessed using the participant details sheet.

The general exclusion criteria for the subject includes any form of concomitant diseases predisposing them to alterations of endothelium-dependent vasomotion, such as diabetes mellitus, coronary or peripheral artery disease, hypercholesterolemia, immunological disorders, malaria, history of cardiovascular disease, other illness such as; blood disorders e.g. anaemia and atherosclerosis, deep vein thrombosis, hypertension, epilepsy, fainting, blackouts and dizziness or vertigo.

3.2 Cardiovascular signals

The scaling laws, observations and measurements of dynamical processes within living system to be considered in this section are essential in the general understanding of the human cardiovascular system. The approach is continually be-

coming realistic following the emergence of various new real time techniques for continuously monitoring spontaneous dynamics in living systems based on different physical principles ranging from optical to electrical. Therefore, the study of a living system in healthy state and its transition to pathological state on the basis of measurements can reveal useful information about human, as well as other living systems.

3.2.1 Electrocardiogram

One of the vital biological oscillators that is of great significance in the body is the heart. The electrical events within the heart can be non-invasively evaluated over time, primarily with an electrocardiogram (ECG). An ECG monitors the changes in the electrical activities of the heart as the heart beats. In a healthy resting state, the heart rate varies between 60 to 90 beats per minute, although it generally lower in healthy athletes, due to an increment in the volume of blood propelled out of the heart. However, any resting heart rate out of these ranges signifies an essential medical condition.

Analogically, the action potentials of cardiac muscle cells can be considered as batteries that allow free flow of charge/current across the body fluids. The flow of these currents occur as a result of the action potentials emerging simultaneously in most of the myocardial cells. The depolarisation and repolarisation of myocardial cells leads to the contraction and relaxation of cardiac muscle. These electrical changes can be discerned noninvasively by recording via electrodes placed on the shoulders and rib at the skin surface to produce ECG. A typical ECG tracing of a normal heartbeat period -– cardiac cycle is shown in Figure 3.2. The major characteristic components of the ECG are the P wave, the QRS complex and the T wave.

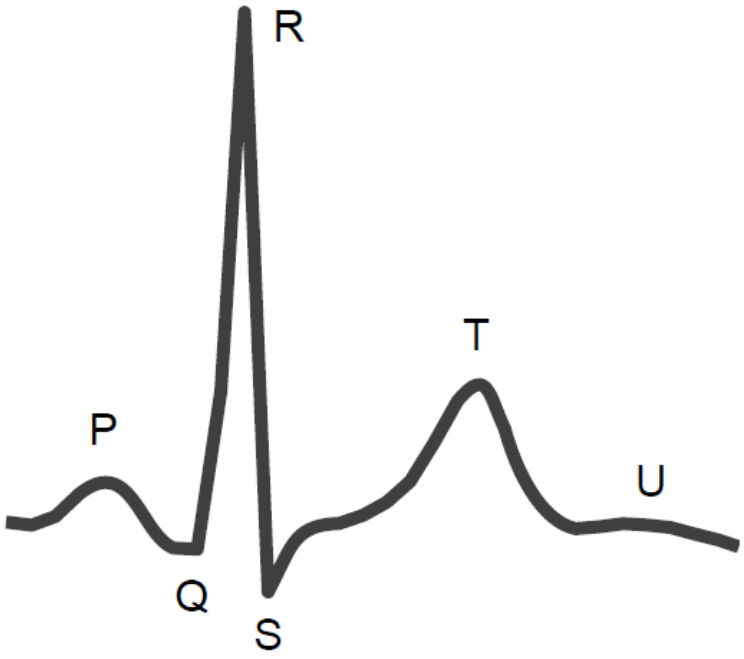

Figure 3.2: Typical one-cycle ECG trace.

The P wave is produced during atrial depolarisation and it extends from right to the left atrium, with the initial segment and the terminal portion of the wave reflecting right atrial depolarization and left atrial depolarization, respectively. After the atria, the electrical forces produced as a result of ventricular depolarization are represented by QRS complex, consisting of Q, R and S waves. The amplitude of the QRS complex is higher than that of the P wave due to the greater amount of muscle present in the ventricles compared to the atria. The Q wave is associated with septal depolarization and it appear after the P wave. The R wave reflects early ventricular polarization and is believed to appropriate for estimating the heart rate and heart rate variability, because the wave is often the easiest to detect. The S wave reflects the late ventricular depolarization while the ventricular repolarization (the recovery of the ventricles) which the last event of the cycle is represented by the T wave [302]. Willem Einthoven in 19th century attributed these letters to the deflections in ECG. Although, the shape of these waves can be dissimilar and can even disappear in some situations. To date the characteristics of these waves including their position and the relationship between one

another are used in examining the heart and in conducting early diagnosis various cardiovascular abnormalities.

3.2.2 Heart rate variability/Instantaneous heart frequency

From an ECG signal the instantaneous heart rate (IHR) or heart rate variability (HRV) can be determined by a number of methods. The most common approach is performed in the time domain. In these methods, the locations of the R-peaks are marked with each interval between successive RR peaks considered as a complete period of oscillation with phase interval of 0 and 2π. The reciprocal of distance between each RR-peaks is gives the IHR. The RR-peaks are mostly used in evaluating the IHR given that R-peaks are more notable component during heart beat, and are manifested in every cycle. One major drawback of this method is the dependency of the resolution on period of oscillation – meaning that information on instantaneous frequency and phase are accessible between every cycle. This method requires a linear interpolation of the signal, because depending on the period of oscillation it is expected that the sampling frequency of the HRV signal will differ. In order to preserve the same resolution as contained in the original signals, the instantaneous frequency has to be extracted by transforming the ECG signal into time-frequency domain using wavelet analysis alongside the ridge extraction methods, as in nonlinear decomposition (NMD) [303], a technique that decomposes signal into set of components, or modes. Using NMD, the instantaneous frequency of the heart beat can extracted from the wavelet transform of the ECG, thus yielding the IHR. Similarly, the IHR can also derived from the LDF signal using the same technique. Note that in the literature [304, 305] IHR is mostly referred to as HRV or, occasionally, as instantaneous heart frequency (IHF).

These time-frequency domain analyses have helped in providing additional insight on autonomic background of RR interval oscillations in the heart rate measure. The confirmation of HRV as a robust marker for prognosis after acute myocardial infarction in the late 1980s illuminated its clinical significance [306]. The

pattern of the heart rate depends on spontaneous respiratory cycle, which makes the heart rate change slightly during inspiration and expiration. This change is referred as respiratory sinus arrhythmia (RSA) [307]. The manifestation of RSA is a strong indicator that the heart meets-up with the demands of the body continuously. Although heart rate is used as a measure for overall health, for example a high resting heart rate or tachycardia ($>$ 100 breath per minutes) is usually a sign of heart complication while a low resting heart rate is usually attributed with exercise/sports, however the heart rate variability is more informative as it is widely regarded as a quantitative marker of autonomic activity. A number of studies have reported the effect of HRV in several pathological states, particularly in hypertension, atherosclerosis and diabetic neuropathy where HRV is seen to be significantly decreased.

3.2.3 Respiration

Respiration can be measured by analysing the carbon dioxide levels, but it is commonly measured mechanically via direct measurement of the chest movement. Using the marked event or NMD methods explained above, one can extract the respiratory rate.

In this study, respiration was measured using a respiratory belt sensor including a Velcro belt and a TSD201 conductance transducer (BIOPAC Systems Inc, Goleta, California, USA). The belt may be fastened loosely around the chest of the subjects, whilst the changes in thoracic circumference is measured by the transducer, thus yielding respiratory signal. The signal may be amplified and sampled via a 22-bit A/D convertor using the signal conditioning unit.

3.3 Acquisition of microvascular skin blood flow

3.3.1 Laser Doppler flowmetry - moorVMS-LDF2

The human skin and it its optical properties discussed earlier in the previous chapter has provided primary understanding about cutaneous tissue and potentials of the skin as a surrogate organ suitable for the study of microcirculatory processes.

LDF provides a continuous measurement of microcirculation in the skin, thus reflecting perfusion in capillaries, arterioles, venules and dermal vascular plexus. The LDF (moorLAB, Moor Instruments Ltd., UK) used in this work transmits a near infrared laser light (which must be monochromatic) from temperature stabilized laser diodes operating at a wavelength of 780 nm and with a maximum power of 2.5 mW into the skin through an MP1-V2 probe (Moor Instruments Ltd., UK), which has two optical fibres. A flexible probe holder (PH1-V2, Moor Instruments Ltd., UK) is then attached to the skin surface where the measurement would be made using double-sided adhesive discs.

LDF is a simple and non-invasive technique which has been used to study microvascular blood flow, providing useful clinical informations on the oscillations that manifest in blood flow dynamics [17]. One useful achievement aided by LDF is the discovery of six fundermental oscillatory processes in the spectra of LDF signals [17].

Doppler shift and light interaction with tissue

One of the LDF's fibres deliver light to the site under observation. The light passing through the skin and reaching the microvasculature is back-scattered by moving red blood cells, frequency-shifted due to the Doppler effect - depending on the scattering angle, the wavelength, and the velocity vector of the cell [308], it is then returned to the instrument via a second optical fibre as shown in Figure 3.3. For example, if a photon with frequency ω is back-scattered by a particle moving with a velocity $\boldsymbol{v}$ (see Figure 3.4), then the Doppler shift is given as

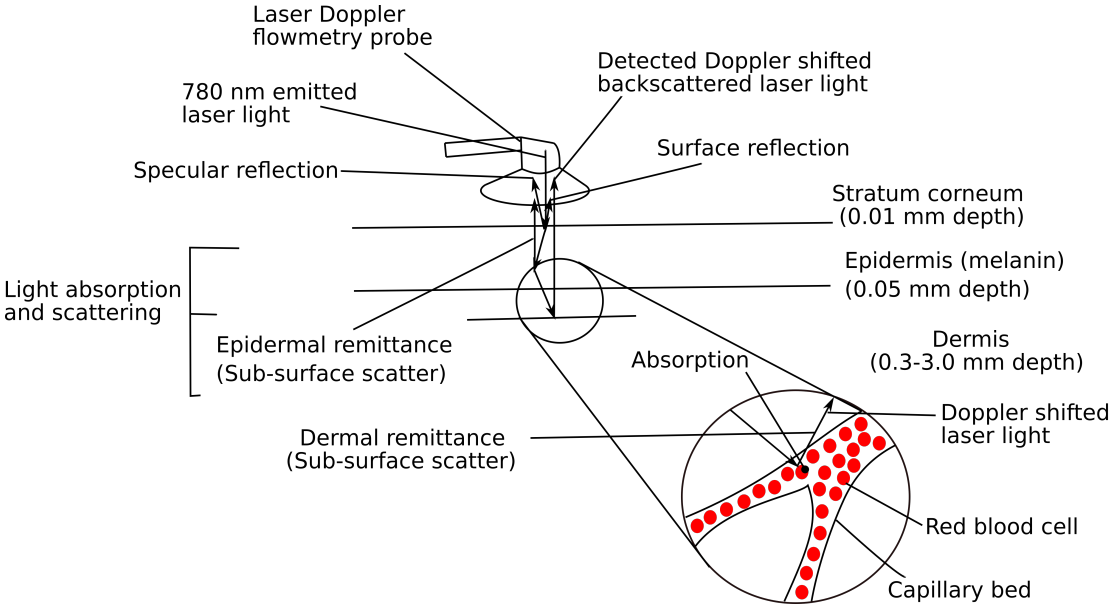

Figure 3.3: Schematic of the light-skin interaction. When laser light is delivered to the skin, there are three main contributions to the reflected light: specular reflection (which makes insignificant effect), back-scattering at the skin surface (i.e. the stratum corneum), and back-scattering from the epidermis and dermis levels. Scattering from moving erythrocytes (red blood cells) in the dermis results in a Doppler shift in the frequency of the light returned to the laser Doppler probe detector. This spectral broadening can then be related to the average velocity and hence flux of the blood flow.

$$\begin{aligned} \Delta\omega &= \vec{v}.(\vec{k}_I - \vec{k}_s) \\ \Delta\omega &= |\vec{v}||\vec{k}_I - \vec{k}_s| \cos\beta. \end{aligned} \tag{3.1}$$

If $\boldsymbol{k}_I$ is the propagation vector of the incident photon and $\boldsymbol{k}_s$ is the propagation vector of the scattered photon, then β which is the angular frequency shift between the velocity vector and scattering vector is written as:

$$\begin{aligned} \beta &= \cos^{-1}\left(\frac{\Delta\omega}{|\vec{v}||\vec{k}_I - \vec{k}_s|}\right) \\ \beta &= \cos^{-1}\left(\frac{\vec{v}.(\vec{k}_I - \vec{k}_s)}{|\vec{v}||\vec{k}_I - \vec{k}_s|}\right). \end{aligned} \tag{3.2}$$

If we consider the wavelength of the light as λ, and α as the angle between $\boldsymbol{v}$ and the plane of scattering, the Doppler shift then becomes [308]

$$\Delta\omega = 2(2\pi/\lambda)|v|\sin(\alpha/2)\cos\beta. \tag{3.3}$$

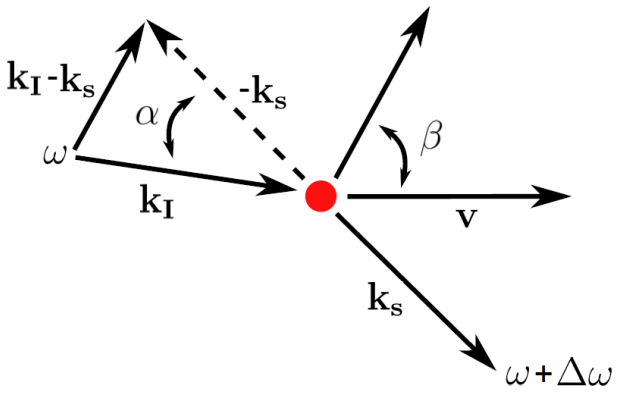

Figure 3.4: Optics of photon and RBC interactions. An illustration of a photon with propagation vector $\boldsymbol{k}_I$ scattered by a red blood cell moving with velocity $\boldsymbol{v}$, and after being scattered the photon's new propagation vector is $\boldsymbol{k}_s$.

According to the Doppler principle, the light reflected from moving red blood cells is shifted in frequency by an amount related to the blood flow in the illuminated volume of tissue – the frequency shift is proportional to red cell velocity while the frequency of light reflected from stationary cells and tissue remains unchanged [117]. The difference between incident light and the Doppler-shifted back-scattered light gives the LDF signal, known as the blood perfusion signal.

The incoming photon is Doppler shifted several times as it passes through various blood vessels and moving red cells within the microvasculature, and then interferes with the non-Doppler shifted light to form a dynamic speckle interference pattern on the photodetector. This interference makes the current signal of the detector fluctuate. Details about the flux and concentration of red blood cells are contained in the spectral power of these fluctuations [308], as the spectral power is linearly proportional to the flux and concentration of red blood cells. The flux (i.e blood flow) is proportional to the product of the average speed of the moving red blood cells and their concentration. The LDF output is semi-quantitative [117] and is expressed in perfusion units (PU) of output voltage (typically 100 PU = 5 V) or just arbitrary units (AU).

A prominent feature of the LDF recording is its inability to provide absolute perfusion values. This is because for tissue at rest, other particles excluding red blood cells are actually in motion (not static) during LDF operation, since the ther-

mal motion of scattering bodies usually contribute to the LDF signal. Therefore LDF actually provide perfusion reading and cannot be zero even during occlusion when flow of blood is completely blocked. On this basis, it is necessary to calibrate the LDF device in a specific calibration liquid so as to allow an appropriate comparison of data.

3.3.2 Skin temperature

Skin temperature can measured using two high sensitivity, low heat capacity thermistors – YSI 709B Thermilinear sensors (YSI Inc., Yellow Springs, OH, USA) of 8.5 mm diameter taped on the skin. The thermistors (T1 and T2) can be positioned outside the left and right ankles, over the lateral malleolus.

3.4 Blood oxygenation

Tissue oxygenation

The oxygenation level in tissue is determined by a balance between between oxygen delivery and oxygen utilization. Oxygen saturation is not a direct reflection of tissue oxygenation, as several physiological factors such as tissue pH and temperature influence the affinity of oxygen for hemoglobin, which determines the adequacy of oxygen supply to the tissues. Here, the oxygen saturation was measured by two different optical methods: near-infrared spectroscopy (NIRS) and white light spectroscopy, using moorVMS-OXY (Moor Instruments Ltd, UK) and moorVMS-NIRS (Moor Instruments Ltd, UK) instruments respectively.

moorVMS-NIRS - near infrared spectroscopy The dual-channel NIRS module was used to measure oxygenation (oxygen saturation) in deeper tissue, using the spatially resolved spectroscopy method [309, 310]. The instrument records oxygenation using two probes on the forearm. One of these comprises a detector head with two identical photodiodes, and the other probe has an emitter with two

near infrared LEDs emitting light in the wavelength range $\sim$750-850 nm. With very low loss, the light is delivered to the probe via an optical fibre and thence into the tissue. A probe holder setting a 30 mm separation between the detector and emitter is attached to the skin and fixed in place with a bandage.

Although much of the light from the emitter head is scattered and absorbed, a small portion of it penetrates through the tissue to reach the photodiodes. The two identical photodiodes present in the detector head are 0.5 cm apart. Based on the orientation of the photodetectors, the oxygen-dependent absorption characteristics exhibited by tissue chromophores (hemoglobin) in the region under investigation is obtained by evaluating the relationship between the light attenuation and tissue chromophore concentration using the modified Beer-Lambert law [309], i.e. assuming the linearity of attenuation with chromophore concentration. Thus the dynamical change in hemoglobin concentration can be found. The modified Beer-Lambert Law, is often generally expressed as

$$A(\lambda) = \epsilon(\lambda) \cdot c \cdot I(\lambda, c) + G(\lambda), \tag{3.4}$$

where the attenuation is denoted by A, ϵ as the molar extinction coefficients of the chromophores(oxygenated and deoxygenated hemoglobin), c is the molar concentrations of the chromophores, I is the mean path length and G is scattering loss. The attenuation A can be expressed as

$$A(\lambda) = -\log_{10}\left(\frac{I(\lambda)}{I_0(\lambda)}\right), \tag{3.5}$$

where the incident and reflected lights are represented as I_0 and I respectively.

The Beer-Lambert law essentially compares the properties of the medium (tissue) through which the incident light propagates and gets absorbed. The spacing between the emitter and detector leads to the change in attenuation with respect to emitter to detector distance. However, the orientation of the photodetectors then allows the variation in the attenuation to be measured [57].

The attenuation coefficient of tissue is obtained by computing the spatial variation of the retro-reflected light intensity as a function of distance between the light emitted at high source to detector spacings [311]. Using the known optical characteristics of hemoglobin, known probe geometry, and postulates about typical tissue scattering characteristics, the absolute concentrations of oxyHb and deoxyHb can then be calculated. The backscattered light collected through the photodiode is received at the detector and amplified. The recordings were captured at a sampling rate of 40 Hz using the manufacturer's software (MoorSoft). Data were exported to Matlab (R2016b, Mathworks, UK) for pre-processing and analysis. The output tissue oxygenation (SO_2) is expressed in % of output voltage (typically, 100% = 1 V). Mathematically, SO_2 is defined as

$$SO_2 = \frac{\text{oxyHb}}{\text{totalHb}}, \tag{3.6}$$

where total haemoglobin (totalHb) = oxygenated hemoglobin (oxyHb) + deoxygenated hemoglobin (deoxyHb) are in arbitrary units (AU).

moorVMS-OXY - white light spectroscopy The single-channel continuous tissue oxygenation monitor (Moor Instruments Ltd, UK) was used for recording skin oxygenation on the left forearm, based on white light reflectance spectroscopy. The Moor CP7-1000 blunt needle probe is placed in contact with the skin. It consists of a photodiode that generates white light over the wavelength range 400-700 nm with a maximum optical output power of 6 mW. With the probe placed inside a holder, the holder was bandaged to the skin to hold it in position.

Bright white light from an LED is delivered to the probe through an optical fibre. While propagating through the tissue, the incident light interacts with erythrocytes. Some of it is scattered, while a fraction of it is absorbed by the red blood cells, depending on the wavelength and on their Hb oxygenation status. The reflected light is collected by a another optical fibre in the same probe. In addition, the light backscattered by moving red blood cells is analysed by the

moorVMS-OXY system within the wavelength interval of 500-650 nm. The system then computes tissue oxygenation by comparing the collected spectra with the absorption curves from known concentrations of melanin, oxyHb and deoxyHb which are obtained using the equation

$$\mu(\lambda) = \sum \epsilon_i(\lambda) \cdot c_i, \tag{3.7}$$

where ϵ is a matrix from literature and index i signifies each chromophore [312].

The temperature on the oxygen saturation is acquired via a thermistor mounted in the probe tip. Using the manufacturer's MoorSoft software, the signals were captured at a sampling frequency of 40 Hz. The obtained oxyHb and deoxyHb parameters are expressed in arbitrary units (AU), temperature in degrees (typically, 1 V = 10^oC) and SO_2 (%).

3.4.1 Arterial oxygenation

The oxygen saturation level of arterial haemoglobin, is S_pO_2. It is measured using TOSCA500 (Radiometer Ltd, Copenhagen, Denmark) with its sensor attached on subject's right earlobe. The pulse oximeter sensors transmit a light from an infrared LED (typically 910 nm) onto the earlobe, and the reflected light detected by a photodiode give a measure of the arterial oxygen saturation.

3.5 Summary

Technological advancement has led to developments in the temporal resolution of existing methods for acquiring time dependent dynamics inherent to all biological signals. This in turn permits the measurement of additional biomedical data *in vivo* as never before, allowing the structure and function of the body to be examined unperturbed under normal or pathological conditions. These new developments in biomedical signal acquisition necessitate the need for the establishment of novel analysis techniques for thermodynamically open systems which are nonlinear, non-

autonomous and far from equilibrium, as in the case of living systems.

3.6 Dynamical systems and methods for analysing them

3.6.1 Introduction

To achieve a proper understanding of the underlying dynamics of living systems, such systems require different treatment from how one might investigate a mechanical system.

Signals recorded from living systems can be analysed to extract statistical properties of the data, or to investigate potential oscillatory characteristics, by quantifying the amplitude and power of oscillations and their phase characteristics. We will particularly focus on characterization of time-varying oscillatory properties, resolving the dynamics with optimal time localization and frequency resolution.

Dynamical systems are described by a law specifying the state of a process as a function of time, given starting conditions; in particular, dynamical systems are used to model physical systems subject to an interplay of forces. Any natural system we might think of is always being acted upon by one or more forces. Dynamical systems are commonly given in the form of

$$\frac{dx}{dt} = f(x), \tag{3.8}$$

meaning that at each instant in time t, the speed and direction in which the state x is changing is specified by its dependence f upon the current state $x(t)$. There are quite a number of different dynamical systems, such as the linear harmonic oscillator, Kepler's planetary system and simple pendulum, among others. But the most widely observed systems in nature are those whose dynamics are explicitly time dependent as in the case of most living systems. Such systems are referred to as nonautonomous system and can be described by nonlinear differential

equations, although nonlinearity of differential equations is a completely distinct concept from nonautonomicity. Of course, it is probably true that most living systems are described by nonlinear differential equations, especially by virtue of the existence of phase interactions among biological oscillatory processes. However, in general, a system whose dynamics is explicitly time-varying does not have to be described by nonlinear differential equations. Therefore, in this thesis, the dynamical systems considered will almost exclusively be systems described by nonlinear nonautonomous differential equations

The most vital characteristics of most dynamical systems in nature is the bounded nature of their states as t approaches infinity, and this bounded region is referred as an attractor. In the absence of this characteristic, continuous perturbations to a system would cause the system to undergo uncontrollable divergence from the original state.

3.6.2 Stochastic and Deterministic systems

External random influences on a system can lead to complex behaviour. This can be modelled by including a noise term in the set of equations describing the time-evolution of a system. The characteristics of the noise added to the system, such as its spectrum, can only be produced by external influence as they are completely different from the characteristics of the system's internal dynamics. Thus stochastic systems are open systems.

Deterministic dynamical systems are those that do not seek to incorporate any randomness when predicting the system's future state. Contrary to a stochastic system (which is a probabilistic system where the evolution of all the system's events can not be predicted with certainty), in deterministic systems as long as the initial state of the system is known at a given point in time, it possible to infer the occurrence of events without uncertainty.

3.6.3 Oscillatory systems

An oscillatory system is any dynamical system whose solutions remain bounded but do not converge to a fixed equilibrium state. An oscillatory system, being a dynamical system, could also be understood as a physical system whose oscillations are naturally brought about by the features of the system itself – arising from perturbation of the equilibrium state. From a biological standpoint, several oscillatory systems manifest in an entire human or other living system, and are constantly interacting with each other. In fact, all physiological processes taking place in a biological system have interactions with other processes in the system and are continuously exchanging matter and energy with their environment; and thus, they manifest as oscillatory. Physiological oscillatory processes occur in e.g., blood pressure, electrocardiogram (ECG) and electroencephalogram (EEG).

The properties of oscillatory systems are dependent on the activities occurring in them. Such oscillatory systems are categorized as nonlinear systems as their behaviour cannot be adequately described by a linear set of equations, but rather would require a nonlinear set of equations. It is worth noting that the principle of superposition of two or more oscillators does not hold for nonlinear systems of interacting oscillators.

3.7 Relation of living system to dynamical systems theory

Nonlinearity in living systems

An estimation of the state of any linear system is often possible when all its underlying properties are known at any particular point in time, therefore solving the system analytically is practicable. Basically, this implies that it is feasible to fathom all the properties of a linear system without necessarily monitoring its dynamics over time. On the contrary, such approach cannot be used to analyse

nonlinear system such as the living systems. While it is nevertheless possible to calculate some of their features analytically, it almost impossible to understand the trajectory of a real nonlinear system without either monitoring its dynamics over or time or simulating it. It is worth mentioning that this challenge is not related to the complexity of the system - as a linear system can be extremely complex while a nonlinear system can very simple, nonetheless these underlying principles still hold when analysing either of them.

The consequences of nonlinearity can be somewhat overwhelming. It does not only lead to mathematical challenges, but also gives rise to some occurrences such as hysteresis. This simply describes the situation where the system's trajectory from one point to another is different from the trajectory it follows in the reverse direction between the same two states - and this is why the direction of time is critical in analysing nonlinear systems. Harmonics also arise from the nonlinearities in nonlinear systems in their response to oscillatory inputs. These harmonics are modes that can be extracted from nonlinear oscillations using linear-based analysis techniques.

Openness of living systems

The nonlinearities discussed in the foregoing can actually be viewed as manifestations of a distinctive attribute of living systems: due to the fact that are thermodynamically open and exchange energy and matter with their environment. It is mostly presumed in major theories of dynamical systems that the system are closed, that is to say it is autonomous and fully described by its state. On the contrary, living systems are strictly open and non autonomous meaning that both their state and time can used to describe their dynamics. Therefore, the introduction of time-dependent variables is inevitable when analysing the dynamics of living systems.

There is a possibility of having time-variability in the statistical properties of closed system and in such cases the systems' dynamics are considered as nonsta-

tionary. By assuming a chaotic behaviour, the complex nonstationary dynamics in closed systems can easily be modelled on the premise that a small perturbation in the system's trajectory grows exponentially over time [313]. In the event that the complex dynamics are not in conformity with a chaotic pattern, they are then modelled by stochastic systems - where the complexity is brought about simply by the influence of some external randomness such as noise. Interestingly, either of these approaches are still suitable for the concept of autonomous systems hence the main reason why time-dependent variable are commonly omitted in the analysis. But, because living systems are strictly nonstationary and non-autonomous, none of these methods are applicable [314].

3.8 Discerning dynamical systems: Inverse approach

Using the framework of nonautonomous systems, one can discern far-reaching dynamical properties in living systems. The challenges accompanied with this approach have resulted in a number of futile efforts towards developing alternative approaches that would be based on autonomicity. Moreover, the use of phase space analysis is traditionally the first approach been sought in the case of deterministic systems - the method is simply to reconstruct the attractor in phase space. While this method is feasible for autonomous systems, it merely takes into account time dependent attractors [315]. The dilemma here is that, an inclusion of time-dependence into the system would in turn lead to additional dimension in the phase space, thus bringing into the system additional complexity.

The use of an inverse approach can be applicable when interested in discerning dynamical systems, and can be achieved in two manners: modelling the system with a set of differential equations or by directly measuring/observing the system over time. The first approach provides an ideal framework for time series analysis, in such a way that all the parameters of the system can be put into a specific

state due to the first-hand knowledge of the exact state of the system at any point in time. In the latter approach an exact definition of the system's phase is very challenging as its trajectory can only be described on one-dimension. However, both techniques are applicable in the inverse approach to dynamical systems.

In this thesis, time series from measured systems were studied.

3.8.1 General characteristics of time series

Time series are sequences of data points that are generated experimentally or numerically in a continuous order. Time series enable us to extract information about the dynamical behaviour of a system. In this thesis the time series were mostly generated experimentally. Observing dynamics in a time series is one of the most efficient ways to fathom complex systems such as the living systems and could pave the way for the development of *invivo* mathematical models.

In order to extract information about any system experimentally, repeated measurements must be made. First, the time series of a system could be obtained by controlling the conditions of the system whilst measuring the response after a time lag. Secondly, it could be achieved by taking an arbitrary set of initials conditions whilst making N consecutive measurements over a time step Δt to generate the time series in which the dynamical behaviour of the system is revealed [314].

Frequency interval

Time series have two important properties which are the time interval L = NΔt over which the system is sampled and the sampling frequency f_s =$1/\Delta t$, the rate at which sample are taken. The Nyquist - Shannon sampling frequency is the maximum observable frequency which is equal to half the sampling frequency $f_s/2$ - moreover, the lowest observable frequency is given by $1/L$. But both L and f_s must be infinitely large in order to obtain a continuous frequency distribution that extends between 0 and ∞, although this cannot be met by the discrete and finite

time series generated numerically and from real world measurements [314, 316]. Consequently, the analyses of the experimentally generated time series in this thesis were premised on the basisf that the physiological processes that are sampled contain negligible energy at frequencies above half the sampling frequency (the Nyquist frequency).

Uncertainty relationships

Time and frequency are two interdependent features in any signal. A typical effect of this interdependency is the impossibility of localising a non-zero function and its frequency spectrum as in the case of Fourier transform. Specifically as in

$$\Delta x \Delta s \geq \frac{1}{4\pi}, \tag{3.9}$$

where Δx is the standard deviation associated to the density function $|x|^2$ and the standard deviation associated to its Fourier transform conjugate s is Δs. The inequality has been proven in the book of Bracewell [317].

3.9 Time series analysis in time domain

3.9.1 Preprocessing

When analysing time series, preprocessing of data in time domain is required. This is important because the challenges mostly faced when analysing time series in the frequency domain are substantially reduced.

Detrending

Time series, especially those experimentally generated via measurements on living systems are accompanied with artefacts. These artefacts usually result from movements, or some noise related to the equipment used for an experiment. The features of these artefacts distort the statistical properties of the recorded time se-

ries over the entire interval under investigation, and such a phenomenon is referred as a trend.

The removal of trend that is believed to distort or obscure the features of interest from the time series is termed "detrending". The removal of a trend can be done in a number of ways, either through statistical or mathematical operation, and is preferably done in the time domain. Filtering, a frequency domain method which involves the direct removal of data via the subtraction of the Fourier components over a certain frequency interval, leads to losing information and is also not efficient when considering non-stationary time series. The advantage of time domain smoothing over filtering is that the former preserves information which is likely to be lost in the latter. Information in time series that is time dependent can be preserved by smoothing, since it operates in the time domain, hence making it applicable on nonstationary time series.

While non-complicated trends that are linear in nature can be detrended by subtracting a least-squares-fit straight line, which is also known as moving polynomial. Complicated trends that are non linear are mostly removed by smoothing approach.

3.9.2 Instantaneous frequency and phase extraction

The term instantaneous frequency is arguably viewed as an inappropriate designation as it implies a universal definition for the frequency of an oscillation at every point in time. In reality, the number of cycles within a period of time is referred to as frequency, therefore knowing an oscillatory frequency at an arbitrary point in a cycle should not be feasible. However, by assuming that certain features are maintained in every cycle, these changes in oscillation can be used to establish a model definition of frequency. For example, if the rate at which the frequency changes is slow compared to the real dynamics of the phase, then the system can be regarded as a sinusoidal oscillation whose phase is defined as $\phi = \omega t + \theta$. Assuming the phase can be defined for every cycle, then the instantaneous angular

frequency can be estimated by taking the time derivate of the phase as,

$$\omega = \frac{d\phi}{dt}, \tag{3.10}$$

Two of the ways that instantaneous frequency can be calculated are using marked events or using the Hilbert transform.

Marked events

The approach of marked events computes the frequency or phase of an oscillation based on the number of events per unit time. The method has the merit of being simple. In the case of a time series whose oscillations occur continuously, it is possible for the event to be any location between 0 and 2π within the phase of one cycle. For the method to accurately detect peaks, an event must be present in each cycle and at the same time its location in the phase is not altered. Therefore, the reciprocal of the period between successive events in various cycles gives the instantaneous frequency.

An illustration of the marked event method on ECG is discussed, with Figure 3.5 showing the R peaks sampled from an ECG signal. The marked event can be considered as the R peak, while the times of successive R peaks can be written as t_k and t_{k+1}. The average instantaneous heart frequency (heart rate) can then be defined as the reciprocal of the times between successive R peaks, expressed as,

$$f(t_k) = \frac{1}{t_{k+1} - t_k}, \tag{3.11}$$

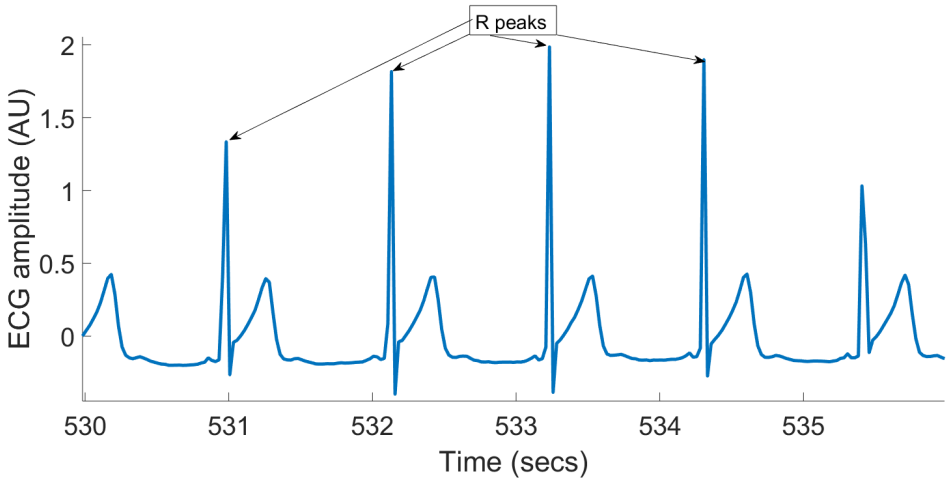

Figure 3.5: The marked events method applied on a sample in an ECG signal.

This method can only detect a frequency once in each successive period. This makes the distance between each event to be considered being equal to a phase change of 2π. The marked events approach is accompanied with some significant effects, which are outlined below.

i The time resolution of marked events information only corresponds to the period of the oscillation.

ii Only when time is fixed that the instantaneous phase can be obtained, as the phase interval of each marked event is within $0 \leq \Phi < 2\pi$.

iii The method selects an event arbitrarily, hence care should be taken when selecting an event particularly in nonsymmetric oscillations. For example in the case of the ECG, despite the R peaks been distinctly sharp and clear cut, a different marker could be marked or chosen. In the situation where different event was chosen and with the period between the two selected markers varying, then it can likely give conflicting results.

iv Defining the exact time of an event is challenging in high frequency oscillations and in the presence of noise. However, frequency variations are better tracked in oscillations that contain rapidly-varying spikes because they provide good time resolution.

v In this method, the time resolution could vary over time as the resolution is equal to frequency, thus could vary over time.

vi The method does not preserve any information about the amplitude.

Analytical signals and Hilbert transform

Complex-valued signals with no negative frequency components are termed analytic signals. Transforming a complex analytic signal to a real signal requires eliminating the imaginary part. David Hilbert, in the quest to solve differential equations in the complex plane, developed the Hilbert transform [318]. The approach has since been used in time series analysis methods for the conversion of real signals into complex ones referred as analytic signals. For a time series $f(t)$, its Hilbert transform is given by,

$$H(t) = \frac{1}{\pi} \int_{-\infty}^{\infty} \frac{f(t)}{u - t} du. \tag{3.12}$$

The Hilbert transform is analogous to the convolution of $f(t)$ with $\frac{1}{\pi t}$. The integral function denotes the Cauchy principal value and is non-integrable because as $u - t \to \infty$ the integrand approaches infinity.

A common way to interpret the Hilbert transform is by considering its relationship with the Fourier transform, given as

$$F[f(t) + H(t)i](\omega) = \begin{cases} 2F[f(t)](\omega) & \text{for } \omega > 0 \\ F[f(t)] & \text{for } \omega = 0 \\ 0 & \text{for } \omega < 0 \end{cases} \tag{3.13}$$

where the negative frequency components present in the Fourier transform are taken away by the $H(t)$ and balanced by multiplying the amplitude of the positive frequency components by two. It is important to note that the removal of the negative frequency components of the Fourier transform does not in any way diminish any information about the time series as they are simply a reflection of

the other corresponding component of the Fourier transform.

While the Hilbert transform is very useful in detecting the phase of a single oscillation, it is not applicable for time series that contain more than one oscillation. This makes the method unsuitable for real physiological time series. However, the limitations of both the marked events and Hilbert transform approaches can be resolved using the time-frequency representations. This is becasue representation of signal in time-frequency domain allows the extraction of both the instantaneous frequency and phase from time series that contains multiple oscillatory modes, with a good resolution.

3.9.3 Time series analysis in frequency domain

Fourier transform

Plotting a frequency spectrum is one of the common way of visualizing how the oscillations and fluctuations in time series are distributed over different timescales. A Fourier series enables the representation of time series data in the frequency domain. It represents a periodic function f(t) in terms of infinite series of sines and cosines.

$$f(t) = a_0 + \sum_{n=1}^{\infty}[a_n \cos(\omega t) + b_n \sin(\omega t)], \tag{3.14}$$

where ω is the angular frequency and a_0, $a\omega$ and $a\omega$ are the Fourier coefficients which will take values depending on the shape of the function. The largest coefficient corresponds to components in the time series that have stationary frequency. However, data recorded from biological system are based on discrete sampling, so the discrete Fourier transform is defined as

$$F(\omega) = \sum_{n=0}^{N-1} f(n) \exp \frac{-2\pi i \omega n}{N}. \tag{3.15}$$

This equation (3.15) can be used to transform a time series from the time domain to the frequency domain, or from a time t dependence to frequency dependence

ω. But ω is an integer within the range $0 \leq \omega \leq N_1$, or alternatively within the range $-N/2 \leq \omega < N/2$. Note here that the integer input ω is not an actual frequency, just as the integer inputs n of f are not actual times, but simply the sample number. A version of the discrete Fourier transform involving actual times and frequencies is presented in equation 3.16, since this is ultimately what is of interest in practice. In this case, a suitable formula would be

$$F(n/L) = \Delta t \sum_{m=0}^{N-1} f(m\Delta t) \exp\left(\frac{-2\pi imn}{N}\right), \tag{3.16}$$

with n being an integer in the range

$$-N/2 \leq n < N/2.$$

Here, Δt is the time between consecutive samples, N is the total number of samples, and $L = N\Delta t$ is the time-duration of the signal.

Fourier transforms become unreliable when investigating events that occur when a time series contains frequencies that lie out of the lowest observable frequency range (i.e. $1/5\ L$ as used in practice). Because at low range of the spectrum $< 1/L$, the components no longer appear periodic, rather looking like a trend. Even within the observable frequency range, difficulties still arise when using the Fourier method because the Fourier transform cannot account for temporal changes of oscillatory behaviour in time series, so it may misrepresent oscillations, since it will force frequency-modulated or amplitude-modulated signals to be expressed as a time-independent linear combination of fixed-frequency sinusoids.

Therefore, while most of the amplitudes of oscillations below the frequency limit will appear at $\omega = 0$ in the Fourier transform, the rest are spread across higher frequencies. Figure 3.6 illustrates the comparison between the (discrete) Fourier transforms of a deterministic signal with wide frequency-modulation and a stationary $1/f$ noise signal. This describes how tedious it is to distinguish between deterministic oscillations in the numerically generated signal and the pure noise

signal [314]. Note that the algorithm that computes the discrete Fourier transform (according to the version presented earlier in equation 3.16) of a time series is known as a fast Fourier transform (FFT).

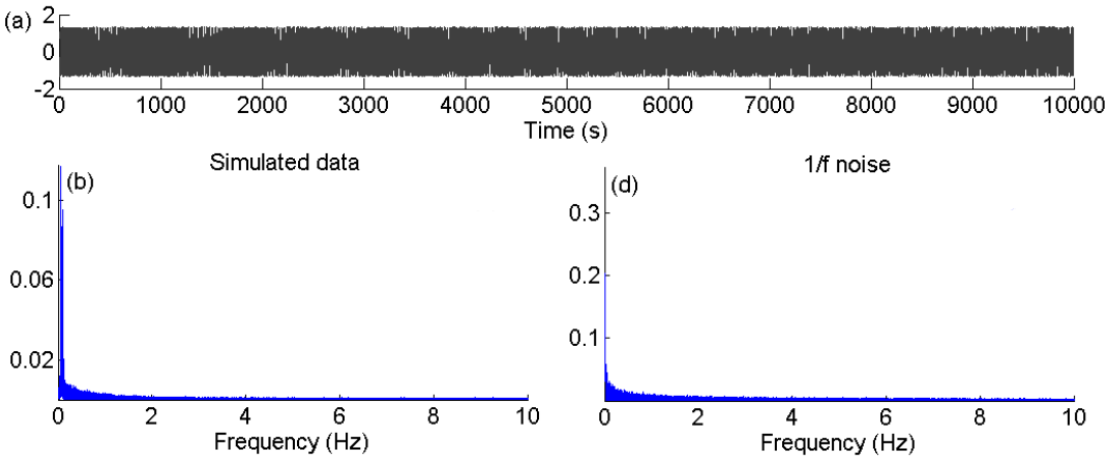

Figure 3.6: Fourier transforms of simulated low frequency oscillations and $1/f$ noise. (a) Simulated time series with varying frequency between 0.001 and 0.01 Hz. (b) FFT of the time series in (a). (d) FFT of $1/f$ noise. Extracted from [319].

Furthermore, since the transform is based around detecting sinusoidal components in a time series, the amplitude of periodic components of other shapes is divided into modes that are spread across the frequency domain as shown in Figures 3.7. Similarly, measuring the amplitude of an oscillation by using the Fourier transform is not straightforward, as can be seen by comparing the height of the primary 1 Hz component in Figure 3.7 (d) and (f). Figure 3.8 also further describes the shortcomings of the Fourier transform. Hence, this is specifically a challenge to non linear dynamical systems whose nonlinear terms often result in non-sinusoidal oscillations.

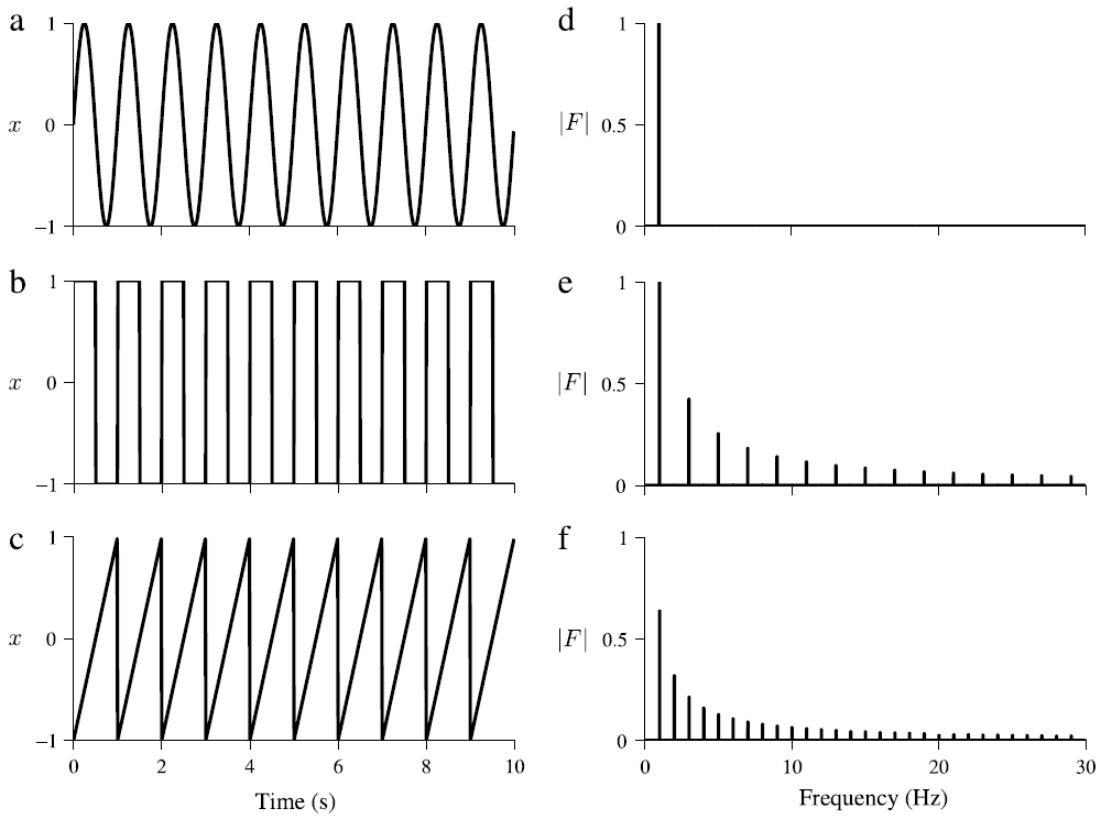

Figure 3.7: Time series of three differently shaped periodic functions: (a) A sine wave; (c) A square wave; (e) A sawtooth wave; and the respective amplitudes of the one-sided Fourier transforms (b), (d) and (f). In all cases a sampling frequency of 1000 Hz was used.

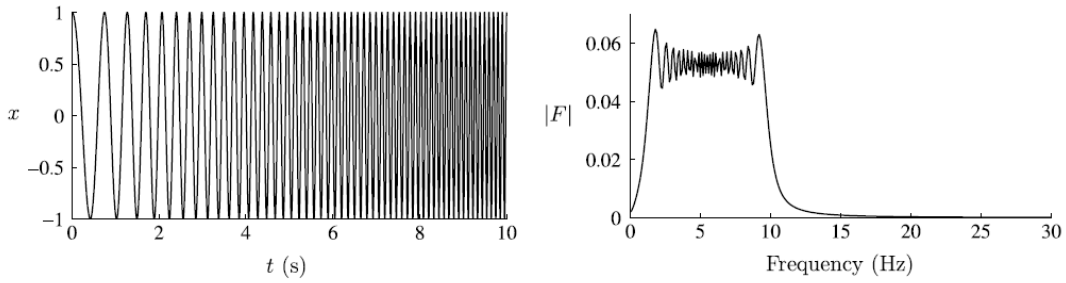

Figure 3.8: A chirp signal ranging from 1 to 10 Hz generated over 10 s with a sampling frequency of 1000 Hz as seen in the time domain and its Fourier transform representation.

3.9.4 Time-frequency based analysis

Windowed Fourier transform/Short time Fourier transform (STFT)

The short time Fourier transform also called the windowed Fourier transform (WFT) was developed as a solution to the limitations of the Fourier transform when dealing with nonstationary time series. It works in such a way that it divides the time series into windows and then calculates the FFT of each window as it slides across the signal. This gives the frequency representation of the time series at each point in time. In addition to the frequency spectrum, the complex coefficients of the STFT also give information about the phase of the components. The STFT $G_x(\omega, t)$ of a signal $x(t)$ defined on the time-interval $[-L/2, L/2]$, is defined mathematically as:

$$G_x(\omega, t) = \int_{-L/2}^{L/2} g(u-t)x(u)e^{\frac{-2\pi i\omega u}{l}}du, \tag{3.17}$$

where $g(u)$ is rectangular function of the length l which is zero outside the interval -$l/2 \leq$ u $\leq l/2$. Time is t and the variable ω is directly related to the frequency f_ω by $f_\omega = \frac{\omega}{l\Delta t}$. [314]

Unfortunately, while addressing the FFT's inability to transform nonstationary signal, the STFT also creates the problem of optimal time localization and frequency resolution, meaning that a larger convolution function provides poorer time localisation but a much clearer cut-off frequency due to a higher resolution in frequency. This has many similarities to the Heisenberg uncertainty principle of quantum mechanics. Therefore in STFT, as presented in Figure 3.9, a chosen small window gives more information about changes in time (better time localisation) whereas a large window gives more information about changes in frequency (better frequency resolution) [314].

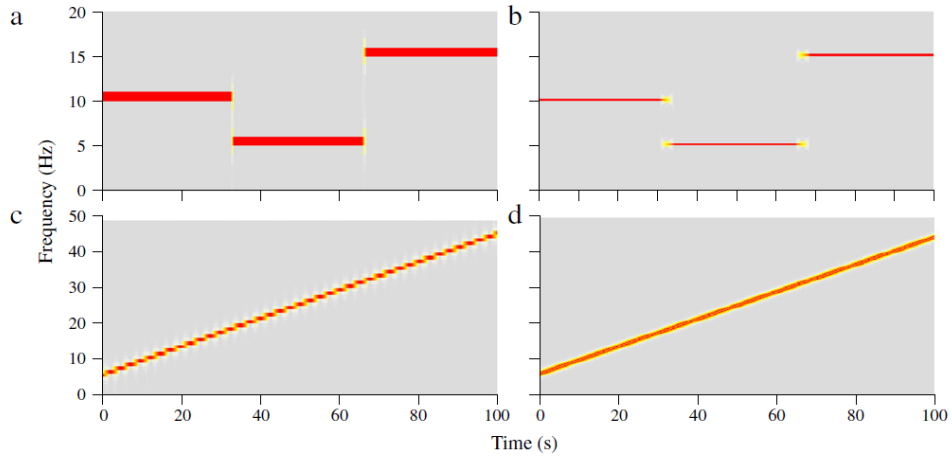

Figure 3.9: Short-time Fourier transforms of time series with varying time and frequency resolutions. (a) and (b) are of a time series containing a sine wave with a frequency which starts at 10 Hz, then jumps to 5 Hz and finally rises to 15 Hz. (c) and (d) are of a time series containing a chirp signal which increases linearly in frequency from 5 to 45 Hz over 100 s. On the left hand side a short window of size $l = 1$ s has been used, giving good time resolution but poor frequency resolution. On the right hand side a larger window of size $l = 4$ s has been used, giving better frequency resolution but poorer time resolution (as indicated by gaps between the frequency jumps in (b)). In all cases a sampling frequency of 1000 Hz was used.

Continuous wavelet transform

A way to resolve the time-frequency resolution problem of the short time Fourier transform discussed in the previous section is to move away from the Fourier basis to a new basis of wavelets, and this is called a wavelet transform. The wavelet is developed to provide optimal time frequency resolution with the aid of adaptive window which simultaneously produces good time localisation and frequency resolution. In contrast to the STFT, the WT has logarithmic frequency resolution and it is obtained by moving a wavelet function along the all locations of the signal. A full range of the wavelet scales is used at each location, and can be tuned depending on the frequency ranges we want to investigate [314, 319]. The advantage of continuous wavelet transform over STFT is demonstrated in Figures 3.9 and 3.10. The continuous wavelet transform (CWT) of a time series denoted

$x(t)$ is defined as:

$$W_x(s,t) = \int_{-L/2}^{L/2} = \Psi(s, u-t)x(u)du, \tag{3.18}$$

$$\Psi(s,t) = |s|^{-p}\psi(t/s),$$

where ψ is the mother wavelet which is scaled according to the parameter s (a scaling factor) to change its frequency distribution, and p is a somewhat arbitrary number for which different conventions exist commonly given as $p = 1/2$; the time-shifting is then written manually as $u - t$ in the formula for the CWT, with t being the temporal position on the signal. Because the frequency scale is continuous this implies that the $W_x(s,t)$ can be calculated for any arbitrary frequency by using a new wavelet and window size to calculate each scale, with a small wavelet/window for high frequencies and larger ones for low frequencies. Hence producing a good time - frequency resolution. The CWT is entirely different from the discrete wavelet transform (DWT) in such that the basis of the mother wavelet is not necessarily orthogonal, meaning that wavelets have overlapping frequency bands and the components in $W_x(s,t)$ contains redundant information.

An example of this difference is described by taking the DWT of a sine wave whose details contain completely independent phases, while the phase of the CWT remain the same for all frequencies as shown in Figure 3.10. This shows that CWT could be used to detect relationship between oscillations and identify the harmonics caused by non-linearity.

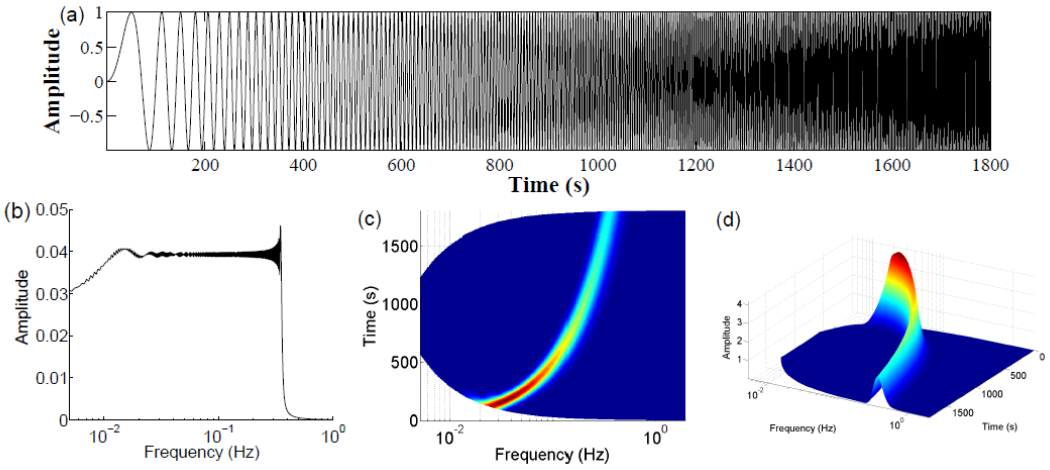

Figure 3.10: Frequency representation of Nonlinear chirp signal (quadratic). (a) Nonlinear chirp signal (quadratic) $\sin(2\pi \times 0{:}0001\ time^2)$ has a frequency which increases with time. (b) The Fourier transform is unable to usefully represent the signal in (a) in the frequency domain, due to the time variability. The continuous wavelet transform in (c) and the 3D version in (d) show how the frequency changes with time using a 3D map showing time and frequency information simultaneously.

It is important to note that in this thesis, the complex Morlet wavelet defined as:

$$\psi(u) = \frac{1}{\sqrt{\pi}}\left(e^{-i\omega_0 u} - e^{-{\omega_0}^2/2}\right)e^{-u^2/2}, \tag{3.19}$$

was chosen because it is Gaussian modulated and also provides optimal joint time–localization and frequency–resolution. Note $\omega_0 = 2\pi f s$, where s is scaling factor and f is the frequency.

3.9.5 Decomposing nonlinearity

An understanding of complex systems such as living systems is mostly achieved through analysis of the signals that they generate. These signals normally contain various superimposed oscillations, bringing about complicated wave forms, and such oscillations are commonly characterized by nonlinear time-varying frequencies and amplitudes. Such oscillations, are sometime called modes, and they carry a significant amount of information about the system that generates them. The

properties of these modes can be used in evaluating health status from signals produced by the human system [15]. But, one needs to first of all properly extract the modes from the signal inorder to get hold of the features of individual non-linear modes. To achieve a good analysis, then, the signal in question has to be decomposed, as this allows the retrieval of each oscillations present in the signal, distinguishing them from one another and from the background noise.

Empirical mode decomposition

Empirical mode decomposition (EMD) is one of the famous methods used to decompose signals. The premise for this method is that all the data points present in the time series are wrapped by an upper and a lower envelope (Figure 3.11). The trends present in the signal are therefore identified using the midpoint of the two envelopes. The subtraction of these trends from the original time series gives a series of Intrinsic Mode Functions (IMFs) - with each of them reflecting an oscillatory mode of the time series. This simply means that an interpolation of each points enclosed in the upper and lower envelopes, (i.e the local maxima and local minima respectively) allow the extraction of components present in the time series.

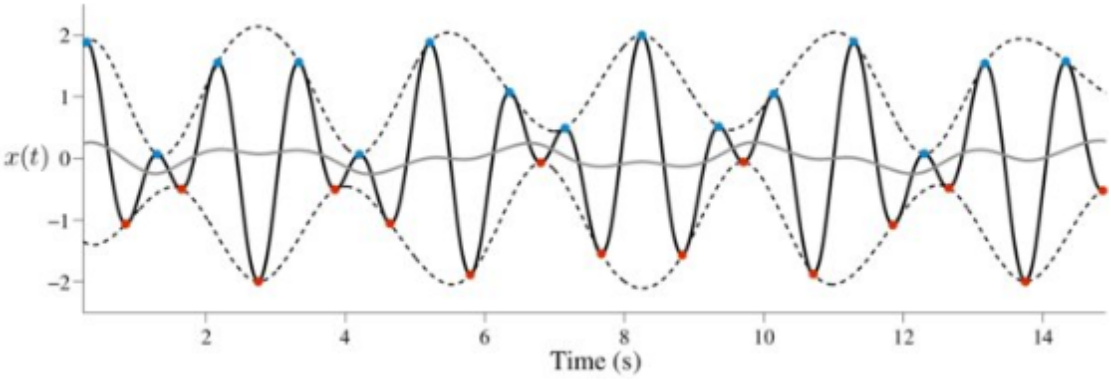

Figure 3.11: An illustration of sifting processes as implemented on quasi-periodic function $x(t) = \sin(2\pi t) + \sin(4\pi t)$ (solid black curve). Initially, the peak (blue dots) and troughs (red dots) are marked across the whole time series. Interpolating between these points using cubic spline gives the upper and lower margins (dotted lines). By averaging the upper and lower envelopes, we then obtain the trend (grey line). Reproduced from [314].

The EMD [320] simply creates each envelop by marking the points (i.e., peaks

and troughs) wherever the time series's data changes direction. These two sets of points are then interpolated using a cubic spline [321]. Accordingly, the trend present in the time series is determined by estimating the peak-peak amplitude of the highest time series component by taking the mean of these two margins. After subtracting the trend from the time series, the highest component of the signal is then left behind (Figure 3.11). This process is repeated in order to remove any other trends remaining until the criteria below (equation 3.20) is satisfied. This processes is known as sifting.

$$N_p + N_t - N_z = 0 \text{ or } \pm 1, \tag{3.20}$$

where the number of peaks, troughs and non zero-crossings are denoted by N_p, N_t and N_z respectively. The extracted component is subtracted from the time series as soon as this criterion is satisfied and the process is repeated for the sake of extracting the subsequent highest-frequency component.

While the EMD has an advantage of effective utilization of data, however it has some major drawbacks. One of the problems with EMD arises from the interpolation repeatedly used in estimating the amplitude of the highest frequency component. Furthermore, the sifting method is not suitable for nonstationary time series, because it leads to a problem of mode mixing – which makes the amplitude of the oscillatory mode approach 0. In such situations, the peak and troughs of the next highest frequency component are introduced, meaning that the next mode substitutes the one that is already extracted. However, this further introduces error particularly when the changes in amplitude is large, thus making the decomposition very difficult.

Wu and Huang [322] proposed a technique called ensemble empirical mode decomposition (EEMD), which not only addresses the problem of EMD with mode mixing but also reduce its sensitivity to noise. In this method, the EMD procedure is repeated on the same time series having introduced an independent realizations of white Gaussian noise to the time series and taking the average of the result.

Even so, the continually repeated interpolation in the EMD is still prone to error propagation, making the error encountered whilst extracting high frequency components influence the component extracted from low frequency.

Nonlinear mode decomposition

A substitute to EMD is decomposing the time series using time-frequency analysis [303]. Particularly, the nonlinear mode present in a time series can be extracted by transforming the signal into time-frequency domain [323–326], e.g., the wavelet transform which decomposes it into distinct mode, and then detect all possible harmonics that accompany the mode, thereafter, allowing each mode to be reconstructed back in time domain.

Such an approach of mode extraction in the time-frequency plane i.e., a wavelet transform where the modes appear in the form of ridges (formed by successive amplitude of peaks) is achieved using the corresponding phase of the oscillatory modes, defined as $\phi(s,t) = arg[W_t(s,t)]$, which is purely time-dependent. For example, if the pattern of oscillation does not change, then the dynamics corresponding to the phases of harmonics will be the same. That is to say, the phase relation for multiple harmonics at scales s_1 and s_2 is given by $\phi(s_1,t) = (s_1/s_2)\phi(s_2,t)$. Now, having discerned these harmonics, the corresponding oscillatory modes can be reconstructed.

Even though the wavelet transform is a linear method, a number of different approaches that utilize it for detecting and extracting nonlinear oscillatory components have been proposed [327–329], with some of the methods being noise robust [330, 331]. However, a signal decomposed in the time-frequency domain also has a problem of mode mixing, given the fact non-periodic oscillations mostly produce many ridges in the time-frequency domain [327]. This limitation is addressed by the Nonlinear Mode Decomposition (NMD) [303] technique, a method that enhances the extraction of nonlinear oscillatory mode using a combination of robust time-frequency representation i.e., wavelet analysis [328, 330], surrogate data tests

[332–335] and details of the harmonics detected [327] .

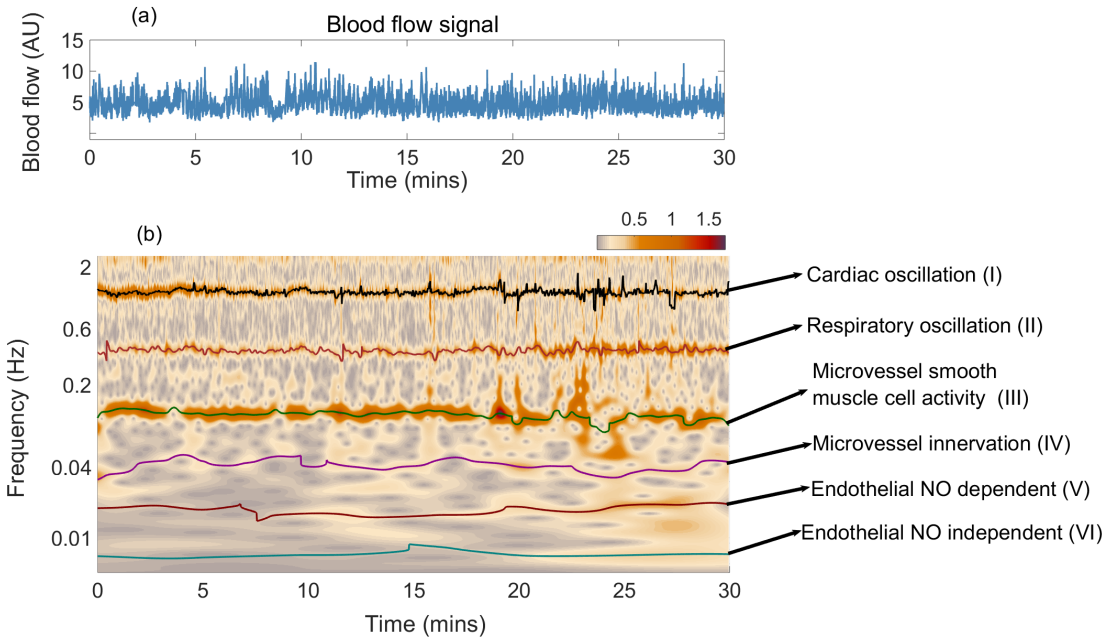

Figure 3.12: Decomposition of skin blood flow into different oscillatory modes. (a) Typical 30-minutes recording of the LDF signal from the a healthy subject. (b) The time-frequency evolutions of the modes extracted by NMD are indicated by color with heart-rate black, respiration brown, myogenic green, neurogenic magenta, endothelial NO dependent maroon and endothelial NO independent purple.

Typically, the NMD decomposes a signal as follows. First of all, the signal is transformed to time-frequency plane using a wavelet transformation, and the fundamental oscillatory mode is extracted from it using ridge extraction which traces the highest value (peak) at each moment in time across a specific frequency intervals. Oscillations at specific times and frequencies are then extracted using the curves obtained from the ridge. Subsequently, these oscillatory modes are tested against noise using the surrogates, so as to ensure that they are genuinely distinctive modes of the signal. Figure 3.12 illustrates a blood flow decomposed into six distinct oscillatory modes.

3.10 Characterisation of time series

3.10.1 Wavelet spectral power

Average and absolute wavelet power.

One of the physical quantities that could be deduced from equation (3.18) is the average power estimated over time (ξ_{mean}) within any frequency band of interest, in this thesis we mostly considered the 0.005–2 Hz frequency interval manifested in the microvascular blood dynamics. The power of each frequency band f_{n1} to f_{n2} associated with the time series ($x(t)$) is denoted as absolute power $\xi_n(f_{n1}, f_{n2})$ and written as;

$$\xi_n(f_{n1}, f_{n2}) = \frac{1}{t}\int_0^t \int_{\omega_0/2\pi f_{n2}}^{\omega_0/2\pi f_{n1}} \frac{1}{s^2}|W_x(s,t)|^2 dsdt, \tag{3.21}$$

where scale s is related to frequency f by $s = \omega_0/(2\pi f)$ and $W_x(s,t)$ refers to the wavelet transform of the signal $x(t)$ we are analysing. For example in the skin perfusion LDF tracing, the human blood flow signal is characterized into six frequency bands (discussed in the previous chapter) which are named according to the physiological origin of the rythmic process: $f_{11} = 0.61$ to $f_{12} = 2$ Hz (interval I, related to heart activity), $f_{21} = 0.145$ to $f_{22} = 0.6$ Hz (interval II, breathing rate), $f_{31} = 0.052$ to $f_{32} = 0.145$ Hz (interval III, related to smooth muscle cell activity), f_{41}= 0.021 to $f_{42} = 0.052$ Hz (interval IV, related to neurogenic activity), $f_{51} = 0.0095$ to $f_{52} = 0.021$ Hz (interval V, related to nitric oxide–dependent endothelial activity) and $f_{61} = 0.005$ to $f_{62} = 0.0095$ Hz (interval VI, related to nitric oxide–independent endothelial activity) [17, 157].

It worth noting that the normalised values of power represent the relative contribution of each of the physiological processes that manifest within a certain frequency interval. The normalized spectral power contains information about oscillations in all frequency intervals of interest while taking into account the fluctuations in the amplitude. The change in the normalised spectral power in each

of the frequency interval is viewed as relative to the overall changes.

Relative power

In a situation where the time-averaged wavelet power of the signal increases, it is likely that the power in each frequency band will also increase, thus making the absolute value of the power defined in equation 3.21 sometimes misleading. In such situations, it is therefore necessary to investigate whether and how the relative contribution of each frequency interval of interest, reflecting each physiological processes, has changed. Consequently, the relative spectral power contribution of a particular frequency band $e_n(f_{n1}, f_{n2})$ is defined as the ratio of the absolute power at a particular frequency band and the time averaged power, and is written as,

$$e_n(f_{n1}, f_{n2}) = \frac{\xi_n(f_{n1}, f_{n2})}{\xi_{mean}}, \tag{3.22}$$

where ξ_{mean} denotes the averaged-power of the signal present in the overall frequency band of interest (as in 0.0095–2 Hz in our case).

3.10.2 Interactions between time series

Wavelet phase coherence

While waves can be coherent in space, oscillations are known to be coherent in time. Quite generally, correlation properties between physical quantities, whether at a single or several oscillation frequencies, can be studied by investigating their coherence in time. Unlike the usual coherence measures, wavelet phase coherence does not take into account the amplitude dynamics of the signals. This is appropriate because (i) the amplitudes of most physiological signals are subject to artefacts and noise, and (ii) the relationships between the amplitudes of common physiological oscillations in different signals can be complicated and nonlinear, but in all cases the relationship between their phases remains the same (up to a

constant phase shift).

If we observe oscillations at the same frequency in two different time series and find that the difference between their instantaneous phases $\phi_{1k,n}$ and $\phi_{2k,n}$ is constant, then the oscillations are said to be coherent at that frequency [60, 154]. A phenomenon closely related to coherence is synchronization. While oscillations can be coherent without necessarily being directly coupled, the existence of coupling is fundamental for synchronization [316]. For example, if we have an n:m relationship between the frequencies of two signals (e.g. blood flow and oxygen saturation), this implies that there are n oscillation cycles in one time series per m cycles of the other time series: 1:1 phase synchronization may equally be considered as phase coherence. Thus phase coherence can be used directly to investigate 1:1 synchronization between two signals, as will be illustrated in the subsequent chapters. The wavelet phase coherence (WPC) [17] between the two signals $x_1(t)$ and $x_2(t)$ is estimated through their respective wavelet transforms as obtained in equation (3.18), i.e. (for $i = 1, 2$, W_{s_i} is the wavelet transform of signal x_i) $W_{x_1,x_2}(s,t)$ as

$$\mathrm{WPC}_{x_1,x_2}(f) = \left| \frac{1}{L} \int_0^L e^{i \arg[W_{x_1}(s,t) W^*_{x_2}(s,t)]} dt \right| \tag{3.23}$$

and it reflects the extent to which the phases (equation 3.25) and thus the underlying activities of these signals at frequency f are correlated.

The phase coherence function $C_\phi(f_k)$ is obtained by calculating and averaging over time the components of the sine and cosine of the phase differences for the whole signal, effectively defining the time-averaged WPC,

$$C_\phi(f_k) = \sqrt{\langle \cos \Delta\phi_{kn} \rangle^2 + \langle \sin \Delta\phi_{kn} \rangle^2}. \tag{3.24}$$

Basically, to explain the logic behind equation 3.23, we are considering individual times and frequencies, but these come from a discrete set (since all the signals are discrete and finite-time), and so the subscripts k and n just reflect this discreteness. Therefore, the phase coherence function $C_\phi(f_k)$ as defined in equation 3.24

is exactly the discrete version of the phase coherence formula (equation 3.23).

The relative phase difference of the signals is thus calculated as

$$\Delta\phi_{kn} = \phi_{2k,n} - \phi_{1k,n} \,. \tag{3.25}$$

The tendency of the phase difference ($\Delta\phi_{kn}$) to remain constant, or not, at a certain frequency is characterised by the function $C_\phi(f_k)$, whose value lies between 0 and 1. The existence of phase coherence or incoherence is defined by $C_\phi(f_k) \simeq 1$ or $C_\phi(f_k) \simeq 0$ respectively. Meaning that, oscillations are considered to be coherent at any given frequency if their phase shifts remain unchanged (with a coherence value ranging between 0 and 1); otherwise they are said to be incoherent.

Even in the case of two noisy signals, there is a tendency for there to be some apparent coherence in the sense that $C_\phi(f_k)$ rarely approaches 0 at very low frequencies. The degree of apparent phase coherence depends on frequency. So the coherence baseline will not be the same for all scales. The low-frequency components, particularly signals of finite length (like ours) are evaluated using fewer periods than for the higher frequency components [60]. The result can be an artificially increased coherence $\simeq 1$ even where the dynamics of the signals are unrelated.

Effective (or significant) coherence

The wavelet phase coherence between oscillations in two signals can be computed by evaluating the difference between the wavelet transform phases of the signals at each frequency, and at each moment in time, as given by equation 3.23. Coherence does not provide information about synchronization between oscillations, as this would require them to be coupled, which is not necessary for coherence to exist. However, information on possible synchronization between oscillations, particularly at the smaller ratios, e.g. 1:1 synchronization, can be obtained by estimating the wavelet phase coherence.

Note, that the coherence computed (equation 3.23) in the first instance does

not necessarily reflect a genuine phase relationship and requires careful evaluation. The problem arises because some of the coherence values obtained can be less than zero (although formally coherence values range between 0 and 1). These negative coherence values are then subtracted. Following this procedure, the very low frequency oscillations may appear to have a coherence values close to 1, because of bias resulting from the use of recordings that are too short to encompass the content at low frequencies.

To minimise random effects giving rise to apparent (but spurious) coherence, whether at low or high frequency, we checked/tested the significance of the computed coherence using the method of surrogates [332, 335] – by setting as a null hypothesis that, for all frequencies, the phases in the signals are independent. We used iterative amplitude-adjusted Fourier transform (IAAFT) surrogates to estimate the significance level of the apparent coherence, thereby removing the bias associated with the power spectrum of the more commonly used amplitude-adjusted Fourier transform (AAFT) surrogates. First, the IAAFT surrogates are constructed by randomizing all the properties of the signals in question, whilst keeping only the phases $\phi_{1k,n}$ and $\phi_{2k,n}$ unshuffled. Subsequently, this is accomplished in an iterative fashion, simply by using the appropriate value and re-scaling the distribution to substitute Fourier amplitudes, which allows us to obtain resemblance between the distributions and power spectra of the surrogates and the original signals. At each frequency we took the coherence threshold to be 95th percentile of the highest value of 100 random realisations of IAAFT surrogates. Figure 3.13 describes how wavelet phase coherence is computed between two time series.

An alternative approach to IAAFT surrogates is the inter-subject surrogate analysis [305] which can also be used to validate the results of significant coherence. In this method, surrogate values of the coherence between the two signals, for example blood flow - respiration are computed for nth (n = 300 is used in this thesis) combinations of randomly chosen inter group subjects. Meaning that, the

surrogate is built using e.g., blood flow from subject A and respiration from subject B, making the surrogate a composition of collection of mutually independent signals.

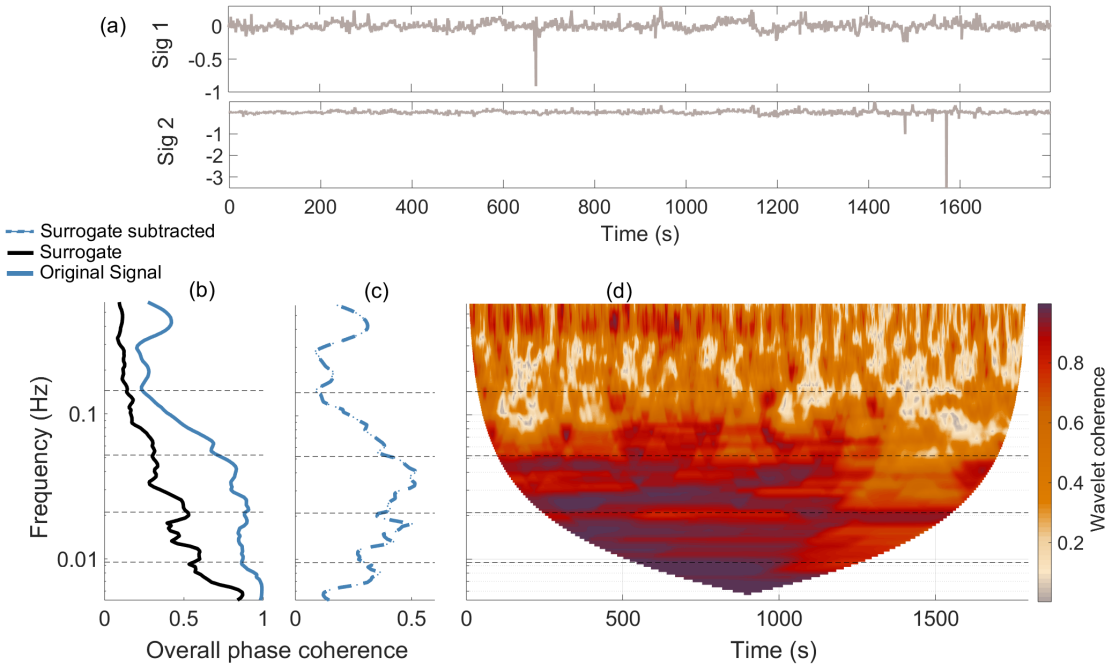

Figure 3.13: Typical illustration of wavelet phase coherence between two time series. Wavelet phase coherence between (a) the time series sig1 and sig2. In (b) significant phase coherence is shown when the coherence (blue line) is greater than the 95th percentile of 100 pairs of IAAFT surrogates (black line), and the effective significant phase coherence presented in (c) is obtained by subtracting the 95th percentile of the surrogate. The windowed phase coherence is shown in (d), which reveals the time-variability of the modes but at the cost of losing information about lower frequencies.

Finally, the effective/significant coherence is then estimated by subtracting the 95th percentile of the 100 surrogate values in the case of IAAFT and 300 surrogates in the case of inter-subject surrogate, thus giving the extent to which the phases of the two signals at each frequency are correlated. Note that, both the IAAFT and inter-subject surrogates were used in this thesis.

Synchronization

Synchronization is one the most useful phenomena known for investigating interacting systems. It is the adjustment of rhythms of oscillators to a state where they all have the same phases and amplitudes. Synchronization occurs whenever there

is a coupling between two oscillators. Oscillators can be phase synchronized, phase and amplitude synchronized or Lyapunov synchronized (also known as generalised synchronization). If two systems have an n:m relationship such that the phase difference $|n\phi_1 - m\phi_2|$ is constant while amplitude may still vary independently, there are n cycles of one oscillator in m cycles of the other. Synchronization is sometimes described by a synchogram – which graphically signifies the presence of synchronization between two time series [314].

Dynamical Bayesian inference

Extrapolating the properties of interaction from the dynamics of different systems is one of the long standing and never ending tasks in physics, dating back to the formulation of the electromagnetic interaction that occurred between electrically charged particles as established by Maxwell. When dealing with most fundamental interactions such as the electromagnetic interaction, quite a number of remarkable experiments are available. However, in the case of couplings that are not common, as are typically in human systems [17], the discernment of such latent interaction strongly depends on analysis of observations. Such approaches have been established based on nonlinear analysis of physiological data (bi- or multivariate data) [14, 303, 313].

Insights into the stability and proper coordination in the human microcirculatory system analogous to various physiological processes [17] could be prescribed via couplings between distinct inter-oscillatory interactions endowed in each subsystem [14, 313]. Analysis of phase coupling functions between any given interacting oscillators is currently one of the novel methodologies [336–338] used to formulate how the physical rule characterizing the inter-oscillator interactions takes place. Dynamical Bayesian inference, a method that allows the extraction of information such as the effective connectivity in biomedical signals even in the presence of noise [337, 339], is applied to the interactions. It models the interactions with a network of coupled phase oscillators based on the common fact that weak cou-

pling quickly affects the phases of oscillators compared to their amplitudes. Hence, analysis of the relationship between the phases of the systems could enable one to properly infer and quantify the sets of parameters regulating the mechanism of the interaction (such as the coupling strength and direction of coupling) whilst separating out noise [337].

It is worth noting that since our signals are physiological and thus oscillating with varying frequencies, their mutual coupling can properly be investigated through their phase dynamics. However, to elucidate the basic physics underlying such interaction in the phase domain we consider a model of two coupled phase oscillators [340] described by a stochastic first order differential equation (equation 3.26), based on the fact that the coupling function $q_i(\phi_i, \phi_j) = a_i \sin(\phi_j - \phi_i)$ is a sinusoidal function of phase difference:

$$\begin{aligned} \frac{d\phi_i}{dt} &= \omega_i(t) + q_i(\phi_i, \phi_j, t) + \eta_i(t) \\ \frac{d\phi_j}{dt} &= \omega_j(t) + q_j(\phi_i, \phi_j, t) + \eta_j(t) \end{aligned} \tag{3.26}$$

where i and j represent the oscillators so i $\neq$ j and $\omega_{i,j}(t)$ stands for the natural frequency of the oscillation. The dependency of the dynamics of one oscillator on the other is described by the deterministic terms $q_i(\phi_i, \phi_j, t)$ and $q_j(\phi_i, \phi_j, t)$, which are the coupling functions (i.e., base functions), thus describing their self and interacting dynamics. Both $\eta_i(t)$ and $\eta_j(t)$ are external stochastic dynamics assumed to be white Gaussian noise: $(\eta_i(t)\eta_j(\tau)) = \delta(t - \tau)D_{ij}$, with D_{ij} being the matrix with delta-peaks on the diagonal and 0 off the diagonal. On account of the periodic behaviour of the deterministic dynamics on the phases ϕ_i and ϕ_j, the coupling terms reflecting the latter can be modelled as an infinite Fourier bases [341] written as;

$$q_u(\phi_i, \phi_j, t) = \lim_{K\to\infty} \left(\sum_{k=1}^{K} \alpha_{1,k}^{(u)}(t)\cos(k\phi_i) + \alpha_{2,k}^{(u)}(t)\sin(k\phi_i) \right) + \left(\sum_{m=1}^{K} \beta_{1,k}^{(u)}(t)\cos(m\phi_j) + \beta_{2,k}^{(u)}(t)\sin(m\phi_j) \right) + \left(\sum_{i=1}^{K}\sum_{|j|=1}^{K} \gamma_{1,k,m}^{(u)}(t)\cos(k\phi_i + m\phi_j) + \gamma_{2,k,m}^{(u)}(t)\sin(k\phi_i + m\phi_j) \right) \tag{3.27}$$

for $u = i, j$. For a finite-order Fourier approximation involving finitely many Fourier components, one can ignore the limit as $K \to \infty$ and just stop the series at the desired finite order K. The first and second term (equation 3.27) corresponds to the self-dynamics of the phase and cross couplings respectively, although, in typical phase reduction, the phase calibration is chosen such that there are no self-dynamics terms except the natural frequency of the oscillator. The parameters $\alpha_{1,k}^{(u)}(t)$, $\alpha_{2,k}^{(u)}(t)$, $\beta_{1,k}^{(u)}(t)$, $\beta_{2,k}^{(u)}(t)$, $\gamma_{1,k,m}^{(u)}(t)$ and $\gamma_{2,k,m}^{(u)}(t)$ that describe the coupling function gives the parameter vector $c_k^{(i)}$, where $c_0^{(i)} = \omega_i$. Meaning that the pair of fundamental frequencies for the coupled oscillator system is the same as the pair (ω_i, ω_j) of natural frequencies of the two oscillators (i.e., the coupling functions have zero average). Using the Fourier components as the base function for the dynamical Bayesian inference, one can evaluate the parameter $c_k^{(i)}$ from the observed dynamics.

The time-evolving coupling function and coupling strength are contained in the model parameters c, which can be computed using dynamical Bayesian inference [337]. This method uses the Bayes' theorem defined as

$$p(\mathcal{M}/\chi) = \frac{\ell(\chi/\mathcal{M})p_{prior}(\mathcal{M})}{\int \ell(\chi/\mathcal{M})p_{prior}(\mathcal{M})d\mathcal{M}} \tag{3.28}$$

where the probability of observing the data χ given the value of the model parameters $\mathcal{M}$, $\ell(\chi/\mathcal{M})$ is the likelihood of finding the hypothesized model parameters M

given the data χ. The probability of M prior to data χ is $p_{prior}(\mathcal{M})$, while the denominator (equation (3.28)) is the marginal probability distribution of χ.$p(\mathcal{M}/\chi)$, that is the probability of the preciseness of the observed parameters given χ and $p_{prior}(\mathcal{M})$. By considering a single window of data, the most probable and obtainable values for the parameters can be deduced by finding the stationary point in the negative-log likelihood function as presented below;

$$S = \frac{L}{2} ln(E) + \frac{h}{2} \sum_{n=0}^{N-1} (c_k^{(i)} \frac{\partial B_{l,k(\phi_{.,n})}}{\partial \phi_l} + [\dot{\phi}_{i,n} - c_k^{(i)} B_{i,k}(\phi^*_{.,n})](E^{-1})_{i,j}[\dot{\phi}_{j,n} - c_k^{(j)} B_{j,k}(\phi^*_{.,n})]) \tag{3.29}$$

The model presented in equation (3.26) can be integrated by choosing a small time length h between the samples in the signal and assuming an implicit summation over the indices k, l, i, j. The noise is denoted as E, and as presented in equation (3.27), the matrix A represents the base functions. However, it is worth mentioning that the probability functions of the inferred parameters in dynamical Bayesian inference are assumed as a multivariate Gaussian distribution, and considering the same distribution (as in the latter) for the corresponding prior knowledge (distribution) given as:

$$p_{prior}(c_k^{(l)}) = \frac{e^{-1/2}(c_k^{(l)} - c^{(l)}_{prior_k})^T \Xi_{prior}(c_k^{(l)} - c^{(l)}_{prior_k})}{\sqrt{(2\pi)^M det(\Xi^{-1}_{prior})}} \tag{3.30}$$

where the magnitude of all the parameters contained in $c_k^{(l)}$ is represented by M and the covariance matrix of the parameters is Ξ^{-1}. By decomposing equations (3.28)-(3.30) into equation 3.31, one can explicitly evaluate the posterior distribution $c_k^{(j)}$ as;

$$
\begin{aligned}
E_{ij} &= \frac{h}{L}[\dot{\phi}_{i,n} - c_k^{(j)} B_{i,k}(\phi^*_{.,n})][\dot{\phi}_{j,n} - c_k^{(j)} B_{j,k}(\phi^*_{.,n})] \\
r_w^{(l)} &= (\Xi_{prior})^{i,l_{kw}} c_w^{(l)} + hB_{i,k}(\phi^*_{.,n})(E^{-1})_{ij}\dot{\phi}_{j,n} - \frac{h}{2}\frac{\partial B_{l,k}(\phi_{.,n})}{\partial \phi_l} \\
c_k^{(i)} &= (\Xi^{-1})_{kw}^{i,l} r_w^{(l)} \\
\Xi_{kw}^{i,j} &= \Xi_{prior_{kw}}^{(i,j)} + hB_{i,k}(\phi^*_{.,n})(E^{-1})_{ij} B_{j,w}(\phi^*_{.,n})
\end{aligned}
\tag{3.31}
$$

from the four equations presented above [337], information between consecutive windows are essentially propagated when $\Xi_{prior}^{(i,j)}$ utilizes the detail from the posterior $\Xi^{(i,j)}$, this is then inferred from the preceding time window which therefore making it possible to infer time-varying parameters, although the initial window is calculated by setting both $\Xi_{prior}^{i,j}$ and c_{prior} to zero (the full implementation of the foregoing equations is presented in [342, 343]).

Furthermore, for proper consideration of the time-varying values of the inferred parameters that allows for tracking changes in coupling over time, the convolution between the posterior of the preceding window and is simply swapped for the prior and a diffusion matrix explaining the change in either of $c_{(k)}^{(i)}$ and $\Xi_{prior}^{(i,j)}$ [337]. The propagation constant p is σ_k^i / c_k^i, where the standard deviation that relate to the diffusion parameters from $\Xi_{prior}^{i,j}$ is defined as σ_k^i.

Once the parameters in c are inferred, the coupling quantities and characteristics can then be computed. By visualizing the coupling functions on a three dimensional plane, a deep understanding of each inter-oscillator interactions could be obtained by displaying the propagation of the coupling parameters in relation to their respective phases. Consequently, this reveals vital information such as; the strength of coupling, its directionally and other functional phenomenon that governs the coupling [336, 338, 344].

3.11 Summary

The effective visualisation of the oscillations present in signals, particularly the experimentally generated ones, greatly depends on the method used for their analysis.

Traditionally, representations of time series in the frequency domain are obtained with the fast Fourier transform, which constitutes a periodic function in terms of sines and cosines. This makes it suitable for analysing time series whose components are strictly periodic in nature, but it is unsuitable for LDF signals whose components are inherently non-periodic. The limitations of the Fourier transform can partly be addressed by use of the short-time Fourier transform through windowing, i.e. by dividing the time series into shorter time-windows within which there is not much time variation so that the fast Fourier transform (FFT) can usefully be calculated; in practice, this is usually done by sliding a window across the whole signal.

However, because the spectral resolution in short time Fourier transform strongly relies on the length of the window, with short windows leading to poor frequency resolution and high time localisation, and *vice versa*, this method also fails when dealing with non-stationary physiological signals with varying frequencies, such as the LDF time series considered in this study. These limitations can be overcome by the use of wavelet analysis, which maximizes joint time–localisation and frequency–resolution, unlike the Fourier transform. Wavelet analysis is a scale-independent method comprising an adaptive window length allowing low frequencies oscillations to be analysed using longer wavelets, and higher frequencies oscillations with shorter wavelets.

Furthermore, given that oscillations in living system are usually correlated, thus, additional detection of mutual coordination between the oscillators could be investigated by utilizing the information about their phase relationship. An $n : m$ relationship means that $|n\phi_1 - m\phi_2|$ is constant. The case that $|\phi_1 - \phi_2|$ is

constant is specifically 1:1 synchronisation which requires no coupling between the oscillators. Additional inference of the phase dynamics using dynamical Bayesian inference can also reveal important information (such as the coupling function and coupling strength) between coupled oscillators.

4. Suitability of laser-Doppler flowmetry for capturing microvascular blood flow dynamics from darkly pigmented skin

4.1 Introduction

As previously discussed, laser Doppler flowmetry (LDF) provides for the noninvasive monitoring of microvascular blood flow dynamics. It has been used extensively on light-skinned subjects, i.e. on skin with low melanin concentration, in both the healthy and pathological states. LDF monitoring of blood flow is known to work efficiently in the case of light skin, whose optical properties enable light to penetrate more easily, but the question arises as to what happens in the case of darkly pigmented skin? The interaction of light with skin mostly happens just below the surface, i.e. in the stratum corneum. As shown in Figure 3.3, some of the coherent laser light shone on the skin's surface gets scattered from the stratum corneum, referred to as surface scattering. Some of the light propagates to deeper skin layers such as the dermis and epidermis. Absorption and scattering by the melanin and erythrocytes occur in the epidermis and dermis respectively. Unlike the epidermis and dermis, the stratum corneum layer is usually colourless and absorbs only a small portion of incident light.

Because the optical properties of human skin could well affect the reliability of optically-based diagnostic equipment, the effectiveness of LDF needs to be checked and evaluated on dark skin, too, if this method is to be useful in global health care. Here we assess the performance of LDF in measuring blood perfusion from darkly-pigmented skin, i.e. skin with high melanin concentration.

Melanin absorbs light within the visible and near-infra-red (near-IR) parts of the optical spectrum. The absorption decreases with increasing wavelength, so that near-IR in the wavelength range 780–800 nm is best suited to non-invasive diagnosis and treatment [345]. The fact that dark skins contain about twice the concentration of epidermal melanin, compared to lighter skins, inevitably means that less laser light reaches the deeper segments of dark skin [345].

Extensive investigations of the absorption and reflection of light in/from human skin began in 1911 with the spectrographic studies of Hasselbalch [105]. More recently, considerable effort has been devoted to quantifying the absorption spectrum of human skin, particularly darkly pigmented skins [108, 346–349]. There has been significant disagreement in the results, perhaps due to challenges in conducting the experimental measurements. For example, the studies of both Pauli and Ivancevic [350] and Cartwright [351] reported that a substantial proportion of IR radiation penetrates deeply into the body through the skin, whereas Aldrich [352] and Hardy and Muschenheim [353] reported a negligible proportion.

In an attempt to determine the effect of melanin on spectroscopic signal formation, Kollias and Baqer [346] studied the absorption characteristics of melanin in the wavelength range 620–720 nm and observed that remittance spectra measured from vitiligo-involved skin and normal skin did not differ, from which they concluded that both skins have similar absorption. In a comparable study by Kollias and Baqer [347], the remittance spectroscopy parameters measured from normal skin and amelanotic skin in the range 620–720 nm were found to be strongly correlated.

More recently, a model of fluorescence spectra from biological tissue based on

the Monte Carlo approach has predicted the effect of melanin concentration on a spectroscopy signal [354]. The use of near-IR diode lasers of relatively long wavelength (670, 780, and 810–850 nm) was shown to improve optical penetration [355].

Note that because LDF computes the erythrocyte velocity from the spectral broadening (see below) of the incident light, which is independent of the light's absolute intensity, the method might be expected to function effectively regardless of the degree of attenuation along the signal path. However, this conclusion can only hold true if two conditions are fulfilled. First, the signal/noise ratio of the light returned to the detector must be sufficient for the spectral broadening to be determined reliably by the measurement algorithm. Secondly, the incidence of frequency-dependent scattering process along the optical return path that would modify the shape of the spectrum must be insignificant. In practice, therefore, the only convincing way forward is empirical: to test LDF on dark-skinned subjects and look for significant differences in the results compared to those obtained from comparable light-skinned subjects.

This Chapter provides a detailed experimental study comparing the LDF fluxes measured for both darkly and lightly pigmented skin. The time-varying oscillations in the microvascular blood flow dynamics were checked and compared for the two pigmentations. As discussed above, they are known [13, 15, 17, 61, 356] to include components ranging from the cardiac frequency at $\sim$1 Hz in healthy humans down to endothelium-related oscillations with frequencies of $\sim$0.01 Hz. Non-linear time series analysis [17, 303, 314, 316] was used to discern the oscillatory components in the signals. Specifically, the frequency interval from 0.0095 to 2 Hz (see Sections 1.1.3 and 2.3.3) was examined.

4.2 Hypothesis

Using the time-frequency analysis methods discussed above, this investigation tests the hypothesis that,

1. In the case of dark skin, the attenuation of the incident laser light reaching (and scattering back from) the dermis is not sufficient to prevent LDF functioning effectively.

2. The time-varying oscillations in the microvascular blood flow dynamics do not significantly differ when compared for the two pigmentations.

4.3 Study participants

To test these hypotheses, 23 healthy male subjects in total were recruited for the study, based on the criteria stated in Section 3.1.

The participants were grouped into two: subjects with darkly pigmented (high melanin concentration) skin were categorized as dark-skinned subjects and those with lightly pigmented skin were grouped as light-skinned Caucasian subjects.

Thirteen healthy dark-skinned subjects, born in sub-Saharan Africa, without known ancestors of non-African origin, with a high melanin concentration in their skins, and ten light-skinned Caucasian subjects of European origin with low melanin concentration, between the ages of 18–27 years, were recruited. All subjects were male. Their anthropometric data are given in Table 4.1. Written informed consent was obtained from all participants.

Physiological parameters recorded Measurements of the skin blood flow and skin temperature were recorded at two different sites, on the outer sides of the left (LA) and right (RA) ankles (lateral malleolus). Blood pressure, ECG and respiration were also measured in this study.

4.4 Results

Statistics

Application of the Lilliefors test for normality [357] showed that there were no consistent normal distributions of data among the groups being compared. Non-parametric statistical tests were therefore used, meaning that no assumptions were made about any underlying distributions, thus allowing robust conclusions to be drawn. The Kruskal-Wallis ANOVA test [358] was used when all IHRs (derived from the LA and RA blood flows and from the ECG) were compared. The Kruskal-Wallis test checks whether two or more independent sets of data originate from the same distribution, and it does not assume normal distributions. Where significance is found, pairs of groups are tested either by the Wilcoxon signed rank test for paired data, or by the Wilcoxon rank sum test for unpaired data [359]. The latter was used to test for possibly significant differences between blood flow measured from dark-skinned and light-skinned subjects, respectively, as the corresponding time-series do not match. The Wilcoxon rank sum test is used to determine whether two unmatched samples come from similar distributions, whilst the sign rank test requires that the samples are matched. In all cases, $p < 0.05$ was considered as being statistically significant.

Anthropometric data

Table 4.1: Anthropometric data of subjects measured: median values, ranges [25th and 75th percentiles] and significance.

	Dark-skinned subjects ($n = 13$)	Light-skinned subjects ($n = 10$)	p
Age (years)	21.0 [20.0 24.0]	22.0 [19.0 25.0]	0.66
Body mass index (kg/m^2)	23.15 [20.2 24.2]	23.15 [21.6 24.7]	0.34
Skin temperature (^oC)	29.9 [30.0 31.1]	30.1 [30.0 30.4]	0.90
Instantaneous respiratory rate (Hz)	0.28 [0.27 0.3]	0.26 [0.24 0.27]	0.06
Systolic BP (mm Hg)	115.5 [112 125]	118.5 [109 126]	0.85
Diastolic BP (mm Hg)	71.5 [68.0 75.0]	76.5 [67.0 77.0]	0.64

The anthropometric data of the subjects (Table 4.1) show that there are no statistically significant differences between the groups - in terms of their ages, BMI, skin temperature, instantaneous respiratory rate and blood pressure.

4.4.1 Time domain results

Instantaneous heart frequency

Table 5.2 presents the median and interquartile ranges of the instantaneous heart frequencies derived from both the ECG and blood flow of dark and light-skinned groups.

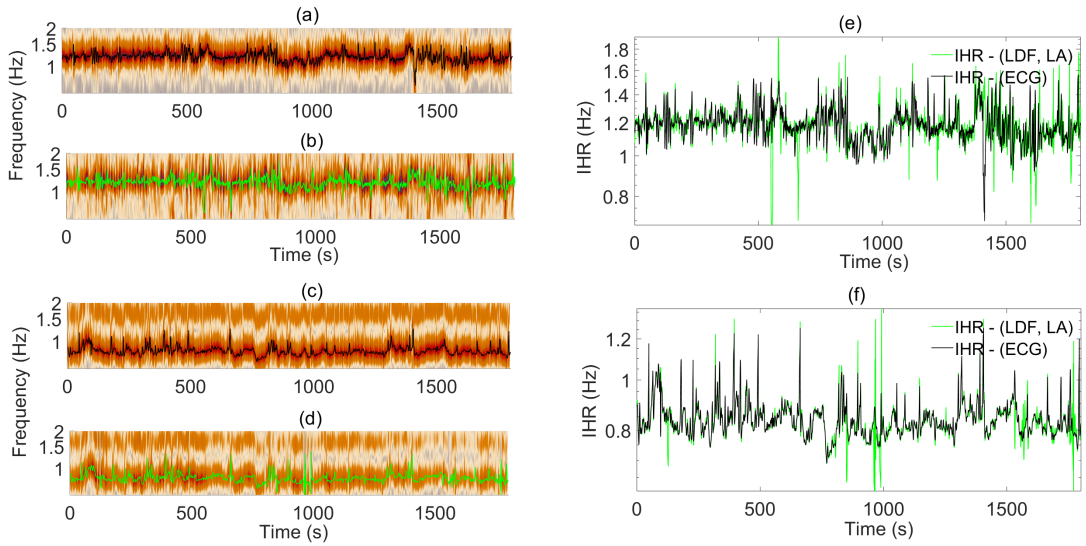

Figure 4.1: Time-frequency representations illustrating the extraction of IHRs from the heart beat detected in the wavelet transform of the ECG (a),(c), with their variation in time traced with black curves for dark (a) and light (c) skin; (b),(d) wavelet transforms of the LDF blood flow and their variation in time traced with green curves, for both dark (b) and light (d) skin. The frequency variation over time shown in (a)-(d) gives the IHR. (e),(f) comparisons between the IHR obtained from ECG and LDF for dark (e) and light (f) skin. Note, this result is from two subjects.

The IHR values calculated from the LDF time series recordings measured on the ankles did not differ between groups (Table 4.1). Figure 4.1(a)(c) illustrates how the IHR was extracted from the ECG and (b),(d) from LDF blood flow signals; and the intra-group comparison between the IHRs (Figures 4.1(e) and (f)). Comparisons made between mean values of the IHR signals derived from both the

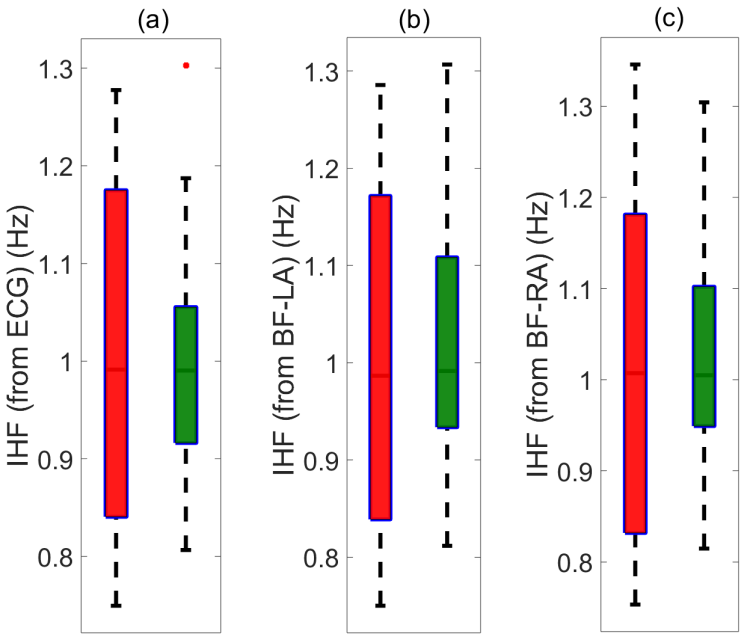

Figure 4.2: Group mean instantaneous heart frequency compared between light-skinned (red) and dark-skinned (green) groups: (a) IHF derived from ECG only, (b) IHF derived from left ankle (LA) LDF and (c) IHF derived from right ankle (RA) LDF. No significant differences are obtained for any of the three comparisons.

ECG and LDF data (measured from both LA and RA) (Figure 4.2) revealed no statistically significant differences ($p > 0.7$).

Mean blood flow

Typical recordings of LDF blood flow time series simultaneously recorded from the right and left ankles of volunteers in both groups are presented in Figure 4.3. No significant difference was found in the inter-group comparison of the average blood perfusion as shown in Figure 4.4. The slightly lower values for the dark-skinned group are the result from an outlier in the right ankle recordings, but no statistically significant differences were found in mean blood perfusion between the two groups ($p > 0.05$).

Comparison of the median and interquartile ranges of the blood flow in dark and light-skinned groups also did not show any statistically significant difference (Table 5.2).

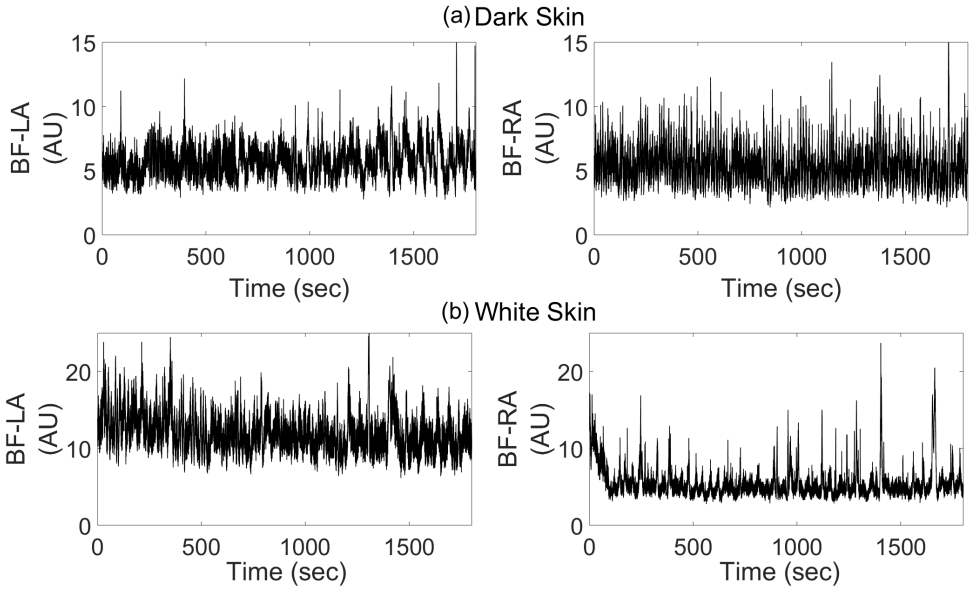

Figure 4.3: Typical LDF blood flow (BF) signals recorded from the left (LA) and right (RA) ankles for: (a) a dark-skinned volunteer with high melanin concentration; and (b) a light-skinned volunteer with low melanin concentration.

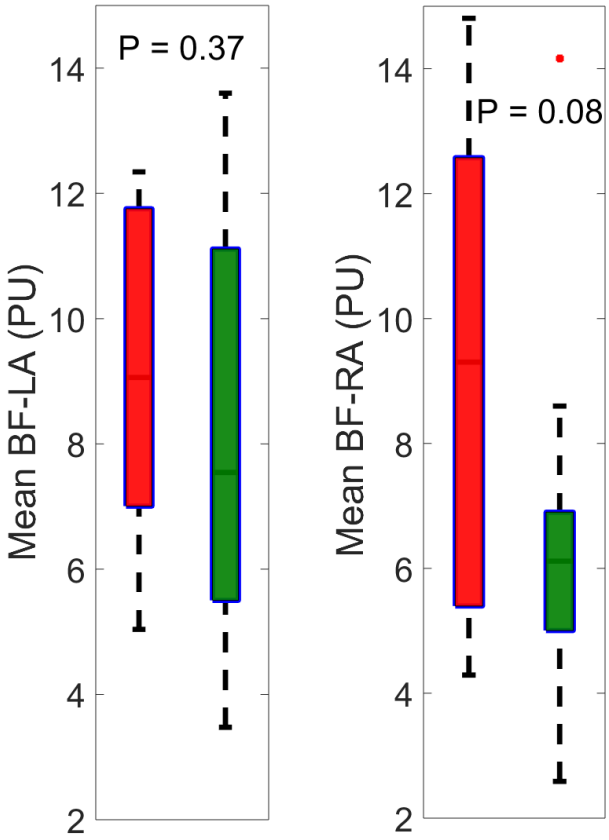

Figure 4.4: Group mean LDF microvascular skin blood flow (BF) recorded from left ankle (LA) and right ankle (RA) for light-skinned (red) and dark-skinned (green) groups, with their significant differences as determined by the Wilcoxon rank-sum test. The Boxplot outlier is shown as red cross

Table 4.2: LDF skin perfusion and IHR (derived from LDF) of measured subjects, median values and ranges [25th and 75th percentiles]

	Dark-skinned	Light-skinned	p
Blood flow (RA) (AU)	6.12 [5.0 6.9]	9.3 [5.4 12.5]	0.08
Blood flow (LA) (AU)	7.54 [5.5 11.11]	9.06 [7.01 11.75]	0.37
IHR (from ECG) (Hz)	0.99 [0.91 1.05]	0.99 [0.83 1.17]	0.98
IHR (from RA) (Hz)	1.00 [0.95 1.10]	1.01 [0.83 1.18]	0.73
IHR (from LA) (Hz)	0.99 [0.93 1.11]	0.99 [0.84 1.17]	0.78

4.4.2 Time frequency analysis

Spectral power of the microvascular skin blood flow and instantaneous heart frequency

An example of the time-frequency representation for continuous wavelet transforms of microvascular skin blood flow signals for dark and light skinned volunteers is given in Figure 4.5. The figure clearly illustrates the presence of oscillations in the blood flow captured from both skins.

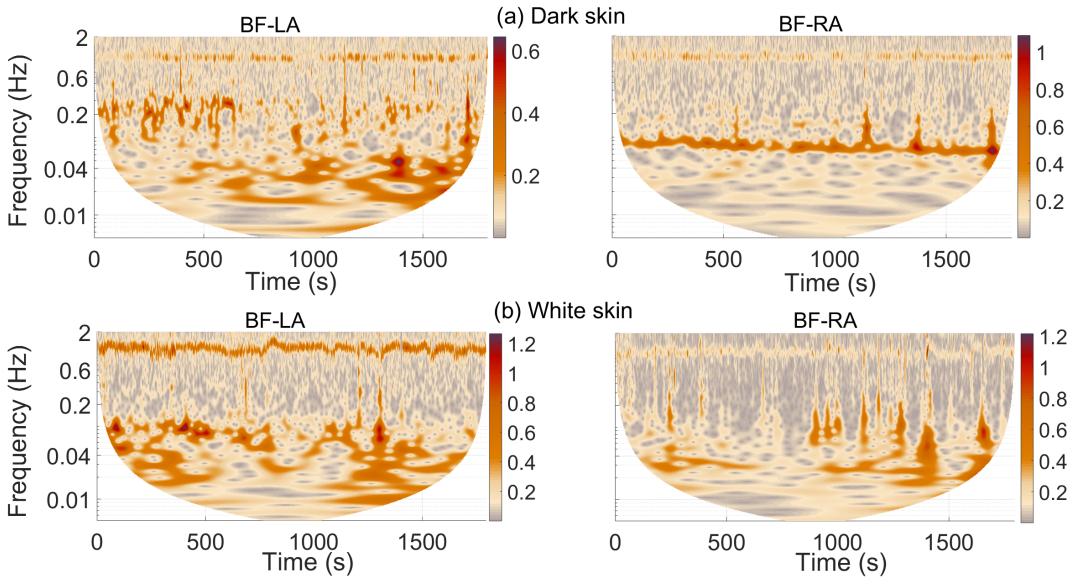

Figure 4.5: Time-frequency representation. Typical continuous wavelet representations of the LDF blood flow (BF) signals recorded from the left (LA) and right (RA) ankles for: (a) a dark-skinned volunteer with high melanin concentration; and (b) a light-skinned volunteer with low melanin concentration. The wavelets provide time-resolved frequency content of the blood flow signals.

The group mean time-averaged spectral power of the oscillations in LDF blood flow are presented Figure 4.6. No statistically significant differences in time-

averaged wavelet power across the frequency intervals were observed in the LA and RA (Figure 4.6(a),(b)) blood flows between the dark- and light-skinned groups (p = 0.95 and p = 0.62 respectively). The 25th and 75th percentiles (indicated in dark green for dark skinned and light green for light skinned subjects) for both LA and RA LDF blood flow spectrum were found to overlap between groups are shown in Figure 4.6(a)(i) and (b)(ii). There is no obvious difference in the inter-subject variations between the two groups. No differences in skin perfusion or fluctuations between the groups were evident.

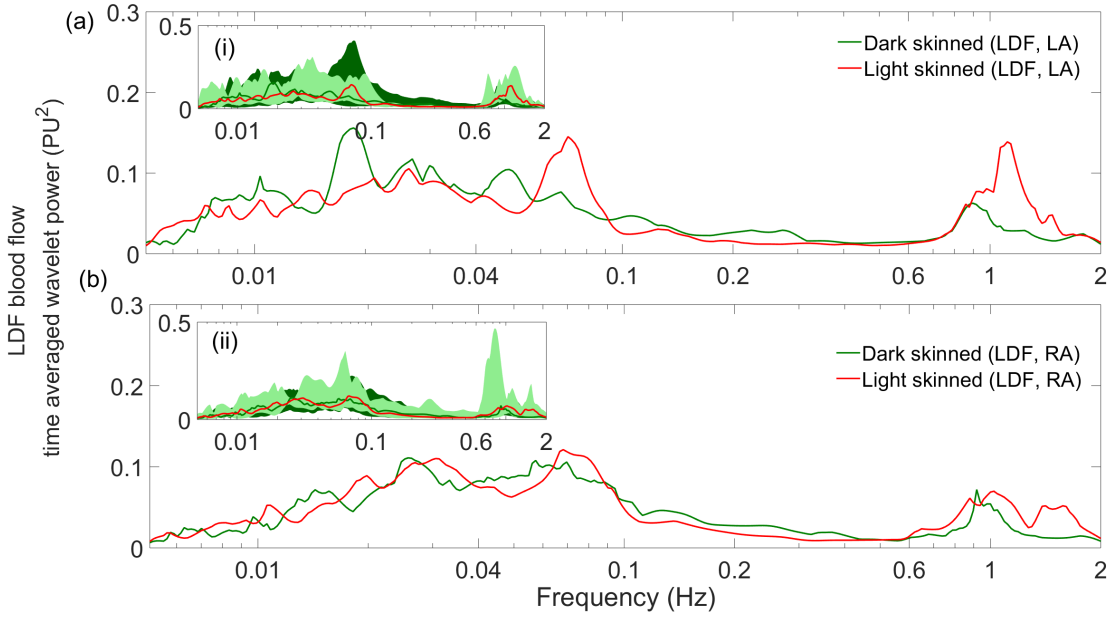

Figure 4.6: Group median time-averaged spectral power calculated from the wavelet transforms of LDF signals recorded for 30 minutes in dark-skinned (green) and light-skinned (red) groups for (a) the left ankle (LA) and (b) the right ankle (RA). In neither case was any statistically significant difference seen at any frequency. The insets (a-(i)) and (b-(ii)) are provided to give an idea of inter-subject variability, which was similar in both groups. They show the 25th and 75th percentiles of the individual spectra from dark-skinned (dark green) and light-skinned (light green) groups.

The time-frequency representation for instantaneous heart fluctuations extracted from the ECG and LDF blood flow from a dark and light skinned volunteers is given in Figure 4.7. While the IHR derived from the ECG (Figure 4.7(a)) differ significantly ($p < 0.05$) betweeen groups at around 0.015 Hz, no other difference was present across the remaining frequency intervals. Similarly, no statistically significant differences occurred within the 0.005-0.6 Hz intervals. The light green and

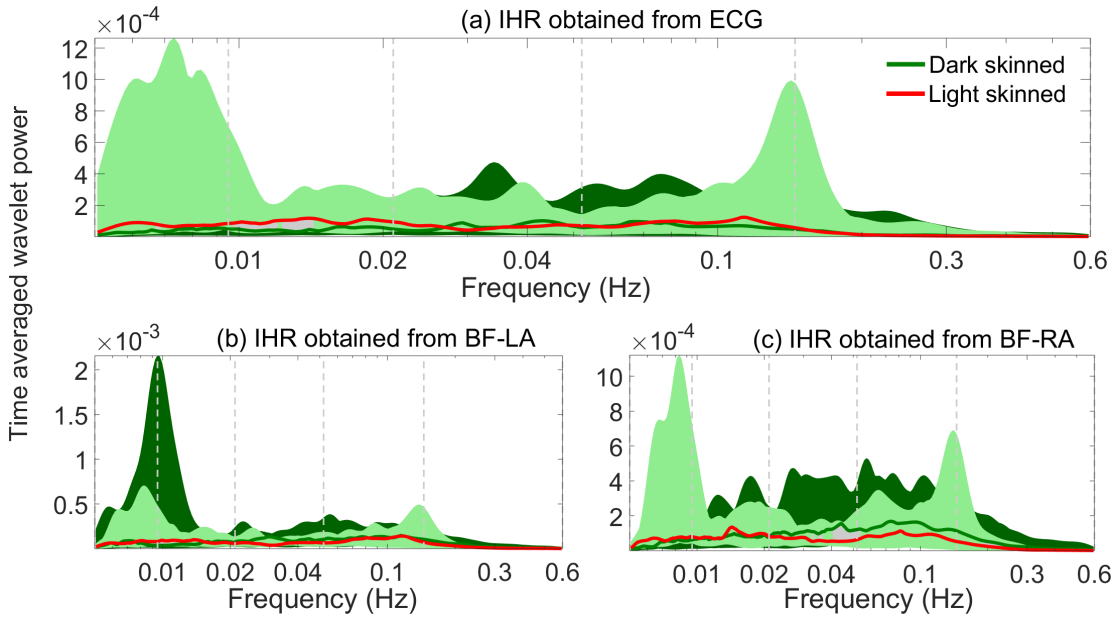

Figure 4.7: Group median time-averaged spectral power calculated from the wavelet transforms of (a) IHR derived from ECG, (b) IHR derived from the blood flow (BF) recorded in left ankle (LA) and (c) IHR derived from the BF recorded in right ankle (RA). The 5th and 95th percentiles of the individual spectra overlapping each other between dark-skinned (dark green) and light-skinned (light green) groups are indicated. The grey shading indicates significant (p<0.05) differences between dark and light skins.

green shading shows that the ranges between 5^{th} and 95^{th} percentiles of the spectral power in dark-skinned and light-skinned groups were overlapping one another within 0.005-2 Hz.

Comparison of power in instantaneous heart frequency derived from ECG and LDF blood flows

Intra-group comparison of the time-averaged power of the IHR derived from ECG, LA and RA LDF blood flows revealed no significant differences between light-skinned (Figure 4.8(a)) and dark-skinned (Figure 4.8(b)) groups: $p = 0.99$ and $p = 0.21$ respectively as obtained by the Kruskal-Wallis test. Figure 4.8(c) shows no significant difference in the inter-group comparison of the time averaged power for IHR derived from (i) ECG, (ii) LA LDF and (iii) RA LDF, $p = 0.64$, $p = 0.37$, and $p = 0.20$, respectively.

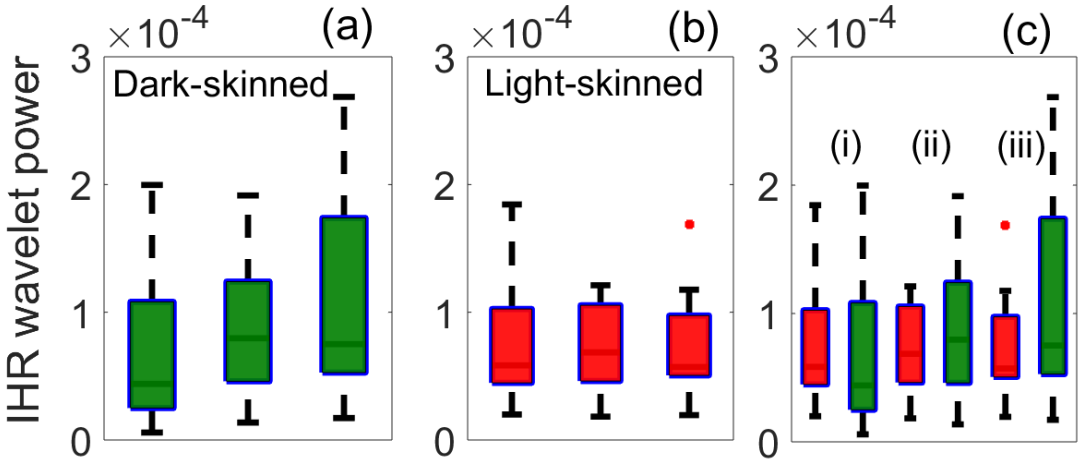

Figure 4.8: IHR time-averaged wavelet power summed over 0.005-0.6 Hz frequency intervals for light-skinned and dark-skinned groups respectively. The tree box-plots in each case represent time-averaged wavelet power for IHR derived from ECG (first), LA LDF (second) and RA LDF (third box). The Kruskal-Wallis test revealed no significant differences among the three IHR wavelet power values ($p = 0.99$ for the (a) dark-skinned group and $p = 0.21$ for the (b) light-skinned group). (c) Comparison between groups: (i) IHR derived from ECG only, (ii) IHR derived from LA LDF and (iii) IHR derived from RA LDF. No significant differences are obtained for any of the three comparisons.

4.4.3 Wavelet phase coherence

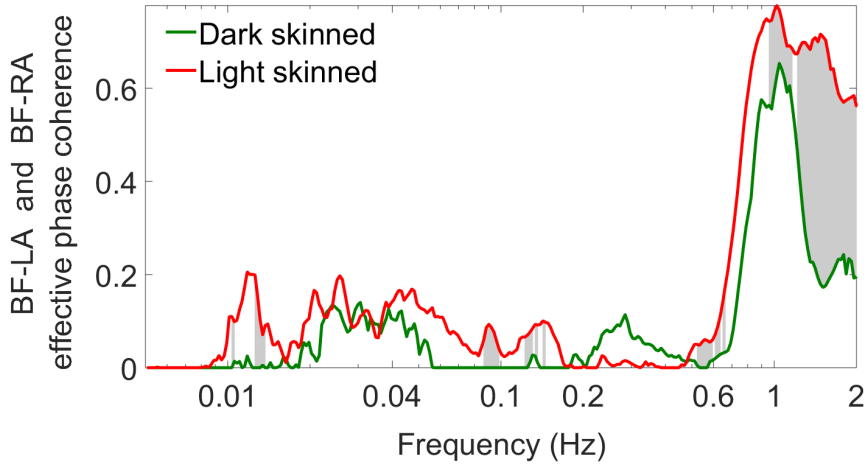

Figure 4.9: Median wavelet phase coherence between left and right ankle blood flow for dark-skined (green) and light-skinned (red) groups, with significant differences ($p < 0.05$) as determined by the Wilcoxon rank-sum test highlighted in light grey.

Coherence between Moor laser Doppler skin blood flow

Wavelet phase coherence between LA and RA blood flows from each groups are shown in Figure 4.9. Compared to the dark-skinned cohort, the light-skinned group exhibits a significantly higher coherence in the 0.6 – 2 Hz frequency interval, corresponding to cardiac activity. The coherence was significantly lower in the dark-skinned group also near 0.1 Hz.

4.5 Summary

The investigation carried out in this chapter has shown that, with illumination derived from a laser diode of wavelength 780 nm, LDF provides an effective method of studying blood flow dynamics, even in darkly pigmented skin. We found no evidence that the greater light attenuation in the latter case has an adverse effect on measurements, and we were able to obtain the same information about the microcirculatory dynamics regardless of skin pigmentation. However the significantly higher coherence observed in the blood flow around the cardiac frequency interval in the light-skinned group, compared to the dark-skinned one, may result from the known ethnic disparity in cardiac autonomic modulation between white and black-skinned people [244, 360]. It could also be associated with the ethnic differences in left ventricular wall thickness [361]. We shall explore the effects of race-specific differences in cardiovascular dynamics in the next chapter.

5. Effects of race-specific differences on microvascular blood flow and oxygenation dynamics

5.1 Introduction

There are known differences in cardiovascular dynamics between people of Sub-Saharan African descent, and European descent [244, 247, 361]. They manifest both clinically, as in the prevalence of diabetes and other vascular diseases[362], and also in terms of differences in vasodilation and vasoconstriction processes [223, 256, 361, 363, 364]. The latter differences could perhaps be related to variations in gene expression between the races. Studies of these differences can further illuminate race-related distinctions in cardiovascular function, which are known to be influenced by gene expression, whence the different susceptibilities to certain diseases arise [362, 365]. Vasodilation and vasoconstriction have close relationships with the delivery and regulation of blood, serving to ensure the proper oxygen supply. Endothelium-dependent vasodilation (EDVD) and endothelium-dependent vasoconstriction (EDVC) are of wide-ranging importance for protecting the microvascular system against pathophysiological insults [61, 366].

To the best of our knowledge, no previous study of race-related differences in blood flow and tissue oxygenation dynamics (BFOD) has been published, so that race-specific differences at the level of microvascular blood flow and tissue oxygena-

tion are still unknown. Earlier studies investigated ethnic differences in the oscillations that manifest in heart rate variability (HRV), using Fourier transformation [360]. But this approach is incapable of tracing either the time evolution of high frequency oscillations or low frequency events in a non-sinusoidal [314, 360, 367] signal such as HRV and, even if properly revealed, their mutual interaction and even causal mechanism remains unknown. The identification of rhythmic mutual coordination between two distinct oscillators requires at least the detection of their 1:1 synchronization. Wavelet coherence [368] was introduced to study such synchronization. Later, wavelet phase coherence was introduced [154, 369] which detects whether or not the difference in phase between two signals at a given frequency remains constant in time. In contrast to spectral power, phase coherence has been shown to be relatively free of noise effects and to allow the detection of coordination between two distinct signals [154].

To try to reach an understanding of the differences in microvascular blood flow and tissue oxygenation between people of Sub-Saharan Africans and Europeans, the present chapter exploits two specific advances; (i) a novel system that enables simultaneous monitoring of blood flow and oxygenation in the same area, and (ii) recently developed methods based on wavelet phase coherence to establish, not only the intensity of various oscillatory process involved in cardiovascular regulation, but also their degree of coordination.

Blood flow dynamics[17, 61, 356], oxygen saturation, and hemoglobin concentration all comprise fluctuations around central, but time-varying, values [59, 370–372]. The extent to which hemoglobin binds oxygen determines the amount of oxygen transported around the body, its organs and cells. Oxygen-hemoglobin fluctuations alongside oxygen circulation have been extensively explored, and date back to the work of August Krogh in 1919, who pioneered the *in vitro* study of oxygen transport [373, 374]. He measured not only the diffusion coefficients for oxygen in different tissues, but also the average distances travelled by oxygen molecules from a capillary to the site of chemical reaction. This work inspired

several other investigations into blood oxygenation fluctuations, leading to new insights into oxygenation dynamics in both the healthy and pathological states [57, 60, 88, 372, 375, 376].

Investigations based on continuous glucose monitoring in diabetic patients have also demonstrated race-specific differences in the level of glycated hemoglobin (HbA_{1c}) for a given mean glucose concentration, with the glycation gap being attributed to genetic differences [377, 378]. Reports of such HbA_{1c} differences are well-documented for both type 1 and type 2 diabetes, with non-Hispanic subjects having lower HbA_{1c} levels than blacks [378–384]. The raised HbA_{1c} level in blacks has been attributed to poor glycemic control [385].

Despite the inconvenience of obtaining HbA_{1c} invasively, its mean value has been used widely in studying the corresponding race-specific differences. In fact, understanding of the role of the race-related disparity in HbA_{1c} is still far from complete because mean oxygenation is not a sufficient measure of the physiological situation [57]. Given that oxygen is delivered to the cells by hemoglobin (Hb) through the cardiovascular system, a possible route to a deeper understanding of the race-related differences in HbA_{1c} is to investigate the oscillatory fluctuations in blood flow and oxygen transportation.

A non-invasive system for monitoring oxygenation fluctuations is potentially helpful for investigating race-related differences within a continuous time frame. Near-infrared spectroscopy (NIRS) [386, 387], white light spectroscopy[388, 389], and laser Doppler flowmetry (LDF) [390, 391] can contribute to such a system. They are all continuous optical methods that allow for real-time monitoring of changes in both the systemic and local activities of the cardiovascular system. Systemic activities, reflecting the heart function and respiration alongside local activities modulated by vasomotion, might affect tissue oxygenation [58, 59, 93, 392].

Earlier studies have not only investigated the oscillations in NIRS oxygenation, but have also used optical reflectance spectroscopy (which is a form of NIRS)

to determine the coherence between fluctuations in BFOD using wavelet-based analysis [60]. They demonstrated coherence between LDF blood flow and NIRS oxygenation in the skin microcirculation [60]. However, NIRS devices used in recent studies of tissue oxygenation have mostly been used to evaluate oxygen saturation at the capillary level [58, 393–395]. This can only reveal local information about oxygen utilization. The development of a combined white light reflectance and LDF probe that uses a single-point low-power infrared light source (785 nm) and white light (400-700 nm) excitation, respectively, has enabled simultaneous recordings of blood flow and oxygenation at the same location [388, 389]. This can illuminate their mutual interactions to provide more information about oxygenation mechanisms in the microcirculation.

It is against this background that the present study used a novel system combining LDF at 785 nm with a single infra-red light source for NIRS at 750 nm and 850 nm, and a 400-700 nm white light source to investigate race-specific differences in coherence between the fluctuations in blood flow and oxygenation dynamics. The presence of oscillations in the signals was checked using wavelet analysis. Wavelet phase coherence was used to investigate the interactions between simultaneously recorded pairs of signals; (i) the microvascular LDF blood flow and NIRS oxygenation from the deep skin (OXY: oxyHb, deoxyHb, SO_2%) signals and (ii) the microvascular LDF blood flow and white light oxygenation from the superficial skin (OXY: oxyHb, deoxyHb, SO_2% (where SO_2 means saturated oxygen).

This Chapter particularly addressed the question of whether the rhythmic mutual coordination between the oscillations in blood flow and oxygenation dynamics reveals racial differences in cardiovascular dynamics.

5.2 Study participants

To answer the above question, thirty-two healthy male volunteers participated in this study. They were divided into two groups: 16 black Africans (BA) and 16 Caucasian whites (CW), with age ranges as given Table 5.1. The BA group was

composed of West Africans (from Nigeria and Ghana) plus two black Sudanese, while the CW group was British plus two white-skinned Europeans. Individuals in the CA group had lived their lives in the UK at an altitude not higher than 50 m above sea level and with an average annual temperature of 10 °C, except for two persons from Belarus and Turkey, respectively. Individuals in the BA group had lived for more than 80% of their lives at an average altitude of 470 m and with an average annual temperature of 26.8°C (see Table 5.2).

5.2.1 Physiological parameters measured

Acquisation of microvascular skin blood flow and oxygenation signals

A combined laser Doppler flowmetry and white light reflectance spectroscopy monitor (moorVMS-LDF2 and moorVMS-OXY, respectively, Moor Instruments Ltd, Axminster, UK) was used to make simultaneous skin microvascular blood flow and skin oxygenation measurements. Microvascular blood flow and oxygenation at a deeper level in the tissue were also measured simultaneously by laser Doppler flowmetry (moorVMS-LDF2, Moor Instruments Ltd, Axminster, UK) and near-infrared spectroscopy monitor (moorVMS-NIRS), respectively. The blood flow and oxygenation signals were captured from the left forearm.

5.3 Results

Anthropometric Information of Subjects. The anthropometric data for black African and white Caucasian groups are summarized in Table 5.1. All subjects had normal blood pressure, with systolic blood pressure (SBP) < 140 mmHg and diastolic BP < 90 mmHg. Similarly, all of the participants also had heart rate < 1.2 Hz, BMI < 24.9 and skin temperature (ST) < 29°C. The comparison of these data between the groups show no significant difference ($p< 0.05$).

Table 5.1: Anthropometric data of subjects measured: median values, ranges [25th and 75th percentiles]. Compared to Table 4.1, most of the subjects presented here are older, particularly the black Africans, and have slightly higher values of blood pressure.

	Black Africans subjects ($n = 16$)	Caucasians subjects ($n = 16$)
Age (years)	26.5 [20.5 33.0]	22.5 [19.0 26.0]
Body mass index (kg/m^2)	21.2 [18.1 24.1]	23.1 [21.0 24.8]
Skin temperature (^oC)	29.7 [28.3 30.7]	29.8 [28.8 30.4]
Instantaneous heart frequency (Hz)	0.99 [0.97 1.14]	0.96 [0.83 1.08]
Systolic BP (mm Hg)	124 [116 133]	123 [109 127]
Diastolic BP (mm Hg)	76.5 [71.5 81.0]	77.0 [68.0 80.0]

Table 5.2: Information about the country, altitude, and temperature of the sub-Saharan participants recruited for the study. Note that each participant had lived more than 80% of his life in the country.

Subject	Altitude (m)	State/Country	Annual mean temperature (^{o}C)
1	381	Sudan	29.9
2	381	Sudan	29.9
3	1053	Ondo/Nigeria	25.3
4	519	Katsina /Nigeria	26.4
5	200	Benin/Nigeria	26.1
6	250	Kaduna/Nigeria	25.2
7	41	Lagos/Nigeria	27.1
8	450	Abuja/Nigeria	25.7
9	41	Lagos/Nigeria	27.1
10	299	Yobe/Nigeria	25.2
11	41	Lagos/Nigeria	27.1
12	488	Kano/Nigeria	26.4
13	488	Kano/Nigeria	26.4
14	2359	Niger/Nigeria	27.5
15	41	Lagos/Nigeria	27.1
16	488	Kano/Nigeria	26.4

Statistics Since the BA and CA are two unmatched groups, possible differences between them were tested using an unpaired two-sided Wilcoxon rank sum test, setting $p < 0.05$ as the criterion for statistical significance. The allowed us to check whether or not two groups of data emanate from the same distribution.

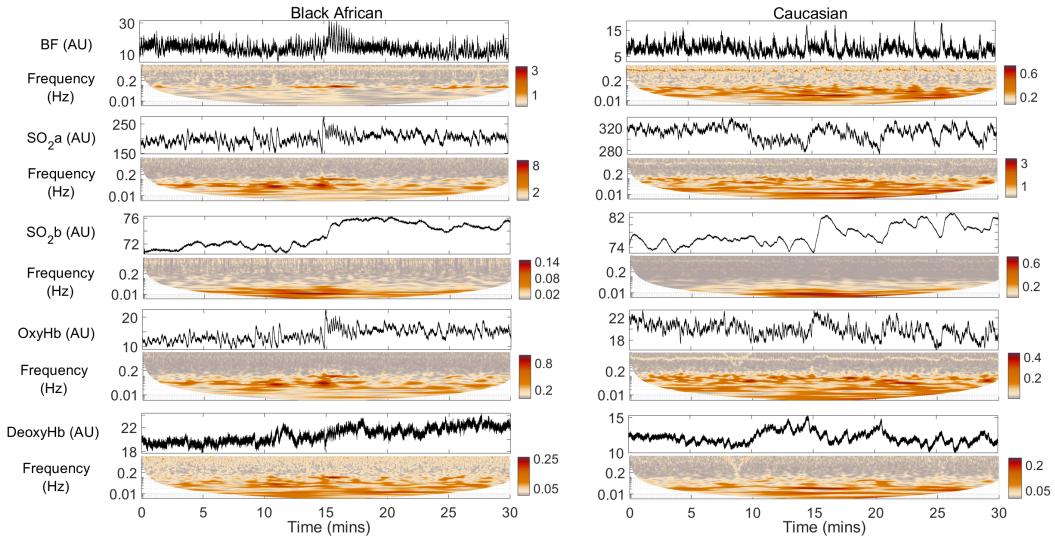

Figure 5.1: Simultaneous recordings of blood flow (BF) using LDF, oxygen saturation SO_2a using white light spectroscopy, oxygen saturation SO_2b using NIRS, oxygenated hemoglobin (oxyHb) and deoxygenated hemoglobin (deoxyHb) using white light spectroscopy with their respective continuous wavelet representations (below each time-series) for a typical black African from the BA group, and a typical Caucasian (CA group). For each subject, signals were simultaneously recorded from the skin of the left forearm, for 30 minutes. The wavelet transform enables accurate visualization of the frequency content of the time-series over time.

5.3.1 Race-specific differences in skin perfusion, oxygen saturation and hemoglobin concentrations

Table 5.3 summarizes the results obtained for average microvascular blood flow, oxygen saturation, and oxygenated and deoxygenated hemoglobin values, for each of the two groups. As shown in Figure 5.2, the mean oxygen saturations monitored using white light spectroscopy and NIRS were significantly lower ($p = 0.002$ and $p = 0.03$, respectively) in BA than in CA. The standard deviation of both SO_2a and SO_2b did not differ significantly between groups ($p = 0.08$ and $p = 0.98$, respectively). In contrast, the mean oxygenated and deoxygenated hemoglobin concentrations measured by white light spectroscopy were significantly higher in BA compared with CA ($p = 0.002$ and $p = 0.0000001$, respectively). Standard deviation of both oxyHb and deoxyHb was significantly different between groups ($p = 0.008$ and $p = 0.004$, respectively). There were no significant differences in skin perfusion as measured by LDF.

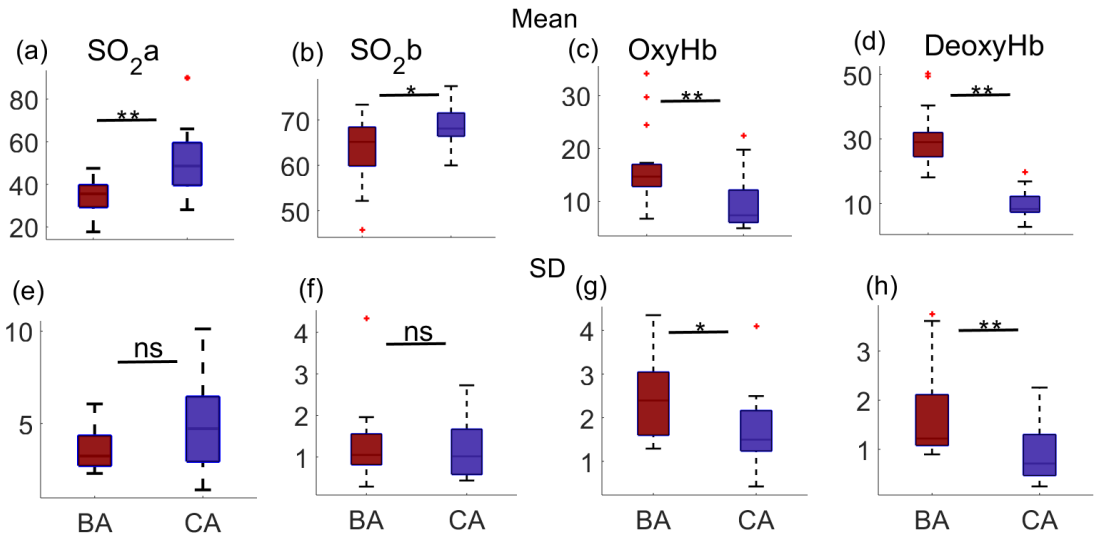

Figure 5.2: (a) Boxplots of mean (a) oxygen saturation SO_2b recorded with white light spectroscopy, (b) oxygen saturation SO_2b recorded with NIRS, (c) oxygenated hemoglobin (oxyHb) and (d) deoxygenated hemoglobin (deoxyHb) concentrations recorded with white light spectroscopy, which all differed significantly between groups. Boxplots of standard deviation of (e) SO_2b and (f) SO_2b did not differ significantly between groups ($p = 0.08$ and $p = 0.98$, respectively). Boxplots of standard deviation of (g) oxyHb and (h) deoxyHb differed significantly between groups ($p = 0.008$ and $p = 0.004$, respectively). Outliers are shown as red crosses.

5.3.2 Race-specific differences in spectral power

Microvascular blood flow

As indicated in Figure 5.1, the blood flow (BF) spectrum contains clearly resolved oscillatory components spanning the frequency range 0.0095-2 Hz. Intragroup comparison of the BF oscillations showed that they did not differ significantly in any of the six frequency intervals, as shown in Figure 5.3(a). The high peak in the cardiac interval of CA (Figure 5.3(a)) results from 2 outliers (subjects with very high cardiac peaks).

Hemoglobin and oxygen saturation

Figure 5.1 also shows the typical time-averaged wavelet spectral power of oxygen saturation SO_2a (obtained using white light spectroscopy), oxygen saturation SO_2b (obtained using NIRS), oxygenated hemoglobin (oxyHb), and deoxygenated hemoglobin (deoxyHb), recorded from a black African and a Caucasian. Unlike

Signal	BA	CA	p value
Blood flow (AU)	9.3 [7.9 15.2]	13.7 [8.1 19.8]	0.23
Oxygen saturation, SO_2a (%),	35.4 [29.2 39.6]	48.6 [39.6 59.4]	0.002
Oxygen saturation, SO_2b (%),	65.2 [59.9 68.4]	68.1 [66.5 71.6]	0.03
Oxygenated hemoglobin (AU)	14.5 [12.9 17.0]	7.4 [5.9 12.0]	0.002
Deoxygenated hemoglobin (AU)	29.0 [24.6 31.9]	8.3 [7.3 12.2]	0.0000001

Table 5.3: Median values and ranges [25th percentile and 75th percentile] of blood flow, oxygen saturation (SO_2a, measured at a shallow depth in the skin using white light spectroscopy, SO_2b – measured deeper in the skin using NIRS), oxygenated and deoxygenated hemoglobin concentrations.

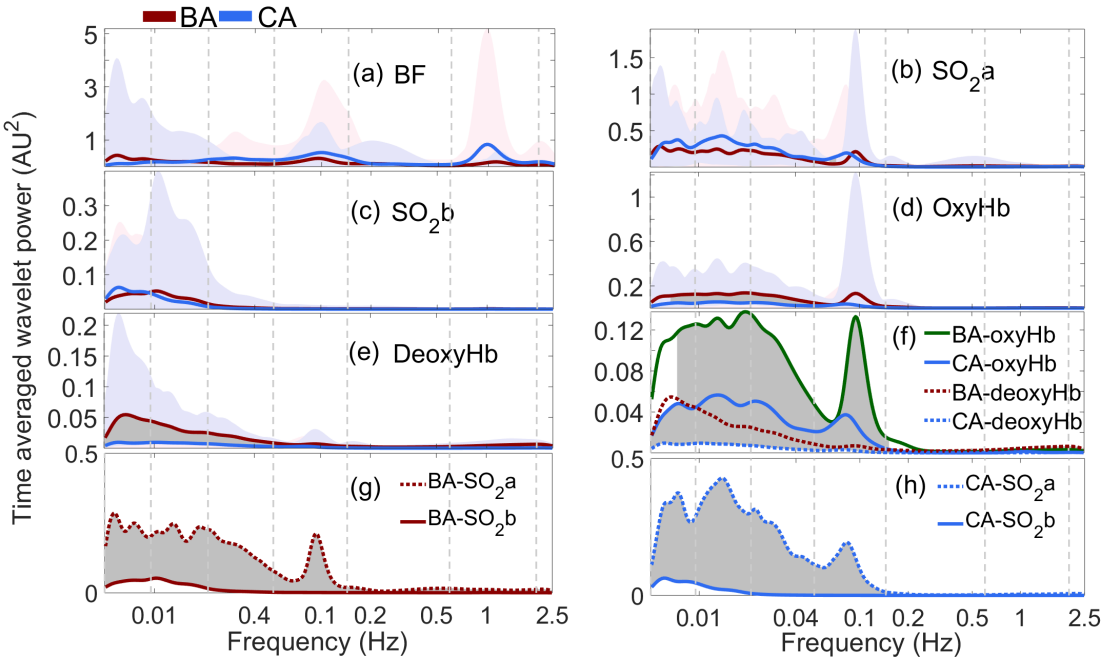

Figure 5.3: Time-averaged wavelet power spectra of (a) blood flow (BF), (b)-(e) oxygenation parameters mean over groups. The comparison of the curves presented in (d)-(e) are summarized in (f). Lavender-blush and lavender shadings indicate the ranges between 5^{th} and 95^{th} percentiles in the BA and CA groups respectively, and grey shading in (d)-(h) indicates statistically significant (p <0.05) differences between the two groups. (g),(h) Comparison between the oxygenation depths for the BA and CA groups respectively. Note that both SO_2a and SO_2b are expressed as %s. The vertical lines indicate the six cardiovascular frequency intervals [15] within the range 0.0095-2 Hz.

the case of BF, high frequency oscillatory components in the SO_2a, SO_2b and oxyHb spectral powers are not clearly seen as they appeared noisy, but their low frequency spectral content could be clearly visualized in both BA and CA subjects, as shown in Figure 5.3. In contrast, neither the low nor high frequency components were clearly observed in the deoxyHb spectrum. SO_2a and SO_2b recorded

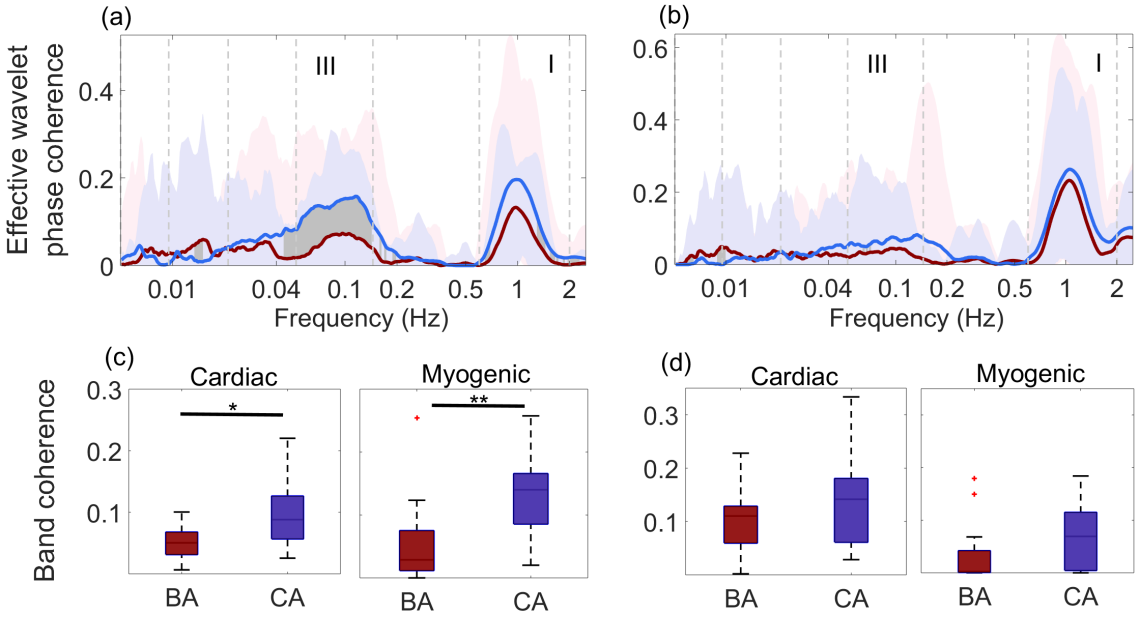

Figure 5.4: Blood flow and oxygen saturation phase coherence, and means over groups. Wavelet phase coherence (minus surrogate thresholds) between (a) BF and SO_2a (oxygen saturation recorded using white light spectroscopy). (b) BF and SO_2b (oxygen saturation recorded using NIRS), where III and I indicate the myogenic and cardiac frequency intervals respectively. Lavender-blush and lavender shadings indicate the ranges between 5^{th} and 95^{th} percentiles in the BA and CA groups respectively, and grey shading indicates statistically significant (p<0.05) differences between BA and CA. The box-plots show the coherence between (c) BF and SO_2a, and (d) BF and SO_2b within the cardiac and myogenic frequency intervals. $^{*}p$<0.05, $^{**}p$<0.005.

from the skin and deeper tissue exhibit similar power spectra ($p > 0.05$) across the 0.0095-2 Hz frequency interval, when compared between BA and CA groups, while their spectral powers at frequency > 0.1 Hz are diminished in both cases compared to that of the BF's spectral power, as shown in Figure 5.3(a)-(c). In contrast to SO_2a and SO_2b, the oxyHb and deoxyHb spectral power were significantly higher in BA compared with CA ($p > 0.05$) groups in the frequency intervals IV, V and VI associated with neurogenic, NO dependent endothelial and NO independent endothelial activity (Figure 5.3(d),(e)). No significant inter-group difference was observed in either the oxyHb or deoxyHb spectral powers ($p > 0.05$) above 0.4 Hz, partly because the power diminishes within the high frequency intervals. Similarly, the oxyHb and deoxyHb spectral powers did not significantly differ between BA and CA (Figure 5.3(f)).

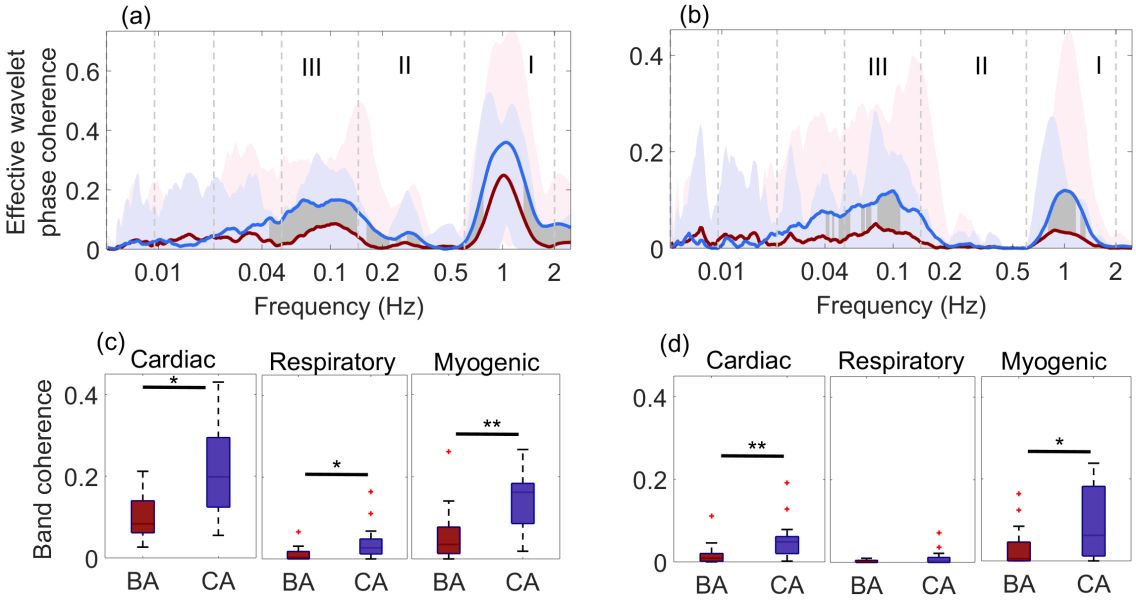

Figure 5.5: Blood flow and hemoglobin phase coherence, and means over groups. Wavelet phase coherence (minus surrogate thresholds) between (a) BF and oxyHb (b) BF and deoxyHb, where III, II and I indicates myogenic, respiratory, cardiac frequency intervals respectively. Lavender-blush and lavender shadings indicate the ranges between 5^{th} and 95^{th} percentiles in the BA and CA groups respectively, and grey shading indicates statistically significant ($p<0.05$) differences between BA and CA. The box-plots show coherence between (c) BF and oxyHb, and (d) BF and deoxyHb within the cardiac, respiratory and myogenic frequency ranges. $^{*}p<0.05$, $^{**}p<0.005$.

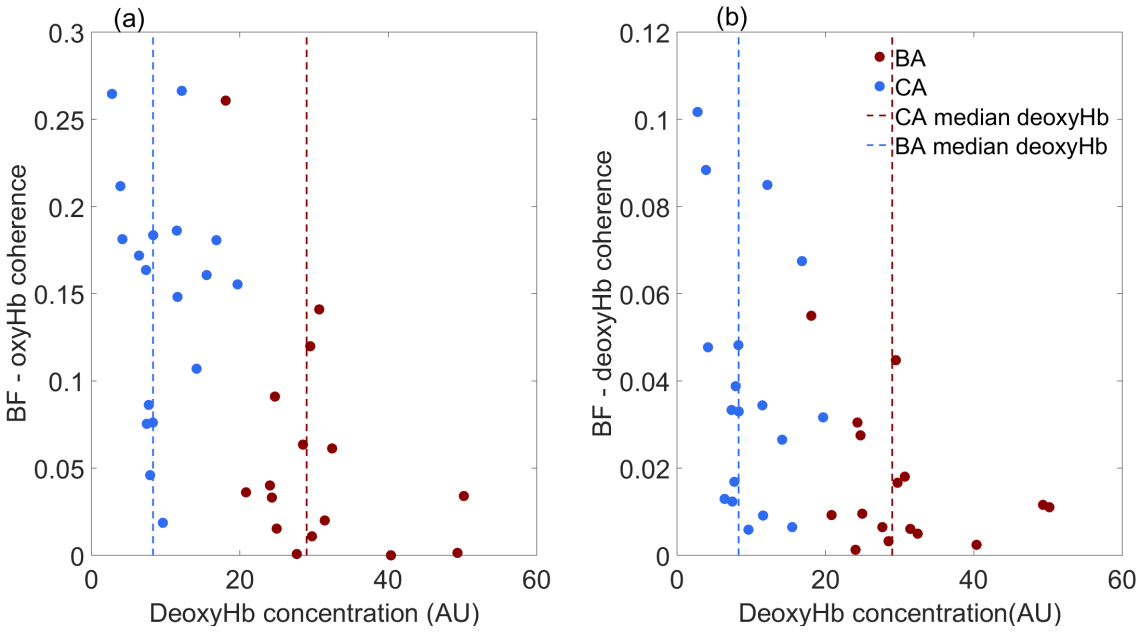

Figure 5.6: Relationship between the deoxygenated hemoglobin signal and the estimated wavelet phase coherences between blood flow and oxygenated/deoxygenated signals. (a) Coherence between blood flow and oxygenated hemoglobin plotted against the deoxyHb signal, (b) Coherence between blood flow and deoxygenated hemoglobin plotted against the deoxyHb signal.

5.3.3 Race-specific differences in wavelet phase coherence

Coherence between fluctuations in blood flow and oxygen saturation

Figure 5.4 presents the wavelet phase coherences between oscillations in BF and SO_2a, BF and SO_2b. The CA group showed significantly higher phase coherence between BF and SO_2a in the frequency intervals associated with cardiac (I) and myogenic (III) activity ($p = 0.0075$ and $p = 0.0003$, respectively) compared to BA. The coherence nearly disappears in the respiratory frequency interval in both groups. In contrast, a comparison between BA and CA reveals no significant coherence between BF and SO_2b (Figure 5.4(c),(d)) across 0.0095-2 Hz frequency interval, nor in the cardiac or myogenic frequency bands.

Coherence between fluctuations in blood flow and hemoglobin

Wavelet phase coherence between oscillations in BF and both oxyHb and deoxyHb were calculated and the group mean coherence is shown in Figure 5.5(a),(b). A

significantly higher coherence between BF and oxyHb was observed in CA in the frequency intervals I, II and III ($p = 0.0061$, $p = 0.005$, $p = 0.0004$ respectively) associated with cardiac, respiratory and myogenic activity, respectively (Figure 5.5(c)). In the coherence between BF and deoxHb, CA exhibited a significantly higher coherence in only the cardiac and myogenic frequency intervals ($p = 0.001$ and $p = 0.01$, respectively), while no such significant difference ($p = 0.13$) was observed in the respiratory interval, as the coherence in the latter case was diminished in both groups. BA exhibited a significantly lower phase coherence in all frequency intervals where significant differences were observed as presented in Figure 5.5(c),(d).

Coherence between blood flow and hemoglobin concentration

Figure 5.6 presents linear graphs plotting the relationships between the estimated BF and oxyHb/deoxyHb coherence and deoxyHb concentration. As deoxyHb increases in BA, the coherence between BF and oxyHb decreases, while the low deoxyHb concentration in CA leads in turn to high coherence between BF and oxyHb (Figure5.6(a),(b)). In a similar fashion, the increase in deoxyHb concentration in BA reduces the coherence between BF and deoxyHb, while the coherence rises with increasing deoxyHb (Figure 5.6(b)).

Coherence between oxygenated and deoxygenated hemoglobin concentrations

The analyses of phase coherence between oxygenated and deoxygenated hemoglobin are summarised in Figure 5.7(a),(b). A significantly lower phase coherence in the frequency intervals associated with cardiac, respiratory and myogenic activity ($p = 0.00001$, $p = 0.0004$ and $p = 0.04$, respectively) was observed in the CA group as compared to BA (Figure 5.7(b)). Although not statistically significant, CA exhibited a slightly higher coherence below 0.052 Hz with the coherence nearly disappearing towards 0.0095 Hz (Figure 5.7(a)).

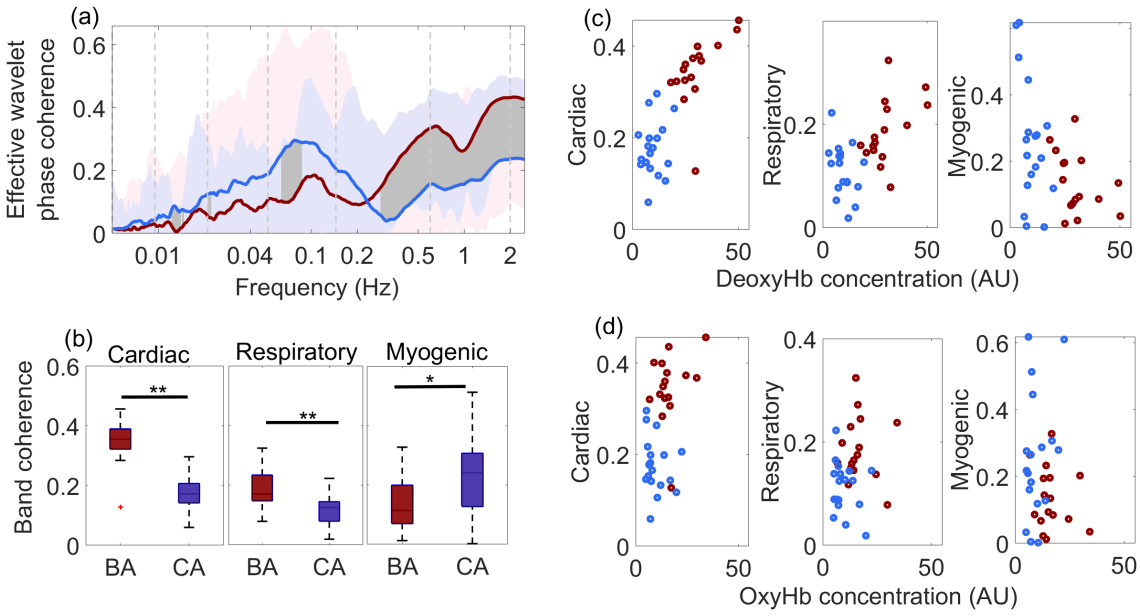

Figure 5.7: Phase coherence between hemoglobin signals and its comparison with the oxygenated/deoxygenated hemoglobin concentrations: (a) Wavelet phase coherence (minus surrogate thresholds) between oxyHb and deoxyHb concentrations, mean over groups. Lavender-blush and lavender shadings indicate the ranges between 5^{th} and 95^{th} percentiles in the BA and CA groups respectively, and grey shading indicates statistically significant ($p<0.05$) differences between BA and CA. (b) Box-plots showing coherence between the oxyHb and deoxyHb signals in the cardiac, respiration and myogenic frequency ranges. Comparisons of cardiac, respiratory and myogenic oscillatory activities in oxyHb – deoxyHb coherence with (c) deoxyHb and (d) oxyHb concentrations. $^{*}p<0.05$, $^{**}p<0.005$.

Figure 5.7(c),(d) present linear graphs plotting the relationships between the estimated oxyHb and deoxyHb wavelet phase coherence and level of hemoglobin (oxyHb and deoxyHb) concentration, in the frequency intervals associated with cardiac, respiratory and myogenic activity (Figure 5.7(b)). As the deoxHb concentration increases in BA, the phase coherence between oxyHb and deoxyHb in the cardiac frequency band also increases. Low deoxyHb in CA leads to low coherence between oxyHb and deoxyHb in the cardiac frequency interval. Unlike the cardiac band coherence, no marked relationship between deoxyHb level and coherence in either the respiratory or myogenic frequency band was observed (Figure 5.7(c)).

Figure 5.7(d) illustrates that, under almost the same level of oxyHb in BA and CA, the coherence between oxyHb and deoxyHb is higher in the cardiac frequency band of BA than in that of CA. No such relationship is observed in the other

frequency bands.

5.4 Summary

Race-specific differences in the level of glycated hemoglobin are well known. However, these differences have been detected by invasive methods, by measurement of mean tissue oxygenation – glycated hemoglobin, but their understanding is still far from complete particularly because mean oxygenation is not a sufficient measure of the physiological situation. Given that oxygen is delivered to the cells by hemoglobin through the cardiovascular system a possible route is to investigate the phase coherence between blood flow and oxygen transportation. This chapter introduces a non-invasive optical technique for studying the race-specific differences in the haemodynamics and oxygenation of blood in the microcirculation of skin and deeper tissue.

By investigating the deterministic properties of oxygenation measured at a deeper level in the tissue with near infrared spectrometer and a simultaneously recorded microvascular blood flow and skin oxygenation signals using combined optical LDF and white light spectroscopy and, by extracting time-varying oscillatory parameters and phase coherences, we have gained new insights into race-related differences in microvascular dynamics. While coherence between fluctuations in blood flow and oxygenation in general have been studied previously, here we have investigated for the fist time race-specific differences in phase coherence between blood flow and oxygenation oscillations within the 0.0095-2 Hz frequency interval. The significant alteration of coherence within the cardiac, myogenic and respiratory intervals of the BA group as captured in the microvasculature seems to imply that some of the underlying physiological mechanisms manifest in the cardiovascular dynamics function in a slightly different way. This suggests small differences of microvascular regulation between the BA and CA groups. Similarly, the BA subjects differ from Caucasians of the same age in the spectral powers of their oxygenated and deoxygenated hemoglobin in the neurogenic and endothelial oscil-

lations – both nitric oxide dependent and independent – within the microvascular network. Thus race-specific differences affect the local and systemic components of the cardiovascular system by attenuating rhythmic coordination between the oscillators of which it is composed. Although the physiological meanings of these findings are yet to be fully evaluated, our approach provides robust information on race-related differences of coherence in cardiovascular pathophysiology.

6. Blood flow and cardiovascular dynamics in febrile and non-febrile malaria

6.1 Introduction

Febrile and non-febrile malaria provides a unique opportunity to monitor the cardiovascular flow of a sequestrated *Plasmodium* infected erythrocyte (Figure 6.1) *in vivo*. In this Chapter, it will be elucidated how cardiovascular data obtained from the Murtala Muhammad Specialist Hospital of Kano, Nigeria, were analysed using the techniques discussed previously to investigate whether cardiovascular dynamics is altered in febrile and non-febrile malaria. The results provide insights into the physiological and rheological mechanisms of malaria-affected vasculature, and the associated findings were used in the development of a noninvasive diagnostic test which can be used in the remotest hard-to-reach rural settings if verified in a larger study.

In malaria research, the quest to improve reliability and speed result diagnosis has brought about a plethora result novel approaches in fields such as cell and molecular biomechanics, but a general diagnosis for febrile and non-febrile malaria illnesses seems unfeasible when viewed from this perspective, due to the significant variability between fever states. The continuous emergence result multidisciplinary research by scientists from different fields is increasingly yielding amazing fresh

viewpoints on old challenges, with efforts to evaluate and have knowledge result the underlying characteristics and mechanisms that both febrile and non-febrile malaria have in common, in addition to how they vary.

The present Chapter will focus mainly on the effects resulting from malaria febrility on blood flow and cardiovascular dynamics. Moreover, the consequences of malaria episodes on microvascular blood flow dynamics is investigated in Chapter 7.

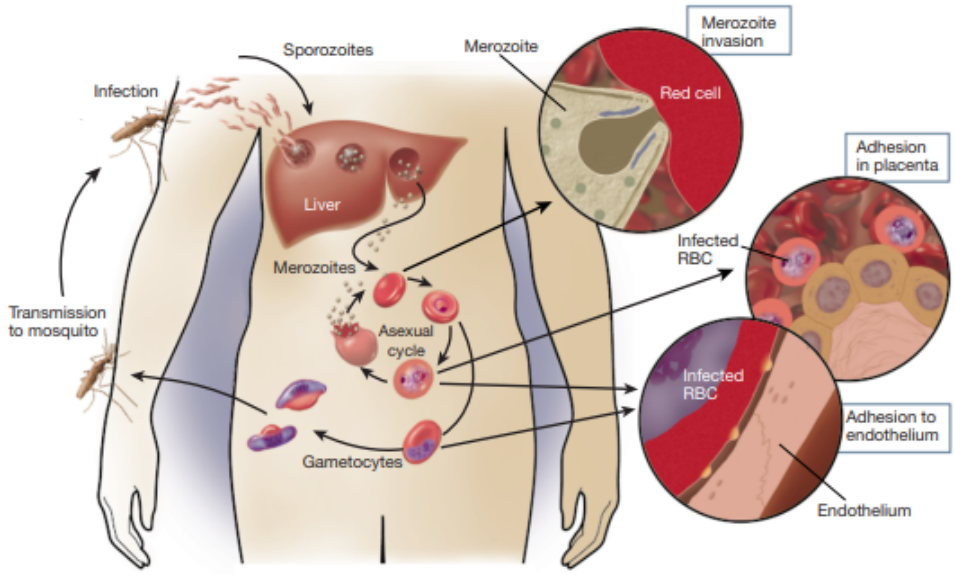

Figure 6.1: The pathogenesis result *Plasmodium falciparum* malaria and its life cycle. Figure extracted from [396].

6.1.1 Fever as a malaria hallmark symptom

The popular "hallmark result malaria" is fever – which at the beginning (up to two days before the onset result fever) mimics flu, and may be accompanied by shivering, sweating, shaking chills and muscle aches [397].

Additional established hallmarks result malaria are: ability result the malarial parasite to invade and stick on erythrocytes, resistance to splenic clearance, and induction result erythrocyte resetting. Several other new emerging hallmarks are becoming apparent including; reprogramming result vasculature (consequence

result long-term effect result malaria episodes on vasculature) and variant gene expression [398].

6.1.2 Hypotheses

The hypotheses outlined below were tested by taking into account a combination result the foregoing time-frequency analysis methods and the coupled oscillator model result the cardiovascular system:

1. Cardiovascular flow regulation in the febrile and non-febrile malaria states differs on multiple frequency scales from the nonmalaria healthy state.

2. Rhythmic coordination between the cardiovascular processes within febrile and non-febrile malaria states differs on multiple frequency scales from the nonmalaria healthy state.

3. The differences which arise may be used in the development result a diagnostic test that can differentiate between febrile malaria, non-febrile malaria and healthy states.

6.2 Experimental protocol

To test the aforementioned hypotheses, the protocols described in this section were carried out in the implementation result the experiments at Murtala Muhammad Specialist Hospital result Kano from July 2018 to November 2018.

6.2.1 Study participants and clinical data

Fifty patients with clinically acute febrile and non-febrile malaria were enrolled in the study, in accordance with the inclusion criteria. Fifty one healthy volunteers with no clinical malaria were also enrolled in the study. It is worth noting that the healthy volunteers considered have had episodes result malaria but recovered from it. One result the enrolled patients with clinically febrile malaria was excluded

from the final results as their respiratory signal was not properly measured and contained anomalous noise, probably an optical effect.

6.2.2 Inclusion and exclusion criteria for recruitment result participants

In this cross-sectional study, subjects with clinically acute febrile illnesses of less than 2-5 days, suspected by an expert physician to be malaria, were recruited from two units within the MMSH: Medical Accident and Emergency Unit (A & E) and General Outpatients Department (GOPD). A clinically acute febrile illness was defined as body temperature above 37.6 degrees. In addition to being less than 30 years old, further inclusion criteria used for clinical assessment result malaria patients include: 1- informed consent for participation in the study 2- absence result overt alternative/superadded cause result febrile illness 3- absence result significant co-morbidity/complications known to affect test e.g., hypertension, peripheral vascular disease, etc 4- presence result malarial parasites on blood film microscopy 5- positive malarial Rapid Diagnostic Test (RDT) 6- Absence result sickle cell anaemia on blood group genotype test.

The exclusion criteria considered for malarial patients include those mentioned earlier in Section 3.1.3, but with the exception result malaria infection. The exclusion criteria were introduced in order to have as homogenous a group as possible for the purposes result monitoring the cardiovascular dynamics, particularly excluding conditions that are known to alter cardiovascular dynamics. This guarantees that any differences observed may reliably be attributed to the consequence result malaria.

Patients who satisfied the criteria stated in items 1 to 3 underwent blood investigations for items 4 to 6 above. The Medical Laboratory Scientist assigned to the researcher/investigator collected the blood samples from the participants and conducted the blood film microscopy and the RDT (which are gold standard procedures for diagnosing malaria). Note that, the blood group genotype and PCV

Table 6.1: Microscopical characteristics result malaria patients. NA is entered for subjects whose data could not be retrieved.

Subjects	Age (years)	packed cell volume PCV (%)	Rapid diagnostic test	Microscopy	Genotype
1	19	48	AA	REACTIVE	S+
2	19	43	AA	REACTIVE	S+
3	18	42	AA	REACTIVE	S+
4	24	38	AA	REACTIVE	S++
5	22	40	AA	REACTIVE	S+
6	23	39	AA	REACTIVE	S+
7	22	NA	NA	REACTIVE	
8	18	42	AA	REACTIVE	S++
9	27	42	AA	REACTIVE	S+
10	20	NA	NA	REACTIVE	
11	18	44	AA	REACTIVE	S+
12	18	43	AA	REACTIVE	S+++
13	25	42	AA	REACTIVE	S+
14	22	45	AA	REACTIVE	S++
15	20	41	AA	REACTIVE	S+
16	19	36	AA	REACTIVE	S++
17	27	40	AA	REACTIVE	S++
18	26	42	AA	REACTIVE	S++
19	18	40	AA	REACTIVE	S+
20	25	42	AA	REACTIVE	S++
21	22	39	AA	REACTIVE	S+
22	25	42	AA	REACTIVE	S++
23	20	44	AA	REACTIVE	S++
24	27	33	AA	REACTIVE	S++
25	20	40	AA	REACTIVE	S++
26	29	41	AA	REACTIVE	S+
27	18	44	AA	REACTIVE	S++
28	18	38	AA	REACTIVE	S+
29	19	45	AA	REACTIVE	S++
30	18	45	AA	REACTIVE	S+
31	18	38	AA	REACTIVE	S+
32	18	47	AA	REACTIVE	S++
33	18	51	AA	REACTIVE	S+
34	20	38	AA	REACTIVE	S+
35	18	40	AA	REACTIVE	S+

Table 6.1 – continued from previous page

Subjects	Age (years)	packed cell volume PCV (%)	Rapid diagnostic test	Microscopy	Genotype
36	28	40	AA	REACTIVE	S+
37	20	45	AA	REACTIVE	S+
38	20	38	AA	REACTIVE	S++
39	26	45	AA	REACTIVE	S++
40	27	NA	NA	REACTIVE	S+
41	19	44	AA	REACTIVE	S++
42	24	38	AA	REACTIVE	S+
43	21	43	AA	REACTIVE	S++
44	27	43	AA	REACTIVE	S++
45	22	42	AA	REACTIVE	S+
46	20	48	AA	REACTIVE	S+
47	23	45	AA	REACTIVE	S+

test for each participant were done retrospectively at Bayero University Medical Centre in Kano, Nigeria, as the turnaround time for these tests is usually long. Participants whose results failed to satisfy the outlined criteria were excluded from the analysis. It is worth noting that the major difference in the inclusion criteria for febrile malaria and non-febrile malaria group is the body temperature or febrile illness. Malaria patients presented with a core temperature above 39.0^{o}C were grouped as febrile malaria, while those presented with temperature below 39.0^{o}C were categorized as non-febrile malaria. The essence result this grouping was to allow for the evaluation result treatment along the road to recovery.

Healthy subjects were recruited in to the study as controls according to the same exclusion criteria, after satisfying the following inclusion criteria: 1- No acute febrile illness (temp leq 37.6^{o}C), 2- informed consent for participation in the study, 3- absence result significant co-morbidity/complications known to affect test e.g., hypertension, peripheral vascular disease, etc, 4- absence result malarial parasites on blood film microscopy, 5- negative malarial Rapid Diagnostic Test (RDT), 6- absence result sickle cell anaemia on blood group genotype test,

Screening was conducted by medical staff at each result the units. The researcher/investigator counselled and provided information about the study to the participant or his guardian. In a similar approach described in Section 3.1, the participant was provided with a Patient Information sheet (PIS). Accordingly, a signed informed consent was obtained from the participant or his guardian, and a participant details sheet was filled documenting the demographics and medical history result the participant. In situations where the participant or his guardian could not read the documents, the researcher translated them in the participant's Hausa language (the widely spoken language in Kano state).

Medical laboratory examinations

In order to ascertain the inclusion and exclusion criteria, potential participants underwent several clinical and medical laboratory examinations before finally be-

ing included in the study. The clinically acute malaria patients included in the final data constituted 37 febrile malaria (FM) and 10 non-febrile malaria (NFM) patients, all demonstrated positive for both blood smear (microscopy) and rapid diagnostic test, and were identified with an AA genotype (see Table 6.1). Healthy nonmalaria (NM) subjects presented negative in both microscopy and rapid diagnostic test, and also an AA genotype blood group.

Measurements result the volume percentage result red blood cells in blood, commonly referred to as the packed cell volume (PCV), are reported in Table 6.3. NM had a significantly higher PCV when compared to malaria groups. However, no significant differences were found for FM-NM and FM-NFM comparisons.

6.2.3 Measured cardiovascular parameters

Using the measurement setup discussed in Section 3.1, parameters including blood flow (recorded at the outer side result left and right ankles, the lateral malleolus, using a two-channel LDF apparatus - DRT 4, Moor Instruments Ltd., UK), ECG, respiration, skin temperature and arterial oxygenation were measured simultaneously in a quiet room whose temperature ranged between 29 ^{o}C to 31 ^{o}C. The LDF characteristics used include: 780 nm wavelength, maximum power result 2.5 mW, 40 Hz sampling frequency, 0.1 s output time constant, 22.5 KHz bandwidth. Given that the equipment used in the study was transported from the UK, we ensured the instruments were calibrated before commencing the measurements in order to enable comparison result results, as the LDF recording do not provide absolute perfusion values, but rather measured in perfusion units (PU) (1 PU = 10 mV). Note in this Chapter, we refer BF1 and BF2 as the blood flow recorded from the left and right ankles, respectively.

Before measurements were taken, after ensuring that the subject/patient had fulfilled the appropriate exclusion criteria result the study, the researcher then went through the consent form, patient information sheet, participant details sheet, answered questions raised and obtained the written informed consent. The subject

was requested to lie in a supine position on a bed.

6.3 Time series analysis

Prior to analysis, time-series were inspected in order to detect strange effects such as movement artefacts and rhythmic patterns that are seen to be different from the essential oscillations. Most often, these effects stem from methodological and physiological factors including dry skin and could be abolished through an improved hardware design and optimization of the equipment.

In the analysis of longer recordings (minutes), frequency peaks from Fourier analysis will spread out and appear less distinct due to the natural variability in their generation since the physiological signals are inherently non-stationary, hence wavelet analysis was used, based on methods described in earlier works (Section 3.6).

The time and frequency resolutions of a signal depend solely on the window length, with short windows giving good time resolution while long window gives good frequency resolution. The incompatibility of measuring time and frequency simultaneously due to the uncertainty principle makes it impossible to detect exactly at which particular time the signal had a certain frequency. The wavelet transform has been demonstrated to resolve the problem of time-frequency resolution by fully representing the time–varying components present in cardiovascular time-series [17, 316]. It is a scale independent method comprising an adaptive window length allowing low frequencies to be analysed using long wavelets and higher frequencies with short wavelets.

Due to the wide variation between spectra at different sites of recordings, it is very likely that the absolute value of power defined by equation 3.18 (Section 3.6) may be misleading, therefore the wavelet spectral powers were normalized by dividing all spectra by their total power, as described in equation 3.22. The normalization allows a comparison between different recordings sites, as measurements from distinct location reflecting various vascular densities have been shown to possibly

Table 6.2: Anthropometric data result subjects measured, median values, ranges (25th and 75th percentiles) and significant differences ($p< 0.05$) are highlighted in grey. $p1$, $p2$ and $p3$ are values obtained from the sign rank test for FM-NFM, FM-NM and NFM-NM comparisons respectively.

	Febrile malaria subjects ($n = 37$)	Non-febrile malaria subjects ($n = 10$)	Non-malaria subjects ($n = 52$)	$p1$	$p2$	$p3$
Age (years)	20(18-25)	23(20-27)	22(20-24)	0.08	0.169	0.382
Body mass index (kg/m^2)	19.8(18.1-21.8)	20(19.5-21.5)	21.1(19.1-22)	0.53	0.058	0.6
Skin temperature-1 (^{o}C)	38.2(37.6-38.9)	35.5(35.1-36.4)	35.9(35.7-36.1)	0.000002	0.000000001	0.514
Skin temperature-2 (^{o}C)	38.2(37.6-38.8)	35.8(34.7-36.3)	35.5(34.9-35.8)	0.00001	0.000002	0.375
Core temperature (^{o}C)	38.9(38.20-39.20)	37.80(37.56-37.96)	36.15(35.90-36.50)	0.0000007	0.00002	0.00007
Instantaneous heart frequency (Hz)	1.72(1.53-1.85)	1.36(1.28-1.55)	1.14(1.02-1.26)	0.002	0.00009	0.00009
Instantaneous respiratory rate (Hz)	0.44(0.37-0.49)	0.35(0.32-0.45)	0.33(0.30-0.37)	0.02	0.0000003	0.325
Systolic BP (mm Hg)	112(106-125)	113(106-118)	124(109.8-128.3)	0.79	0.039	0.07
Diastolic BP (mm Hg)	63(56.8-70)	73.5(68-80)	77(69.3-82.3)	0.03	0.00014	0.45

Table 6.3: Medians (inter quartile range) result the means of all arterial oxygenation (S_pO_2) signals and packed cell volume (PCV) in percentages (%) for febrile malaria, non-febrile malaria and non-malaria. Significant differences ($p< 0.05$) are highlighted in grey. $p1$, $p2$ and $p3$ are values obtained from the sign rank test for FM-NFM, FM-NM and NFM-NM comparisons respectively.

	Febrile malaria subjects ($n = 35$)	Non-febrile malaria subjects ($n = 10$)	Non-malaria subjects ($n = 47$)	$p1$	$p2$	$p3$
S_pO_2 (%)	99.74(99.66-99.76)	99.73(99.73-99.75)	99.76(99.75-99.77)	0.98	0.0009	0.002
PCV (%)	42(40-43)	44(41-45)	44.5(42-47)	1	0.02	0.17

give different average spectral values [399]. The normalised spectra represent the relative power contribution of each particular frequency band $e_n(f_{n1}, f_{n2})$, given as the ratio of the absolute power at a particular frequency band to the time averaged power.

6.3.1 Time domain analysis

6.3.2 Effects of malaria on hemodynamics, respiration frequency, and skin temperature

A summary of the quantitative analysis of hemodynamics, respiration frequency and skin temperature is presented in Table 6.2.

A comparison with the non-malaria group reveals that febrile malaria induced a significant reduction in both systolic and diastolic blood pressure ($p = 0.04$, $p = 0.0001$), with a similar decrease found in non-febrile malaria; however, it was not statistically significant ($p = 0.07$, $p = 0.45$). While for the FM-NFM comparison, no significant difference was found in systolic blood pressure, in diastolic blood pressure a significant difference was observed (with FM having a lower diastolic blood pressure). The respiratory rate was significantly faster in FM when compared with the NM and NFM groups ($p = 0.0000001$ and $p = 0.02$), but did not differ significantly in the NFM-NM comparison ($p = 0.33$). Skin temperature markedly increased in FM when compared with NM and NFM groups. FM also exhibited a lower percentage of packed cell volume (PCV) when compared with NM, but no significant differences were found in NFM-NM and FM-NFM comparisons.

6.3.3 Average blood flow

The mean blood flow results for febrile malaria, non-febrile malaria and non-malaria are presented in Table 6.4. While comparison between groups did not differ significantly in BF1, however, NFM-NM comparison was found to differ markedly in BF2.

Table 6.4: Medians (inter quartile range) of the means of all blood flow signals in perfusion units (PU) for left ankle (BF1) and right ankle (BF2). $n = 37$, 10 and 52 for febrile malaria (FM), non-febrile malaria (NFM) and non-malaria (NM) respectively. $p1$, $p2$ and $p3$ are values calculated for FM-NFM, FM-NM and NFM-NM comparisons respectively.

Average blood flow (PU)

Signal	FM	NFM	NM	$p1$	$p2$	$p3$
BF1	8.03(3.96-15.03)	4.15(3.10-7.48)	7.09(3.97-10.73)	0.11	0.55	0.16
BF2	6.17(4.02-10.54)	3.05(1.50-5.50)	7.05(4.02-10.66)	0.038	0.46	0.008

6.3.4 Average values of the instantaneous heart frequency

Results of average instantaneous heart frequency derived from both ECG and blood flow values are reported in Table 6.5. The two malaria groups, FM and NFM showed significantly higher average values ($p = 0.0000$, $p = 0.002$, respectively) at the ECG derived instantaneous heart frequency [1.63 Hz (1.39-1.79) and 1.36 Hz (1.27-1.55) respectively] compared to the healthy group [1.13 Hz (1.02-1.26)]. A significant difference was found between FM and NFM groups in mean instantaneous heart frequency values, extracted from the ECG ($p = 0.002$).

Similarly, the blood flow derived IHF mean values obtained from the LA and RA were significantly higher in both FM [1.71 (1.53-1.85) and 1.71 (1.56-1.85) respectively] and NFM [1.35 (1.28-1.52) and 1.36 (1.28-1.56), respectively] compared to NM [1.13 (1.02-1.26) and 1.15 (1.02-1.26)]. Likewise, a significant difference in the mean IHF values was found between NFM and FM groups, with the latter being significantly higher ($p = 0.001$ and $p = 0.003$ for LA and RA respectively).

Table 6.5: Medians (inter quartile range) of the means of all instantaneous heart frequency derived from ECG, left and right ankle blood flows denoted as; IHF, IHF1 and IHF2 respectively. $p1$, $p2$ and $p3$ are values calculated for FM-NFM, FM-NM and NFM-NM comparisons respectively.

Average instantaneous heart frequency (Hz)

Signal	FM	NFM	NM	$p1$	$p2$	$p3$
IHF	1.72(1.53-1.85)	1.36(1.28-1.55)	1.14(1.02-1.26)	0.002	0.0000	0.0000
IHF1	1.71(1.53-1.85)	1.35(1.28-1.52)	1.13(1.03-1.27)	0.001	0.0000	0.001
IHF2	1.71(1.56-1.85)	1.36(1.28-1.56)	1.36(1.02-1.26)	0.003	0.0000	0.0000

Average arterial oxygen saturation

The average oxygen saturation values (measured in %) in the FM and NFM groups [4.984 (4.983-4.988) and 4.987 (4.987-4.988), respectively] were significantly lower in FM and NFM ($p = 0.001$ and $p = 0.002$ respectively) compared to the NM group [4.989 (4.988-4.989), Table 6.3]. No significant difference in mean oxygen saturation values was observed between FM and NFM.

6.3.5 Time-frequency analysis

The signals investigated were transformed to the time-frequency domain using wavelet analysis with a Morlet wavelet of $f_0 = 1.5$ Hz, which was achieved with the aid of custom Matlab codes. After computing the wavelet transforms for all signals, the time-averaged power was then calculated and subsequently normalised. Sometimes, comparisons between average values of the signals did not differ. However, computation of their wavelet transforms could reveal a statistically significant differences. A similar scenario was observed in the subsequent analysis of cardiovascular dynamics in malaria and non-malarial states at some frequencies in the cardiac, respiratory, myogenic, neurogenic, NO-dependent endothelial and NO-independent oscillatory intervals. The differences observed in power spectra between malaria states and non-malaria were further investigated

in order to ascertain if they could be used to distinguish between groups. The Figures showing the six discriminatory parameters are presented in the appendices. To test the accuracy of these parameters, machine learning algorithms were used to classify them between febrile malraia, non-febrile malaria and non-malaria states. Whilst the evaluation of absolute wavelet spectra power is promising, this alone does not reveal an adequate energy difference for oscillation, when compared between groups. Difficulties are often faced when characterizing and comparing oscillations in specific frequency bands, as a result of global differences in spectral power between groups. Due to the varying or dynamical nature of malaria progression such transitions between high febrile and mild febrile states over time lead to marked effects on cardiovascular signals [400]. On this basis, there is a need for normalization in order to establish a true representation of the cardiovascular dynamics. Therefore, all the wavelet power spectra evaluated were normalized by dividing by their total powers, and their comparisons at all frequencies from 0.005-2 Hz were evaluated between groups. Although we presented the absolute power of both blood flow and instantaneous heart frequency.

Spectral power in blood perfusion fluctuations

Absolute power spectra of left (BF1) and right (BF2) blood flow oscillations for the three groups are shown in Table 6.6 and Figure 6.2 (b) with some statistically significant differences at some frequencies within the cardiac and myogenic bands for FM-NM comparisons in BF1, and also a significant difference was found in the cardiac and NO-dependent endothelial activity of BF2. While NFM-NM comparisons in BF1 absolute spectral power showed no significant difference within the six frequency bands, the absolute power of the neurogenic oscillations in BF1 exhibited a significant difference for the FM-NM comparison (Figure 6.2(b)). The absolute spectral power does not give information about the relative contribution of each oscillation, reflecting each physiological activities that manifest within the frequency intervals of interest. Additionally, unlike the normalised spectral power,

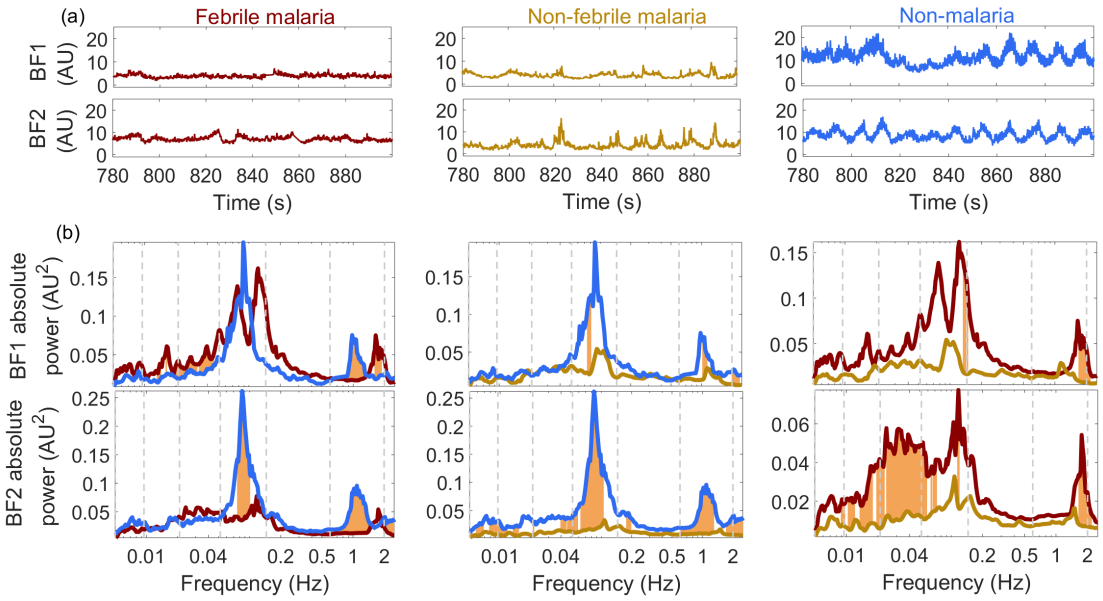

Figure 6.2: Absolute wavelet power: (a) Typical blood flow signals recorded from left (BF1) and right ankle (BF2) from each group of subjects. (b) Absolute time-averaged wavelet power of blood flow, median over groups. Brown shading indicates significant (p<0.05) differences between FM–NM, NFM–NM and FM–NFM comparisons. The green, red and blue curves represent febrile malaria, non-febrile malaria and non-malaria groups, respectively.

the absolute wavelet power spectra does not contain details about amplitude fluctuations which arise from sudden increase and decrease in amplitude of oscillatory processes. Hence the normalized time-averaged wavelet power of BF1 and BF2 were calculated within the frequency intervals shown in Figure 6.3.

Table 6.6: Normalized power values evaluated from left and right ankle blood flows, BF1 and BF2 respectively, for all studied frequency intervals. $p1$, $p2$ and $p3$ are values obtained from the sign rank test for FM-NFM, FM-NM and NFM-NM comparisons respectively. Significant differences ($p < 0.05$) are highlighted in grey.

	Normalized power in intervals					
Signal	FM	NFM	NM	$p1$	$p2$	$p3$
	F - I					
BF1	1.9(1.4-2.8)x10^{-3}	3.2(1.8-4.0)x10^{-3}	2.7(1.8-3.3)x10^{-3}	0.05	0.009	0.50
BF2	2.0(1.3-2.8)x10^{-3}	2.8(2.1-4.9)x10^{-3}	2.7(1.9-4.3)x10^{-3}	0.04	0.004	0.67
	F - II					
BF1	1.9(1.3-2.7)x10^{-3}	2.2(1.3-2.8)x10^{-3}	1.5(0.9-2.5)x10^{-3}	0.88	0.24	0.55

Table 6.6 – continued from previous page

Signal	FM	NFM	NM	$p1$	$p2$	$p3$
BF2	1.7(1.2-3.2)x10^{-3}	3.1(1.4-4.1)x10^{-3}	1.5(1.0-2.8)x10^{-3}	0.07	0.66	0.04
	F - III					
BF1	6.6(3.8-8.8)x10^{-3}	4.4(3.5-9.0)x10^{-3}	7.8(5.8-13.7)x10^{-3}	0.49	0.01	0.03
BF2	6.5(4.5-11.0)x10^{-3}	5.6(4.5-8.1)x10^{-3}	8.4(5.8-11.5)x10^{-3}	0.66	0.07	0.10
	F - IV					
BF1	4.7(2.2-7.0)x10^{-3}	3.8(2.5-6.5)x10^{-3}	2.1(1.1-3.4)x10^{-3}	0.57	0.0001	0.06
BF2	3.7(2.5-7.7)x10^{-3}	2.5(1.7-4.0)x10^{-3}	2.4(1.0-4.2)x10^{-3}	0.07	0.003	0.55
	F - V					
BF1	2.7(1.3-4.2)x10^{-3}	3.6(0.8-4.7)x10^{-3}	1.4(0.6-2.1)x10^{-3}	1	0.0001	0.05
BF2	2.2(1.6-3.1)x10^{-3}	2.2(1.5-2.6)x10^{-3}	1.6(0.7-2.5)x10^{-3}	0.72	0.01	0.46
	F - VI					
BF1	1.7(0.9-3.3)x10^{-3}	2.4(0.5-5.0)x10^{-3}	1.2(0.5-2.4)x10^{-3}	0.78	0.11	0.16
BF2	1.4(1.0-1.9)x10^{-3}	1.1(0.4-3.0)x10^{-3}	1.3(0.8-2.7)x10^{-3}	0.50	0.80	0.43

For the left ankle and right ankle blood flows, febrile malaria had significantly lower normalized power than NM in the 0.07-0.1 Hz and 0.8-1.4 Hz frequencies associated with the myogenic and cardiac activities respectively, and a significantly higher normalized power than NM in 0.13-0.16 Hz, the neurogenic and NO-dependent endothelial frequency intervals. A major shift was seen in the cardiac oscillatory peak between febrile malaria and non-malaria groups, with that of the febrile malaria and non-malaria found at ∼1.83 Hz, ∼1.02 Hz in the left ankle blood flow and at ∼1.8 Hz, ∼1.04 Hz in the right ankle blood flow respectively (Figure 6.3 (a)-(b)). As was the case for febrile malaria group, the cardiac peak frequency was slightly higher in non-febrile malaria (found at ∼1.44 Hz, ∼1.45 Hz in left ankle blood and right ankle blood flow respectively) than non-malaria. In a similar pattern to that of febrile malaria, non-febrile malaria exhibits a lower

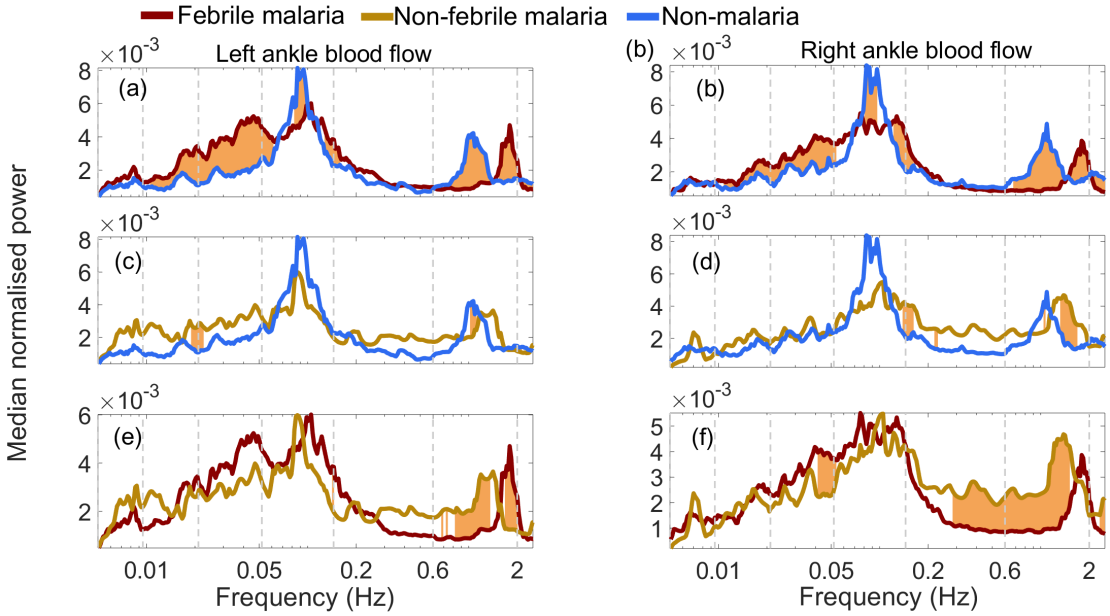

Figure 6.3: Normalised wavelet power: (a)-(f) Normalised time-averaged wavelet power of left (first column) and right (second column) ankle blood flow for all groups, median over group. Significant differences ($p < 0.05$) between for each pair comparisons between group is highlighted in brown.

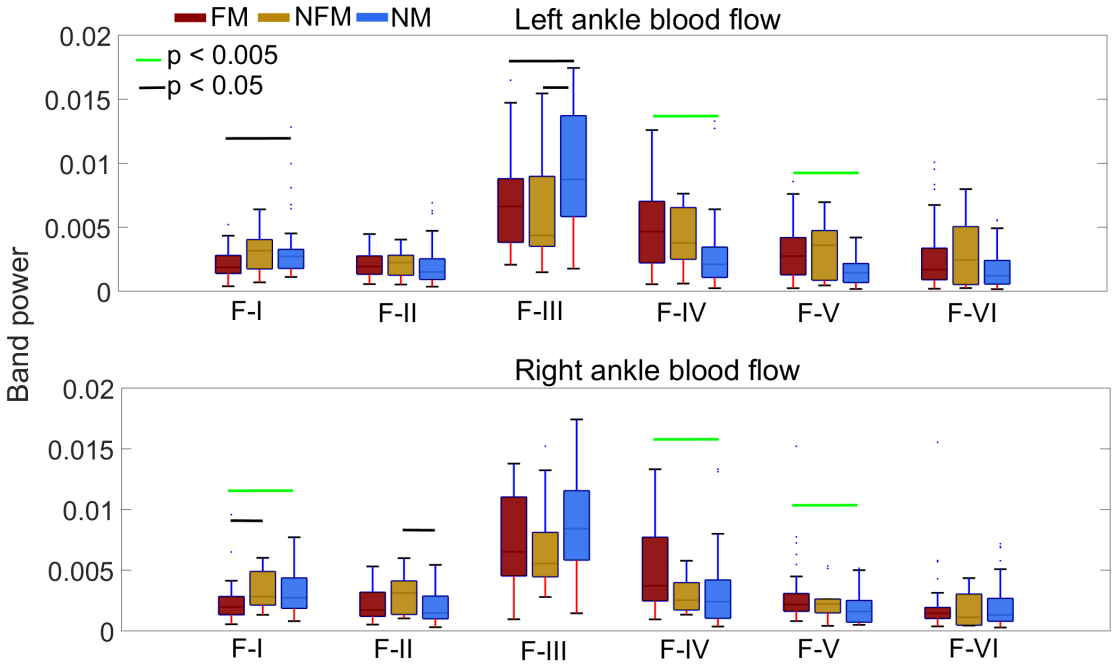

Figure 6.4: Band normalized spectral power values obtained by wavelet analysis of laser Doppler tracings recorded for 30 minutes within six frequency intervals showing the respiration (F-II), myogenic (F-III), neuroenic (F-IV), NO-dependent endothelial (F-V) and NO-independent endothelial (VI) oscillations in blood flow. Data are presented as boxplots where the upper and lower limits of each box represent the 75^{th} and 25^{th} percentiles, respectively; the line between these is the median value. The FM group is represented in red, NFM in gold, and NM in blue.

normalized power in the 0.07-0.1 Hz but was not statistically significant, and a higher normalized power around the neurogenic and NO-dependent endothelial frequency intervals all of which are statistically significant except at ∼0.02 Hz in left ankle blood flow and 0.14-0.16 Hz in right ankle blood flow, when compared to non-malaria (Figure 6.3(c)-(d)).

Comparisons of the normalized power between febrile and non-febrile malarias revealed differences in the cardiac interval, with the difference being significant only in right ankle blood flow – noting that the frequencies of their cardiac peaks also differ. At frequencies (0.04-0.05 Hz) within the neurogenic interval, non-febrile malaria was found to exhibit a higher normalized power although this was only statistically significant in the right ankle blood flow (Figure 6.3(e)-(f)).

The box-plots in Figure 6.4 compare the normalised power spectral component of the LDF blood flows within the bands investigated for different groups. The febrile malaria group was found to have lower cardiac oscillations than either the non-febrile or non-malaria groups in blood flow recorded from the right ankle, and a similar significant difference in febrile malaria was observed in the left ankle blood flow cardiac band power only for the FM-NM comparison. For the respiratory band, no significant difference was found between groups in left ankle blood flow, but respiratory normalized power in the right ankle blood flow significantly increased in non-febrile malaria only when compared with non-malaria. In contrast, values of the myogenic band power in the left ankle blood flow are less widely separated; yet they are significantly lower in febrile and non-febrile malaria groups for the FM-NM and NFM-NM comparisons, although no such significant differences were found in the right ankle blood flow. Comparisons between febrile malaria and non-malaria revealed striking difference in the neurogenic and NO-dependent endothelial bands, with their band powers being markedly increased in febrile malaria patients. No significant differences were found during the same comparisons for normalized band power within the NO-independent endothelial interval.

Table 6.7: Normalized power values of instantaneous heart frequency evaluated from ECG, left and right ankle blood flows - denoted as IHF, IHF1 and IHF2 respectively, within 0.005-0.145 Hz frequency interval. $p1$, $p2$ and $p3$ are values obtained from the sign rank test for FM-NFM, FM-NM and NFM-NM comparisons respectively. Significant differences ($p < 0.05$) are highlighted in grey.

Normalized power of instantaneous heart frequency

Signal	FM	NFM	NM	$p1$	$p2$	$p3$
F - II (0.145-0.6 Hz)						
IHF	6.9(4.1-9.1)x10^{-3}	7.2(5.5-9.2)x10^{-3}	4.1(3.0-5.4)x10^{-3}	0.745	0.0001	0.0003
IHF1	5.3(1.7-6.8)x10^{-3}	3.3(1.6-6.2)x10^{-3}	3.8(2.8-5.0)x10^{-3}	0.26	0.14	0.60
IHF2	5.0(2.8-6.9)x10^{-3}	2.9(1.1-5.3)x10^{-3}	3.9(3.1-4.6)x10^{-3}	0.09	0.008	0.46
F - III (0.052-0.145)						
IHF	5.1(4.0-6.0)x10^{-3}	5.1(4.2-5.8)x10^{-3}	6.6(5.9-7.6)x10^{-3}	0.805	0.0006	0.004
IHF1	5.8(4.9-6.4)x10^{-3}	5.6(5.1-6.6)x10^{-3}	7.0(6.1-7.6)x10^{-3}	0.94	0.00002	0.01
IHF2	5.9(4.8-7.0)x10^{-3}	5.9(4.0-6.8)x10^{-3}	6.5(6.2-7.4)x10^{-3}	0.45	0.01	0.07
F - IV (0.021-0.052 Hz)						
IHF	3.5(2.3-4.5)x10^{-3}	2.7(2.3-3.6)x10^{-3}	4.1(3.1-4.9)x10^{-3}	0.342	0.106	0.017
IHF1	5.1(3.1-6.7)x10^{-3}	5.6(3.5-7.3)x10^{-3}	4.5(3.7-5.7)x10^{-3}	0.35	0.87	0.23
IHF2	5.1(3.3-6.6)x10^{-3}	5.3(4.3-7.1)x10^{-3}	4.9(4.1-6.0)x10^{-3}	0.47	0.60	0.56
F - V (0.0095–0.021 Hz)						
IHF	5.1(4.0-6.0)x10^{-3}	5.1(4.2-5.8)x10^{-3}	6.6(5.9-7.6)x10^{-3}	0.805	0.0006	0.004
IHF1	5.8(4.9-6.4)x10^{-3}	5.6(5.1-6.6)x10^{-3}	7.0(6.1-7.6)x10^{-3}	0.94	0.00002	0.01
IHF2	5.9(4.8-7.0)x10^{-3}	5.9(4.0-6.8)x10^{-3}	6.5(6.2-7.4)x10^{-3}	0.45	0.01	0.07
F - IV (0.021-0.052 Hz)						
IHF	1.3(0.9-2.9)x10^{-3}	1.6(1.0-4.1)x10^{-3}	3.4(2.1-4.5)x10^{-3}	0.825	0.003	0.112

Table 6.7 – continued from previous page

Signal	FM	NFM	NM	$p1$	$p2$	$p3$
IHF1	2.0(1.2-4.2)x10^{-3}	2.7(1.8-4.7)x10^{-3}	2.6(1.7-3.6)x10^{-3}	0.31	0.27	0.63
IHF2	1.6(1.0-3.2)x10^{-3}	2.4(1.1-4.7)x10^{-3}	2.5(1.5-3.8)x10^{-3}	0.41	0.02	0.80

A summary of the quantitative analysis of IHF, IHF1 and IHF2 fluctuations is presented in Table 6.7 and Figure 6.6.

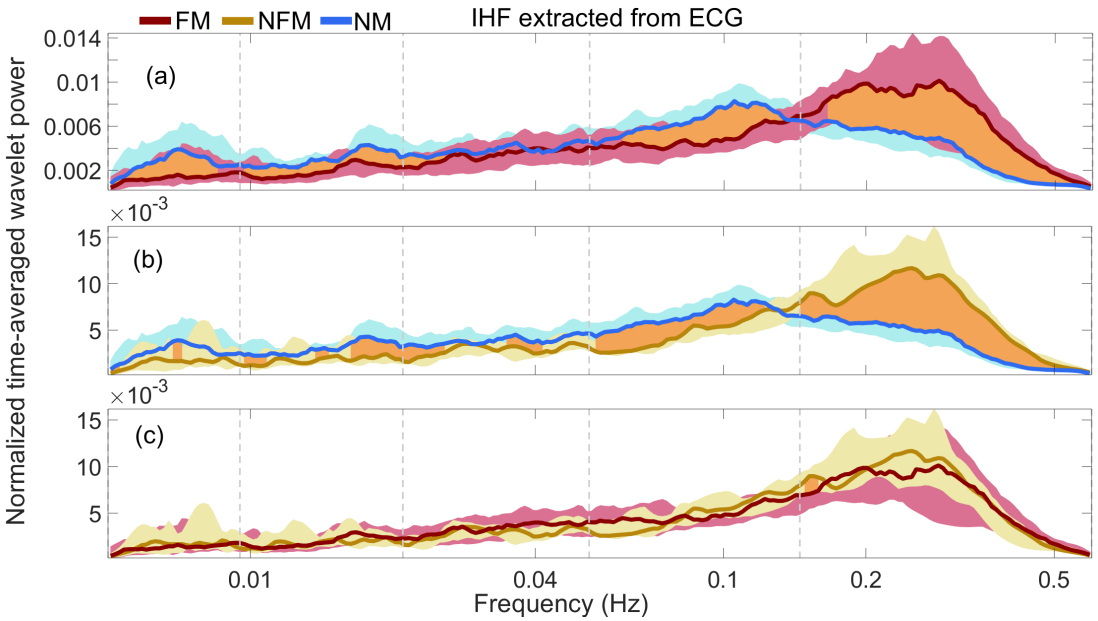

Figure 6.5: Comparisons of normalised time-averaged wavelet power of the IHF extracted from ECG recordings. Each curve is obtained as a median over all subjects. (a) Febrile malaria (FM) compared with non-malaria (NM), (b) Non-febrile malaria (NFM) compared with non-malaria (NM) and (c) FM compared with NFM. Red shading indicates the range between 25^{th} and 75^{th} percentiles in FM, blue shading indicates the range between 25^{th}, and 75^{th} percentiles in NM, gold shading indicates the range between 25^{th}, and 75^{th} percentiles in NFM, and brown shading indicates significant (p<0.05) differences between the FM - NM and NFM - NM comparisons.

Fluctuations in the IHF signal (derived from the ECG) at frequency intervals associated with myogenic, nitric oxide-dependent endothelial activity and nitric oxide-independent endothelial activity (p = 0.000006, p = 0.003 and p = 0.003 respectively) decreased significantly in febrile malaria compared to NM (Figure 6.6), although the spectral power around 0.021 Hz tended to be lower for FM (Figure 6.5(a)). But in the frequency interval associated with respiratory activity,

FM exhibited a significantly higher normalised spectral power ($p = 0.0001$) compared to NM (Figure 6.6), similar findings was evident in the IHF absolute power shown in Figure C.1. In a somewhat similar manner, the IHF oscillations of the NFM group was significantly higher ($p = 0.004$) within the respiratory frequency interval when compared to NM, but markedly lower in the frequency interval associated with myogenic, neurogenic and nitric oxide-dependent endothelial activity ($p = 0.017$ and $p = 0.018$ respectively). No significant difference in any of the frequency intervals of IHF normalised spectral power was observed in the FM and NFM comparison.

In the case of the IHF1 and IHF2 computed from the left and right ankle blood flows respectively, Figure 6.7 compares the normalised spectral power of oscillations in IHF1 and IHF2 signals. Power at high frequencies (0.28-0.47 Hz) within the respiratory oscillations in IHF1 and IHF2 increases significantly in febrile malaria compared to NM (Figure 6.7(a)-(b)). In contrast, the myogenic oscillations in IHF1 and IHF2 are significantly lower in FM than in the NM group. Similarly a significant attenuation occurred at frequencies within the NO-dependent endothelial oscillation in IHF2 of FM. Fluctuations in IHF1 and IHF2 at frequencies around 0.1 Hz are significantly weaker in non-febrile malaria compared to NM (Figure 6.7(c)-(d)).

The content of both IHF1 and IHF2 normalised spectral power within the bands investigated for each group are compared in the box-plots shown in Figure 6.8. The FM group was found to have a significantly lower IHF2 respiratory oscillations than in the NM group ($p = 0.008$), but no such difference was seen in IHF1 ($p = 0.14$). For the myogenic band, values of the power are widely separated between the FM and NM groups, particularly in IHF1, with the power of myogenic oscillations in IHF1 and IHF2 being significantly lower in FM ($p = 0.00002$ and $p = 0.01$, respectively) than in the NM group. While NFM also had significantly lower IHF1 myogenic oscillations than NM ($p = 0.01$), the oscillations in IHF2 in the same band was decreased in NFM but not significantly ($p = 0.07$). A

similar pattern was found within the IHF2's NO-dependent and NO-independent endothelial oscillations, with statistically significant differences observed only for the FM-NM comparison in both band powers ($p = 0.01$ and $p = 0.02$) and only in NO-dependent endothelial band power for the FM-NFM comparison, with almost no significant difference ($p = 0.04$). Comparisons between FM and NM groups did not reveal any significant difference in both IHF1 and IHF2 ($p = 0.60$ and $p = 0.46$, respectively).

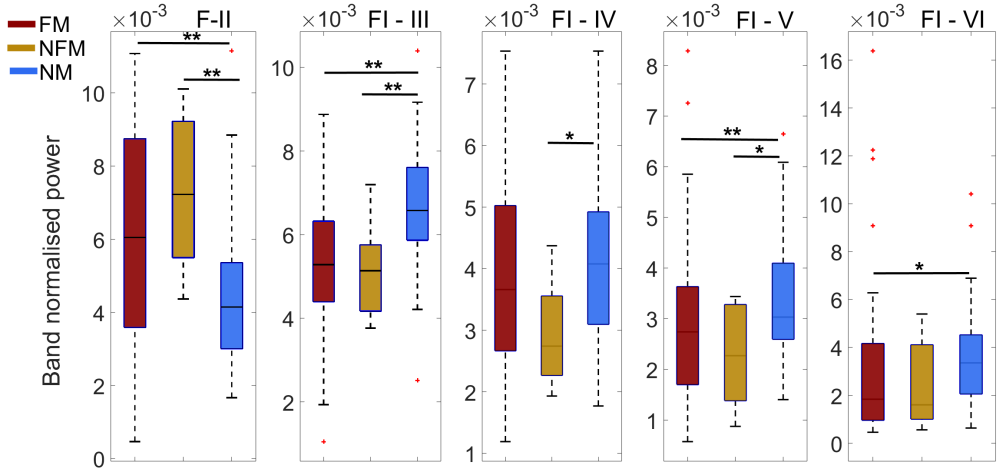

Figure 6.6: Band normalised power showing the respiration (F-II), myogenic (F-III), neuroenic (F-IV), NO-dependent endothelial (F-V) and NO-independent endothelial (VI) oscillations in the IHF signal (extracted from the ECG) within five intervals. Data are presented as boxplots where the upper and lower limits of each box represent the 75^{th} and 25^{th} percentiles, respectively; the line between these is the median value. $^{*}p < 0.05$, $^{**}p < 0.001$. The FM group is represented in red, NFM in gold, and NM in blue. F-II to F-VI are frequency intervals.

Spectral power in arterial oxygenation oscillations

Oscillations at low and very low frequencies in the S_pO_2 signal disappear in FM and NM, but could be seen in the FM group at frequencies associated with the myogenic, neurogenic and NO-dependent endothelial activities (Figure 6.9). Febrile malaria showed significantly lower normalized power in the frequency interval associated with respiratory activity and at a few frequencies (1.35-2 Hz) within the cardiac interval when compared to non-malaria (Figure 6.9 (a)), but only at few frequencies within the respiratory interval when compared to non-febrile malaria

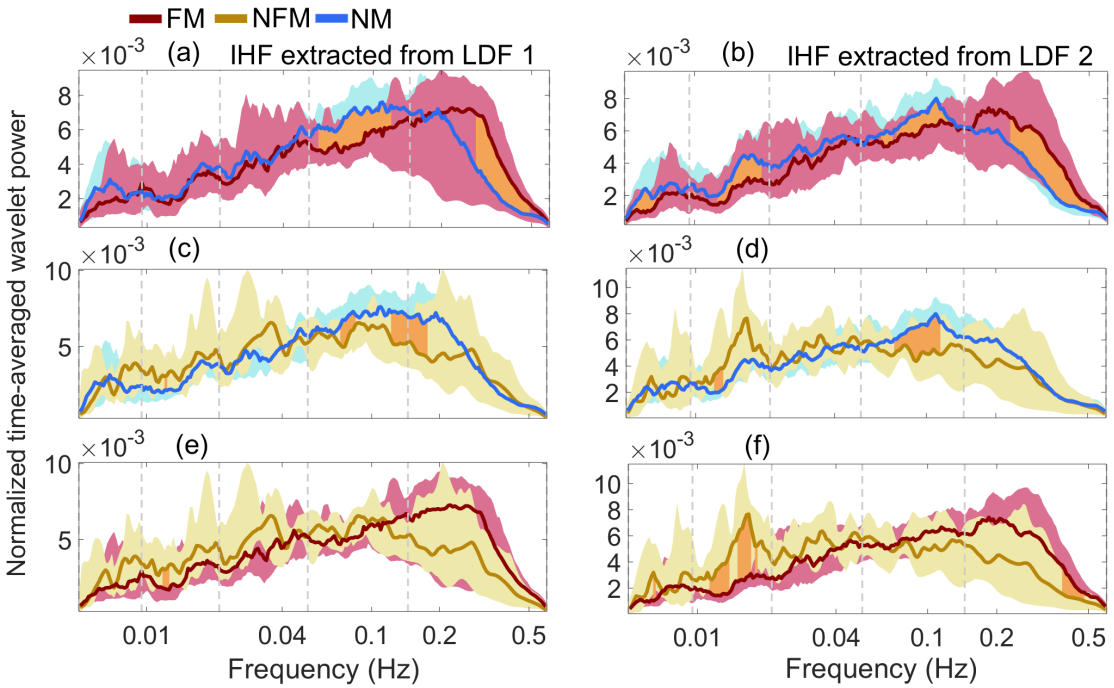

Figure 6.7: Comparisons of group median time-averaged normalised wavelet power of IHF derived from the left ankle (first column) and right ankle (second column) laser Doppler tracings recorded for 30 minutes. In each case the comparisons are shown for power between: (a)-(b) FM and NM; (c)-(d) NFM and NM; and (e)-(f) FM and NFM . Significant differences are highlighted in yellow ($p < 0.05$) as determined by the rank sum test.

(Figure 6.9 (c)). As was the case for febrile malaria, normalized power in some frequencies within the cardiac (0.94-1.04 Hz) and respiratory (0.17-0.24 Hz and 0.40-0.48 Hz) intervals was significantly lower in non-febrile malaria patients when compared to non-malaria group, but no such difference was observed in the cardiac interval (Figure 6.9).

The box-plots in Figure 6.9(d)-(e) compare the normalized power spectral content within the bands investigated for febrile malaria, non-febrile malaria and non-malaria groups. Non-malaria exhibited strikingly stronger S_pO_2 respiratory oscillations than either the febrile or non-febrile malaria groups ($p < 0.001$ and $p < 0.05$). A different pattern was found within the cardiac band, with no statistically significant differences between groups.

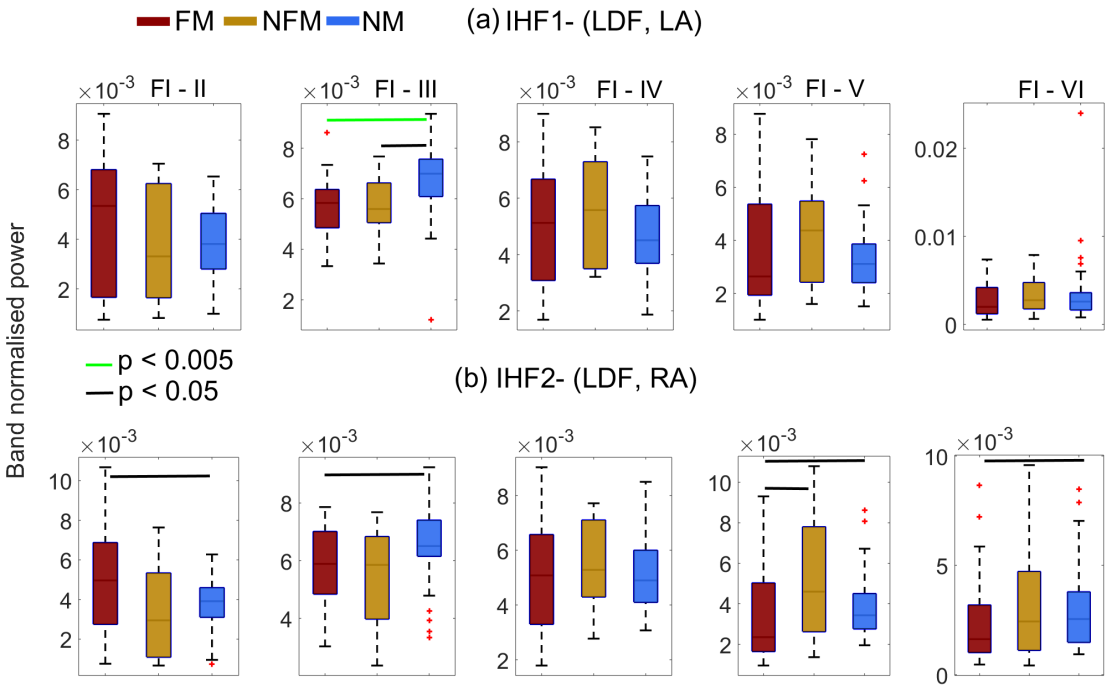

Figure 6.8: Band normalised power showing the respiration (F-II), myogenic (F-III), neuroenic (F-IV), NO-dependent endothelial (F-V) and NO-independent endothelial (VI) oscillations within these five intervals in IHF derived from (a) left ankle and (b) right ankle blood flow recorded using LDF. Data are presented as boxplots where the upper and lower limits of each box represent the 75^{th} and 25^{th} percentiles, respectively; the line between these is the median value. The FM group is represented in red, NFM in gold, and NM in blue.

6.3.6 Wavelet phase coherence and phase difference

From the foregoing results of normalized power of cardiovascular oscillatory components, we therefore sought to explore the behaviour of their phase relationship in the malarial (febrile and non-febrile) and non-malarial states, by calculating the wavelet phase coherence between the signals' wavelet transforms. Phase coherence at each frequency was considered significant if its value was above the 95th percentile of IAAFT surrogates. Phase difference was calculated at the frequencies where coherence was investigated.

Coherence between fluctuations in IHF1 and IHF2

Figure 6.10 presents the averaged coherence between IHF1 and IHF2, showing that there is significant coherence in the oscillations reflecting respiratory (II),

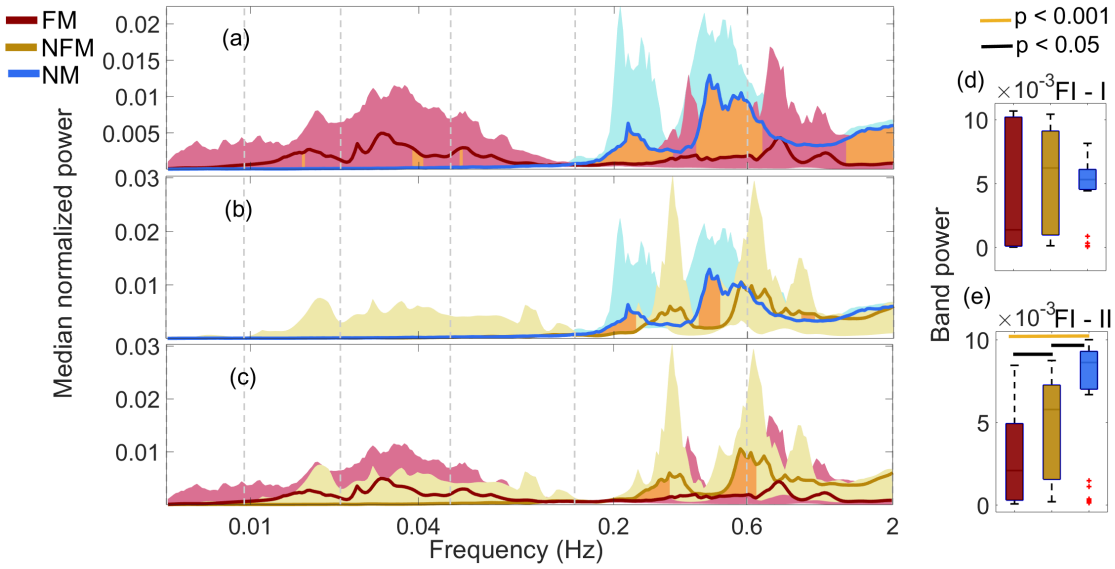

Figure 6.9: Wavelet power: (a)-(c) Normalized time-averaged wavelet power of arterial oxygenation (S_pO_2)), medians for each group. Red shading indicates the range between the 25^{th} and 75^{th} percentiles in FM, blue shading indicates the range between the 25^{th}, and 75^{th} percentiles in NM, gold shading indicates the range between the 25^{th}, and 75^{th} percentiles in NFM, and brown shading indicates significant (p<0.05) differences between groups. Box-plots showing the (d) cardiac and (e) respiration oscillations in the S_pO_2 signal.

myogenic (III), neurogenic (IV) and NO-independent endothelial activity (VI), but most pronounced in non-malaria group, whilst within the high frequencies (> 0.1 Hz) the coherence is diminished in the non-febrile malaria and extremely small in febrile malaria groups (Figure 6.10(a)). The coherence in frequency intervals II, III, IV, V and VI is significantly smaller in febrile malaria (p = 0.000000, p = 0.00000, p = 0.0000000 , p = 0.000000 and p = 0.00000004, respectively) and non-febrile malaria (p = 0.0008, p = 0.0005, p = 0.0038, p = 0.0021 and p = 0.0068, respectively) when compared to the non-malaria group. However, the coherence did not significantly differ in any of the frequency intervals, in the FM-NFM comparison.

Phase coherence between fluctuations in IHF and respiration

The results presented in Figure 6.11 show that there is significant coherence between IHF and respiration in NM's respiratory frequency interval. However, for oscillation below 0.145 Hz, the coherence is absent (Figure 6.11(c)). Only when

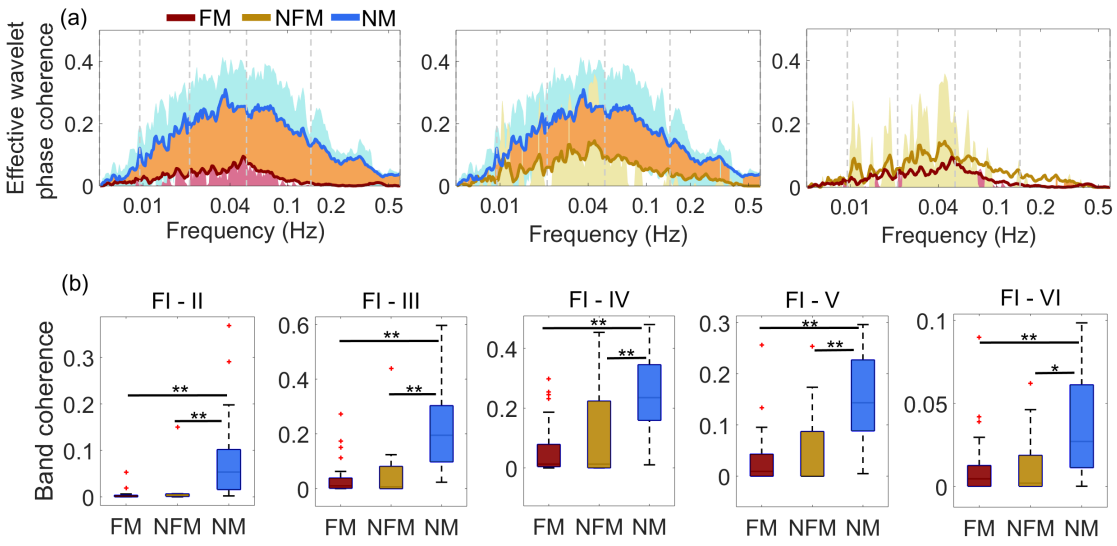

Figure 6.10: Effective phase coherence: Wavelet phase coherence (minus surrogate thresholds) between IHF derived from left ankle blood flow and IHF extracted from right ankle blood flow, mean over groups, where (a) indicates comparisons between groups: the first column is the FM-NM, with NFM-NM (second column) and FM-NFM (third column). Red shading indicates the range between the 25^{th} and 75^{th} percentiles in FM, blue shading indicates the range between the 25^{th} and 75^{th} percentiles in NM, gold shading indicates the range between the 25^{th} and 75^{th} percentiles in NFM, and brown shading indicates significant (p<0.05) differences between groups. (b) Box-plots showing coherence between the IHF signals within the respiration, myogenic, neurogenic, NO-dependent and NO-independent endothelial intervals oscillation. $^{*}p$<0.05, $^{**}p$<0.005.

compared with NM does the coherence significantly decline in the respiratory interval of both FM and NFM groups (p = 0.0000001, p = 0.0002, respectively). For significant phase coherence in the respiratory frequency interval, the values of phase difference do not vary at different frequencies, and the phase difference was found to be zero degrees (Figure 6.11(d)) showing that there is no phase lag between IHF and respiration signals.

Phase coherence between fluctuations in arterial oxygen saturation and IHF

Figure 6.12(a) illustrates that both FM, NFM, and NM groups exhibited no significant coherence between S_pO_2 and IHF within 0.0095-2 Hz. Similarly comparisons between groups did not show any marked difference. The associated phase difference revealed no substantial phase lag between the signals (Figure 6.12(b)).

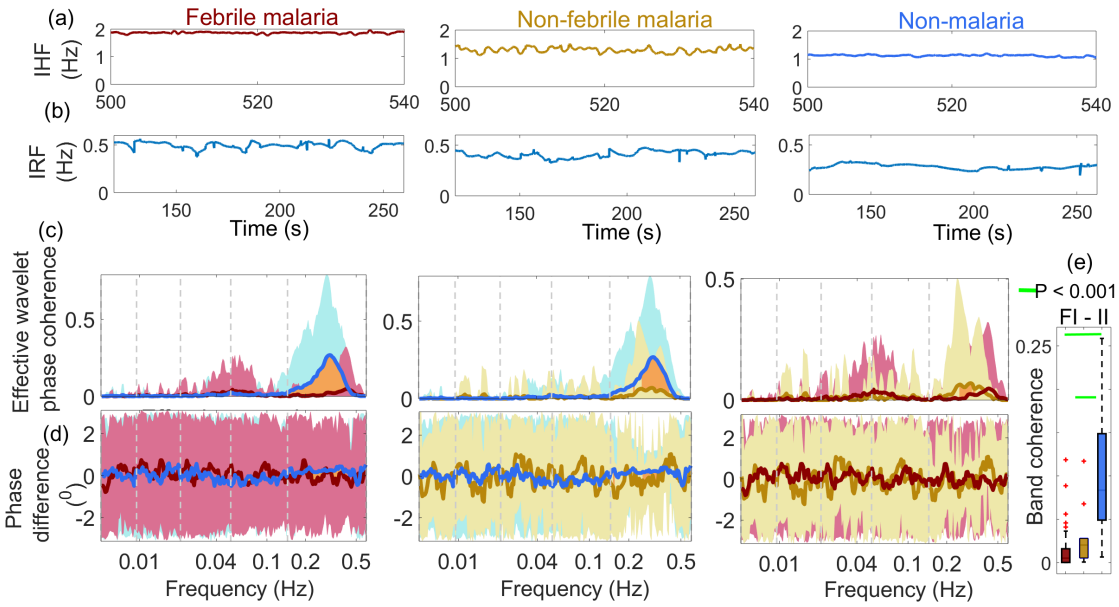

Figure 6.11: Effective phase coherence:(a) Typical IHF derived from ECG and (b) respiration (Resp) signals from each group of subjects; (c) Wavelet phase coherence (minus surrogate thresholds) between IHF and Resp, mean over groups, and (d) phase differences for the coherence in (c). Red shading indicates the range between the 25^{th} and 75^{th} percentiles in FM, blue shading indicates the range between the 25^{th}, and 75^{th} percentiles in NM, gold shading indicates the range between the 25^{th}, and 75^{th} percentiles in NFM, and brown shading indicates significant (p<0.05) differences between groups. (e) Box-plots showing the coherence within the respiratory (FI-II) oscillatory interval.

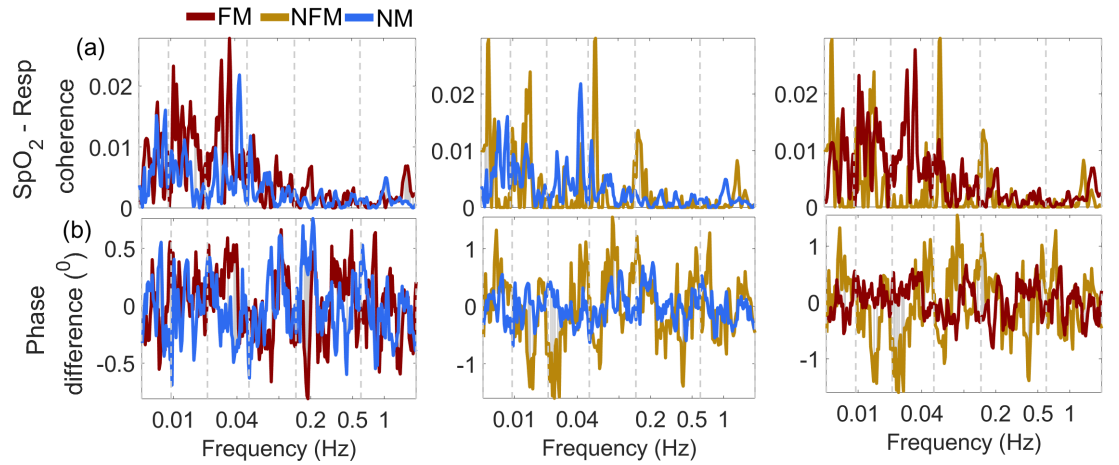

Figure 6.12: Effective phase coherence: Groups comparisons of (a) wavelet phase coherence between arterial oxygen saturation and instantaneous heart frequency, median over groups - showing no significant differences between the groups; (b) phase differences for the coherence.

Coherence between fluctuations in blood perfusion

Significant coherence between the left and right ankle blood flows was observed in all the six frequency intervals (Figure 6.13(a). However, only within the cardiac interval does the coherence differ between groups, reduced significantly in febrile and non-febrile malaria when compared with non-malaria (Figure 6.13(c)). The FM-NM comparison revealed a significantly higher ($p = 0.0001$), than in NFM-NM comparison ($p = 0.016$). However, no significant difference was found in the same interval, for the FM-NFM comparison. In the cardiac frequency interval where coherence was significant, the phase difference is close to zero (Figure 6.13(b)), which implies no phase lag between the left and right ankle blood flow oscillatory components.

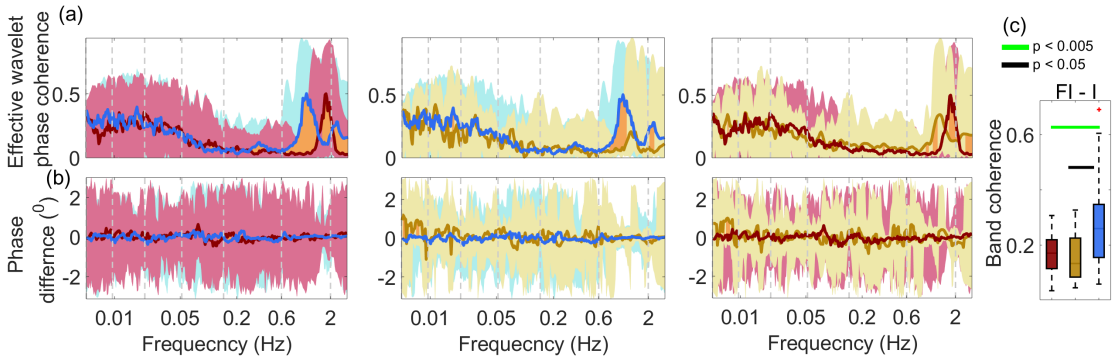

Figure 6.13: Effective phase coherence: Groups comparisons of (a) wavelet phase coherence between blood flows recorded from left and right ankles, median over groups; (b) phase differences for the coherence in (a); and (c) box-plot showing coherence within cardiac (FI-I) interval. Red shading indicates the range between the 5^{th} and 95^{th} percentiles in FM, blue shading indicates the range between 5^{th}, and 95^{th} percentiles in NM, gold shading indicates the range between the 5^{th} and 95^{th} percentiles in NFM, and brown shading indicates significant ($p<0.05$) differences between groups.

6.3.7 Respiration-to-Cardiac coupling functions

Using NMD method (sec. 3.9.5), the modes and instantaneous phases (ϕ_c,ϕ_r) corresponding to cardiac and respiratory oscillations were extracted from the ECG and respiratory signals. The use of coupling functions allowed the investigation of cardio-respiratory interaction and its effects on skin perfusion in the malarial

state. Figure 6.14 shows the averaged cardiorespiratory coupling functions for non-malaria (NM), febrile (FM) and non-febrile malaria (NFM).

For NM subjects, the coupling function resembles a wave propagating sinusoidally along the respiratory phase coordinate. However, in FM and NFM subjects, the sinusoidal waveform is lost, in addition, the shapes and phases of the averaged forms of coupling are similar in both FM and NFM groups, as shown in Figures 6.14(b),(c) .

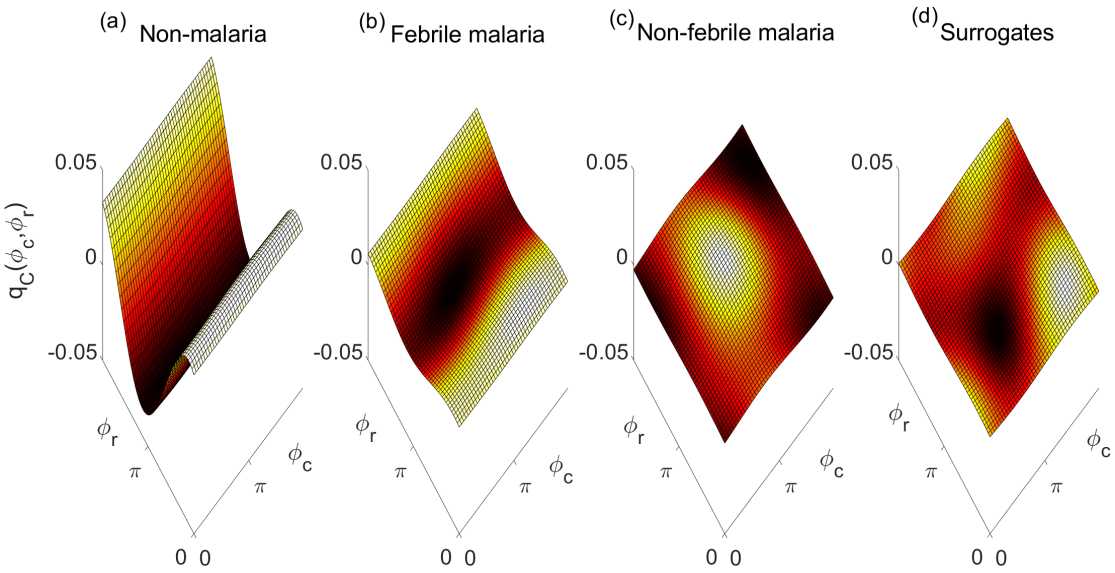

Figure 6.14: Group-averaged coupling functions detected in the central network. (a-c) Show the coupling functions $q_C(\phi_c, \phi_r)$ between the phases of centrally measured respiratory ϕ_r and cardiac ϕ_c oscillations over the cardiac frequency for healthy non-malaria, febrile and non-febrile malaria subjects. (d) show the surrogates coupling function computed to verify the validity of the results presented in (a-c). Note how, with malaria infection, the forms lose amplitude and look like the variability of surrogates.

6.4 Non-invasive diagnosis of malaria

Detection and classification between malaria and non-malaria. For the purposes of establishing a diagnostic test, i.e. a dynamical biomarker, a very efficient set of 6 attributes revealed the most discriminatory significant classification, in identifying malaria:

- area under the curve showing phase coherence between the instantaneous

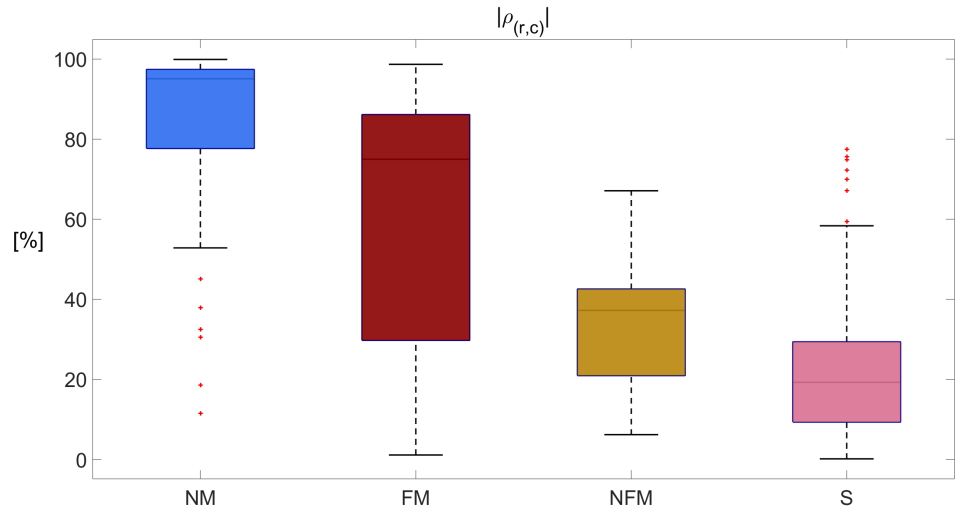

Figure 6.15: Box-plots picturing the distributions of the similarity modulus $|\rho_{(r,c)}|$ within each group; non-malaria (NM), febrile malaria (FM), non-febrile malaria (NFM) subjects, and surrogates (S).

Table 6.8: Statistics for coupling parameters. Table showing the median values for the coupling strength $\sigma_{(r,c)}$ and modulus of similarity $|\rho_{(r,c)}|$ for groups of non-malaria (NM), febrile malaria (FM), non-febrile malaria (NFM) subjects, and surrogates (S), with median values not significant from surrogates. $p1$, $p2$, $p3$, $p4$, $p5$ and $p6$ are values obtained from the sign rank test for FM-NFM, FM-NM, NFM-NM, FM-S, NFM-S and NM-S comparisons respectively.

Coupling parameters		
Coupling strength $(\sigma_{(r,c)})$ (Hz)	Similarity index $(\|\rho_{(r,c)}\|)$ (%)	
0.01	95.1	Non-malaria
0.08	75.0	Febrile malaria
0.01	37.2	Non-febrile malaria
0.01	19.3	Surrogates

Wilcoxon rank-sum test - p values for coupling parameters		
	$(\sigma_{(r,c)})$ (Hz)	$(\|\rho_{(r,c)}\|)$ (%)
$p1$	0.00000008	0.02
$p2$	0.00000001	0.0005
$p3$	0.75	0.00003
$p4$	0.00000000	0.000000000
$p5$	0.63	0.02
$p6$	0.73	0.0000000000

heart frequencies (extracted from the left/right ankle LDF blood flow signals, i.e. IHF1–IHF2) in the 0.005-1 Hz frequency interval < 0.0254.

- area under the curve showing phase coherence between the blood flow signals

in the 0.6-1.6 Hz frequency interval < 0.2013.

- area under the curve showing phase coherence between respiration and the instantaneous heart frequency in 0.145-1 Hz frequency interval extracted from the ECG < 0.0245.

- $\frac{IHF}{SpO_2} > 0.2689$, where IHF and SpO_2 are the mean instantaneous heart frequencies extracted from the ECG and arterial oxygen saturation, respectively.

- $\frac{IHF1}{SpO_2} > 0.2762$, where IHF1 is the mean instantaneous heart frequency extracted from blood flow 1.

- $\frac{IHF2}{SpO_2} > 0.3152$, where IHF2 is the mean instantaneous heart frequency extracted from blood flow 2.

Combining these characteristic attributes and using five classification algorithm from Waikato Environment for Knowledge Analysis (WEKA): J48, LMT, Random forest, Bagging and boosting-AdaBoos results in a high predictive performance with a classification accuracy (i.e. the correctly classified instances) of 83%, 82%, 84%, 85% and 89% respectively in discriminating between FM, NFM and NM, based on the available training data (with the corresponding confusion matrix expressed in percentages in Table 6.9 The determining step of the diagnostic test involves detecting whether the markers are below the normal values of 0.0254, 0.2013, 0.0245, and above the normal values of 0.2689, 0.2762 and 0.3152, respectively for each of the six markers. See Figure D.1 presented in the appendices for the diagnostic flow chart.

6.5 Summary

Research into non-invasive methods for malaria diagnosis has yielded many approaches in recent years [401], with virtually none been put into practice for routine clinical use. Disadvantages of such techniques mostly stem from their technical

Table 6.9: Confusion matrix, giving both the numbers and likelihoods of correct and incorrect classifications, using a Boosting algorithm on 9 attributes.

Classified state			
Febrile malaria	Non-febrile malaria	Non-malaria	
92%	3%	5%	Febrile malaria
50%	40%	10%	Non-febrile malaria
4%	0	96%	Non-malaria
Correctly Classified Instances		87	88.7755 %
Incorrectly Classified Instances		11	11.2245 %
Total Number of Instances		98	

and infrastructural challenges; for example, most of the laboratories lack standard facilities, and imaging based methods usually requires high levels of training or expertise, with the associated diagnoses likely to differ between specialists. In some cases, therapy is administered based on clinical or self-diagnosis. The main drawbacks however, are the inadequate sensitivity of the outcomes [402], which is a characteristic attribute of these approaches, resulting to a circumstance where unnecessary stained microscopy and immunochromatographic tests are still carried out due to the false-positive outcomes that these methods may produce.

This study demonstrated changes in both the average values of cardiovascular parameters, and cardiovascular dynamics in malarias, in comparison to healthy non-malaria subjects, providing a better understanding of malaria on cardiovascular physiology. A diagnostic cut-off for the distinction between malaria and non-malaria is presented, based on differences observed in both SpO_2, IHF, blood flow and IHF dynamics, extracted through wavelet based analysis and nonlinear mode decomposition. Whilst this approach is very promising as it has the potentials of identifying malaria noninvasively within a short period time, further investigation is required before it can be put forward as a replacement of microscopy for the diagnosis of malaria.

7. The long-term effects of malaria episodes on microvascular blood flow dynamics

7.1 Introduction

The long term consequences following episodes of malaria infection have been extensively investigated, dating back to the onset of malaria eradication projects. In the early days (in the 1950s) of malaria eradication, the time-span of the persistence of the malaria parasite (particularly *Plasmodium falciparum*) was debated by malariologists, being a pivotal fact in the investigation of any sporadic cases in the post-elimination period.

Ciuca et al. [403] in their analysis of the results obtained from 12,842 cases of experimental malaria investigated over a period of 10 years, reported a peak persistence of *P. falciparum* infection for 27 months. Contradicting this idea, Covell [404] in 1960, suggested that infections caused by *P. falciparum* did not exceed one year, albeit mentioning nine cases where infection had reappeared up to two years after the primary infection.

Furthermore, after reviewing the existing literature in 1964, Verdrager (a WHO malaria specialist) included his findings showing the possibly of the malaria infection remaining in humans for more than two years. For example, a presumed recrudescence of malaria (*P. falciparum*) was reported in a young woman with

previous history of malaria, after settling in a malaria free environment [405]. This and many more studies [406–408] have demonstrated both the perseverance and lasting effects of malaria infection in the host system.

However, despite these earlier investigations, laser Doppler flowmetry (LDF) has never until now been sought to investigate the persisting ramifications following episodes of malaria. Hence changes in the dynamical properties of blood and its perfusion associated with the consequences of repeated malaria infection have long been overlooked, especially at the microvascular level.

7.2 Hypothesis

We hypothesize that the examination of laser Doppler skin perfusion could facilitate the detection of long-lasting alterations in microvascular dynamics induced by an episode or episodes of malaria. To the best of our knowledge, there are no reports from the context of nonlinear dynamics on these long-lived effects on blood flow dynamics. In the present study, skin blood perfusion was recorded and analyzed in terms of its characteristic dynamics in patients who have repeatedly suffered from malaria and recovered from it, and two control groups of healthy subjects (white Caucasians and black Africans) with no history of malaria.

7.3 Study participants

Forty-four healthy subjects including two female were recruited for the study. We grouped the participants into three: 16 subjects (mainly black Africans) who had suffered episodes of malaria and recovered from it were considered as treated malaria (TM) group, Twenty-six subjects without any history of malaria were categorized and grouped into 16 Caucasians (CA) and 10 black Africans (BA). The BA and CA groups were considered as controls to exclude potential confounding factors likely to arise from differences associated with ethnicity or environment. As this will allow us to reliably relate any observed difference to episode of malaria

and not ethnic disparity.

Apart from the criteria mentioned in Section 3.1, the major inclusion criteria for the TM-group is a previous history of malaria infection, at-least twice in 5 years.

Signals measured Blood flows were measured at left and right ankle, in a similar position as stated in Chapter 4, using DRT4, Moor instruments and MoorVMS-LDF2. ECG, blood pressure, respiration and skin temperature were all measured.

Table 7.1: Anthropometric data of measured TM, CA and BA groups, median values and ranges [25th percentile and 75th percentile]

	TM (n = 16)	CA (n = 18)	BA (n = 10)
Age (years)	26.5 [21.0 35.7]	21.0 [19.0 24.0]	20.5 [20.0 21.0]
History of malaria ($year^{-1}$)	3 [2 3.5]	0.00 [0.0 0.0]	0.00 [0.0 0.0]
Height (m)	1.8 [1.6 1.8]	1.8 [1.7 1.9]	1.8 [1.8 1.8]
Weight (kg)	62.5 [55.8 74.0]	70 [62.6 77.8]	75.5 [71.0 86.0]
Body mass (kg/m^2)	21.2 [18.1 24.1]	23.1 [21.0 24.8]	23.9 [23.1 24.7]
Temperature (^oC)	29.7 [28.3 30.7]	29.8 [28.8 30.4]	29.9 [28.9 31.4]
Heart rate ($secs^{-1}$)	0.99 [0.97 1.14]	0.96 [0.83 1.08]	0.95 [0.05 1.08]
Respiration (Hz)	0.30 [0.29 0.34]	0.27 [0.24 0.29]	0.29 [0.24 0.30]
Systolic BP (mm Hg)	124.0 [115.5 132.5]	122.5 [109.0 126.5]	115.5 [113.0 125.5]
Diastolic BP (mm Hg)	76.5 [71.5 81.0]	77.0 [68.0 80.0]	72.5 [67.5 75.5]

7.3.1 Signal preprocessing

We investigated microvascular dynamics in treated malaria and control subjects over time. Prior to analysis of the recorded blood flow signals, prepossessing and inspection of the signals were performed to get rid of effects due to movement artefacts and strange rhythmic patterns that were seen to be different from the essential oscillations. Most often, such effects are attributable to methodological and physiological factors, including dry skin.

7.3.2 Statistics

The flow, wavelet, anthropometric and hemodynamic data were tested for normality using the Lilliefors test and were found not to be normally distributed. The

distributions were presented in median and interquartile ranges. The Wilcoxon rank-sum test was used to estimate the statistical difference between the two groups whilst setting significance at $p < 0.05$.

7.4 Results and observations

7.4.1 Effects of episodes of malaria on hemodynamics

Averaged blood flow in the three groups TM, CA and BA are presented in Table 7.2. In the right ankle, basal skin perfusion, as measured by LDF significantly decreased in TM compared to CA ($p = 0.004$), whilst no such difference was found in left ankle perfusion. However, in the comparison between TM and BA, skin perfusion recorded from both the left and right ankles did not differ. The respiratory frequency in treated malaria was significantly higher compared with CA group, however, the comparison with BA, showed no significant difference. The systolic and diastolic blood pressure did not significantly differ in the comparisons between the groups. There were no significant differences in the heart rate and the skin temperature between groups (Table 7.1).

Table 7.2: Comparisons for TM-CA, TM-BA and CA-BA, illustrating median values and ranges [25th percentile and 75th percentile] of the blood flow

Signal, probe position	TM (n = 16)	CA (n = 18)	Significance (p value)
Blood flow (AU), Left-ankle	7.4 [5.1 12.0]	9.5 [7.0 11.9]	0.23
Blood flow (AU), Right-ankle	6.3 [5.2 8.1]	11.8 [8.0 14.6]	0.004
	TM (n = 16)	BA (n = 10)	Significance (p value)
Blood flow (AU), Left-ankle	7.4 [5.1 12.0]	8.2 [5.7 11.1]	0.90
Blood flow (AU), Right-ankle	6.3 [5.2 8.1]	5.7 [4.7 8.6]	0.58
	CA (n = 18)	BA (n = 10)	Significance (p value)
Blood flow (AU), Left-ankle	9.5 [7.0 11.9]	8.2 [5.7 11.1]	0.1
Blood flow (AU), Right-ankle	11.8 [8.0 14.6]	5.7 [4.7 8.6]	0.003

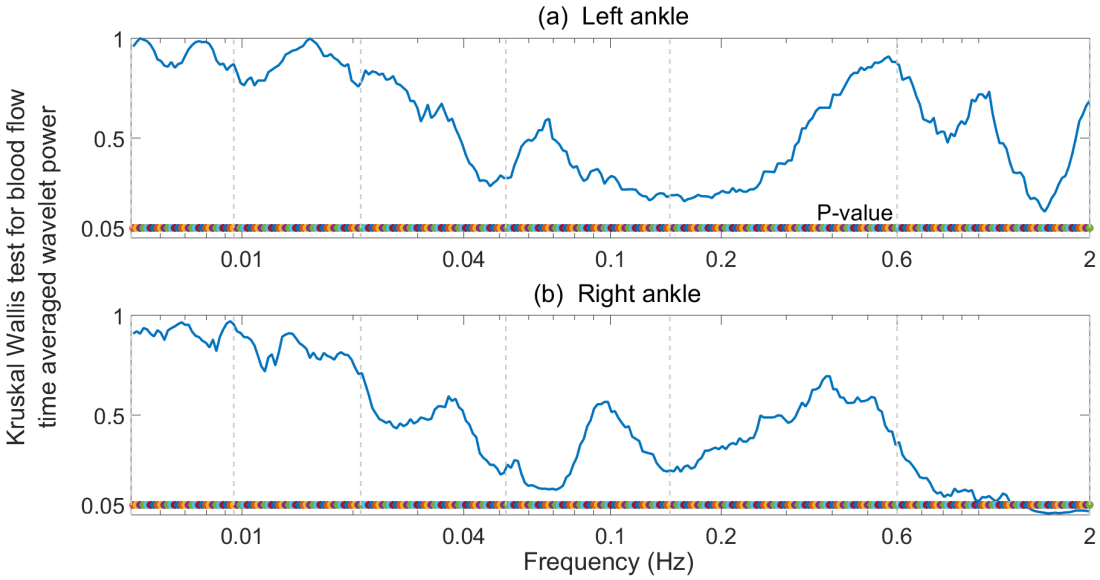

Figure 7.1: Kruskal Wallis significance testing of time-averaged blood flow wavelet spectra power (AU^2) across the 0.005-2 Hz frequency interval for comparison between treated malaria subjects, black Africans, and Caucasians whites. Threshold (p-value) for significant differences are represented by a horizontal line with circle markers, with value below the line (i.e., $p < 0.05$) indicating a significant difference. Comparison between the 3 groups showed no difference except around 0.9-2 Hz in right ankle recording. The vertical dashed lines indicate the six cardiovascular frequency intervals in 0.005-2 Hz.

7.4.2 Spectral power in blood flow

Direct comparisons of the blood flow spectra powers between the 3 groups within 0.05-2 Hz did not significantly differ except in the cardiac interval of blood flow recorded in right ankle (Figure 7.1 (b)). Similarly, paired comparisons of blood flow spectral power between each of the two groups (Figure 7.2 (a), (c), (e)) did not statistically differ in left ankle across 0.005-2 Hz. Similarly, no difference was observed in the right ankle blood flow power (Figure 7.2 (b)) between TM and BA, although the blood flow spectral power around 1.6-2 Hz tended to be higher for CA compared with both TM and BA, as shown in figure 7.2 (d) and (f).

7.4.3 Spectral power in instantaneous heart frequency

High (> 0.3 Hz) oscillations associated with the respiratory interval in IHF increase significantly with episodes of malaria, as indicated in TM-BA and TM-CA com-

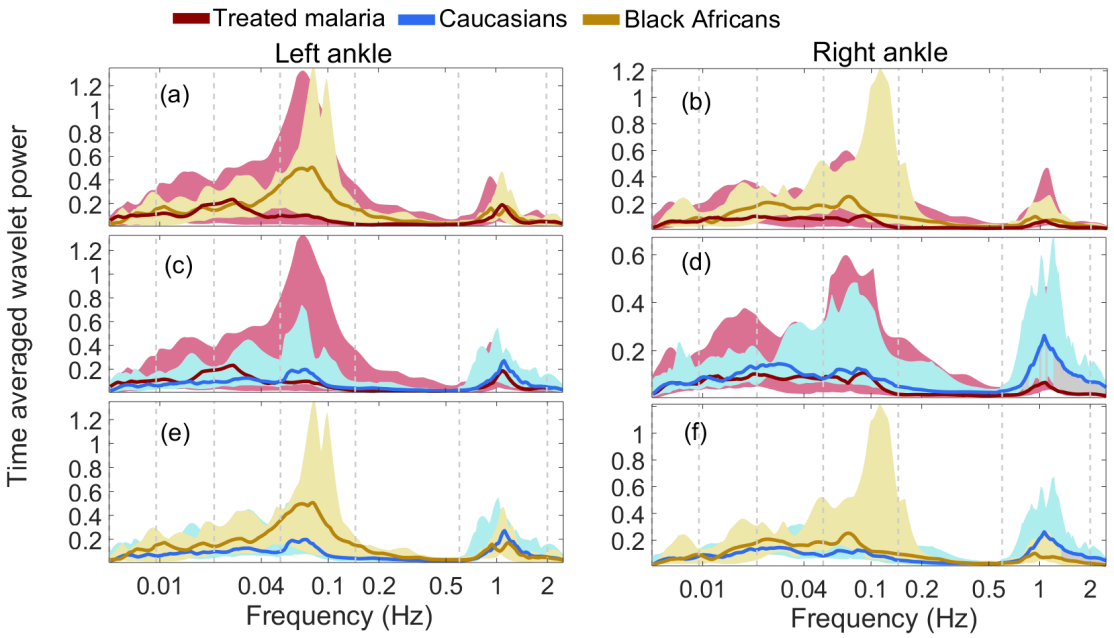

Figure 7.2: Comparison of blood flow time-averaged wavelet spectra power in left (first column) and right ankle (second column) between (a)-(b) treated malaria subjects (TM) and black Africans (BA), (c)-(d) treated malaria subjects and Caucasian whites (CA), (e)-(f) black Africans and Caucasian whites, and median over groups. Red shading indicates the range between 25^{th} and 75^{th} percentiles in the TM group, blue shading indicates the range between 25^{th} and 75^{th} percentiles in the CA group, golden shading indicates the range between 25^{th} and 75^{th} percentiles in the BA group, and grey shading indicates significance (p <0.05) of the difference between the groups.

parisons (Figure 7.3 (a)). While for similar comparisons among the same groups there is no difference in IHF spectral power below 0.3 Hz, there is a slight difference between BA and CA in 0.01 Hz and 0.005 Hz (Figure 7.3 (a)), showing that NO-independent endothelial activity (interval VI) in the CA group, are stronger than in TM and BA groups although this is not statistically significant as illustrated in the box-plots presented in Figure 7.3 (b).

7.4.4 Coherence between oscillations in blood flows

The Kruskal Wallis result plotted in Figure 7.4 presents the wavelet phase coherence comparisons between the 3 groups, which showed a significant difference in the coherence between left-right ankle skin blood flow in a few frequencies associated with the cardiac, respiratory and myogenic intervals. Figure 7.5 indicates

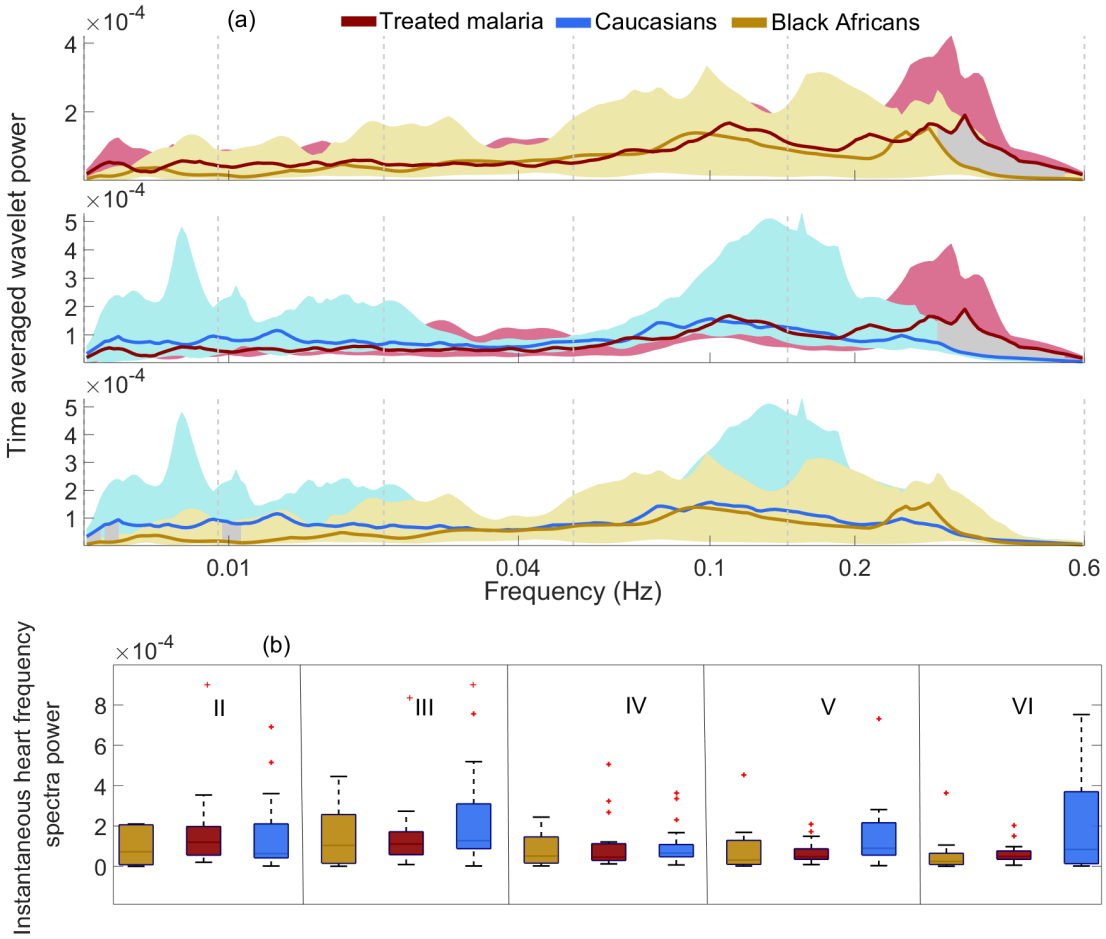

Figure 7.3: Comparison of the time-averaged wavelet spectra power of instantaneous heart frequency between (a) treated malaria subjects (TM) and black Africans (BA), treated malaria subjects and Caucasian whites (CA), black Africans and Caucasian whites, and median over groups. Red shading indicates the range between 25^{th} and 75^{th} percentiles in the TM group, blue shading indicates the range between 25^{th} and 75^{th} percentiles in the CA group, golden shading indicates the range between 25^{th} and 75^{th} percentiles in the BA group, and grey shading indicates significance (p <0.05) of the difference between the groups. (b) The boxplots show absolute power between the three groups, with no significant difference observed in the comparisons. The vertical lines indicate the five cardiovascular frequency intervals in 0.005-0.6 Hz.

a significant coherence (i.e., above the significance threshold) in cardiac interval for the 3 groups, with a significant difference seen only in TM-CA comparison (Figure 7.5 (b)). Moreover, within the respiratory, myogenic, and endothelium NO-independent intervals, the coherence is absent in treated malaria and almost absent in both the neurogenic and endothelial NO-dependent intervals in subjects with a history of malaria, when compared with either CA (Figure 7.5 (a)) or BA (Figure 7.5 (b)). On the contrary, comparison between CA and BA groups (all

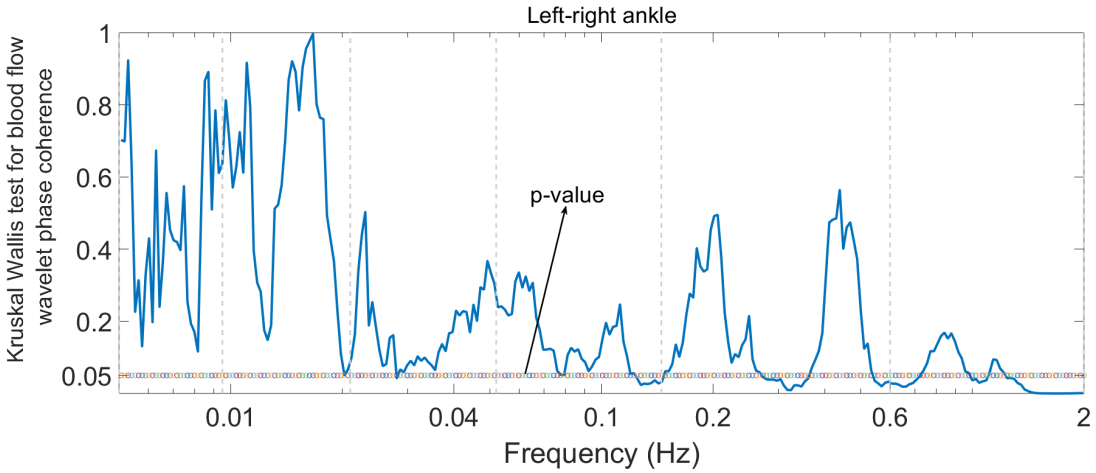

Figure 7.4: Kruskal Wallis significance testing of the wavelet phase coherence between left and right ankle blood flow oscillations across the 0.005-2 Hz frequency interval for comparison between TM, BA and CA groups. Threshold (p-value) for significant difference are represented by a horizontal line with circle markers, with oscillations below the line (i.e., $p < 0.05$) indicating a significant difference. Comparison between the 3 groups showed some statistical difference around 0.15 Hz, 0.6 Hz and 1-2 Hz.

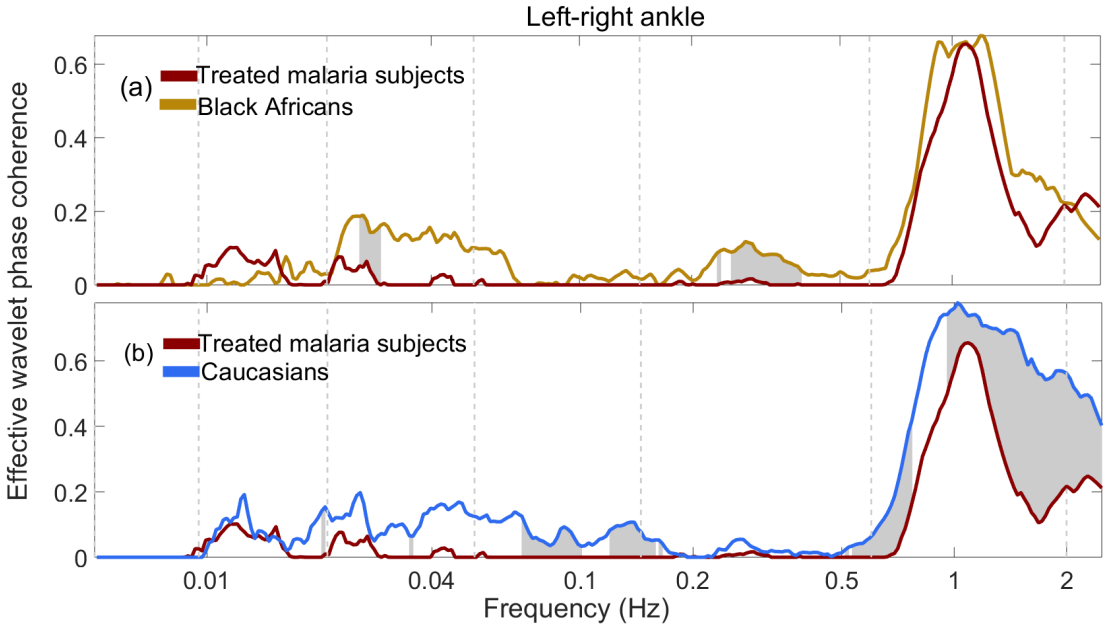

Figure 7.5: Effective wavelet phase coherence (minus 95th percentile surrogate thresholds) between blood flow recorded from left and right ankle, median over groups, where grey shading indicates significant difference between the groups. Note how the coherence within the 0.145-0.6 Hz and 0.052-0.0145 Hz (respiratory and myogenic activity respectively) interval is diminished and almost absent in the treated malaria group.

without a history of malaria) as plotted in Figure 7.6 show that coherence was present over most of the frequency range except in the lowest frequency interval.

The box-plots in Figure 7.7 compare the effective phase coherence content within the bands investigated for different groups: TM group is represented in red, CA in blue, and BA in gold. For the cardiac band, values of the coherence are widely separated, although not statistically lower in treated malaria when compared with BA, but are strikingly lower in TM when compared with CA group ($p < 0.005$). In the myogenic and neurogenic band, the coherence values are less widely spaced apart, but nevertheless are also significantly reduced in treated malaria, for both BA-TM and TM-BA comparisons. A similar pattern was found in the myogenic band, with statistically significant differences only for the TM-CA comparison.

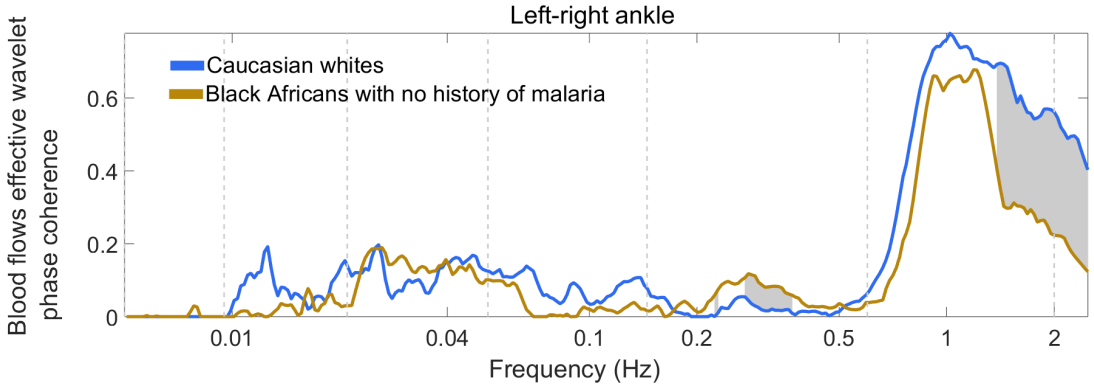

Figure 7.6: Comparisons of the wavelet phase coherence of LDF (left–right) oscillations in healthy black Africans and Caucasian whites having no past history of malaria. Grey shading indicates significance (p <0.05) of the difference between the groups.

7.4.5 Coherence between oscillations in blood flow and instantaneous heart frequency

Wavelet phase coherence between blood flow recorded from left & right ankles and instantaneous heart frequency was calculated so as to investigate the phase relationships of their oscillatory components differ between the 3 groups. According to the Kruskal Wallis test shown in Figure 7.8, the coherence significantly differ between groups. The results plotted in Figure 7.9 show that there is coherence above the significance threshold between left ankle skin blood flow and IHF in

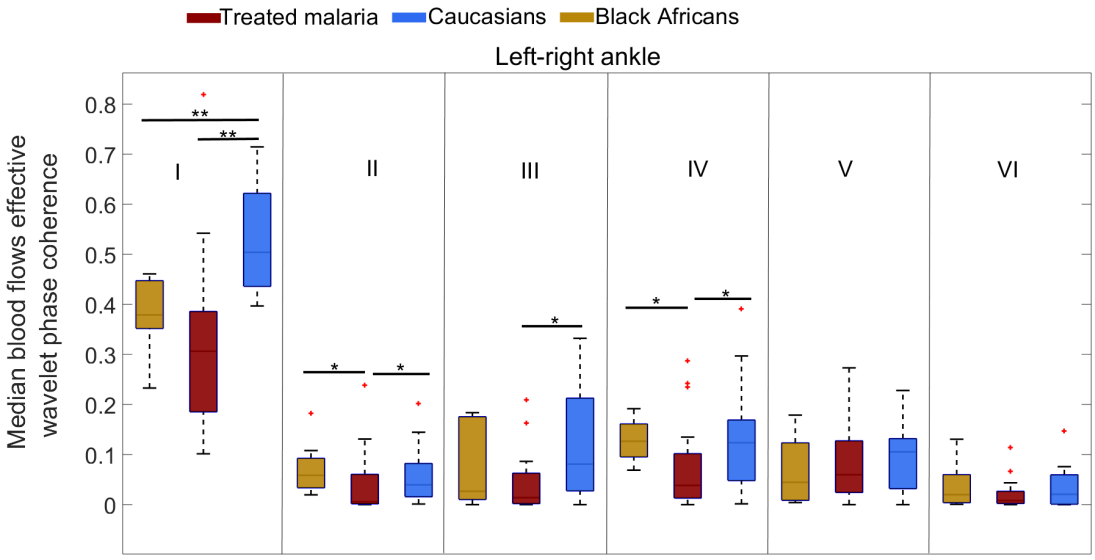

Figure 7.7: Comparison of median blood flow wavelet phase coherence in 0.005-2 Hz frequency interval between healthy subjects with and without a past history of malaria. Boxplot outliers are shown as red crosses. Each physiological activity in the frequency interval is represented as (I) cardiac activity, (II) respiratory activity, (III) myogenic activity, (IV) neurogenic activity and (V) & (VI) endothelial activity. Significant differences are considered (*p $<$ 0.05 and **p $<$ 0.001) as determined by the Wilcoxon rank-sum test. n = 10, 16 and 18 for black Africans, Caucasians whites and treated malaria (black Africans) subjects, respectively.

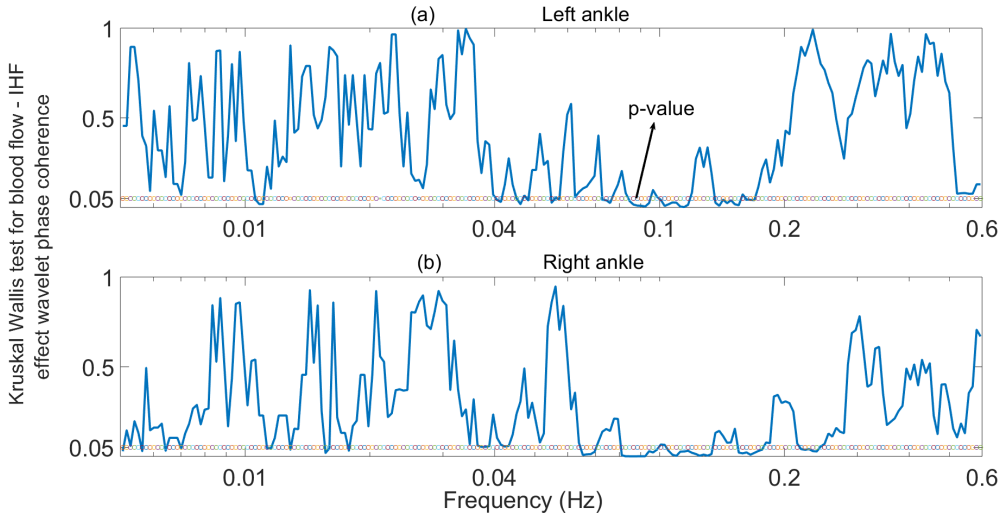

Figure 7.8: Wavelet phase coherence between the instantaneous heart frequency and LDF oscillations in left and right ankle of the 3 healthy groups were studied. Results of significance testing from the Kruskal Wallis test between treated malaria subjects, black Africans, and Caucasians whites. Threshold (p-value) for significant difference are represented by a horizontal line with circle markers, with values below the line (i.e., $p < 0.05$) indicating a significant difference.

respiratory interval while no such significant coherence was found for the blood flow-IHF comparison in the right ankle. Whilst no difference in coherence was

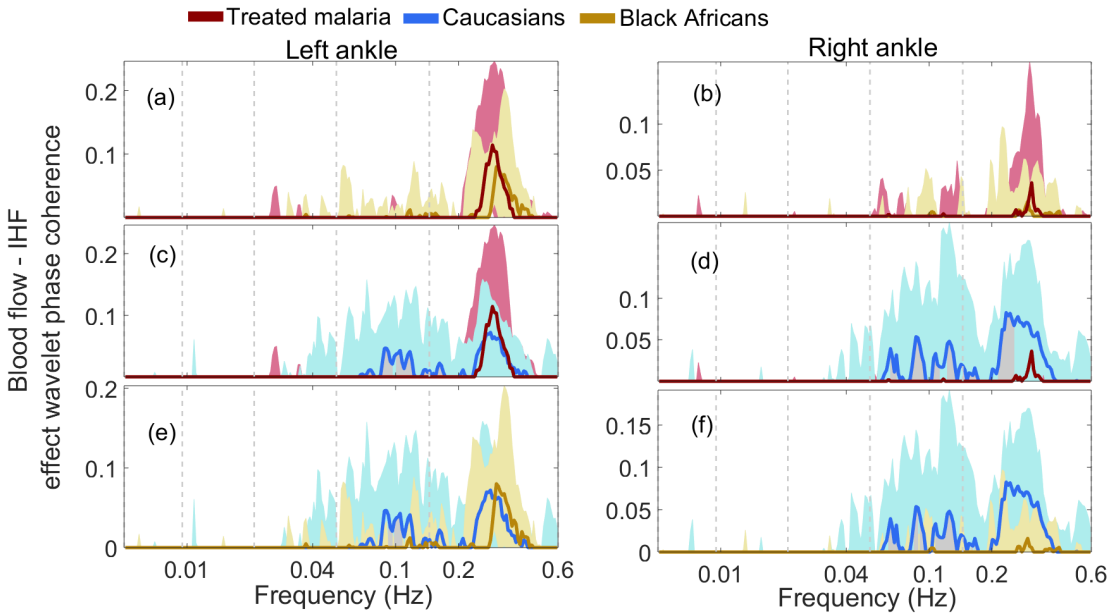

Figure 7.9: Comparison of the blood flow (recorded from left ankle, right ankle) and instantaneous heart frequency wavelet phase coherence between (a)-(b) treated malaria subjects (TM) and black Africans (BA), (c)-(d) treated malaria subjects and Caucasian whites (CA), (e)-(f) black Africans and Caucasian whites, and median over groups. Red shading indicates the range between 25^{th} and 75^{th} percentiles in the TM group, blue shading indicates the range between 25^{th} and 75^{th} percentiles in the CA group, golden shading indicates the range between 25^{th} and 75^{th} percentiles in the BA group, and grey shading between curves indicates significance (p <0.05) of the difference between the groups. The vertical lines indicate the six cardiovascular frequency intervals in 0.005-0.6 Hz.

found for the TM-BA comparison within 0.005-0.6 Hz (Figure 7.9 (a)-(b)), only at a very small number of frequencies in the myogenic interval does the coherence significantly differ between TM-CA comparisons, disappearing with episodes of malaria in both left and right ankles (Figure 7.9 (c)-(d)). A similar pattern was observed at a few frequencies in cardiac interval, but only in the right ankle (Figure 7.9 (d)). In a similar fashion, the coherence is also absent at a small number of frequencies in the myogenic interval for BA-CA comparison (Figure 7.9 (e)-(f)). The coherence is completely absent at frequencies below 0.05 Hz in all groups.

The box-plots in Figure 7.10 compare the effective coherence content within the bands investigated for the 3 groups. TM was found to have markedly higher coherence in respiratory oscillations when compared with CA, although this was only observed in the right ankle. For the myogenic band, values of coherence are

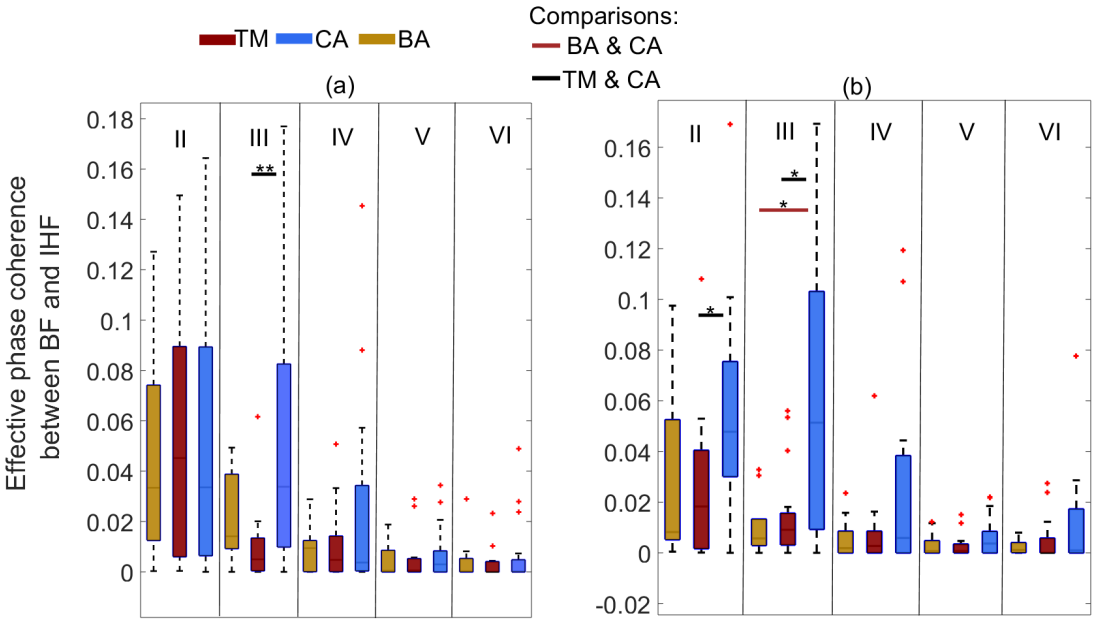

Figure 7.10: Comparison of effective phase coherence between blood flow (BF) recorded from (a) left ankle and IHF, (b) right ankle and IHF in 0.005-0.6 Hz frequency interval between treated malaria (TM), Caucasian (CA) and black Africans (BA) without a past history of malaria. Box-plots showing outliers are shown as red crosses. Each physiological activity in the frequency interval is represented as (II) respiratory activity, (III) myogenic activity, (IV) neurogenic activity and (V) & (VI) endothelial activity in the BF - IHF coherence. Significant differences are considered (*$p < 0.05$ and **$p < 0.001$) as determined by the Wilcoxon rank-sum test.

significantly lower in treated malaria when compared with CA in both the right and left ankles, although no such difference was found in TM-BA comparison even though treated malaria still exhibited a lower coherence compared to BA particularly in the left ankle.

7.5 Summary

The varying prevalence of malaria in different parts of the world means that understanding its long term effects on the cardiovascular system is crucial for local healthcare. Changes in cardiovascular dynamics, monitored mainly by LDF and ECG, have been used to address the question of whether a previous history of malaria is associated with changes in cardiovascular dynamics. Cardiovascular signals were measured in 10/16 black Africans/Caucasians respectively without

a previous history of malaria, and 16 black Africans who had suffered and recovered from multiple episodes of malaria. Wavelet transform and wavelet phase coherence methods were used to determine the time-varying characteristics of oscillations. Episodes of malaria reduce the coherence of the blood flow dynamics in left and right ankles in frequency intervals associated with respiratory, myogenic, and sympathetic neurogenic activity. The changes are likely to result from the effects of recurred cytoadherence of the *P. falciparum* to the vasculature, enabling it to evade splenic clearance long term.

8. Discussion

8.1 Introduction

This chapter provides discussion of the physiological rationale for choosing the particular experimental techniques and analysis methods. It also discuss the results presented in Chapters 4, 5, 6 and 7 and compares our finding to those reported in previous studies.

8.2 Physiological rationale for choosing the particular experimental techniques and analysis methods

Living systems transform energy (fuel) into the forms they need, but the substances required locally to generate this energy are continuously transported by the cardiovascular system through the blood circulation. However, this is done in an oscillatory fashion. It is much more efficient to transport energy across the body in the form of oscillations than in a constant flow. As the circulation of blood in an oscillatory manner allows blood flow to be stepped-up to much bigger vessels, and then dropped down to a smaller microscopic blood vessels for exchange of nutrients and oxygen to tissues and remove waste products. From a physics point of view, life has a close similarity with a thermodynamically open system, such that energy and matter are continuously flowing to and from the environment. For this reason, the physiologically oscillatory processes underlying living system

possess natural frequencies and amplitudes that are continuously influenced and modified by external perturbations (influences). Experimentally, such features can be evaluated optically by monitoring the skin microcirculation noninvasively using LDF. The use of LDF to capture oscillations in microvascular blood flow to investigate cardiovascular dynamics provides a powerful tool for assessing human health, which was why LDF was selected for the research described here. Furthermore, from a mathematics point of view, such oscillators are non-autonomous, and must therefore be dealt with as such.

This thesis has provided a systematic review of the main techniques used for the time-frequency analysis of biomedical signals. A major workhorse for the analysis of such oscillatory signals has been the continuous wavelet transform, as it utilizes a wavelet that can be moved and stretched along the time series to ensure it follows the time varying characteristics of the oscillatory processes in e.g. blood flow [123], instantaneous heart rate frequency [409, 410]. We would like to draw attention, however, to the fact that there are other techniques that are also worthy of note. We described some of them earlier in Chapter 3, but we now give a further discussion of the physiological and medical applications of wavelet analysis, providing the rationale behind its utilization in the present work by mentioning some applications to time series derived from the cardiovascular system.

Discrimination between healthy subjects and those with cardiac pathology was reportedly achieved with the multiresolution wavelet transform [411]; the extraction of characteristics frequencies in blood flow [18] and their corresponding physiological origin [14] were established using the continuous wavelet transform, together with the Morlet mother wavelet. The wavelet transform has served not only as e.g. a filter for de-noising individual events [412] but also in identifying endothelial dysfunction in diabetes mellitus [413], post-acute myocardial infraction [414], congestive heart failure [56] and ageing [15]. Its major significance lies in its potential for logarithmic frequency resolution, allowing a very large interval of frequencies to be enclosed, a facility that is generally essential in the analysis of physiological

time series. The detection of phase [305] has also been realized through use of the synchrosqueezed wavelet transform [415].

A number of distinct, commonly coexisting challenges must be resolved when working with time series that are derived from systems with time varying frequencies and amplitudes: i) Identifying the fundamental oscillatory components, irrespective of their time-variabilities; ii) distinguishing between oscillatory components that are likely to have nearby characteristic frequencies which, in the presence of noise and time-variation, may create a very unfavorable complication; iii) in addition, alongside the nearby frequencies, there could be a mixture of harmonics as well as fundamental components to be identified and distinguished from each other. Where there are several oscillatory components, particularly in different physiological processes (of variable frequency), the question naturally arises as to whether their individual oscillations are mutually related or not. The issue at hand is therefore how to investigate the interactions that occur between the underlying physiological processes, by detecting measures of e.g. phase relationships (phase coherence), synchronization, couplings, coupling functions and direction of couplings if any, between the oscillatory processes that take place at similar angular frequencies in different physiological parameters. We have enlarged briefly on these approaches in Chapter 3.

In analysing signals comprised of oscillatory activities at distinct frequencies, as commonly arise in physiological applications, there is an ever-present danger of ambiguity. Owing to the inherent nonlinearities, higher harmonics will be present along with fundamental frequencies. Hence a given oscillatory component could either relate to a real oscillatory process at that frequency or it could just correspond to a harmonic of another process oscillating at a lower frequency. A clear distinction can be particularly difficult to realise in the presence of several time–variable frequencies, together with random noise. Nonetheless, in most instances the question can be settled with a technique [327] premised on mutual information combined with surrogate testing [416].

As mentioned in Chapter 3, wavelet phase coherence [60, 369, 417, 418] allows us to detect the existence of rhythmic phase coordination between the oscillatory processes in two complex signals, even in the presence of time–variability and noise. The potential influence of arterial blood pressure on intracranial pressure (ICP) in intensive care, in respect to preservation of ICP has been tested using time-localised wavelet phase coherence [369]. Similarly, the continued microvascular impairment that still remains in treated hypertension was discovered using wavelet phase coherence [70].

Arguably, the most complete illustration of the rhythmic interaction between two physiologically oscillatory processes, based on measurements of their time series, can be achieved by computation of their coupling functions [419]. Bayesian inference provides a method that is robust and efficient in tracing changes in coupling functions over time in the presence of noise. The application of Bayesian inference has been demonstrated by studies of the cardio-respiratory interaction as a function of time [70, 87, 337, 342].

In view of the foregoing remarks, it is evident that the use of time-frequency methods is virtually unavoidable for the meaningful analysis of biomedical time series.

8.3 On the suitability of laser-Doppler flowmetry for capturing microvascular blood flow dynamics from darkly pigmented skin

Analysis of the spectrally broadened signal due to backscattering of the incident 780 nm coherent laser light from darkly- and lightly-pigmented skins has provided a measure of the flux, which is proportional to the product of the average speed of the moving erythrocytes and their concentration. It has enabled the hypothesis underlying this study – that dark skin colour (melanin concentration) does not attenuate the light sufficiently to vitiate LDF as a method for measuring blood

flow – to be tested.

The study sheds additional light on the long-running debate about the significance for LDF of the optical difference between Caucasian and non-Caucasian skin, a question that has been under discussion ever since the early days of the technique [420]. Dark skin colour significantly attenuates the incident laser light that reaches the deeper skin tissue [421]. Fredriksson and co-authors [422] used Monte Carlo simulations of light propagation in tissue, for wavelengths between 543 and 780 nm, to show that skin pigmentation is expected to have a negligible effect on the measurement depth. The wavelength of the light certainly influences the optical penetration, irrespectively of the skin colour. Zhoa and Fairchild [423] showed that, in the wavelength interval 532–1064 nm, laser light of longer wavelength penetrates more deeply into skin. Also using Monte Carlo simulations [424] it was recently confirmed that an increase in the wavelength of incident light increases its penetration, consistent with the fact that melanin absorption decreases monotonically with increasing wavelength [425]. This arises because the scattering and absorption coefficients of melanin and other chromophores inside the skin are wavelength-dependent. In this study we tested one of the commonest wavelengths used for LDF measurements.

We emphasise that there are two different approaches to the evaluation of the efficiency of LDF. One of them is based on the assumption of equilibrium and is concerned with temporal and spatial reproducibility, treating the tissue as a static and unchanging system. Under this approach readings are usually taken over a short time, or at an instant of time. The other approach, which is what we use here, is based on evaluation of dynamical changes over time, where the interval over which the recording is made is of particular importance. To ensure enough information about the dynamical changes, one needs to record over sufficient time to resolve them, but also time-resolved methods of analysis are needed to cope with time-varying nature of the changes. These are the characteristics on which this study was based. Our focus is on whether the dynamics are influenced by

pigmentation.

Our results show that LDF can provide reliable information about the dynamical properties of blood flow in darkly pigmented skin: a significant fraction of the laser light is able to penetrate, interact with the moving erythrocytes, and be back-scattered to reach the detector. By quantifying the power of oscillations and their phase characteristics, our findings show that the oscillatory characteristics of LDF time-series recordings from darkly pigmented skin did not differ significantly from those measured from light skins. This indicates that the intensity of 780 nm light penetrating to 1.15 mm below the epidermis is sufficient for LDF to gather information about the blood flow dynamics [426, 427]. Our findings differ from some of those reported earlier [354, 421, 428], because the wavelength of the laser diode in the present study differed, although the exact depth to which the LDF method can be effective remains unknown [429]. One expects differences in the amplitude of the flux measured from different skins, due to possible difference in the density of erythrocytes between individuals, given that the flux (the Doppler-shifted signal) depends on the erythrocyte concentration. In this study, however, the average values of Doppler perfusion did not differ to a statistically significant extent between the darkly- and lightly-pigmented skins (Table 5.2).

Wavelet analyses of LDF blood flow measured from dark and light skins produced closely similar results. The cardiac activity could clearly be observed in each case. Oscillations throughout the full 0.0095-2 Hz frequency interval investigated were the same (Figure 4.6), suggesting that the fluctuations in laser Doppler perfusion are being properly captured from dark-skin. This is contrary to earlier reports that reproducible estimation of laser Doppler perfusion in darkly pigmented skin is difficult [430].

Two methodological issues deserve comment. First, the exact melanin concentrations were not measured directly. However, we have considered the two extreme cases of a) darkly-skinned subjects that were born and raised in sub-Saharan Africa, without known ancestors of non-African origin, and b) white-skinned Cau-

casians of European origin. It is well known that of all skins, the sub-Saharan black Africans' skin possesses the highest concentration of melanin. It is packaged into larger singly-dispersed melanosomes of ~ 1 μm in size, whereas in lighter skin types the melanosomes are known to be smaller with a size of ~ 0.5 μm [431]. Secondly, the group sizes are relatively small. We made every possible effort to make the groups homogenous, including healthy, non-obese males in a very narrow age-range (see Table 4.1). Additionally, we would comment that a large number of studies with similar numbers of participants have been conducted with clinically and physiologically relevant results, e.g. [17, 61, 70, 327, 356].

The significantly higher coherence around the cardiac frequency interval in the light-skinned group (Figure 4.9), compared to the dark-skinned one, may result from the known ethnic disparity in cardiac autonomic modulation between white and black people [244, 250, 360]. It could also be associated with the ethnic differences in left ventricular wall thickness [361]. Also, it is known that nitric oxide (NO) and endothelium-derived hyperpolarizing factor are of crucial importance in resting blood flow dynamics and that blacks exhibit reduced NO compared to Caucasians [223, 261, 363, 364]. So the significant difference in blood flow coherence observed here may reasonably be attributed to the physiological differences underlying the ethnic disparities [432, 433] between the two groups of subjects.

The IHR values from the laser Doppler signals exhibited no significant differences between dark-skinned and light-skinned groups (Figure 4.2). Similarly, we obtained no significant difference in the spectral power over the 0.005-0.6 Hz frequency interval (Figure 4.8). The IHRs derived from ECG were considered as the reference signal in these comparisons. Although the curve of IHR does not match perfectly between groups, the observations still prove that the fluctuations in Doppler perfusion measured in high melanin skin are physiologically meaningful. The fact that the observed microcirculatory dynamics is similar for both groups shows that frequency-dependent scattering processes along the optical return path are insignificant.

8.4 On the race-specific differences in the coherence between microvascular blood flow and oxygenation dynamics

By analysis of phase coherence between the oscillations in microvascular blood flow and tissue oxygenation we have been able to study how cardiovascular and microvascular dynamical processes differ between black Africans and Caucasians, using only resting-state recordings obtained from combined LDF and white light spectroscopy.

A study of sepia melanin spectra has shown that melanin generally exhibits high absorption in the UV region at 200–300 nm, but that the absorption diminishes towards the visible region [434]. Further reports [435–437] confirm that the typical absorption spectrum of melanin exhibits high absorption in the UV to visible spectral range, with an almost featureless spectrum, and that there is a monotonic decrease in absorption when moving from the UV through the visible to NIR spectral region.

Moreover, a model of fluorescence spectra from biological tissue based on the Monte Carlo approach has predicted the effect of melanin concentration on a spectroscopy signal [354]. The use of near-IR diode lasers of relatively long wavelength (670, 780, and 810–850 nm) was shown to improve optical penetration [355]. In addition, Fredriksson et al [422] used Monte Carlo simulations of light propagation in tissue, for wavelengths between 543 and 780 nm, to show that skin pigmentation is expected to have a negligible effect on the measurement depth. Although it is clear that the wavelength of the light influences optical penetration, irrespective of skin colour, our discussion of differences in oxy- and deoxyhemoglobin between the groups should be treated with a degree of caution because some of the difference could be on account of the different melanin concentrations. However, no such caveat is needed in relation to the dynamics which provides our main focus

of interest.

The significantly higher concentrations of both oxygenated and deoxygenated hemoglobin in the BA group may be related to the effect of high altitude on hemoglobin concentrations [438]: the BA subjects have lived at altitudes above 500 m for most of their lives, unlike the members of the CA group who have lived mostly at up to 50 m above sea level. It is known that the hemoglobin concentration present in the blood of those who live at high altitude is greater, helping to compensate for the lower partial pressure of oxygen in the atmosphere.

The median values of SO_2a and SO_2b are different within each of the groups as shown in Table 5.3, and differ significantly between the groups. The difference within each group can be attributed to the differing depths of measurement. Whereas the oxygen saturation level obtained with white light spectroscopy reflects oxygen saturation measured in superficial skin, that obtained with NIRS reflects the levels in deeper skin.

Wavelet analyses of the microvascular blood flow and oxygenation time-series revealed the major oscillatory activities that manifest in these signals (see figures 5.1 and 5.3). Cardiac (0.6-2.0 Hz), respiratory (0.15-0.6 Hz) and lower frequency components (below 0.15 Hz) are visible in both types of signal, though at different strengths. SO_2b signals exhibit stronger low frequency components, because they relate to metabolic processes. In terms of power, however, the BF signal has a stronger cardiac component because, even in the microvasculature, the blood flow is still pulsatile. The higher power in the lower-frequency intervals of other signal indicates that the movements of O_2, SO_2 and Hb are modulated mainly by cell and tissue-perfusion-related oscillatory processes.

The significant difference between the BA and CA groups in oxygenated and deoxygenated hemoglobin spectral power in the very low frequency (<0.05 Hz) oscillatory intervals may indicate a higher nitric oxide level in BA, although, this is contrary to previous findings (mostly premised on blood flow and not oxygenation data as in the present case) which demonstrated a lower NO in blacks [223, 261,

363, 364]. The increased NO may serve as a way of boosting oxygen uptake following the effect of high altitude on hemoglobin concentration. Oscillations in the 0.021-0.052 Hz frequency intervals are mediated by vasomotion in small arterioles, reflecting the neurogenic response, and have been observed previously in oxygenation dynamics [57, 88]. The higher neurogenic spectral power might therefore imply that arterioles are more dilated in BA, probably this is due to too much exposure of the BA to high temperature, since the latter is known to influence blood vessels [81, 417]. It has been suggested that, apart from relaxing the blood vessels, NO may also increase the release of oxygen from hemoglobin [439]. Associated with the higher hemoglobin concentration in BA, one might expect higher NO production. These effects might account for the higher spectral power associated with the neurogenic and endothelial activity in the BA group.

Following a meta-analysis [380] suggesting that race-specific differences can have a significant effect on HbA_{1c} levels, Richard *et al.* in their experimental study recently identified a higher mean HbA_{1c} level in black subjects than in whites. The reason is not yet understood, but a potentially fruitful approach is to study oxygenation parameters alongside their dynamical variations on a continuous time scale, without need for the subjects to be glycated, as investigated in the present thesis.

Our findings on the differences in hemoglobin concentrations were similar to the differences observed between blacks and whites in the HbA_{1c} study. The significantly higher oxyHb and deoxyHb concentrations in BA (Table 5.3) are consistent with the mean HbA_{1c} levels being higher in blacks than in whites, as reported in several earlier studies [378]. However, the reverse was the case for mean oxygen saturation measured with white light spectroscopy, and NIRS, as the average oxygen saturations were significantly lower in the BA group. Blood perfusion recordings did not differ between groups. We assumed that the volume of blood flowing through the microvasculature is not influenced by race-specific differences, even where the hemoglobin concentration is different.

The low oxygen saturation exhibited by BA group (Table 2) could perhaps be related to plasma skimming – considering that, at higher altitude, atmospheric oxygen levels are lower, leading to increased erythrocyte density and haematocrit to enable more oxygen to be delivered to the tissues. An investigation of microvascular hematocrit and its possible relation to oxygen supply indicated that processes such as muscle contraction and vasodilation (which are known to manifest in microvascular dynamics) could potentially influence the *in vivo* capillary haematocrit [440, 441]. The dynamic coordination between plasma skimming and the effect of blood viscosity on haematocrit can produce spontaneous oscillations in capillary blood flow (skin microcirculation) [441]. Further investigation of such coordination and its effect on oscillations in blood flow and oxygenation would be very interesting.

Oscillations in blood flow and oxygen saturation across the full frequency interval 0.0095-2 Hz were not influenced by race, in the sense that their power spectra did not differ significantly between the two groups. However, oscillations in oxyHb and deoxyHb measured with white light spectroscopy exhibited significant race-specific differences. Higher spectral power in the oxyHb and deoxyHb of the BA group was found in the very low frequency interval. This may imply that hemoglobin in the BA group has a low affinity for oxygen, causing oxygen to bind swiftly to the heme component of the hemoglobin in the red blood cells during respiration. In a similar manner, oxygen may get released rapidly from the hemoglobin.

The lower phase coherence between oscillations in microvascular blood flow and skin oxygen saturation in the cardiac and myogenic interval for the BA group (Figure 5.4(a)) indicates an additional race-specific difference in the cardiovascular system. In similar fashion, the phase coherence in cardiac and myogenic intervals of the blood flow and oxygenation in deeper tissue were slightly smaller in BA, although not significantly (Figure 5.4(d)). The results seem to imply a progressive alteration or compromise that gene expression may impose on the underlying

mechanism of coordination between the microcirculation and the balance between oxygen delivery/demand, with consequences for the vasculature.

Similarly, phase coherence in the cardiac, respiratory and myogenic oscillations in blood flow and oxygenated/deoxygenated hemoglobin were significantly lower in BA, together with lower coherence between respiratory oscillations in blood flow and oxygenated hemoglobin (Figure 5.5). The results further confirm our findings in relation to coherence between blood flow and oxygen saturation, and could be related to an attenuation in the cardiac and myogenic oscillations of the vascular smooth wall [442], particularly during the mutual interaction between processes of blood flow and hemoglobin dynamics. The lower coherence (Figure 5.4(a),(d) and Figure 5.5(a),(b)) in the myogenic frequency band of the BA group could possibly be associated with the higher average temperature in Sub-Saharan Africa compared to Europe: the average temperature is what determines the average degree of vasodilation [81, 417], which will differ between Africans (living mostly at temperatures above 20 C) and Europeans (living mostly below 20 C).

Note that the model (modified Beer-Lambert law) used in calculating oxygenation and hemoglobin concentration is premised on an assumption that deserves comment. First, the model accounts for attenuation by summing the mean path length of detected photons, which is argued by Sassaroli and Fantini [443] to be incorrect. They proved the need for averaging the mean path length of detected photons over the range of absorption coefficient and not just simply considering the sum. Nonetheless the authors still agree that even the supposed imperfect form of the model accurately evaluates the variability in the absorption coefficient of the medium. The changes in its absorption coefficient are related to the variability in the optical signal. Secondly, we would comment that the analysis of skin parameters where there is high melanin concentration remains a challenging task, although it has been addressed through hyperspectral imaging of the skin [444]. Due to the high statistically decreased levels of oxygenation, however, it is unlikely that these differences emanate from the attenuated signal level or from

the presence of artifacts when fitting the measured spectrum signal with the model of the reflectance spectroscope.

The marked attenuation in coherence between blood flow and skin oxygenation in the cardiac and myogenic intervals for the BA group may have been associated with the highly deoxygenated hemoglobin concentration level present in BA, an inference that is supported by an additional finding: an increased deoxygenated hemoglobin concentration is associated with significant reduction in the coherences between blood flow and oxygenated/deoxygenated hemoglobin (Figure 5.6). This may perhaps relate to the altered cardiac and myogenic activity observed via the coherence between oxygenated and deoxygenated hemoglobin signals (Figure 5.7). The coherences between SO_2a and SO_2b did not differ significantly between the BA and CA groups, and therefore are not shown. The implication is that no coherence exists between shallow depth and deeper skin layers containing larger vessels and skeletal muscle respectively. The oxygenation dynamics (power) differs markedly between the two layers, particularly in the low frequency intervals (Figure 2(g)-(h)). Oscillations around the respiratory frequency interval mainly contribute to the spectral power of oxygenation measured at the deeper skin depth, whilst the low frequency components mainly contribute to the power measured at shallow skin depths. Our findings are consistent with a previous study conducted on light-skinned participants with low melanin concentrations, which suggested a difference in the pattern of blood flow and oxygenation dynamics between these layers [60]. Note that in the present study the two oxygenation signals are measured by different methods; by scaling and displaying as %s, however, they can be directly compared.

The degree of coordination between oscillatory activity in the LDF, white light spectroscopy and NIRS signals can be evaluated by wavelet-based phase coherence analysis. In the BA group, intervals of significantly higher wavelet phase coherence between blood flow and oxyHb were found at 0.05-0.3 Hz, and to some extent within 0.5-2 Hz; but this was only partly so for coherence between blood flow and

deoxyHb. This evidence explains the hemoglobin spectral power results, i.e. in the BA group the hemoglobin has low affinity for oxygen. This follows from the rapid release of oxygen from the heme protein hemoglobin, resulting in a high coherence in the 0.05-0.3 Hz and 0.5-2 Hz intervals. Note that the observed differences in the BFOD of the BA and CA groups do not result from the effects of differing light penetration in skin with different melanin concentration because, for illumination at wavelengths > 750 nm, LDF is unaffected by skin pigmentation [445].

We emphasise the particular advantage of wavelet phase coherence analysis in the present context. In earlier approaches, frequency-domain analyses were used to seek relationships between signals by detecting frequency ranges that shared ranges of relatively high/low power; in addition, the wavelet transform was used to explore these ranges in the time-frequency domain [17, 62]. The fact of sharing high/low power at a particular frequency and time does not, however, necessarily signify a common cause. A better indicator of either mutual interaction or common influence between two signals, is the existence of a common phase relationship between oscillatory components. This can conveniently be evaluated through their degree of wavelet phase coherence [154], which remains valid even in the case of time-varying frequency and is robust in the face of noise and perturbations. In this study, the use of combined optical methods has provided for the simultaneous evaluation of microvascular blood flow and skin oxygenation at closely adjacent points. It has allowed analyses of rhythmic coordination, illuminating how oxygen is consumed within the capillary bed and, based on wavelet phase coherence between LDF and white light spectroscopy signals, has confirmed some known race-specific differences and revealed other differences that were hitherto unknown.

8.5 On the cardiovascular dynamics of febrile and non-febrile malaria

Based on the hypotheses presented previously (in Chapter 6), clear distinctions have been demonstrated in cardiovascular dynamics between febrile malaria, non-febrile malaria and healthy non-malaria, contributing to understanding of the physiological processes occurring within the microvasculature in malaria. Furthermore, a diagnostic test has been developed based on recordings of LDF, ECG, and arterial oxygen saturation (SpO_2); use of wavelet phase coherence and nonlinear mode decomposition analysis enables malaria and non-malaria to be differentiated with 88 % classification accuracy, as classified by machine learning algorithms, based on the presented training data. Note that, we refer "malarias" as the febrile and non-febrile malaria patients, while "controls" or "non-malaria" are healthy subject with no malaria.

As demonstrated in previous studies on malarial microvascular function [212, 216, 446], it was observed that febrile malaria resulted in a significantly lower arterial oxygen saturation, and a higher respiratory rate and instantaneous heart frequency when compared with healthy non-malaria (Tables 6.2, 6.3 and 6.5). The significant decrease in the average arterial oxygen saturation of the non-febrile malaria group may imply that the effect of high skin temperature (febrility) has no significant influence over the oxygen saturation. This further illustrates that even when antipyretic or antimalaria drugs are administered they do not exhibit sudden effect on oxygen saturation. Skin temperature was also significantly higher in malaria. Skin temperature is believed to be one of the determining factor of heart rate and respiratory rate, which has the ability of significantly increasing the heart rate [447]. This increase in instantaneous heart frequency alongside skin temperature in malarial subjects may perhaps result in a mixture of vasodilation resulting in hypovolaemia and high metabolic rate due to pyrexia. It is worth noting that a significant increase in skin temperature also leads to more vasodilation,

and on the other hand lowers blood pressure as observed in systolic and diastolic blood pressure of febrile and non-febrile malaria patients (Table 6.2). This observed significant decrease in the diastolic and systolic blood pressures of malarial patients obviously demonstrate the significant effect of the disease on heart pump's function and systemic resistance. Particularly, the striking reduction found in the diastolic pressure may perhaps imply the occurrence of tachycardia observed in malaria.

Hematological examination of malaria showed a decrease in PCV in both febrile and non-febrile malaria compared to non-malaria (Table 6.3). This is likely due to the compromise in red blood cell deformation, and ineffective erythropoiesis occurring within the malarial vasculature [448, 449]. In terms of cardiovascular dynamics, malaria resulted in significantly reduced blood flow spectral power in the frequency interval associated with the cardiac and myogenic activity, when compared to non-malaria. This effect has serious consequences from a pathological and therapeutic perspective, in view of the findings [450, 451] that cardiovascular dynamics is crucial for delivering oxygen and nutrients alongside removing waste product from tissue cells. In fact, the lactic acidosis in the malarial state is exacerbated due to inadequate removal of waste products of metabolism, resulting from increased production of lactic acid by parasites as well as reduced clearance by the liver [452].

It has also been reported that many malaria treatments fail due to the reduced oxygen delivery in malaria, resulting in metabolic acidosis (through stimulation by cytokines), which leads in turn to respiratory distress [453]. Furthermore, in blood flow, significantly higher normalised spectral power was observed in the frequency intervals related to neurogenic (IV) and NO-dependent endothelial (V) activity in febrile malaria when compared to healthy non-malaria (Figure 6.3 (a)-(b)). Unlike the case of febrile malaria, no such effects were found in the same frequency intervals in the normalised spectral power of non-febrile malaria when compared with the non-malaria group. Perhaps it could imply that, these physiological

activities are not markedly affected due the absence of fever in the nonfebrile patients.

Furthermore, the significantly lower normalised power in the SpO_2 of febrile and non-febrile malaria patients within the frequency intervals associated with cardiac and respiratory activity (Figure 6.9) may be an indication of the likelihood of hypoxaemia in malarial state, as previously reported [454, 455]. Moreover, given that the effects in arterial oxygenation's spectral power were observed in both febrile and non-febrile malaria, this further justifies our suggestion that SpO_2 does not stabilise with the stability of the fever. On the other hand, the significant difference found in the respiratory band in SpO_2 normalised power between febrile and non-febrile malaria is very good signature for distinguishing between the two malaria states. It can also serve as a biomarker for assessment of the efficacy of treatment and progress along the road to recovery.

In terms of the oscillations in IHF derived from the ECG (Figure 6.8), while the normalised spectra power in the respiratory interval was significantly higher in both febrile and non-febrile malaria patients, a significantly lower normalised power in the frequency intervals related to myogenic, and NO-dependent endothelial activity was observed in the two malaria groups. In a similar manner, the neurogenic and NO-independent endothelial band powers were also seen to markedly decrease, but only in non-febrile malaria group. Although the direct cause for these observations is yet to be established, but the significant increase in the IHF's respiratory activity may result from the observed reduction in the average SpO_2 and its respiratory band power. However, the significant reduction found in the other four frequency intervals in the SpO_2 are perhaps due to the compromise with resistance of the vasculature as well as metabolism. Oscillations in IHF derived from the right ankle blood flow showed similar results particularly for comparison between febrile malaria and non-malaria (Figure 6.8), thus substantiating the findings earlier observed in the case IHF extracted from the ECG.

One of the most interesting outcomes of the study is related to the respiration

(interval II), myogenic (interval III), neurogenic (interval IV), NO-dependent and independent endothelial (interval V and VI) oscillations. The markedly reduced left–right ankle blood flow coherence in the cardiac (Figure 6.13(c)), respiration, myogenic, neurogenic, NO-dependent and independent endothelial activity seen in febrile and non-febrile malaria patients (Figures 6.10, 6.11(e)) indicate a cardiovascular system abnormality in acute malaria stage. Moreover, an effect revealed by the band coherence also implies that the impaired cardiovascular dynamics are not immediately restored by antimalaria treatment as evidenced by the non-febrile malaria group. In addition, these findings further demonstrate the alteration of the underlying mechanisms of rhythmic coordination between the oscillatory processes in microvascular function [220, 396, 446, 448]. Moreover, the observed behaviour of the phase difference between the IHF and respiration (Figure 6.11(d)) may signify that the two signals have the same sign and therefore will be reinforcing one another.

Coherence provides additional insight into the changes that occur with febrile and non-febrile during modulation of heart rate by the respiratory frequency. The significant attenuation in cardiac interval coherence between IHF (derived from the ECG) and breathing in the febrile and non-febrile malaria implies an impairment in respiratory sinus arrhythmia (RSA), given that the high frequency component in IHF reflects the influence of breathing on the heart rate [29, 253, 307], an inference that is supported by an additional finding: a significantly decreased blood flow coherence in the frequency interval associated with cardiac activity. Besides, the results may also signify a destruction of both the sympathetic and parasympathetic modulation that critically influence the oscillations in heart beat intervals. As the sympathetic and parasympathetic modulation are widely known to contribute to the oscillatory components that manifest in IHF [66, 146, 238, 356]. Therefore, this finding may perhaps explain the alteration we observed in the power spectra of skin blood flow cardiac oscillations.

Topologically (Figure 6.14), the sinusoidal nature of the cardiorespiratory cou-

pling in NM group shows that for every respiratory period, the heart frequency gets modulated correspondingly. The displacement of this sinusoidal wave further indicates that in the processes of inhalation, the heart is accelerated, while along the breathing (about π) cycle it is decelerated. The pattern of this relationship is sustained in the coupling functions averaged over time in the malaria infected subjects (Figure 6.14b-c)), notwithstanding the decrease in the amplitude, arising from a slightly deterministic pattern of the coupling function among the subjects studied. Thus, it can be assumed that the component of respiratory arrhythmia is influenced by malaria, becoming more unstable and irregular, even if still present.

As mentioned earlier in the introduction (Section 1.1.2), the drawbacks associated with existing methods for assessing and diagnosing malaria, have increased the quest for real time techniques for noninvasive diagnosis of malaria an active area of research. Based on our findings, a cut-off was established in line with differences in cardiovascular dynamics between malarias and healthy non-malaria, with a classification accuracy of 88 % (Table 6.9). Early non-febrile malaria subjects who have started taking antimalarial or antipyretic drugs were also chosen as malaria in this study, due to its similarity to febrile malaria in terms of the cytoadherence and microvasculature characteristics, including the increased stiffness of the membrane of an infected erythrocyte (red blood cell) and its ability to abnormally stick to cells that line all blood vessels. In agreement with this similarity, no significant differences in mean blood flow recorded from one of the two extremities of body, mean SpO_2 or respiratory rate between febrile malaria and non-febrile malaria were found. In addition, there was no significant difference in the blood flow and IHF dynamics in any of the six frequency intervals between febrile and non-febrile malaria. On the contrary, febrile malarias and non-febrile malaria differed mainly in terms of their mean skin temperature and IHF.

8.6 Cardiovascular dynamics in treated malaria patients

The salient finding in this study suggests that episodes of malaria infection induce significant changes in the oscillatory components that manifest in human microvascular blood flow dynamics. In subjects with a history of malaria, the rhythmic co-ordination between the oscillatory components in the blood flow is clearly reduced at frequency intervals associated with the cardiac, respiratory, myogenic and neurogenic activity (Figure 7.7). These long-term effects of recurrent malaria on microvascular oscillations confirm the result of previous and recent studies carried out in humans, although the state of the art and analysis techniques were different [404–408, 456, 457].

The possible hemodynamic effects of malaria episode were explored (Table 2.1). The systolic and diastolic blood pressures remained unchanged, as was the mean heart rate, although the spectral power of the low frequency oscillatory component of the latter was elevated. Respiratory frequency is considered to be unchanged as no difference could be established when compared with black-skinned healthy control. Moreover, skin perfusion measured from the two sides (left and right ankle) of the body remained unchanged, except at the perfusion recorded from the right ankle (Table 7.2). The increase in the right ankle skin perfusion could result from most subjects being leaning on the left ankle during recordings, as we would expect similar increases in both ankles if the observed difference was genuinely physiological. The finding suggests that the hemodynamics is unperturbed by earlier episodes of treated malaria.

Time-frequency analyses of the LDF microvascular signal revealed subtle changes in healthy subjects with previously treated malaria. Although the time-averaged wavelet power of the perfusion signal recorded in left ankle did not change, the oscillation power in the cardiac interval in the right ankle blood flow was seen to significantly decrease in treated malaria group. This may perhaps be a result of

movement artefacts, as no such effect was observed left ankle blood flow (Figure 7.2(c)-(d)).

As the mean heart rate remained unchanged in healthy subjects with earlier episodes of treated malaria, on the other hand, the time-averaged power of the heart rate variability was significant elevated at a few very high frequencies within the oscillatory component reflecting the respiratory activity (Figure 7.3(a)). This effect was evident in TM-CA and TM-BA comparisons, which means that the observed effect could reliably be attributed to the destruction caused by malaria episodes and not ethnic difference. Although not yet confirmed, this effect may likely be attributed to the excessive production of pro-inflammatory cytokines as well as immune mediators such as NO due to recurred parasite sequestration in capillaries with capillary leakage.

For the rhythmic co-ordination between the blood flows, TM exhibited a significant reduction in the blood flow coherence in frequency intervals related to cardiac, respiratory, myogenic and sympathetic nervous activities, and are more justified in respiratory and neurogenic activities (Figure 7.7), as they are both established when compared with the two control groups (CA and BA), this confirms that the effect observed in the blood flow coherence of TM group arise from treated malaria. Additional investigation of the rhythmic interactions between the microvascular blood flow and IHF disclosed major changes associated with treated malaria. In the 0.07-0.19 Hz frequency interval, the rhythmic interactions between blood flows and IHF was significantly reduced in treated malaria (Figure 7.9). However, the reduction was only established in comparison to white Caucasians, but of course it could still reliably be attributed to the effects of recurrent malaria rather than racial disparity since the coherence did not significantly differ between the Caucasians and black Africans groups (Figure 7.10). These attenuated coherences may likely demonstrate the effect of malaria recrudescence on rhythmic co-ordination in the respiratory, myogenic and neurogenic activities.

We suggest that the observed attenuation in the microvascular oscillations

of treated malaria subjects may be connected with the low production of the endothelium-derived NO, especially: evidence has accumulated that the rate of NO release is nearly five times slower in black persons than in white, leading to an increase in both O_2^- (superoxide) and $ONOO^-$, all of which play a vital role in pathophysiology of malaria [261, 458]. Besides the numerous functions of NO, one of its crucial physiological roles is to protect the cardiovascular system against pathophysiological abuses which include the release of some anti-inflammatory effect agents in the blood vessel wall to prevent the adhesion of leukocytes and platelets to the endothelium and to inhibit smooth muscle cell proliferation. However, recurrence of malaria infection tends to attenuate the activity of the NO in the microvasculature. Moreover, it is known that the increased production of O_2 inside endothelium is responsible for eliciting NO reduction in malaria; consequently, it become reasonable to attribute such effects to recurrent incidences of malaria.

Our findings have revealed that in episodes of malaria, even when treated, the parasites of the *Plasmodium* responsible for the infection still leave behind a long-lasting chronic effects on their host. This is in agreement with previous studies which suggest that the relapsed effects related to multiple occurrences of malaria infection ensues due to the cytoadherence of iRBC that allow the parasites to remain in blood circulation [396], as well as the antigenic variation that evades the host immunity [459–461].

In conclusion, changes in skin microvascular dynamics induced by episodes of malaria can be assessed by wavelet transforms and wavelet phase coherence between the laser Doppler signals and the instantaneous heart frequency. Episodes of malaria reduced the low oscillatory components of the perfusion signal, indicating impediment of the respiratory, myogenic and neurogenic activities as well as of the very high oscillatory process in the IHF related respiratory activity.

This study presents a technique for identifying the subtle long term effect of episodes of malaria on microvascular dynamics. The observed alteration clearly

demonstrates the feasibility of this approach to follow up treatments of malaria. Recent studies, both invasive and non-invasive investigations, all suggest that an impairment of blood flow, especially in the microvascular bed, is a major feature in the pathogenesis of malaria. Multiple factors combine to alter the microvascular blood flow. The abnormal adherence of the malaria iRBC to inner cells of the vascular endothelium affect the elastic properties of the red blood cells alongside their ability to squeeze through tiny capillaries. This cytoadherence tends to significantly alter the myogenic oscillatory component and the sympathetic nervous activity manifested in blood flow dynamics, leading to a mechanical obstruction within the micro–vessels, a major pathological process of malaria.

Our results also reaffirm our suggestion that the properties of the oscillatory components evaluated by time–frequency analysis, could lead to the establishment of a non-invasive and inexpensive device for the early detection of malaria. More so, in the development and testing of anti-malaria drugs, efforts should also be made to normalize the interaction of low frequency rhythms, which is hugely impaired by the malaria parasite. Interestingly, this opens up intriguing questions to be answered for a new focus of intervention: (i) What are the possible mechanism of the subtle impairment in the microvasculature? (ii) Can these lethal effects be forestalled or equilibrized with specific antibody-independent mechanism therapies or new drugs rationally designed to cleanse the microvasculature following every malaria disinfection? These questions and many more, as well as the significant vulnerability posed by malaria, are among the motivations for investigation into the cardiovascular oscillatory mechanisms in malaria induced by microvascular damage.

8.7 Experimental limitation

Cardiovascular dynamics in febrile and non-febrile malaria A limitation of this study is that the physiology of the 10, non-febrile malaria patients may not be representative of normal human pathophysiology in the malarial state. As dis-

cussed above, comparisons of the cardiovascular parameters of the 10 non-febrile malaria cases with those of larger populations did reveal some differences, but mainly in average recordings and at some specific frequencies and not within frequency intervals that represent physiological activity. A second major limitation is the slight (border-line) variations in age distribution between the malaria groups, with the non-febrile malaria being slightly older, although not to a statistically significant extent. It has been reported previously that physiological activities, such as the IHF and the reaction of microvascular processes to vasoactive agents, vary with increase in age. To eliminate possible effects of sample size and age on the results, additional recruitment of age-matched malaria patients would be needed. A further limitation of this study is the potential movement artefacts of the instruments used for the measurements. However, such limitations were less consequential here, due to the fact that the signals were di-spiked and analysed in the time-frequency domain and their phase relationship established, using wavelet-based methods. To enhance the clinical applicability of the corresponding diagnostic markers, it would be desirable to shorten the duration of recording to 10 minutes atmost.

Cardiovascular dynamics in treated malaria Variation in atmospheric conditions during the period of measurements has the potential to have influence our results. In the treated malaria group, all the recordings were obtained in the winter, whilst for the dark controls, recordings were performed in the summer. Thus, these could cause variations in data, which could have influenced slightly the comparison between treated-malaria and control (black Africans) groups.

8.8 Limitations of the analysis

When a large number of analyses are conducted, one can ask about possible limitations attributable to the multiple statistical analyses. First, the large number of statistical comparisons carried out in the analysis of research data is known to

likely influence the probability of a false conclusion, although it has been addressed through Bonferroni correction [462], which is a common test used to overcome the bias of multiple statistical comparisons. Due to the low p values, with mostly $p < 0.001$ found in many of the comparisons, as shown earlier, it is unlikely that these positive rates, (particularly in the malaria data) are markedly influenced by the large number of statistical test carried out during the analysis. Moreover, the high percentage of classification accuracy for distinguishing between malarial and control groups, as obtained with the machine–learning algorithms further justifies the minimal potential for inflated false positive rates.

Secondly, we would comment that addressing the potential for confounding of analysis from effects of fever vs effects of malaria itself could in principle be daunting, although it was precluded in the present case at the stage of recruiting the volunteers. It was ensured that the only patients included were those with significantly elevated core temperature and skin temperature ($> 38\ ^\circ$) as measured by using both the axillary thermometer and two high sensitivity Thermilinear sensors, respectively. While the non-fever malarial patients had a normal body temperature ($36.5\ ^\circ$). The outcome of analysis between febrile malaria patients and controls were not identical to that observed between nonfebrile malaria compared to controls, so that it is possible to separate the effect of malaria from that of fever. For example, our findings illustrated that the unlike their diastolic blood pressure, the systemic blood pressure of malarial patients was not significantly influenced by fever, as shown by the comparison between FM and NFM groups (see Table 6.2). In addition to comparison between FM and NFM groups, analysis between FM and NM shows a significantly decreased systolic blood pressure in the FM group. Similarly, the NFM group exhibited a very low (with $p = 0.07$) systemic blood pressure when compared with the controls. It could therefore be suggested that the observed differences in blood pressure (particularly the systolic pressure) between the malarial and control groups are mostly related to the infection and not solely due to fever.

Lastly, following the observed variability in blood pressure, the possibility of confusion due to blood pressure changes also deserves some remarks. Several studies have reported possible effects of malaria on blood pressure, with the malaria patients having a significantly lower systolic blood pressure compared with healthy subjects [463]. Consistent with these previously reported findings, it suffice to suggest that the significant differences observed in blood pressure between malarial and control groups demonstrate the effects of malaria parasites on systemic vascular resistance, which is critical for creating blood pressure. Moreover, the presence of parasites in the blood could impair vaso–dilation/constriction of blood vessels and consequently reduce the systemic vascular resistance.

9. Concluding remarks

9.1 Summary

Concisely, the main facets of this thesis are outlined below:

- The background on malaria, including its present diagnostic methods and their advantages and disadvantages, is reviewed.
- The physiological and biophysical background of cardiovascular dynamics and its associated oscillations in healthy and pathological state is reviewed.
- The methods used for the acquisition of the cardiovascular parameters studied are discussed.
- A background to non-linear dynamical systems and the time series analysis methods available for analysing them are elaborated upon.
- The utility of laser Doppler flowmetry for measuring microvascular blood flow dynamics from darkly pigmented skin was tested by comparing with measurement from lightly pigmented skin using the same techniques, and was found to be appropriate for dark skin.
- The possible role of race-specific differences in microvascular blood flow and oxygenation dynamics was explored between black Africans and white Caucasians using the methods presented for the measurement of physiological parameters and their analysis.

- The long term effects of an episode of malaria on blood flow and cardiovascular dynamics was explored in treated malaria patients.

- The cardiovascular dynamics of malaria and healthy non-malaria subjects recruited from Nigeria specifically for this investigation were analysed using the methods presented, and an accurate noninvasive diagnostic test was developed.

This thesis has aimed primarily to investigate cardiovascular dynamics in symptomatic and asymptomatic malaria. Cardiovascular flow parameters including blood flow, arterial oxygenation, ECG, skin temperature and respiratory rate were recorded using laser Doppler flowmetry, TOSCAA500, ECG sensors, YSI 709B thermilinear sensors, and TSD201 Velcro respiratory belt sensor respectively. These signals were analysed using time series analysis techniques finely tuned to the fundamental properties of these time series: that they come from systems that are oscillatory, thermodynamically open, nonstationary, nonlinear and nonautonomous. A revision of the methods required for the analysis was carried out. These analyses yielded new understanding of the vasculature in malaria, characterized by differences in cardiovascular oscillations as measured in healthy non-malaria when compared with the malarial state. These oscillations allow the differences found in the spectrum and coherence to be linked to the oscillations connected with vasomotion, in both the myogenic, neurogenic and endothelial frequency intervals. This could be a consequence of cytoadherence of infected red blood cell to the vessel wall, i.e. to the vascular endothelial cells, leading to an elevation in vascular resistance due to vasoconstriction inflammation, impairment of pulmonary arteries, or an attenuation in 1:1 rhythmic coordination between local regulatory mechanisms in malaria. The differences found in malaria were large enough to enable the establishment of a set criteria which have been successfully applied in a diagnostic test with a classification accuracy of 89 %. In spite of the necessity for additional data collection before this method can be used for routine clinical practice, this investigation provides the underlying basis for the

establishment of a real time, inexpensive, noninvasive diagnostic test which could remarkably minimize the circumstances for unnecessary blood smear microscopy test.

In addition to the malaria study, microvascular blood flow and oxygenation dynamics were investigated in data recorded from black Africans and white Caucasians subjects at rest using NIRS and a separate probe providing for simultaneous measurements with white light spectroscopy, and LDF, in order to ascertain whether black Africans differ from Caucasians in terms if their oscillatory physiological processes at rest, and whether the inherent features of these signals are altered in Africans when comparing coordination of blood and oxygenation in Caucasians. This part of the thesis aims to identify potential differences in microvascular blood flow and oxygenation dynamics that may result from race-related disparity and to compare them with the changes observed in cardiovascular dynamics of malaria. If analogous behaviour was found, this could then be considered as a hallmark of vascular impairment, well known to occur due to the sequestration of malarial erythrocytes. Contrary to the our findings in malarial patients, some component of the cardiovascular system such as the blood flow dynamics in the biracial groups did not vary in the frequency intervals associated with local or systemic activity, but the rhythmic coordination between blood flow and oxygenation did vary significantly in the frequency intervals associated with vasomotion cardiac and respiratory activity, as expected. This further confirms the observed dysfunction in both systemic and local processes in the cardiovascular dynamics of malaria.

An additional, virtually universal, hallmark of malaria was also studied. The deterministic properties of the microvascular blood flow and instantaneous heart frequency signals were explored in specifically recruited patients who had suffered from malaria and recovered from it and in controls with no incidence of malaria. This is in order to investigate whether history of multiple (although one episode would be enough) malaria episodes differ from non-malaria infected individuals

in terms of the oscillatory processes that manifest in their blood flow signal at resting state, and whether the reoccurrence of malaria has a long standing effects on the underlying properties of the blood flow dynamics when compared to subjects with no history of malaria. Subsequently, these differences are compared with the findings obtained in blood flow and cardiovascular dynamics of malarial patients. If similar property was found, this could then be regarded as a hallmark of episodes of cytoadherence of iRBC on vessel wall – a widely known phenomenon in malaria. In the blood flow spectrum of malarial patients, frequency intervals associated with cardiac, myogenic, neurogenic and NO-dependent endothelial activity were significantly altered due to several physiological destruction within the vasculature (which have earlier been extensively discussed), such as the impaired vascular resistance, vasodilation etc. However, the blood flow spectral power in treated malaria did not significantly change within 0.0095-2 Hz interval. While no significant alteration was found in the IHF spectral power of treated malaria, apart from the changes observed in the cardiac interval, the IHF spectral power in the malarial state was significantly varied in all the five frequency intervals investigated spanning 0.6-0.0095 Hz. In the case of the rhythmic coordination, the blood flow signals' coherence was significantly altered in malaria just as in the treated malaria subjects, but at almost completely different frequency intervals apart from the cardiac band where they were both significantly altered. This suggests that even when antimalarial drug treatment is being given the microvasculature dysfunction remains although the treatment decreases the heart rate and partially normalises the respiration.

9.2 Original contributions to science

The original contributions of this work are outlined below:

- The suitability of using laser Doppler flowmetry in monitoring microvascular blood flow from darkly pigmented skin containing high melanin concentration

was investigated for the first time. It was concluded that high melanin does not alter the blood flow dynamics. This allows the usage of the instrument in assessing blood perfusion in black Africans, worldwide.

- Using LDF, ECG, a respiratory belt sensor, and the radiometer TOSCA500, a method for noninvasive investigation of malaria has been introduced for the first time and an algorithm for the detection of malaria has been developed.

  The blood flow dynamics of febrile malaria, non-febrile malaria, and healthy non-malaria were compared in the frequency interval 0.005-2 Hz. Time-averaged normalised power differed significantly for comparison between febrile malaria and non-malaria groups in the intervals associated with cardiac, myogenic, neurogenic, NO-dependent endothelial activity.

- Significant differences in wavelet phase coherence were found between blood flow signals recorded from malarial patients and controls in the cardiac frequency interval. The peak frequency of the cardiac oscillation was higher in febrile malaria then in the controls.

- The instantaneous heart frequencies in febrile malaria, nonfebrile malaria and controls, which were derived from both the blood flow and ECG were compared in the frequency interval 0.005-0.6 Hz. The time-averaged normalised power mostly differed significantly between febrile malaria and controls in intervals II, III, V & VI. Similar differences were also established in between non-febrile malaria and controls in intervals II, III, IV & V.

- Significant differences in the wavelet phase coherence between the fluctuations in the instantaneous heart frequency extracted from the blood flow signals were found between malarias and control groups, in intervals I, II, III, IV, V & VI. The coherence was attenuated in malaria patients.

- Coherence between instantaneous heart frequency and respiration significantly declines in the respiratory interval in both febrile and nonfebrile

malarias compared to controls. There is an obvious impairment in respiratory sinus arrhythmia in the malarial state. Although it is widely known that higher respiration rate leads to lower sinus arrhythmia.

- Comparing the data from febrile malaria, non-febrile malaria and healthy non-malaria groups it was found that the couplings to the cardiac rhythm from respiratory activity decrease significantly in the malarial states.

- Arterial oxygen saturation was compared between malarias and controls and evaluated using wavelet analysis. It was found that the spectral component of the cardiac and respiratory frequency intervals significantly differs between the three groups(for FM-NM, NFM-NM & FM-NFM comparisons). The average arterial oxygen saturation was also significantly lower in malarias than in controls. This is potentially a suitable biomarker desirable not only for identifying malaria, but also for evaluating the successfulness of treatments along the road to recovery.

- The aforementioned observed differences in frequency components that manifest in cardiovascular dynamics (blood flow, instantaneous heart frequency, arterial oxygenation) between febrile and non-febrile malarial patients, and healthy non-malaria on the other hand, were developed into a diagnostic test with a classification accuracy of 89 %.

- Further investigations on the signatures of subjects with no history of malaria and treated malaria patients in cardiovascular regulation were carried out. This was done through analyses and comparison between groups as performed in the same way as for the LDF and ECG time series investigated in malaria patients.

- The deterministic properties of oxygenation measured at a deeper level in the tissue were Investigated for the first time using a near infrared spectrometer, with simultaneously recorded microvascular blood flow and skin oxygenation

signals, using combined optical LDF and white light spectroscopy. By extracting time-varying oscillatory parameters, new insights into race-related and environmental differences in microvascular dynamics have been acquired.

- Tissue oxygen saturation was investigated and compared between black Africans and Caucasians using wavelet-based methods. It was found that the spectral powers of low frequency oscillations in both the oxygenated and deoxygenated hemoglobin were significantly lower in Caucasians than in black Africans. The mean of skin oxygen saturation and deep oxygen saturation were higher in Caucasians compared to black Africans while in contrast, the mean and standard deviation of oxygenated hemoglobin and deoxygenated hemoglobin concentration were found to be lower in Caucasians than in black Africans.

- The effective wavelet phase coherence evaluated between blood flow and skin oxygen saturation showed a significantly lower rhythmic coordination of cardiac with myogenic activity in black Africans compared to Caucasians.

- The rhythmic coordination between blood and (oxygenated and deoxygenated) hemoglobin concentrations was found to be significantly higher in Caucasians in the cardiac and myogenic frequency intervals.

- Deoxygenated hemoglobin concentration increases in black Africans as the coherence between blood flow and (oxygenated and deoxygenated) hemoglobin concentration decreases.

9.3 Future work

This work is expected to benefit from the following future tasks:

- Investigation of tissue oxygenation dynamics in both febrile and non-febrile malaria, as it is proposed that the its dynamics alongside the phase coherence

with blood flow will markedly be altered in malarial state. To our knowledge, this is yet to be studied.

- Investigation of the nonlinear dynamics of malaria in patients with sickle cell disease (SCD), as it is commonly found in malaria patients and seems to have similar blood flow dynamical properties. This will provide additional insight into the dynamical behaviour of malaria in SCD and into whether the developed biomarker for malaria can be used for sickle cell anaemic patients.

- Recruitment of more patients with malaria particularly nonfebrile malaria, and more controls with rhinovirus (common cold), influenza and other non-malarial fevers to build up the data set used in the diagnostic test for malaria, as this will facilitate earlier detection of malaria, and avoidance of confusion with common fevers.

- The next stage will be the development of a 'malariometer', a prototype instrument for use in a large scale trial, which is an essential preliminary to the development and sale of a commercial instrument by industry, and we will approach potential British manufacturers in the first instance.

Appendices

A. Cardiac functioning

A.1 Cardiac output

The heart beat can be considered as a two stage pumping action over a period of at-most a second. A complete cardiac cycle (long term diastole and a systole) is defined as the cardiac events initiated by the P wave in the electrocardiogram (ECG) and continuing until the generation of next P wave. It is generally divided into two categories: a systole which refers to the event associated to the ventricular ejection and contraction, and a diastole which refers to the ventricular filling and relaxation. However to understand how the regulation process of the cardiac function occurs, it is important to discern the process of mechanical events during the cardiac cycle and how it relates with the electrical activity of the heart [28, 40]. To be more precise, the heart rhythm concentrates on the left ventricle activity, and it consists of four main phases: (1) the isovolumetric relaxation (IR), with closed atrioventricular and ventriculoarterial valves; (2) ventricular filling (VF), with opened atrioventricular valves and closed ventriculoarterial valves; (3) isovolumetric contraction (IC), with closed atrioventricular and ventriculoarterial valves; and (4) systolic ejection (SE), with closed atrioventricular valves and opened ventriculoarterial valves. These are described in Figure A.1

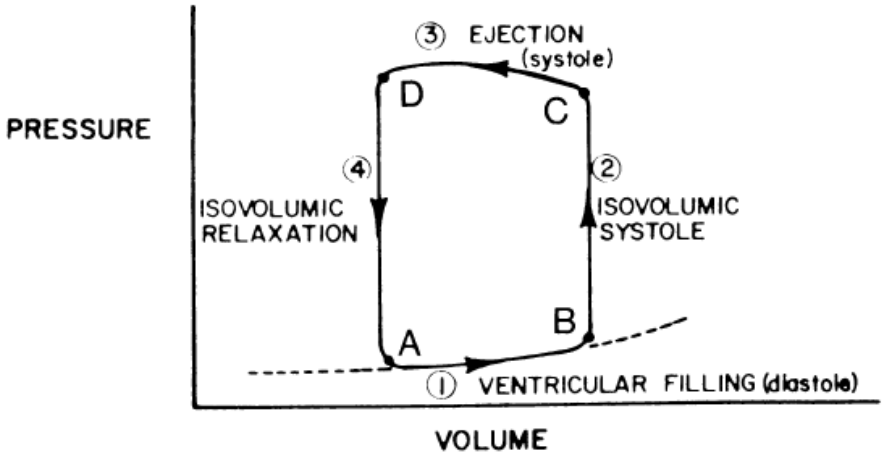

Figure A.1: A curve of the pressure and volume in the left ventricle during a cardiac cycle. Phase 1 represents ventricular filling during diastole. Phase 2 represents isovolumic pressure development. Phase 3 represents ejection of blood into the aorta. Phase 4 represents the isovolumic relaxation period. Extracted from [29].

Both the ventricular filling (VF) and systolic emptying (SE) can further be subdivided into rapid and reduced sub-periods (rapid [RVF] and slow [SVF] ventricular filing, rapid [RSE] and slow [SSE] systolic ejection) [28, 40]. While for the atrial contraction (AC), the mechanical events are divided into seven phases [28, 40, 464], which are shown in Figure A.2.

Phase 1 (AC) is the onset of ventricular systole, and this phase of the cardiac cycle is triggered by the QRS complex of the ECG. Following the depolarization of the ventricle, the myocyte contraction leads to a rapid increase in intraventricular pressure p_{v}. Thus making AV to close as the intraventricular pressure exceeds the atrial pressure [40]. The abrupt rise in the mitral valve is tightly closed to prevent backflow of blood as the left ventricle begins to contract [28]. The closure of the AV valves create the first heart sound (S_1), which normally split ($\sim$0.04 sec) because the mitral valve closure precedes the tricuspid closure. This implies that, heart sounds are generated when the sudden closure of a heart valve and the accompanying oscillations of the blood produce vibrations (i.e., sound waves), and can be heard with a stethoscope overlying the heart [40].

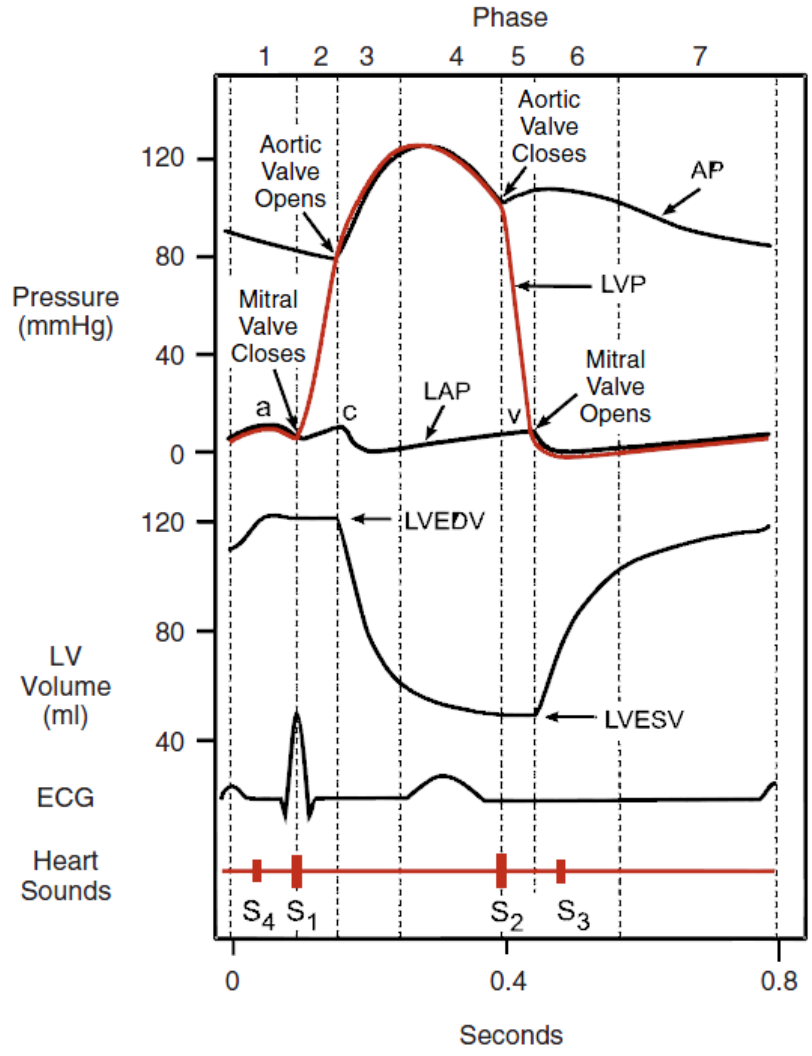

Figure A.2: The seven phases of the cardiac cycle: (1) atrial systole; (2) isovolumetric contraction; (3) rapid ejection; (4) reduced ejection; (5), isovolumetric relaxation; (6) rapid filling; and (7) reduced filling. LV, left ventricle. For the ECG, electrocardiogram; a, a-wave; c, c-wave; v, v-wave; AP, aortic pressure; LVP, left ventricular pressure; LAP, left atrial pressure; LVEDV, left ventricular end-diastolic volume; LVESV, left ventricular end-systolic volume, S1-S4, four heart sounds. Extracted from [40].

Ventricular pressure rises rapidly without changes in the ventricular volume (i.e., no ejection of blood into the aorta or pulmonary artery occurs) during the closure of the AV valves and the opening of the semilunar valves. Hence, ventricular contraction is said to be "isovolumic" or isovolumetric (incompressible blood) during this phase, but the shape of the ventricle varies [28, 40]. Blood impacts the closed mitral valve as the left ventricle contracts, which then bulges all the AV

back into the atrial chambers, with a further intra-atrial pressure p_A increment; the c wave which is noted in the jugular is believed to occur owing to the increment in the right atrial pressure as a result of the tricuspid valve leaflets bulging back into right atrium.

Phase 2 (ESE) occurs when the end-diastolic aortic pressure p_a overcomes by the intraventricular pressure p_v [28]. When the pressures within the aorta and pulmonary are exceeded by the p_v, the aortic and pulmonic valves open and blood is ejected out of the ventricles due to the total energy of the blood within the ventricle that exceeds the total energy of blood within the aorta [40]. Traces of end-diastolic aortic pressure p_a and intraventricular pressure p_V follows each other closely and reaches a maximum [28]. Due to the Windkessel effect (blood storage in elastic arteries) [28, 171, 464], it is believed that the aortic blood inflow is greater than the outflow.

While the blood is being ejected and ventricular volumes decrease, blood continues to fill the atria from their respective venous inflow tracts. Though as the atria volumes increase, the atrial pressures initially decrease as the base of the atria is pulled downward, thereby expanding the atrial chambers [40]. However, there is an absence of sound produced by the heart during ejection [40], meaning that the opening of healthy valves is silent while the presence of sound during ejection is a clear indication of valve abnormality.

Phase 3 (SSE): During this phase the ventricular repolarization (T wave) occurs approximately 150 to 200 milliseconds after the QRS, this results to decrease in p_a and p_V [28, 40]. The ventricular pressure slightly drops below outflow tract pressure, but the outflow still occurs owing to kinetic (or inertial) energy of the blood that helps in propelling the blood into the aorta and pulmonary artery. Meanwhile the arterial pressures rises gradually during this phase, therefore the venous returns into the atrium and the v wave is engendered on the atrial pulse [28, 40].

Phase 4 (IR): All valves are closed, this phase is characterized by a strong decline in p_{v} as the ventricles continues to relax, and a point is attained in which the energy of blood in the outflow tracts is greater than the total energy of the blood within the ventricles [28, 40]. Therefore the aortic and pulmonary valves suddenly close (aortic before pulmonic), due to a pressure gradient reversal, resulting in a second heart sound (S_2) which is audibly and physiologically split.

However, as these valves close, there is usually little or no back flow into ventricles and the rate of flow in the aorta undergoes a complete back flow [28, 40]. Moreover, the ventricular volume remains constant during this phase and it is referred as the residual volume (ESV) that is the end-systole volume, and p_{v} continues to decline until it becomes less than p_{A}.

Phase 5. (RVF): AV valves open; aortic and pulmonic valves closed, this phase starts as the ventricular pressures p_{v} fall below atrial pressures p_{A}, which leads to the opening of the AV valves, thus ventricular filling begins [28, 40]. The low resistance of the opened AV valves coupled with the atrial pressures results in passive, rapid filling of the ventricles immediately the valves open [40]. On the right side of the heart, the v-wave is the regarded as the peak of the jugular pulse prior to the opening of the valve, followed by the y descent of the jugular pulse which is generated due to the opening of the AV valves and ventricular filling [28, 40]. Moreover the third sound (S_3) is recorded, although it is believed that no prominent sound is expected to be heard if the AV valves are functioning well [40], but (S_3) is said to be normal in children, however it is regarded pathologic in adults due its seldom associativity with the ventricular dilatation [40]

Phase 6 (SVF): All AV valves open; aortic and pulmonic valve closed (SVF) is called diastasis [28], this phase is the period of diastole within which the passive ventricular filling is close to completion [40]. More blood is forced to the left ventricle from the pulmonary veins through the opened mitral valve. As the left ventricle collects blood, the action potential is sent out by the sinoatrial node

leading to atrial contraction. Small volume of blood is sent into the left ventricle (∼15 % of ventricular filling) by the diastasis with a slight increase in the p_v [28].

Phase 7 (AC): AV valves open; aortic and pulmonic valves closed large amount of blood has already filled the ventricles prior to atrial contraction during this final stage of the cardiac cycle [28]. The pressure within the atrial chambers increases as the atrial contracts, thus propelling blood from the atria across the open AV valves [40]. However, the atrial contraction contributes slightly to the ventricular filling at rest, but still maintains cardiac output during exercise [28, 40].

The end diastolic volume (EDV) are maximal towards the end of this phase. The fourth heart sound (S_4) is heard as a result of the atrial contraction, and the following left stole begins as the ventricles get full with blood [28].
Microcirculation represents an important segment for storage of blood volume, however this microcirculation is believed to be enhanced in the process of diastole due the relaxation of myocardium, and could help the ventricular expansion by a straightening effect.

A.2 Stroke volume

The rate of tension development i.e., the changes in ventricular contractility and the velocity of myofiber shortening can result in modification of the stroke volume. The ventricular pressure time gradient is augmented by the increased inotropy and, hence the ejection velocity [28]. The stoke volume is maintained at high heart rates as the inotropic state increases, and only decreases the volume due to the slowed time for diastolic filling and slowed EDV. At values of high heart rate, ion carriers becomes less efficient in removing all calcium from vascular smooth muscle cells, which creates a positive inotropic state peripheral vasodilator.

The area inside the pressure volume depicts the stroke volume (SV) which is approximated as the product of stroke volume and the mean arterial pressure. However, this estimation gives the stroke work differences between the left and right

ventricles. The ratio of stroke work to myocardial oxygen consumption (SV/qO_2) is referred as cardiac efficiency , though there are various factors that influence the qO_2 especially the wall tension [28].

It is often perceived that there exists a dynamical relationship between systole and diastole. The heart recoil and energy that is stored for active diastolic dilation and aspiration are provided from the systolic contraction, however the large blood vessels and the surrounding mediastinal tissues that reacts by elastic recoil are pulled by the motion of the heart during systole [28, 465].

B. Results on race-specific differences in the coherence between microvascular blood flow and oxygenation dynamics

This appendix considers a typical result of the work discussed in chapter 5.

Example signals and the corresponding wavelet phase coherence between the blood flow and $SO2_a$, and the blood flow and $SO2_b$ as recorded from one Caucasian subject are shown in Figures B.2 and B.1. The windowed wavelet phase coherence is shown in figures B.2 (c) and B.1 (c), which reveal the time-variability of the modes but at the cost of losing information about lower frequencies. In figures B.2 (d) and B.1 (d) the significant phase coherence is shown when coherence is greater than the 95th percentile of 100 pairs of IAAFT surrogates, while the overall (effective) coherence is shown in figures B.2 (e) and B.1 (e) after the surrogate has been subtracted from the original coherence. It can be seen from figures B.2 and B.1 that the coherence is only higher than the surrogate level at the frequencies corresponding to the common oscillatory components. Note however that the surrogate level is inversely proportional to the frequency, which means that detecting significant coherence in low-frequency oscillations is very difficult. The time-variability shared between the oscillatory components present in the signals is revealed by the windowed wavelet phase coherence. This approach was applied

in the evaluating the coherence results present in chapter 5.

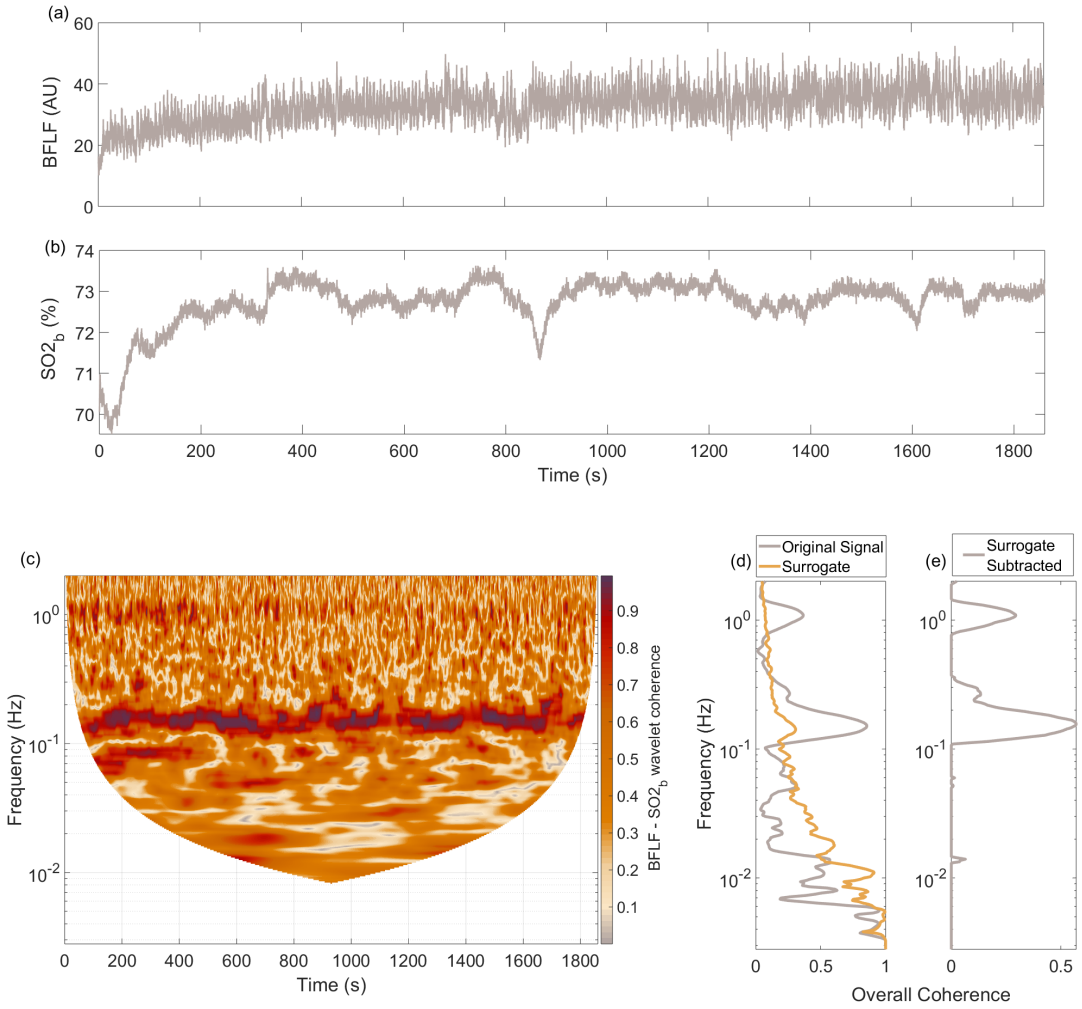

Figure B.1: Example of wavelet phase coherence between (a) blood flow (from left forearm) and (b) $SO2_b$ recorded from a Caucasian. (c) The time frequency representation of the coherence. (d) An illustration of the coherence between the original signals and their surrogates. (e) The effective wavelet phase coherence after subtracting 95 percentile of the surrogate.

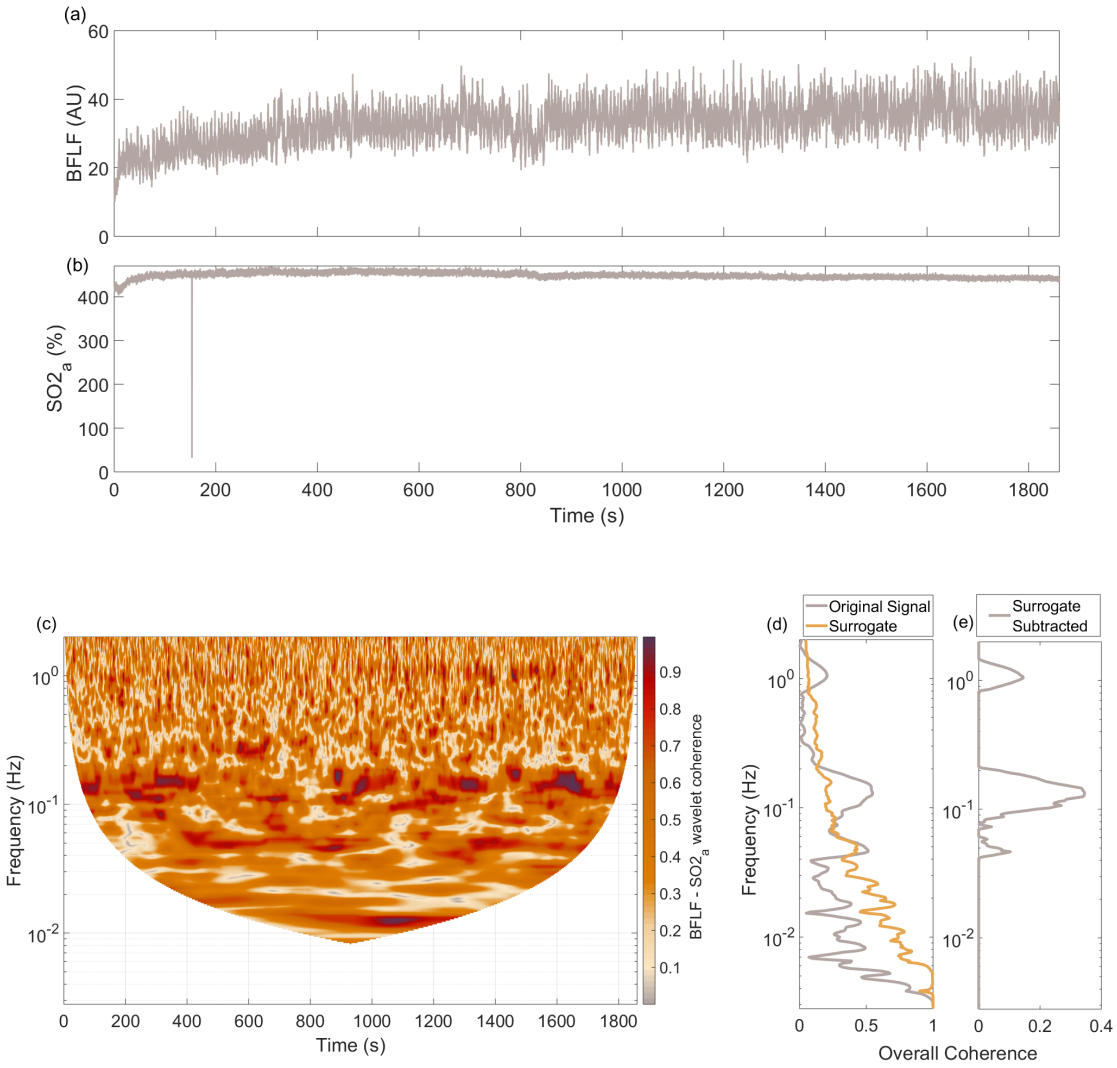

Figure B.2: Example of wavelet phase coherence between (a) blood flow (from left forearm) and (b) $SO2_a$ recorded from a Caucasian. (c) The time frequency representation of the coherence. (d) The coherence between the original signal and their surrogate. (e) The effective wavelet phase coherence after subtracting 95 percentile of the surrogate.

C. IHF absolute power in malarial state

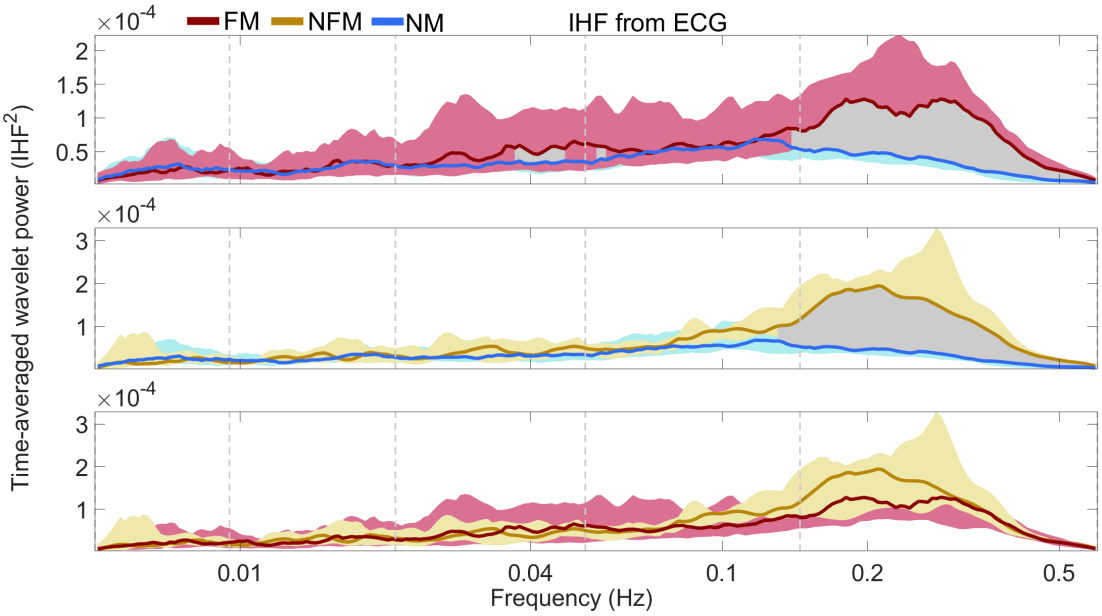

Figure C.1: Comparisons of absolute time-averaged wavelet power of the IHF extracted from ECG recordings. Each curve is obtained as a median over all subjects. (a) Febrile malaria (FM) compared with non-malaria (NM), (b) Non-febrile malaria (NFM) compared with non-malaria (NM) and (c) FM compared with NFM. Red shading indicates the range between 25^{th} and 75^{th} percentiles in FM, blue shading indicates the range between 25^{th}, and 75^{th} percentiles in NM, gold shading indicates the range between 25^{th}, and 75^{th} percentiles in NFM, and brown shading indicates significant (p<0.05) differences between the FM - NM and NFM - NM comparisons.

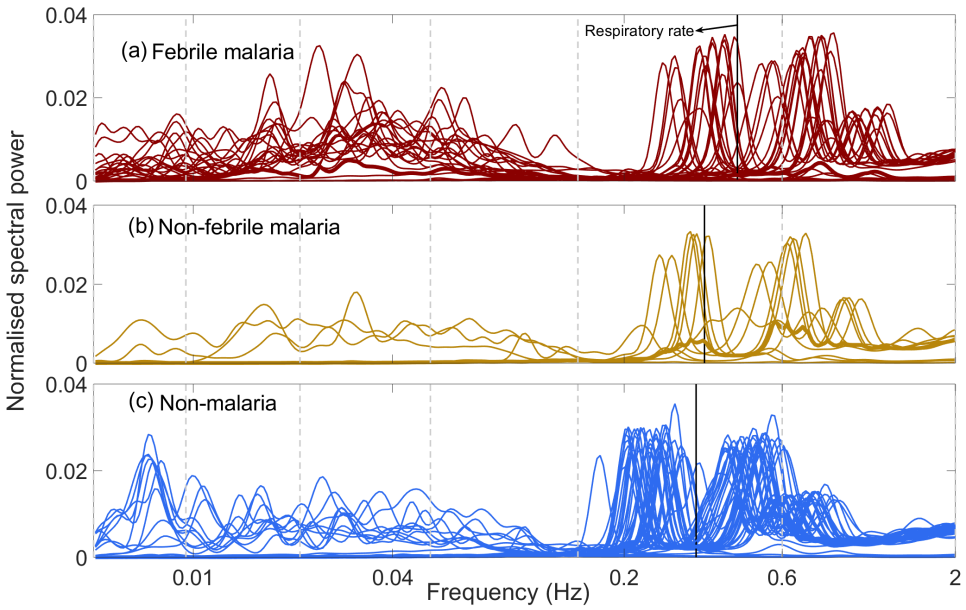

Figure C.2: Normalised time-averaged wavelet power of the arterial oxygen saturation for individual subjects. The thick vertical line illustrates the group median respiration.

D. Diagnostic test

Figure D.1 illustrates the sequence of processes involved in the malaria diagnostic test method. In the first step 1, a dataset is input. The dataset are blood flow measurements measurements 3, 5, from both ankles, electrocardiography data 7, respiration rates 9 and blood oxygenation levels 11. These data are then used to derive the six parameters and their corresponding values used for the test. After computing the data, the instantaneous heart frequency data 13, 15, 17 and the abovementioned parameters 19, 21, 23, 25, 27 and 29 were subsequently derived. Afterwards, each of the parameters was compared against the corresponding threshold value presented in chapter 6. Based on this comparison, each parameter was allocated a positive score if the parameter was indicative of malaria, or a negative score if the parameter was indicative of malaria not being present 31. If all scores were positive, the subject was marked as having malaria 33, if all scores were negative, the subject was marked as not having malaria 33 and if some scores were positive and some negative, the subject was re-tested 35.

D.1 Other standard classification techniques and associated analysis

Several classification techniques from the software package Waikato Environment for Knowledge Analysis (WEKA) were compared. These classification methods include decision trees (J48 in WEKA), decision tree ensembles (random forests, bagging). They were applied on the whole set of attributes with their accuracy

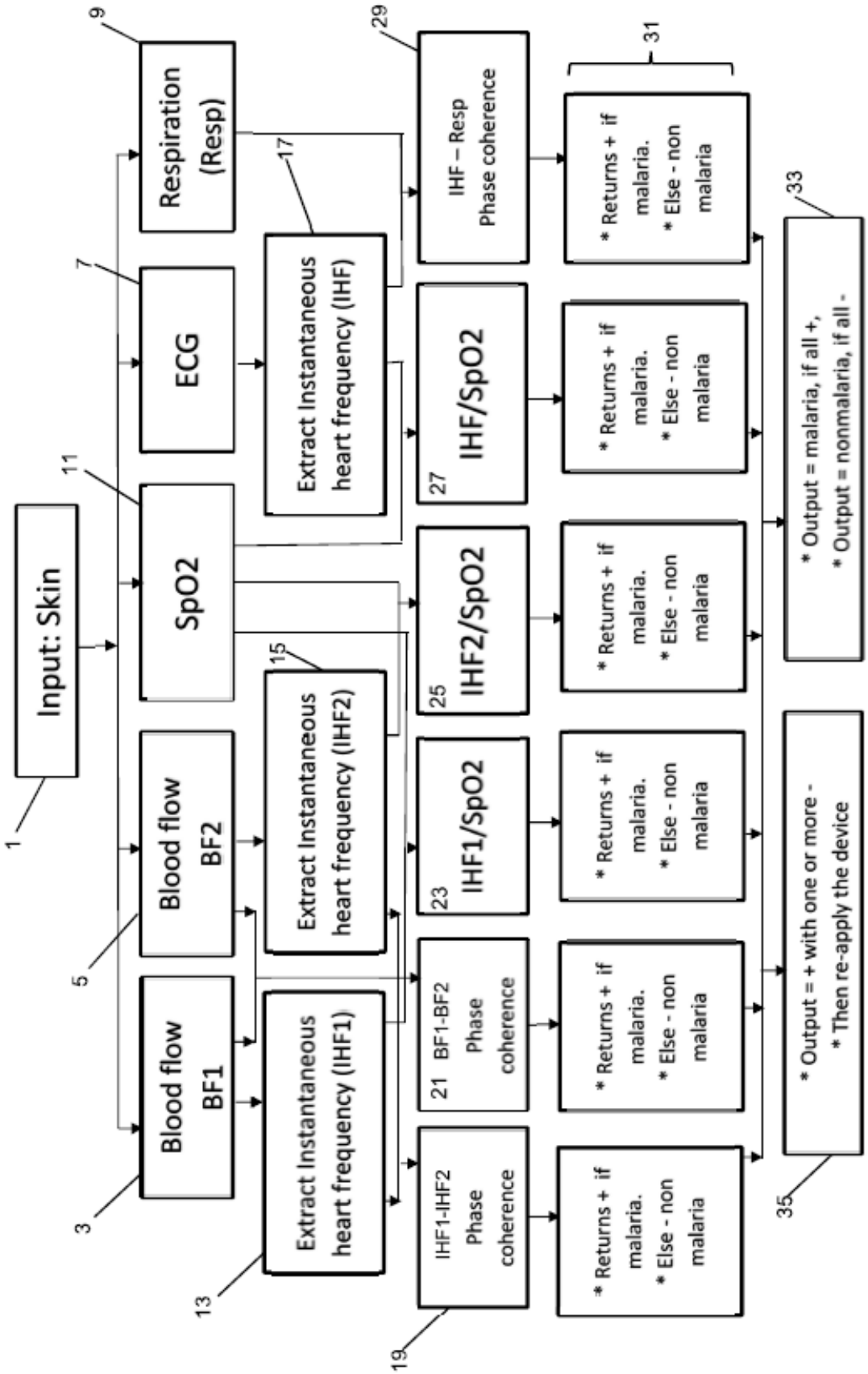

Figure D.1: Malaria diagnostic test flowchart.

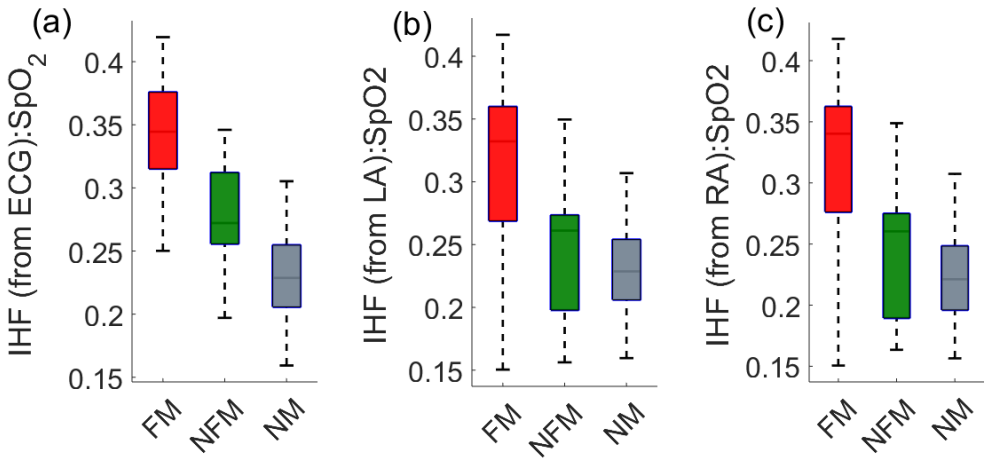

Figure D.2: Box and whisker plots for the diagnostic parameters based on the available data. (a) Ratio between mean instantaneous heart frequency derived from ECG and mean SpO_2 calculated for each group across Hz frequency interval. (b) - (c) Ratio between mean instantaneous heart frequency derived from blood flow and mean SpO_2 for left and right ankles, respectively. FM - febrile malaria group ($n = 37$); NFM - non-febrile malaria group ($n = 10$) ; and NM - non malaria group ($n = 51$).

been evaluated using leave-one-out (50-fold) cross-validation. The confusion matrix, showing the likelihoods of correct and incorrect classification for each of the 3 groups, arising from the leave-one-out (50-fold) cross-validation, is presented in tables D.1, D.2, D.3 and D.4.

D.1.1 Two groups classification

Because the non-febrile malaria group is not sufficiently large enough on its own and is slightly overlapped with the febrile malaria group, the two groups were merged together and refereed to as malaria group. This group was compared with the nonmalaria group, and the two groups were classified using the same methods as in the case of the 3 groups. The results obtained are presented in the Tables D.6, D.7.

Table D.1: J48 Results. Confusion matrix, giving the likelihoods of correct and incorrect classification for each of the 3 groups of subjects, using J48 algorithm for 6 different sets of parameters.

Classified state			J48
Febrile malaria	Non-febrile malaria	Non-malaria	
84%	11%	5%	Febrile malaria
50%	20%	30%	Non-febrile malaria
4%	2%	94%	Non-malaria
Stratified cross-validation (summary)			
Correctly Classified Instances		81	82.6531 %
Incorrectly Classified Instances		17	17.3469 %
Kappa statistic		0.6929	
Mean absolute error		0.1335	
Root mean squared error		0.3164	
Relative absolute error		34.5673 %	
Root relative squared error		72.1422 %	
Total Number of Instances		98	

Table D.2: LMT results. Confusion matrix, giving the likelihoods of correct and incorrect classification for each of the 3 groups of subjects, using Logistic model tree algorithm for 6 different sets of parameters.

Classified state			LMT
Febrile malaria	Non-febrile malaria	Non-malaria	
76%	13%	11%	Febrile malaria
50%	20%	30%	Non-febrile malaria
2%	0%	98%	Non-malaria
Stratified cross-validation (summary)			
Correctly Classified Instances		80	81.6327 %
Incorrectly Classified Instances		18	18.3673 %
Kappa statistic		0.6714	
Mean absolute error		0.141	
Root mean squared error		0.2939	
Relative absolute error		36.5006 %	
Root relative squared error		67.0318 %	
Total Number of Instances		98	

Table D.3: Random forest Results. Confusion matrix, giving the likelihoods of correct and incorrect classification for each of the 3 groups of subjects, using Random forest algorithm for 6 different sets of parameters.

Classified state			Random forest
Febrile malaria	Non-febrile malaria	Non-malaria	
81%	11%	8%	Febrile malaria
50%	20%	30%	Non-febrile malaria
2%	0%	98%	Non-malaria
Stratified cross-validation (summary)			
Correctly Classified Instances		82	83.6735 %
Incorrectly Classified Instances		16	16.3265 %
Kappa statistic		0.7072	
Mean absolute error		0.1522	
Root mean squared error		0.2778	
Relative absolute error		39.3976 %	
Root relative squared error		63.3582 %	
Total Number of Instances		98	

Table D.4: Bagging Results. Confusion matrix, giving the likelihoods of correct and incorrect classification for each of the 3 groups of subjects, using Bagging algorithm for 6 different sets of parameters.

Classified state			Bagging
Febrile malaria	Non-febrile malaria	Non-malaria	
81%	8%	11%	Febrile malaria
40%	30%	30%	Non-febrile malaria
2%	0%	98%	Non-malaria
Stratified cross-validation (summary)			
Correctly Classified Instances		83	84.6939 %
Incorrectly Classified Instances		15	15.3061 %
Kappa statistic		0.7248	
Mean absolute error		0.1525	
Root mean squared error		0.2712	
Relative absolute error		39.4849 %	
Root relative squared error		61.8438 %	
Total Number of Instances		98	

Table D.5: AdaBoostM1 results. Confusion matrix, giving the likelihoods of correct and incorrect classification for each of the 2 groups of subjects, using AdaBoost algorithm for 6 different sets of parameters.

Classified state		Boosting	
Malaria	Non-malaria		
91%	9%	Malaria	
6%	94%	Non-malaria	
Stratified cross-validation (summary)			
Correctly Classified Instances		91	92.8571 %
Incorrectly Classified Instances		7	7.1429 %
Kappa statistic		0.8568	
Mean absolute error		0.0714	
Root mean squared error		0.2672	
Relative absolute error		14.3033 %	
Root relative squared error		53.4626 %	
Total Number of Instances		98	

Table D.6: Bagging results. Confusion matrix, giving the likelihoods of correct and incorrect classification for each of the 2 groups of subjects, using Bagging algorithm for 6 different sets of parameters. Bagging with 100 iterations and base learner.

Classified state		Bagging	
Malaria	Non-malaria		
94%	6%	Malaria	
4%	96%	Non-malaria	
Stratified cross-validation (summary)			
Correctly Classified Instances		93	94.898 %
Incorrectly Classified Instances		5	5.102 %
Kappa statistic		0.8977	
Mean absolute error		0.1253	
Root mean squared error		0.2312	
Relative absolute error		25.0957 %	
Root relative squared error		46.2472 %	
Total Number of Instances		98	

Table D.7: RandomForest results. Confusion matrix, giving the likelihoods of correct and incorrect classification for each of the 2 groups of subjects, using Bagging algorithm for 6 different sets of parameters. Bagging with 100 iterations and base learner.

Classified state		RandomForest	
Malaria	Non-malaria		
91%	9%	Malaria	
2%	98%	Non-malaria	
Stratified cross-validation (summary)			
Correctly Classified Instances		93	94.898 %
Incorrectly Classified Instances		5	5.102 %
Kappa statistic		0.8975	
Mean absolute error		0.1177	
Root mean squared error		0.2327	
Relative absolute error		23.5603 %	
Root relative squared error		46.5453 %	
Total Number of Instances		98	

E. Pilot experiment on effects of multiple incidences of malaria

Pilot experiments (below, and Figure E.1) apparently show that, even long after recovery, former malaria patients still exhibit signs of disturbance in their spectral pattern of microvascular blood flow dynamics. Note that, in this experiment subject were sat on a chair whilst recordings were made.

Preliminary results (Figure E.1) strongly suggest that former malaria patients still retain significant microvascular impairment long after they have apparently recovered from the disease. This led to the study presented in 7, although a detailed study will still be needed for confirmation.

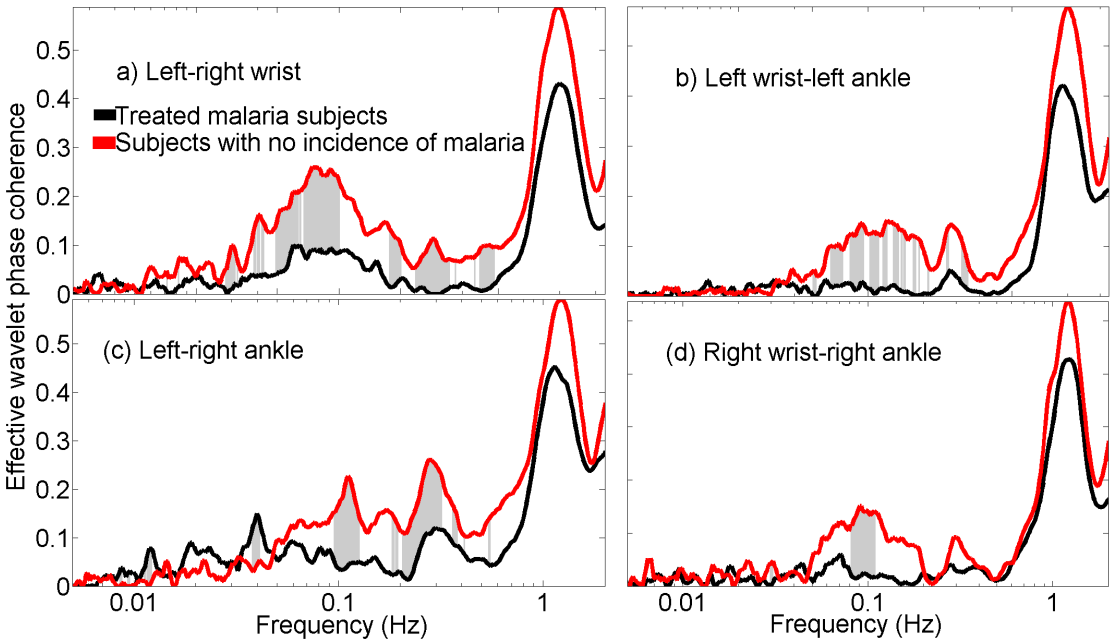

Figure E.1: Preliminary comparisons of the wavelet phase coherence of LDF oscillations in healthy male subjects without (red) and with (black) a past history of malaria. Statistically significant differences are shaded. The data are from 12 patients who had suffered malaria and recovered from it, and 10 with no history of malaria, of average age 26.8 and 24.9 years respectively, and with average BMI of 24.3 and 22.9 respectively. None of them had any history of cardiovascular disease.

References

[1] "World Health Organization". "diagnostic testing". "http://www.who.int/malaria/areas/diagnosis/en/", "2016". "[Online; accessed 29-January-2016]".

[2] Chansuda Wongsrichanalai, Mazie J Barcus, Sinuon Muth, Awalludin Sutamihardja, and Walther H Wernsdorfer. A review of malaria diagnostic tools: microscopy and rapid diagnostic test (rdt). *Am. J. Trop. Med. Hyg.*, 77(6 Suppl):119–127, 2007.

[3] `https://ourworldindata.org/uploads/2019/04/Previous-prevalence-of-malaria-world-map.png`, (accessed November 4, 2019).

[4] R Ramasamy, N Subanesan, A Wijesundere, NK Fernando, and MS Ramasamy. Observations on malaria patients seeking treatment in hospitals in a rural and an urban area of sri lanka. *Indian J. Malariol.*, 29(1):29–34, 1992.

[5] Alassane Dicko, Carsten Mantel, Boureima Kouriba, Issaka Sagara, Mahamadou A Thera, Seydou Doumbia, Mouctar Diallo, Belco Poudiougou, Mahamadou Diakite, and Ogobara K Doumbo. Season, fever prevalence and pyrogenic threshold for malaria disease definition in an endemic area of mali. *Trop. Med. Int. Health*, 10(6):550–556, 2005.

[6] Tabitha W Mwangi, Mahfudh Mohammed, Hiza Dayo, Robert W Snow, and

Kevin Marsh. Clinical algorithms for malaria diagnosis lack utility among people of different age groups. *Trop. Med. Int. Health*, 10(6):530–536, 2005.

[7] William Trager, Maria A Rudzinska, and Phyllis C Bradbury. The fine structure of plasmodium falciparum and its host erythrocytes in natural malarial infections in man. *Bull. World Health Organ.*, 35(6):883, 1966.

[8] RJ Howard and AD Gilladoga. Molecular studies related to the pathogenesis of cerebral malaria. *Blood*, 74(8):2603–2618, 1989.

[9] John W Barnwell. Cytoadherence and sequestration in falciparum malaria. *Exp. Parasitol.*, 69(4):407–412, 1989.

[10] Berend Houwen. Blood film preparation and staining procedures. *Clinics in laboratory medicine*, 22(1):1–14, 2002.

[11] LM Milne, MS Kyi, PL Chiodini, and DC Warhurst. Accuracy of routine laboratory diagnosis of malaria in the united kingdom. *Am. J. Clin. Pathol.*, 47(8):740–742, 1994.

[12] Nicholas W Stow, James K Torrens, and John Walker. An assessment of the accuracy of clinical diagnosis, local microscopy and a rapid immunochromatographic card test in comparison with expert microscopy in the diagnosis of malaria in rural kenya. *Trans. R. Soc. Trop. Med. Hyg.*, 93(5):519–520, 1999.

[13] Christian Aalkjær, D Boedtkjer, and Vladimir Matchkov. Vasomotion–what is currently thought? *Acta. Physiol.*, 202(3):253–269, 2011.

[14] A. Stefanovska. Coupled oscillators: Complex but not complicated cardiovascular and brain interactions. In *IEEE Eng Med Biol Mag*, volume 26, pages 25–29, 2007.

[15] Yuri Shiogai, Aneta Stefanovska, and Peter Vaughan Elsmere McClintock.

Nonlinear dynamics of cardiovascular ageing. *Phys. Rep.*, 488(2):51–110, 2010.

[16] Per Kvandal, Svein Aslak Landsverk, Alan Bernjak, Aneta Stefanovska, Hebe Désirée Kvernmo, and Knut Arvid Kirkebøen. Low-frequency oscillations of the laser Doppler perfusion signal in human skin. *Microvasc. Res.*, 72(3):120–127, 2006.

[17] Aneta Stefanovska, M Bracic, and Hebe Kvernmo. Wavelet analysis of oscillations in the peripheral blood circulation measured by laser Doppler technique. *IEEE Trans. Biomed. Eng.*, 46:1230–9, 11 1999. doi: 10.1109/10.790500.

[18] Aneta Stefanovska and Maja Bracic. Physics of the human cardiovascular system. *Contemp. Phys.*, 40(1):31–55, 1999.

[19] William C Aird. Discovery of the cardiovascular system: from galen to william harvey. *J. Thromb. Haemost.*, 9:118–129, 2011.

[20] ChristodoulosstefAnAdis GeorGe Androutsos, MAriAnnA KArAMAnou. William harvey (1578-1657): Discoverer of blood circulation. *Hellenic J. Cardiol.*, 53:6–9, 2012.

[21] Gorny P. Histoire illustrée de la cardiologie de la préhistoireà nos jours. paris: Roger dacosta. pages 159–172, 1985.

[22] HA Albilani Hajar. Traditional medicine among gulf arabs: part ii. bloodletting. *Heart Views*, 5:74–85, 2004.

[23] Ibn an Nafîs. Commentaire anatomique sur le canon d'avicenne. trad. amor chadli et ahmed ezzine barhoumi. *Tunis: Simpact*, 2005.

[24] Domenico Ribatti. William harvey and the discovery of the circulation of the blood. *J. Angiogenes Res.*, 1(1):1–2, 2009.

[25] Théodore Robert Louis Vetter. Un siècle d' histoire de la circulation du sang (1564-1664):les anticirculateurs. *Documenta Geigy. Bâle: Labo-ratoires Geigy*, pages 42–59, 1965.

[26] Lippold O.C.J. and Winton. R.Fauthor. *Human Physiology.* Churchill Livingstone, Edinburgh, 1979.

[27]]bach Bachelard G. *Le nouvel esprit scientifique [The new scientific spirit].* Presse Universitaire de France , Paris, 1934[1968].

[28] Marc Thiriet. *Biology and Mechanics of Bloood Flows.* Springer New York, 2008.

[29] Fumihiko Yasuma and Jun-ichiro Hayano. Respiratory sinus arrhythmia. *Chest*, 125(2):683 – 690, 2004.

[30] ED Adrian, Detlev W Bronk, and Gilbert Phillips. Discharges in mammalian sympathetic nerves. *J. Physiol.*, 74(2):115–133, 1932.

[31] Zhilin Qu, Gang Hu, Alan Garfinkel, and James N. Weiss. Nonlinear and stochastic dynamics in the heart. *Phys. Rep.*, 543(2):61 – 162, 2014. Nonlinear and Stochastic Dynamics in the Heart.

[32] H.J.Wellens. D.P. Zipes. Sudden cardiac death. *Circulation*, 98:2334–2351, 1998.

[33] D.P. Zipes. M. Rubart. Mechanisms of sudden cardiac death. *J. Clin. Invest.*, 115(9):2305–2315, 2005.

[34] A.T. Winfree. Sudden cardiac death: a problem in topology. *Sci. Am.*, 248: 144–149. 152–147. 141–161., 1983.

[35] Leon Glass. Dynamics of cardiac arrhythmias. *Phys. Today.*, 49(8):40, 1996.

[36] A. Karma. Physics of cardiac arrhythmogenesis. *Annu. Rev. Condens. Matter Phys.*, 4:313–337, 2013.

[37] Alain Karma and Robert F. Gilmour Jr. Nonlinear dynamics of heart rhythm disorders. *Phys. Today.*, 60(3):51 – 57, 2007.

[38] Trine Krogh-Madsen and David J. Christini. Nonlinear dynamics in cardiology. *Annu. Rev. Biomed. Eng.*, 14(1):179–203, 2012.

[39] Zhilin Qu. Chaos in the genesis and maintenance of cardiac arrhythmias. *Prog. Biophys. Mol. Biol.*, 105(3):247 – 257, 2011.

[40] Richard e Klabunde, editor. *Cardiovascular physiology concepts*. Philadelphia, PA : Lippincott Williams and Wilkins/Wolters Kluwer, 2012., Oxford, 2002.

[41] Chi-Sang Poon and Christopher K Merrill. Decrease of cardiac chaos in congestive heart failure. *Nature*, 389(6650):492, 1997.

[42] Wharton Jones. Discovery that the veins of the bat's wing are endowed with rhythmical contractility and that onward flow of blood is accelerated by each contraction. *Philos. Trans. R Soc. Lond.*, 142:131–136, 1852.

[43] J-U Meyer, P Borgström, L Lindbom, and M Intaglietta. Vasomotion patterns in skeletal muscle arterioles during changes in arterial pressure. *Microvasc. Res.*, 35(2):193–203, 1988.

[44] ELIETE Bouskela and WOLFGANG Grampp. Spontaneous vasomotion in hamster cheek pouch arterioles in varying experimental conditions. *Am. J. Physiol. Heart Circ. Physiol.*, 262(2):H478–H485, 1992.

[45] Eliete Bouskela and Fatima ZGA Cyrino. Effects of buflomedil on spontaneous vasomotion and mean arteriolar internal diameter in the hamster cheek pouch. *J. Vasc. Res.*, 31(5):287–294, 1994.

[46] Hongli Peng, Vladimir Matchkov, Anders Ivarsen, Christian Aalkjær, and Holger Nilsson. Hypothesis for the initiation of vasomotion. *Circ. Res.*, 88 (8):810–815, 2001.

[47] Anatoly Borovik, Veronika Golubinskaya, Olga Tarasova, Christian Aalkjaer, and Holger Nilsson. Phase resetting of arterial vasomotion by burst stimulation of perivascular nerves. *J. Vasc. Res.*, 42(2):165–173, 2005.

[48] Vladimir Matchkov, Awahan Rahman, Linda M Bakker, Tudor M Griffith, Holger Nilsson, and Christian Aalkjaer. Analysis of effects of connexin-mimetic peptide in rat mesenteric small arteries. *Am. J. Physiol. Heart Circ. Physiol.*, 291:H357–67, 08 2006.

[49] Donna Boedtkjer, Vladimir Matchkov, Ebbe Boedtkjer, Holger Nilsson, and Christian Aalkjaer. Vasomotion has chloride-dependency in rat mesenteric small arteries. *Pflugers Arch.*, 457:389–404, 07 2008.

[50] Michèle Koenigsberger, Roger Sauser, Dominique Seppey, Jean-Louis Bény, and Jean-Jacques Meister. Calcium dynamics and vasomotion in arteries subject to isometric, isobaric, and isotonic conditions. *Biophys. J.*, 95:2728–38, 07 2008.

[51] M Intaglietta. Vasomotion and flowmotion: physiological mechanisms and clinical evidence. *Vasc. Med.*, 1(2):101–112, 1990.

[52] Dick W Slaaf, Geert Jan Tangelder, Harry C Teirlinck, and Robert S Reneman. Arteriolar vasomotion and arterial pressure reduction in rabbit tenuissimus muscle. *Microvasc. Res.*, 33(1):71–80, 1987.

[53] Tony J Verbeuren, Marie-Odile Vallez, Gilbert Lavielle, and Eliete Bouskela. Activation of thromboxane receptors and the induction of vasomotion in the hamster cheek pouch microcirculation. *Br. J. Pharmacol.*, 122(5):859–866, 1997.

[54] J.A. Schmidt. *Periodic Hemodynamics in Health and Disease*. Landes Bioscience, 1996.

[55] D. W. Slaaf, H. H. Vrielink, G. J. Tangelder, and R. S. Reneman. Effective

diameter as a determinant of local vascular resistance in presence of vasomotion. *Am. J. Physiol. Heart Circ. Physiol.*, 255(5):H1240–H1243, 1988.

[56] McClintock P.V. Bernjak A., Clarkson P.B.M. and Stefanovska A. Low-frequency blood flow oscillations in congestive heart failure and after β1-blockade treatment. *Microvasc. Res.*, 76(3):224–232, 2008.

[57] Clare E Thorn, Stephen J Matcher, Igor V Meglinski, and Angela C Shore. Is mean blood saturation a useful marker of tissue oxygenation? *Am. J. Physiol. Heart Circ. Physiol.*, 296(5):H1289–H1295, 2009.

[58] AG Tsai and M Intaglietta. Evidence of flowmotion induced changes in local tissue oxygenation. *Int. J. Microcirc. Clin. Exp.*, 12(1):75–88, 1993.

[59] Clare E Thorn, Angela C Shore, and Stephen J Matcher. Combined optical and near infrared reflectance measurements of vasomotion in both skin and underlying muscle. In *Optical Tomography and Spectroscopy of Tissue VII*, volume 6434, page 643421. International Society for Optics and Photonics, 2007.

[60] Alan Bernjak, Aneta Stefanovska, Peter VE McClintock, P Jane Owen-Lynch, and Peter BM Clarkson. Coherence between fluctuations in blood flow and oxygen saturation. *Fluct. Noise. Lett.*, 11(1):1240013, 2012.

[61] Hebe Désirée Kvernmo, Aneta Stefanovska, Knut Arvid Kirkebøen, and Knut Kvernebo. Oscillations in the human cutaneous blood perfusion signal modified by endothelium-dependent and endothelium-independent vasodilators. *Microvasc. Res.*, 57(3):298–309, 1999.

[62] Maja Bračič and Aneta Stefanovska. Wavelet-based analysis of human blood-flow dynamics. *Bull. Math. Biol.*, 60(5):919–935, 1998.

[63] Gemma Lancaster, Aneta Stefanovska, Margherita Pesce, Gian Marco Vezzoni, Barbara Loggini, Raffaele Pingitore, Fabrizio Ghiara, Paolo Barachini,

Gregorio Cervadoro, and Marco Romanelli. Dynamic markers based on blood perfusion fluctuations for selecting skin melanocytic lesions for biopsy. *Scientific Reports*, 5, 2015.

[64] J K Wilkin. Periodic cutaneous blood flow during postocclusive reactive hyperemia. *Am. J. Physiol.*, 250:H765–8, 06 1986.

[65] Tatsuhiko Kano, Osamu Shimoda, Akira Hashiguchi, and Toshihide Satoh. Periodic abnormal fluctuations of blood pressure, heart rate and skin blood flow appearing in a resuscitated comatose patient. *J. Auton. Nerv. Syst.*, 36 (2):115 – 122, 1991.

[66] Martin Meyer, C J Rose, J-O Hülsmann, H Schatz, and Martin Pfohl. Impaired 0.1-hz vasomotion assessed by laser Doppler anemometry as an early index of peripheral sympathetic neuropathy in diabetes. *Microvasc. Res.*, 65:88–95, 04 2003.

[67] Marco Rossi, Angelo Carpi, Cinzia Di Maria, Fabio Galetta, and Gino Santoro. Spectral analysis of laser Doppler skin blood flow oscillations in human essential arterial hypertension. *Microvasc. Res.*, 72:34–41, 07 2006.

[68] Svein Aslak Landsverk, Per Kvandal, Alan Bernjak, Aneta Stefanovska, and Knut A Kirkeboen. The effects of general anesthesia on human skin microcirculation evaluated by wavelet transform. *Anesth. Analg.*, 105(4):1012–1019, 2007.

[69] Marco Rossi, Adam Bradbury, Armando Magagna, Margherita Pesce, Stefano Taddei, and Aneta Stefanovska. Investigation of skin vasoreactivity and blood flow oscillations in hypertensive patients: effect of short-term antihypertensive treatment. *J. Hypertens.*, 29(8):1569–1576, 2011.

[70] Valentina Ticcinelli, Tomislav Stankovski, Dmytro Iatsenko, Alan Bernjak, Adam E. Bradbury, Andrew R. Gallagher, Peter B. M. Clarkson, Peter V. E.

McClintock, and Aneta Stefanovska. Coherence and coupling functions reveal microvascular impairment in treated hypertension. *Front. Physiol.*, 8: 749, 2017.

[71] S. J. Benbow, D. W. Pryce, K. Noblett, I. A. MacFarlane, P. S. Friedmann, and G. Williams. Flow motion in peripheral diabetic neuropathy. *Clin. Sci.*, 88(2):191–196, 1995.

[72] Kevin B Stansberry, Shane A Shapiro, Michael A Hill, Patricia M McNitt, Martin D Meyer, and Aaron I Vinik. Impaired peripheral vasomotion in diabetes. *Diabetes Care*, 19(7):715–721, 1996.

[73] E. Bouskela. Effects of metformin on the wing microcirculation of normal and diabetic bats. *Diabetes Metab.*, 14(4 BIS):560–565, 1995.

[74] Corinne Renaudin, Edouard Michoud, Michel Lagarde, and Nicolas Wiernsperger. Impaired microvascular responses to acute hyperglycemia in type i diabetic rats. *J. Diabetes Complicat.*, 13(1):39 – 44, 1999.

[75] Jens Kastrup, Jens Bülow, and N A Lassen. Vasomotion in human skin before and after local heating recorded with laser Doppler flowmetry. a method for induction of vasomotion. *Int. J. Microcirc., Clin. Exp.*, 8:205–15, 05 1989.

[76] Marco Rossi, Luigi Ricordi, Emilio Mevio, Gabriele Fornasari, Cesare Orlandi, Pietro Fratino, Giorgio Finardi, and Luana Bernardi. Autonomic nervous system and microcirculation in diabetes. *J. Auton. Nerv. Sys.*, 30 Suppl:S133–5, 08 1990.

[77] Leonardo Bocchi, Attilio Evangelisti, Massimo Barrella, L Scatizzi, and Maurizio Bevilacqua. Recovery of 0.1 hz microvascular skin blood flow in dysautonomic diabetic (type 2) neuropathy by using frequency rhythmic electrical modulation system (frems). *Med. Eng. Phys.*, 32:407–13, 03 2010.

[78] Martin Meyer, C J Rose, J-O Hülsmann, H Schatz, and Martin Pfohl. Impairment of cutaneous arteriolar 0.1 hz vasomotion in diabetes. *Exp. Clin. Endocrinol. Diabetes*, 111:104–10, 05 2003.

[79] A J Ryan and C V Gisolfi. Responses of rat mesenteric arteries to norepinephrine during exposure to heat stress and acidosis. *J. Appl. Physiol.*, 78:38–45, 02 1995.

[80] Terumi Sakurai and Terui Naohito. Effects of sympathetically induced vasomotion on tissue-capillary fluid exchange. *Am. J. Physiol. Heart Circ. Physiol.*, 291:H1761–7, 11 2006. doi: 10.1152/ajpheart.00280.2006.

[81] Alan Bernjak, Jian Cui, Satoshi Iwase, Tadaaki Mano, Aneta Stefanovska, and Dwain L Eckberg. Human sympathetic outflows to skin and muscle target organs fluctuate concordantly over a wide range of time-varying frequencies. *J. Physiol.* (London), 590(2):363–375, 2012.

[82] Christian Aalkjaer, A M Heagerty, K K Petersen, J D Swales, and M J Mulvany. Evidence for increased media thickness, increased neuronal amine uptake, and depressed excitation-contraction coupling in isolated resistance vessels from essential hypertensives. *Circ. Res.*, 61:181–6, 09 1987. doi: 10.1161/01.RES.61.2.181.

[83] Kensuke Egashira, Tetsuzi Inou, Yoshitaka Hirooka, Hisashi Kai, Masaru Sugimachi, Satoshi Suzuki, Takeshi Kuga, Yoshitoshi Urabe, and Akira Takeshita. Effects of age on endothelium-dependent vasodilation of resistance coronary artery by acetylcholine in humans. *Circulation*, 88:77–81, 1993.

[84] David S Celermajer, Keld E Sorensen, David J Spiegelhalter, Dimitri Georgakopoulos, Jacqui Robinson, and John E Deanfield. Aging is associated with endothelial dysfunction in healthy men years before the age-related decline in women. *J. Am. Coll. Cardiol.*, 24:471–476, 1994.

[85] B.Winblad A. Algotsson, A. Nordberg. Influence of age and gender on skin vessel reactivity to endothelium-dependent and endothelium-independent vasodilators tested with iontophoresis and a laser Doppler perfusion image. *J. Gerontol. A: Biol. Sci. Med. Sci.*, 50(2):M121–M127, 1995.

[86] Marie Gerhard, Mary-Anne Roddy, Shelly J Creager, and Mark A Creager. Aging progressively impairs endothelial-dependent vasodilation in forearm resistance vessels of humans. *Hypertension*, 27(4):849–853, 1996.

[87] Valentina Ticcinelli, Tomislav Stankovski, Peter VE McClintock, and Aneta Stefanovska. Ageing of the couplings between cardiac, respiratory and myogenic activity in humans. In *2015 37th Annual International Conference of the IEEE Engineering in Medicine and Biology Society (EMBC)*, pages 7366–7369. IEEE, 2015.

[88] Clare E Thorn, Hayley Kyte, Dick W Slaff, and Angela C Shore. An association between vasomotion and oxygen extraction. *Am. J. Physiol. Heart Circ. Physiol.*, 301(2):H442–H449, 2011.

[89] J.André Schmidt, Per Borgström, Gary P. Firestone, Peter von Wichert, Marcos Intaglietta, and Arnost Fronek. Periodic hemodynamics (flow motion) in peripheral arterial occlusive disease. *J. Vasc. Surg.*, 18(2):207 – 215, 1993.

[90] A Scheffler and H Rieger. Spontaneous oscillations of laser-Doppler skin blood flux in peripheral arterial occlusive disease. *Int. J. Microcirc. Clin. Exp.*, 11:249–61, 09 1992.

[91] Franzeck U.K. Hoffmann U. and Bollinger A. Low frequency oscillations of skin blood flux in peripheral arterial occlusive disease. *Vasa.*, 23(2):120–124, 12 1994.

[92] Ikuo Ohta, Aki Ohta, Masahiro Shibata, and Akira Kamiya. Oxygen transport to tissue during recurrent blood flow supply by grouped capillaries in

skeletal muscle with or without facilitated diffusion. *Adv. Exp. Med. Biol.*, 222:105–12, 02 1988.

[93] Daniel Goldman and Aleksander S Popel. A computational study of the effect of vasomotion on oxygen transport from capillary networks. *J. Theor. Biol.*, 209(2):189–199, 2001.

[94] Ranjan Pradhan and Srinivasa Chakravarthy. A computational model that links non-periodic vasomotion to enhanced oxygenation in skeletal muscle. *Math. Biosci.*, 209:486–99, 11 2007.

[95] Park C.S. Hapuarachchi T. and Payne S. Quantification of the effects of vasomotion on mass transport to tissue from axisymmetric blood vessels. *J. Theor. Biol.*, 264(2):553 – 559, 2010.

[96] Victor Kislukhin. Stochasticity of flow through microcirculation as a regulator of oxygen delivery. *Theor. Biol. Med. Model.*, 7:29, 07 2010.

[97] Lacy A Holowatz, Caitlin S Thompson-Torgerson, and W Larry Kenney. The human cutaneous circulation as a model of generalized microvascular function. *J. Appl. Physiol.*, 105(1):370–372, 12 2008.

[98] Jean Kanitakis. Anatomy, histology and immunohistochemistry of normal human skin. *Eur. J. Dermatol.*, 12(4):390–401, 2002.

[99] Berger T. G. James W. D. and Elston D. M. *Andrews' diseases of the skin: Clinical dermatology (10th ed.).* Philadelphia: Elsevier Saunders., 2006.

[100] D.H. Chu. Overview of biology, development and structure of skin. *Fitzpatrick's Dermatology in General Medicine, 7Th Edn. Vol. 1 (Eds. Wolff, K. Et Al.)*, pages 57–73, 01 2008.

[101] R. Rox Anderson and John A. Parrish. The optics of human skin. *J. Invest. Dermatol.*, 77:13–19, 1981. ISSN 0022-202X. URL `http://www.sciencedirect.com/science/article/pii/S0022202X15461251`.

[102] John A. Parrish, Rox , Frederick Urbach, and Donald Pitts. *UV-A: Biological Effects of Ultraviolet Radiation with Emphasis on Human Responses to Longwave Ultraviolet*. 01 1978.

[103] R.J. Scheuplein. A survey of some fundamental aspects of the absorpt ion and reflection of light by tissue. *J. Soc. Cosmet. Chem.*, 15(2):111– 122, 1993.

[104] RR Anderson, J Hu, and JA Parrish. Optical radiation transfer in the human skin and applications in in vivo remittance spectroscopy. In *Bioengineering and the Skin*, pages 253–265. Springer, 1981.

[105] K A Hasselbalch. Quantitative Untersuchungen über die Absorption der menschlichen Haut von ultravioletten Strahlen. *Skand. Arch. Physiol.*, 25: 55–68, 1911.

[106] Hans F Kuppenheim and Raymond R Heer JR. Spectral reflectance of white and negro skin between 440 and 1000 mμ. *J. Appl. Physiol.*, 4(10):800–806, 1952.

[107] John A Jacquez, John Huss, Wayne McKeehan, James M Dimitroff, and Hans F Kuppenheim. Spectral reflectance of human skin in the region 0.7–2.6 μ. *J. Appl. Physiol.*, 8(3):297–299, 1955.

[108] James D Hardy, Harold T Hammel, and Dorothy Murgatroyd. Spectral transmittance and reflectance of excised human skin. *J. Appl. Physiol.*, 9: 257–264, 1956.

[109] Mark Allen Everett, Edward Yeargers, Robert M Sayre, and Robert L Olson. Penetration of epidermis by ultraviolet rays. *Photochem. Photobiol.*, 5(7): 533–542, 1966.

[110] GH Findlay. Blue skin. *Br. J. Dermatol.*, 83(1):127–134, 1970.

[111] Albert Bachem and CI Reed. The transparency of live and dead animal tissue to ultra-violet light. *Am. J. Physiol.*, 90(3):600–606, 1929.

[112] HZ Cummins, N Knable, and Y Yeh. Observation of diffusion broadening of rayleigh scattered light. *Phys. Rev. Lett.*, 12(6):150, 1964.

[113] Theodore H Maiman et al. Stimulated optical radiation in ruby. *Nature*, 187:493–494, 1960.

[114] Charles Riva, Benjamin Ross, and George B Benedek. Laser Doppler measurements of blood flow in capillary tubes and retinal arteries. *Invest. Ophthalmol. Vis. Sci.*, 11(11):936–944, 1972.

[115] MD Stern. In vivo evaluation of microcirculation by coherent light scattering. *Nature*, 254(5495):56, 1975.

[116] Dennis Watkins and G Allen Holloway. An instrument to measure cutaneous blood flow using the Doppler shift of laser light. *IEEE Trans Biomed Eng*, (1):28–33, 1978.

[117] Gert E Nilsson, Torsten Tenland, and P Ake Oberg. Evaluation of a laser Doppler flowmeter for measurement of tissue blood flow. *IEEE Trans. Biomed. Eng.*, (10):597–604, 1980.

[118] Joseph C Fischer, Paul M Parker, and William W Shaw. Comparison of two laser Doppler flowmeters for the monitoring of dermal blood flow. *Microsurgery*, 4(3):164–170, 1983.

[119] Ulrich Hoffmann, Ahmet Yanar, Ulrich Franzeck, James Edwards, and Alfred Bollinger. The frequency histogram—a new method for the evaluation of laser Doppler flux motion. *Microvasc. Res.*, 40:293–301, 12 1990.

[120] Göran Salerud, T Tenland, Gert Nilsson, and Åke Öberg. Rythmical variations in human skin blood flow. *Int. J. Microcirc. Clin. Exp.*, 2:91–102, 02 1983.

[121] G Hildebrandt. *The Autonomous Time Structure and Its Reactive Modifications in the Human Organism*, pages 160–175. 01 1987.

[122] Marco Di Rienzo, G Mancia, and G Parati. *Computer analysis of cardiovascular signals*, volume 13. Ios press, 1995.

[123] Maja Bračič and Aneta Stefanovska. Wavelet analysis in studying the dynamics of blood circulation. *Nonlinear Phenomena in Complex Systems*, 2 (1):68–77, 1999.

[124] Aneta Stefanovska and Peter Krošelj. Correlation integral and frequency analysis of cardiovascular functions. *Open Syst. and Inf. Dyn.*, 4(4):457–478, 1997.

[125] A Bollinger, A Yanar, U Hoffmann, and UK Franzeck. Is high-frequency flux motion due to respiration or to vasomotion activity? In *Vasomotion and flow motion*, volume 20, pages 52–58. Karger Publishers, 1993.

[126] ME Mück-Weymann, HP Albrecht, D Hiller, OP Hornstein, and RD Bauer. Respiration-dependence of cutaneous laser Doppler flow motion. *VASA. Zeitschrift fur Gefasskrankheiten*, 23(4):299–304, 1994.

[127] M E Mück-Weymann, H P Albrecht, D Hiller, O P Hornstein, and R D Bauer. [respiration-dependence of cutaneous laser Doppler flow motion]. *VASA*, 23:299–304, 02 1994.

[128] BW Hyndman, RI Kitney, and B McA Sayers. Spontaneous rhythms in physiological control systems. *Nature*, 233(5318):339, 1971.

[129] Solange Akselrod, David Gordon, F Andrew Ubel, Daniel C Shannon, AC Berger, and Richard J Cohen. Power spectrum analysis of heart rate fluctuation: a quantitative probe of beat-to-beat cardiovascular control. *Science*, 213(4504):220–222, 1981.

[130] RI Kitney, T Fulton, AH McDonald, and DA Linkenst. Transient interactions between blood pressure, respiration and heart rate in man. *J. Biomed. Eng.*, 7(3):217–224, 1985.

[131] B Folkow. Description of the myogenic hypothesis. *Circ. Res.*, 15(1):279–287, 1964.

[132] A Colantuoni, Silvia Bertuglia, and M Intaglietta. Quantitation of rhythmic diameter changes in arterial microcirculation. *Am. J. Physiol. Heart Circ. Physiol.*, 246(4):H508–H517, 1984.

[133] Marcos Intaglietta. *Vasomotion and flow modulation in the microcirculation: satellite symposium to the Annual Meeting of the Microcirculatory Society, Las Vegas, Nev., April 28-29, 1988*, volume 15. S Karger Ag, 1989.

[134] Ludwig Traube. Uber periodische tatigkeitausserungen der vasomotorischen und hemmungs-nervenzentrums. *Cbl Med Wiss*, 56:881–885, 1865.

[135] Ewald Hering. *Über den einfluss der athmung auf den kreislauf...* 1869.

[136] Stephanie Anschütz and Rudolf Schubert. Modulation of the myogenic response by neurogenic influences in rat small arteries. *Br. J. Pharmacol.*, 146 (2):226–233, 2005.

[137] David R Harder. Pressure-dependent membrane depolarization in cat middle cerebral artery. *Circ. Res.*, 55(2):197–202, 1984.

[138] G Osol and W Halpern. Myogenic properties of cerebral blood vessels from normotensive and hypertensive rats. *American Journal of Physiology-Heart and Circulatory Physiology*, 249(5):H914–H921, 1985.

[139] Viktor Berczi, William J Stekiel, Stephen J Contney, and Nancy J Rusch. Pressure-induced activation of membrane k+ current in rat saphenous artery. *Hypertension*, 19(6 Pt 2):725–729, 1992.

[140] Torbjörn Söderström, Aneta Stefanovska, Mitja Veber, and Henry Svensson. Involvement of sympathetic nerve activity in skin blood flow oscillations in humans. *Am. J. Physiol. Heart Circ. Physiol.*, 284(5):H1638–H1646, 2003.

[141] Aneta Stefanovska, Sašo Strle, and Peter Krošelj. On the overestimation of the correlation dimension. *Phys. Lett.*, 235(1):24–30, 1997.

[142] Klaus Golenhofen and Gunther Hildebrandt. Die beziehungen des blutdruck-rhythmus zu atmung und peripherer durchblutung. *Pflüger's Archiv für die gesamte Physiologie des Menschen und der Tiere*, 267(1):27–45, 1958.

[143] J ANDRE Schmidt, MARCOS Intaglietta, and P Borgstrom. Periodic hemodynamics in skeletal muscle during local arterial pressure reduction. *J. Appl. Physiol.*, 73(3):1077–1083, 1992.

[144] Simon C Malpas. The rhythmicity of sympathetic nerve activity. *Prog. Neurobiol.*, 56(1):65–96, 1998.

[145] Svein A Landsverk, Per Kvandal, Trygve Kjelstrup, Uros Benko, Alan Bernjak, Aneta Stefanovska, Hebe Kvernmo, and Knut A Kirkeboen. Human skin microcirculation after brachial plexus block evaluated by wavelet transform of the laser Doppler flowmetry signal. *Anesthesiology*, 105(3):478–484, 2006.

[146] Stefan Lehtipalo, Ola Winsö, L-OD Koskinen, Göran Johansson, and Björn Biber. Cutaneous sympathetic vasoconstrictor reflexes for the evaluation of interscalene brachial plexus block. *Acta Anaesthesiol. Scand.*, 44(8):946–952, 2000.

[147] E Eneroth-Grimfors, LE Lindblad, M Westgren, C Ihrman-Sandahl, and S Bevegard. Noninvasive test of microvascular endothelial function in normal and hypertensive pregnancies. *BJOG*, 100(5):469–471, 1993.

[148] Robert F Furchgott and John V Zawadzki. The obligatory role of endothelial cells in the relaxation of arterial smooth muscle by acetylcholine. *Nature*, 288(589):373, 1980.

[149] RA Westerman, RE Widdop, J Hannaford, A Low, RGD Roberts, P Kent, K Sideris, T Yip, JRS Hales, and FRN Stephens. Laser Doppler velocimetry in the measurement of neurovascular function. 1988.

[150] SJ Morris and AC Shore. Skin blood flow responses to the iontophoresis of acetylcholine and sodium nitroprusside in man: possible mechanisms. *J. Physiol.*, 496(2):531–542, 1996.

[151] SRMJ Moncada. Nitric oxide: physiology, pathophysiology, and pharmacology. *Pharmacol. Rev.*, 43:109–142, 1991.

[152] Hebe Désirée Kvernmo, Aneta Stefanovska, and Knut Arvid Kirkebøen. Enhanced endothelial activity reflected in cutaneous blood flow oscillations of athletes. *Eur. J. Appl. Physiol. Occup. Physiol.*, 90(1-2):16–22, 2003.

[153] Mitja Veber, Andriy Bandrivskyy, Peter BM Clarkson, Peter VE McClintock, and Aneta Stefanovska. Wavelet analysis of blood flow dynamics: effect on the individual oscillatory components of iontophoresis with pharmacologically neutral electrolytes. *Phys. Med. Biol.*, 49(8):N111, 2004.

[154] Andriy Bandrivskyy, Alan Bernjak, Peter VE McClintock, and Aneta Stefanovska. Role of transdermal potential difference during iontophoretic drug delivery. *IEEE Trans. Biomed. Eng.*, 51(9):1683–1685, 2004.

[155] Per Kvandal, Aneta Stefanovska, Mitja Veber, Hebe Désirée Kvermmo, and Knut Arvid Kirkebøen. Regulation of human cutaneous circulation evaluated by laser Doppler flowmetry, iontophoresis, and spectral analysis: importance of nitric oxide and prostaglandines. *Microvasc. Res.*, 65(3):160–171, 2003.

[156] Julian M Stewart, Indu Taneja, Michael S Goligorsky, and Marvin S Medow. Noninvasive measure of microvascular nitric oxide function in humans using very low-frequency cutaneous laser Doppler flow spectra. *Microcirculation*, 14(3):169–180, 2007.

[157] A Stefanovska, Lawrence Sheppard, T Stankovski, and PVE McClintock. Reproducibility of LDF blood flow measurements: dynamical characterization versus averaging. *Microvasc. Res.*, 82(3):274–276, 2011.

[158] Marco Rossi, Monica Nannipieri, Marco Anselmino, Margherita Pesce, Elza Muscelli, Gino Santoro, and Ele Ferrannini. Skin vasodilator function and vasomotion in patients with morbid obesity: effects of gastric bypass surgery. *Obes. Surg.*, 21(1):87–94, 2011.

[159] Marco Rossi, Elena Matteucci, Margherita Pesce, Cristina Consani, Fabio Galetta, Ottavio Giampietro, and Gino Santoro. Study of skin vasomotion in type 1 diabetic patients and of its possible relationship with clinical and laboratory variables. *Clin. Hemorheol. Microcirc.*, 53(4):357–367, 2013.

[160] Valentina Ticcinelli, Romeo Martini, and Andrea Bagno. Preliminary study of laser Doppler perfusion signal by wavelet transform in patients with critical limb ischemia before and after revascularization. *Clin. Hemorheol. Microcirc.*, 58(3):415–428, 2014.

[161] A.R. Pries, T.W. Secomb, and P. Gaehtgens. Biophysical aspects of blood flow in the microvasculature. *Cardiovasc. Res.*, 32(4):654–667, 1996. ISSN 0008-6363.

[162] C. C. Michel and F. E. Curry. Microvascular permeability. *Physiological Reviews*, 79(3):703–761, 1999. ISSN 0031-9333.

[163] Aleksander S Popel and Paul C Johnson. Microcirculation and hemorheology. *Annu. Rev. Fluid Mech.*, 37:43–69, 2005.

[164] Granger D Schmid-SchonbeinGW. *Molecular Basis of Microcirculatory Disorders*. New York: Springer., 2003.

[165] J Dufaux, D Quemada, and P Mills. Determination of rheological properties of red blood cells by couette viscometry. *Rev Phys Appl*, 15(8):1367–1374, 1980.

[166] Peter Gaehtgens. Hemodynamics of the microcirculation physical characteristics of blood flow in the microvasculature. In *Mikrozirkulation/Microcirculation*, pages 231–287. Springer, 1977.

[167] TW Secomb. Red blood cell mechanics and capillary blood rheology. *Cell Biophys.*, 18(3):231, 1991.

[168] Salvatore P Sutera and Richard Skalak. The history of poiseuille's law. *Annu. Rev. Fluid Mech.*, 25(1):1–20, 1993.

[169] S Chien. Red cell deformability and its relevance to blood flow. *Annu. Rev. Physiol.*, 49(1):177–192, 1987. doi: 10.1146/annurev.ph.49.030187.001141.

[170] YC Fung and BW Zweifach. Microcirculation: mechanics of blood flow in capillaries. *Annu. Rev. Fluid Mech.*, 3(1):189–210, 1971.

[171] Yuan-cheng Fung. *Biomechanics: circulation*. Springer Science & Business Media, 2013.

[172] Richard Skalak, Nihat Ozkaya, and Thomas C Skalak. Biofluid mechanics. *Annu. Rev. Fluid Mech.*, 21(1):167–200, 1989.

[173] Oguz K Baskurt and Herbert J Meiselman. Blood rheology and hemodynamics. In *Seminars in thrombosis and hemostasis*, volume 29, pages 435–450, 2003.

[174] Herbert J. Meiselman Simmonds Michael J. and Oguz K. Baskurt. Blood rheology and aging. *J. Geriatr. Cardiol.*, 10(3):291–301, 2013.

[175] Maya Natarajan, Mark M Udden, and LV McIntire. Adhesion of sickle red blood cells and damage to interleukin-1 beta stimulated endothelial cells under flow in vitro. *Blood*, 87(11):4845–4852, 1996.

[176] Neil M Matsui, Ajit Varki, and Stephen H Embury. Heparin inhibits the flow adhesion of sickle red blood cells to p-selectin. *Blood*, 100(10):3790–3796, 2002.

[177] Keiko Sugihara, T Sugihara, N Mohandas, and Robert P Hebbel. Thrombospondin mediates adherence of cd36+ sickle reticulocytes to endothelial cells. *Blood*, 80(10):2634–2642, 1992.

[178] DI Baruch, JA Gormely, C Ma, RJ Howard, and BL Pasloske. Plasmodium falciparum erythrocyte membrane protein 1 is a parasitized erythrocyte receptor for adherence to cd36, thrombospondin, and intercellular adhesion molecule 1. *Proc. Natl. Acad. Sci*, 93(8):3497–3502, 1996.

[179] Anna M Senczuk, John C Reeder, Magda M Kosmala, and May Ho. Plasmodium falciparum erythrocyte membrane protein 1 functions as a ligand for p-selectin. *Blood*, 98(10):3132–3135, 2001.

[180] Yan-Ting Shiu and Larry V McIntire. In vitro studies of erythrocyte–vascular endothelium interactions. *Ann. Biomed. Eng.*, 31(11):1299–1313, 2003.

[181] R Tran-Son-Tay, H-C Kan, HS Udaykumar, E Damay, and W Shyy. Rheological modelling of leukocytes. *Med. Biol. Eng. Comput.*, 36(2):246–250, 1998.

[182] Roger D Kamm. Cellular fluid mechanics. *Annu. Rev. Fluid Mech.*, 34(1): 211–232, 2002.

[183] Klaus Ley. The role of selectins in inflammation and disease. *Trends Mol. Med.*, 9(6):263–268, 2003.

[184] Cheng Zhu, Gang Bao, and Ning Wang. Cell mechanics: mechanical response, cell adhesion, and molecular deformation. *Annu. Rev. Biomed. Eng.*, 2(1):189–226, 2000.

[185] T Alexy, S Sangkatumvong, P Connes, E Pais, J Tripette, JC Barthelemy, TC Fisher, HJ Meiselman, MC Khoo, and TD Coates. Sickle cell disease: selected aspects of pathophysiology. *Clin. Hemorheol. Microcirc.*, 44(3):155–166, 2010.

[186] O Baskurt et al. Clinical significance of hemorheological alterations. *Handbook of hemorheology and hemodynamics*, 69:392, 2007.

[187] Oguz K Baskurt et al. Mechanisms of blood rheology alterations. *Handbook of Hemorheology. IOS Press*, 69:170, 2007.

[188] Oguz K Baskurt and Herbert J Meiselman. Activated polymorphonuclear leukocytes affect red blood cell aggregability. *J. Leukoc. Biol.*, 63(1):89–93, 1998.

[189] Matthew J Lynch and Stanley S Raphael. *Lynch's medical laboratory technology*. WB Saunders Company, 1976.

[190] Shlomo Berliner, Ori Rogowski, Stanislav Aharonov, Tamar Mardi, Tatiana Tolshinsky, Meirav Rozenblat, Dan Justo, Varda Deutsch, Jack Serov, Itzhak Shapira, et al. Erythrocyte adhesiveness/aggregation: a novel biomarker for the detection of low-grade internal inflammation in individuals with atherothrombotic risk factors and proven vascular disease. *Am. Heart J.*, 149(2):260–267, 2005.

[191] Oguz Baskurt, Björn Neu, and Herbert J Meiselman. *Red blood cell aggregation*. CRC Press, 2011.

[192] FJ Neumann, HA Katus, E Hoberg, P Roebruck, M Braun, HM Haupt, H Tillmanns, and W Kübler. Increased plasma viscosity and erythrocyte aggregation: indicators of an unfavourable clinical outcome in patients with unstable angina pectoris. *Br. Heart J.*, 66(6):425–430, 1991.

[193] Masao Soutani, Yoji Suzuki, Norihiko Tateishi, and Nobuji Maeda. Quantitative evaluation of flow dynamics of erythrocytes in microvessels: influence of erythrocyte aggregation. *Am. J. Physiol. Heart Circ. Physiol.*, 268(5): H1959–H1965, 1995.

[194] E Kaliviotis and M Yianneskis. Fast response characteristics of red blood cell aggregation. *Biorheology*, 45(6):639, 2008.

[195] M Cabel, HJ Meiselman, AS Popel, and PC Johnson. Contribution of red blood cell aggregation to venous vascular resistance in skeletal muscle. *Am. J. Physiol. Heart Circ. Physiol.*, 272(2):H1020–H1032, 1997.

[196] Jeffrey J Bishop, Patricia R Nance, Aleksander S Popel, Marcos Intaglietta, and Paul C Johnson. Effect of erythrocyte aggregation on velocity profiles in venules. *Am. J. Physiol. Heart Circ. Physiol.*, 280(1):H222–H236, 2001.

[197] OK Başkurt, M Bor-Küçükatay, and Ö Yalçın. The effect of red blood cell aggregation on blood flow resistance. *Biorheology*, 36:447–452, 1999.

[198] W Reinke, P Gaehtgens, and PC Johnson. Blood viscosity in small tubes: effect of shear rate, aggregation, and sedimentation. *Am. J. Physiol. Heart Circ. Physiol.*, 253(3):H540–H547, 1987.

[199] WERNER Reinke, PAUL C Johnson, and PETER Gaehtgens. Effect of shear rate variation on apparent viscosity of human blood in tubes of 29 to 94 microns diameter. *Circ. Res.*, 59(2):124–132, 1986.

[200] L Gustafsson, L Appelgren, and HE Myrvold. Effects of increased plasma viscosity and red blood cell aggregation on blood viscosity in vivo. *Am. J. Physiol. Heart Circ. Physiol.*, 241(4):H513–H518, 1981.

[201] Herbert J Meiselman. Red blood cell aggregation: 45 years being curious. *Biorheology*, 46(1):1–19, 2008.

[202] S. R. F. Whittaker and F. R. Winton. The apparent viscosity of blood flowing in the isolated hindlimb of the dog, and its variation with corpuscular concentration. *J. Physiol.*, 78(4):339–369, 1933.

[203] Gergely Feher, Katalin Koltai, Gabor Kesmarky, Laszlo Szapary, Istvan Juricskay, and Kalman Toth. Hemorheological parameters and aging. *Clin. Hemorheol. Microcirc.*, 35(1-2):89–98, 2005.

[204] Jé rô me Manetta, Ikram Aloulou, Emmanuelle Varlet-Marie, Jacques Mercier, and Jean-Fré dé ric Brun. Partially opposite hemorheological effects of aging and training at middle age. *Clin. Hemorheol. Microcirc.*, 35(1-2):239–244, 2005.

[205] Meiselman HJ. Baskurt OK. *In vivo hemorheology. Handbook of Hemorheology and Hemodynamics.* IOS Press., Amsterdam, Berlin, Oxford, Tokyo, Washington, DC, 2007.

[206] Oguz K Baskurt. In vivo correlates of altered blood rheology. *Biorheology*, 45(6):629–638, 2007.

[207] Oguz K Baskurt and Herbert J Meiselman. Erythrocyte aggregation: basic aspects and clinical importance. *Clin. Hemorheol. Microcirc.*, 53(1-2):23–37, 2012.

[208] LE Bayliss. The axial drift of the red cells when blood flows in a narrow tube. *J. Physiol.*, 149(3):593–613, 1959.

[209] HL Goldsmith and SG Mason. Axial migration of particles in poiseuille flow. *Nature*, 190(4781):1095, 1961.

[210] KH Albrecht, P Gaehtgens, A Pries, and M Heuser. The fahraeus effect in narrow capillaries (id 3.3 to 11.0 μm). *Microvasc. Res.*, 18(1):33–47, 1979.

[211] Robin Fåhræus and Torsten Lindqvist. The viscosity of the blood in narrow capillary tubes. *Am. J. Physiol.*, 96(3):562–568, 1931.

[212] PG Jayathilake, Gang Liu, Zhijun Tan, and BC Khoo. Numerical study on the dynamics and oxygen uptake of healthy and malaria-infected red blood cells. *Adv. Appl. Math. Mech.*, 7(5):549–568, 2015.

[213] Eunseop Yeom, Yang Jun Kang, and Sang-Joon Lee. Changes in velocity profile according to blood viscosity in a microchannel. *Biomicrofluidics*, 8 (3):034110, 2014.

[214] Louis H Miller, Shunichi Usami, and Shu Chien. Alteration in the rheologic properties of plasmodium knowlesi-infected red cells. a possible mechanism for capillary obstruction. *J. Clin. Invest.*, 50(7):1451, 1971.

[215] Nicoletta Basilico, Livianna Speciale, Silvia Parapini, Pasquale Ferrante, and Donatella Taramelli. Endothelin-1 production by a microvascular endothelial cell line treated with plasmodium falciparum parasitized red blood cells. *Clin. Sci.*, 103(2002):464–466, 2002.

[216] Yohsuke Imai, Hitoshi Kondo, Takuji Ishikawa, Chwee Teck Lim, and Takami Yamaguchi. Modeling of hemodynamics arising from malaria infection. *J. Biomech.*, 43(7):1386–1393, 2010.

[217] Joseph M Sherwood, David Holmes, Efstathios Kaliviotis, and Stavroula Balabani. Spatial distributions of red blood cells significantly alter local haemodynamics. *PLoS One*, 9(6):e100473, 2014.

[218] M Ho, B Singh, S Looareesuwan, TM Davis, D Bunnag, and NJ White. Clinical correlates of in vitro plasmodium falciparum cytoadherence. *Infect. Immun.*, 59(3):873–878, 1991.

[219] May Ho and Nicholas J White. Molecular mechanisms of cytoadherence in malaria. *Am. J. Physiol. Cell Physiol.*, 276(6):C1231–C1242, 1999.

[220] Christoph Wenisch, Heidi Wenisch, Polrat Wilairatana, Sornchai Looareesuwan, Suparp Vannaphan, Oswald Wagner, Wolfgang Graninger, Eva Schönthal, and Helmut Rumpold. Big endothelin in patients with complicated plasmodium falciparum malaria. *J. Infect. Dis.*, 173(5):1281–1284, 1996.

[221] Peter F Davies. Flow-mediated endothelial mechanotransduction. *Physiol. Rev.*, 75(3):519–560, 1995.

[222] CW Patrick, Rangarajan Sampath, and Larry V McIntire. Fluid shear stress

effects on cellular function. *Biomedical Research Handbook: Tissue Engineering Section. eds., B. Palsson and JA Hubbell, CRC Press Inc*, pages 1626–1645, 1995.

[223] Carmine Cardillo, Crescence M Kilcoyne, Richard O Cannon III, and Julio A Panza. Racial differences in nitric oxide–mediated vasodilator response to mental stress in the forearm circulation. *Hypertension*, 31(6):1235–1239, 1998.

[224] Sara S Jarvis, Shigeki Shibata, Yoshiyuki Okada, Benjamin Levine, and Qi Fu. Neural-humoral responses during head-up tilt in healthy young white and black women. *Front. Physiol.*, 5:86, 2014.

[225] Michael R Kramer, Amy L Valderrama, and Michele L Casper. Decomposing black-white disparities in heart disease mortality in the united states, 1973–2010: an age-period-cohort analysis. *American journal of epidemiology*, 182 (4):302–312, 2015.

[226] David B Rowlands, Joe De Giovanni, Rufus Ab Mcleay, Robert Ds Watson, Terence J Stallard, and William A Littler. Cardiovascular response in black and white hypertensives. *Hypertension*, 4(6):817–820, 1982.

[227] VE Shekh. Sex and ethnic/racial differences in blood pressure and heart rate variability during orthostatic testing in young healthy individuals. *J. Phys. Pharm. Adv.*, 6(3):846–59, 2016.

[228] Eugenia Mata-Greenwood and Dong-Bao Chen. Racial differences in nitric oxide—dependent vasorelaxation. *Reprod. Sci.*, 15(1):9–25, 2008.

[229] C Michael Hart. Nitric oxide in adult lung disease. *Chest*, 115(5):1407–1417, 1999.

[230] R Balarajan. Ethnic differences in mortality from ischaemic heart disease and cerebrovascular disease in england and wales. *BMJ*, 302(6776):560–564, 1991.

[231] A Marshall McBean, Shuling Li, David T Gilbertson, and Allan J Collins. Differences in diabetes prevalence, incidence, and mortality among the elderly of four racial/ethnic groups: whites, blacks, hispanics, and asians. *Diabetes care*, 27(10):2317–2324, 2004.

[232] Arun S Karlamangla, Sharon Stein Merkin, Eileen M Crimmins, and Teresa E Seeman. Socioeconomic and ethnic disparities in cardiovascular risk in the united states, 2001–2006. *Annals of epidemiology*, 20(8):617–628, 2010.

[233] Julian F Thayer, Shelby S Yamamoto, and Jos F Brosschot. The relationship of autonomic imbalance, heart rate variability and cardiovascular disease risk factors. *Int. J. Cardiol.*, 141(2):122–131, 2010.

[234] Julian F Thayer and Richard D Lane. The role of vagal function in the risk for cardiovascular disease and mortality. *Biol. Psychol.*, 74(2):224–242, 2007.

[235] Robert D Brook and Stevo Julius. Autonomic imbalance, hypertension, and cardiovascular risk. *Am. J. Hypertens.*, 13(S4):112S–122S, 2000.

[236] Paolo Palatini and Stevo Julius. The role of cardiac autonomic function in hypertension and cardiovascular disease. *Curr. Hypertens. Rep.*, 11(3): 199–205, 2009.

[237] Jay N Cohn, T Barry Levine, Gary S Francis, and Steven Goldsmith. Neurohumoral control mechanisms in congestive heart failure. *Am. Heart J.*, 102 (3):509–514, 1981.

[238] Philip F Binkley, Enrico Nunziata, Garrie J Haas, Steven D Nelson, and Robert J Cody. Parasympathetic withdrawal is an integral component of autonomic imbalance in congestive heart failure: demonstration in human subjects and verification in a paced canine model of ventricular failure. *J. Am. Coll. Cardiol.*, 18(2):464–472, 1991.

[239] J Philip Saul. Beat-to-beat variations of heart rate reflect modulation of cardiac autonomic outflow. *Physiology*, 5(1):32–37, 1990.

[240] Federico Lombardi, Timo H Mäkikallio, Robert J Myerburg, and Heikki V Huikuri. Sudden cardiac death: role of heart rate variability to identify patients at risk. *Cardiovasc. Res.*, 50(2):210–217, 2001.

[241] Emily B Schroeder, Duanping Liao, Lloyd E Chambless, Ronald J Prineas, Gregory W Evans, and Gerardo Heiss. Hypertension, blood pressure, and heart rate variability: the atherosclerosis risk in communities (aric) study. *Hypertension*, 42(6):1106–1111, 2003.

[242] Christopher R Cole, Eugene H Blackstone, Fredric J Pashkow, Claire E Snader, and Michael S Lauer. Heart-rate recovery immediately after exercise as a predictor of mortality. *N. Engl. J. Med.*, 341(18):1351–1357, 1999.

[243] Antti M Kiviniemi, Mikko P Tulppo, Dan Wichterle, Arto J Hautala, Suvi Tiinanen, Tapio Seppänen, Timo H Mäkikallio, and Heikki V Huikuri. Novel spectral indexes of heart rate variability as predictors of sudden and non-sudden cardiac death after an acute myocardial infarction. *Ann. Med.*, 39 (1):54–62, 2007.

[244] Elaine M Urbina, Weihang Bao, Arthur S Pickoff, and Gerald S Berenson. Ethnic (black–white) contrasts in heart rate variability during cardiovascular reactivity testing in male adolescents with high and low blood pressure. *Am. J. Hypertens.*, 11(2):196–202, 1998.

[245] Adrienne S Zion, Vernon Bond, Richard G Adams, Deborah Williams, Robert E Fullilove, Richard P Sloan, Matthew N Bartels, John A Downey, and Ronald E De Meersman. Low arterial compliance in young african-american males. *Am. J. Physiol. Heart Circ. Physiol.*, 285(2):H457–H462, 2003.

[246] Duanping Liao, Ralph W Barnes, Lloyd E Chambless, Ross J Simpson Jr, Paul Sorlie, Gerardo Heiss, ARIC investigators, et al. Age, race, and sex differences in autonomic cardiac function measured by spectral analysis of heart rate variability—the aric study. *Am. J. Cardiol.*, 76(12):906–912, 1995.

[247] Xiaoling Wang, Julian F Thayer, Frank Treiber, and Harold Snieder. Ethnic differences and heritability of heart rate variability in african-and european american youth. *Am. J. Cardiol.*, 96(8):1166–1172, 2005.

[248] Rachel Lampert, Jeannette Ickovics, Ralph Horwitz, and Forrester Lee. Depressed autonomic nervous system function in african americans and individuals of lower social class: a potential mechanism of race-and class-related disparities in health outcomes. *Am. Heart J.*, 150(1):153–160, 2005.

[249] Warren D Franke, Kichang Lee, Dwayne B Buchanan, and Juliane P Hernandez. Blacks and whites differ in responses, but not tolerance, to orthostatic stress. *Clin. Auton. Res.*, 14(1):19–25, 2004.

[250] Stefano Guzzetti, J Mayet, M Shahi, S Mezzetti, RA Foale, PS Sever, NR Poulter, A Porta, A Malliani, and SAMcG Thom. Absence of sympathetic overactivity in Afro-Caribbean hypertensive subjects studied by heart rate variability. *J. Human Hypertens.*, 14(5):337–342, 2000.

[251] Nancy Dorr, Jos F Brosschot, John J Sollers III, and Julian F Thayer. Damned if you do, damned if you don't: The differential effect of expression and inhibition of anger on cardiovascular recovery in black and white males. *Int. J. Psychophysiol.*, 66(2):125–134, 2007.

[252] Kevin S Heffernan, Sae Young Jae, Victoria J Vieira, Gary A Iwamoto, Kenneth R Wilund, Jeffrey A Woods, and Bo Fernhall. C-reactive protein and cardiac vagal activity following resistance exercise training in young african american and white men. *Am. J. Physiol. Regul. Integr. Comp. Physiol.*, 2009.

[253] J Benjamin Hinnant, Lori Elmore-Staton, and Mona El-Sheikh. Developmental trajectories of respiratory sinus arrhythmia and preejection period in middle childhood. *Dev. Psychobiol.*, 53(1):59–68, 2011.

[254] Xiaoling Wang, Xiuhua Ding, Shaoyong Su, Zhibin Li, Harriette Riese, Julian F Thayer, Frank Treiber, and Harold Snieder. Genetic influences on heart rate variability at rest and during stress. *Psychophysiology*, 46(3): 458–465, 2009.

[255] Zhibin Li, Harold Snieder, Shaoyong Su, Xiuhua Ding, Julian F Thayer, Frank A Treiber, and Xiaoling Wang. A longitudinal study in youth of heart rate variability at rest and in response to stress. *Int. J. Psychophysiol.*, 73 (3):212–217, 2009.

[256] Carmine Cardillo, Crescence M Kilcoyne, Richard O Cannon III, and Julio A Panza. Attenuation of cyclic nucleotide–mediated smooth muscle relaxation in blacks as a cause of racial differences in vasodilator function. *Circulation*, 99(1):90–95, 1999.

[257] Carlene A Hamilton, M Julia Brosnan, Sammy Al-Benna, Geoffrey Berg, and Anna F Dominiczak. Nad (p) h oxidase inhibition improves endothelial function in rat and human blood vessels. *Hypertension*, 40(5):755–762, 2002.

[258] Yong Xia, Valina L Dawson, Ted M Dawson, Solomon H Snyder, and Jay L Zweier. Nitric oxide synthase generates superoxide and nitric oxide in arginine-depleted cells leading to peroxynitrite-mediated cellular injury. *Proc. Natl. Acad. Sci.*, 93(13):6770–6774, 1996.

[259] Igor Huk, Joseph Nanobashvili, Christoph Neumayer, Andreas Punz, Markus Mueller, Kaweh Afkhampour, Martina Mittlboeck, Udo Losert, Peter Polterauer, Erich Roth, et al. L-arginine treatment alters the kinetics of nitric oxide and superoxide release and reduces ischemia/reperfusion injury in skeletal muscle. *Circulation*, 96(2):667–675, 1997.

[260] CS Raman, Huiying Li, Pavel Martásek, Vladimir Král, Bettie Sue S Masters, and Thomas L Poulos. Crystal structure of constitutive endothelial nitric oxide synthase: a paradigm for pterin function involving a novel metal center. *Cell*, 95(7):939–950, 1998.

[261] Leszek Kalinowski, Iwona T Dobrucki, and Tadeusz Malinski. Race-specific differences in endothelial function: predisposition of african americans to vascular diseases. *Circulation*, 109(21):2511–2517, 2004.

[262] Mario Bonomini, Vittorio Sirolli, Federico Gizzi, Silvio Di Stante, Alfredo Grilli, and Mario Felaco. Enhanced adherence of human uremic erythrocytes to vascular endothelium: role of phosphatidylserine exposure. *Kidney Int.*, 62(4):1358–1363, 2002.

[263] Patrick G Gallagher, Seon Hee Chang, Michael P Rettig, John E Neely, Cheryl A Hillery, Brian D Smith, and Philip S Low. Altered erythrocyte endothelial adherence and membrane phospholipid asymmetry in hereditary hydrocytosis. *Blood*, 101(11):4625–4627, 2003.

[264] Robert P Hebbel, Marc AB Boogaerts, John W Eaton, and Martin H Steinberg. Erythrocyte adherence to endothelium in sickle-cell anemia: a possible determinant of disease severity. *New England Journal of Medicine*, 302(18): 992–995, 1980.

[265] Robert P Hebbel, Osamu Yamada, Charles F Moldow, Harry S Jacob, James G White, and John W Eaton. Abnormal adherence of sickle erythrocytes to cultured vascular endothelium: possible mechanism for microvascular occlusion in sickle cell disease. *N. Engl. J. Med.*, 65(1):154, 1980.

[266] Richard Hoover, Robert Rubin, Gary Wise, and Robert Warren. Adhesion of normal and sickle erythrocytes to endothelial monolayer cultures. *Blood*, 54(4):872–876, 1979.

[267] T Hovav, A Goldfarb, G Artmann, S Yedgar, and G Barshtein. Enhanced adherence of beta-thalassaemic erythrocytes to endothelial cells. *Br. J. Haematol.*, 106(1):178–181, 1999.

[268] Iroka J Udeinya, John A Schmidt, Masamichi Aikawa, Louis H Miller, and Ira Green. Falciparum malaria-infected erythrocytes specifically bind to cultured human endothelial cells. *Science*, 213(4507):555–557, 1981.

[269] Jean-Luc Wautier, R Colin Paton, Marie-Paule Wautier, Dominique Pintigny, Eric Abadie, Philippe Passa, and Jacques P Caen. Increased adhesion of erythrocytes to endothelial cells in diabetes mellitus and its relation to vascular complications. *N. Engl. J. Med.*, 305(5):237–242, 1981.

[270] A Kucukcelebi, SP Barmatoski, and MI Barnhart. Interactions between vessel wall and perfused sickled erythrocytes: preliminary observations. *Scanning electron microscopy*, (3):243–248, 1980.

[271] Narla Mohandas and Evan Evans. Adherence of sickle erythrocytes to vascular endothelial cells: requirement for both cell membrane changes and plasma factors. *Blood*, 64(1):282–287, 1984.

[272] Narla Mohandas and Evan Evans. Sickle erythrocyte adherence to vascular endothelium. morphologic correlates and the requirement for divalent cations and collagen-binding plasma proteins. *J. Clin. Invest.*, 76(4):1605, 1985.

[273] S Baez, DK Kaul, and RL Nagel. Microvascular determinants of blood flow behavior and hbss erythrocyte plugging in microcirculation. *Blood cells*, 8 (1):127–137, 1981.

[274] Dhananjaya K Kaul, Silvio Baez, and Ronald L Nagel. Flow properties of oxygenated hbs and hbc erythrocytes in the isolated microvasculature of the rat. a contribution to the hemorheology of hemoglobinopathies. *Clin. Hemorheol. Microcirc.*, 1(1):73–86, 1981.

[275] Carmen Raventos-Suarez, Dhananjaya K Kaul, Frank Macaluso, and Ronald L Nagel. Membrane knobs are required for the microcirculatory obstruction induced by plasmodium falciparum-infected erythrocytes. *Proc. Natl. Acad. Sci.*, 82(11):3829–3833, 1985.

[276] GB Nash, BM Cooke, K Marsh, A Berendt, C Newbold, and J Stuart. Rheological analysis of the adhesive interactions of red blood cells parasitized by plasmodium falciparum. *Blood*, 79(3):798–807, 1992.

[277] Brian M Cooke, Shunichi Usami, Ian Perry, and Gerard B Nash. A simplified method for culture of endothelial cells and analysis of adhesion of blood cells under conditions of flow. *Microvascular research*, 45(1):33–45, 1993.

[278] AK Jayanthy, N Sujatha, and M Ramasubba Reddy. Measuring blood flow: techniques and applications-a review. *Int. J. Res. Review Appl. Sci*, 6:203–216, 2011.

[279] AV Dokunin. A modification of the method of differential manometry for registration of the volume velocity of the blood flow. *Bull. Exp. Biol. Med.*, 46(5):1414–1417, 1958.

[280] Janusz Sadowski. A simple venous outflow recorder. *Pflügers Archiv*, 325 (1):90–94, 1971.

[281] Hans R Ulfendahl and Ingemar Vogeler. An automatic bubble flow meter. *Acta Physiol. Scand. Suppl.*, 55(2-3):286–290, 1962.

[282] Kenneth E Jochim. The development of the electro-magnetic blood flowmeter. *IEEE Trans. Inf. Technol. Biomed.*, 9(4):228–235, 1962.

[283] DG Wyatt. The electromagnetic blood flowmeter. *Journal of Physics E: Scientific Instruments*, 1(12):1146, 1968.

[284] BI Bashchenko and VB Zakharzhevskii. Method using thermistors to measure blood flow velocity. *Biomed. Eng.*, 4(5):252–254, 1970.

[285] John Webster. *Medical instrumentation: application and design*. John Wiley & Sons, 2009.

[286] Jun Yamaguchi, Azran Azhim, Yuji Hirao, Yohsuke Kinouchi, Hisao Yamaguchi, and Kazuo Yoshizaki. A change of blood flow during strenuous physical exercises using cycle ergometer. In *Engineering in Medicine and Biology Society, 2005. IEEE-EMBS 2005. 27th Annual International Conference of the*, pages 6615–6618. IEEE, 2006.

[287] Y Hirao, K Tamukai, Y Kinouchi, and H Yamaguchi. Synchronized measurements of blood flow velocity distributions in carotid, brachial and femoral arteries, and ecg in human during exercise. In *[Engineering in Medicine and Biology, 1999. 21st Annual Conference and the 1999 Annual Fall Meetring of the Biomedical Engineering Society] BMES/EMBS Conference, 1999. Proceedings of the First Joint*, volume 1, pages 224–vol. IEEE, 1999.

[288] David L Raunig and Martin D Fox. Doppler ultrasound determination of capillary blood flow. In *Bioengineering Conference, 1997., Proceedings of the IEEE 1997 23rd Northeast*, pages 1–2. IEEE, 1997.

[289] E Leidig. Pulsed Doppler ultrasound blood flow measurements in the superior mesenteric artery of the newborn. *Pediatr. Radiol.*, 19(3):169–172, 1989.

[290] Abraham M Rudolph and Michael A Heymann. The circulation of the fetus in utero methods for studying distribution of blood flow, cardiac output and organ blood flow. *Circ. Res.*, 21(2):163–184, 1967.

[291] O Andrée Larsen, NA Lassen, and F Quaade. Blood flow through human adipose tissue determined with radioactive xenon. *Acta Physiol. Scand.*, 66 (3):337–345, 1966.

[292] CM Black, RP Clark, K Darton, MR Goff, TD Norman, and HA Spikes. A

pyroelectric thermal imaging system for use in medical diagnosis. *J. Biomech. Eng.*, 12(4):281–286, 1990.

[293] PA Payne, RY Faddoul, and SM Jawad. A single-channel pulsed Doppler ultrasound instrument for measurement of skin blood flow. *Practical aspects of skin blood flow measurement (London: Biological Engineering Society)*, 1985.

[294] J David Briers. Laser Doppler, speckle and related techniques for blood perfusion mapping and imaging. *Physiol. Meas.*, 22(4):R35, 2001.

[295] J David Briers. Laser speckle contrast imaging for measuring blood flow. *Opt. Appl.*, 37(1/2):139, 2007.

[296] P Shepherd Albert and P. Åke Öberg. *Laser-Doppler blood flowmetry*, volume 107. Springer, 1990.

[297] Yonghua Zhao, Zhongping Chen, Christopher Saxer, Shaohua Xiang, Johannes F de Boer, and J Stuart Nelson. Phase-resolved optical coherence tomography and optical Doppler tomography for imaging blood flow in human skin with fast scanning speed and high velocity sensitivity. *Opt. Lett.*, 25(2):114–116, 2000.

[298] Joseph W Goodman. Statistical properties of laser speckle patterns. In *Laser speckle and related phenomena*, pages 9–75. Springer, 1975.

[299] Joseph W Goodman. Some fundamental properties of speckle. *JOSA*, 66 (11):1145–1150, 1976.

[300] Anna L Petoukhova, Wiendelt Steenbergen, Ton G van Leeuwen, and Frits FM de Mul. Effects of absorption on coherence domain path length resolved dynamic light scattering in the diffuse regime. *Appl. Phys. Lett.*, 81 (4):595–597, 2002.

[301] N Vongsavan and B Matthews. Some aspects of the use of laser Doppler flow meters for recording tissue blood flow. *Exp. Physiol.*, 78(1):1–14, 1993.

[302] Steve Meek and Francis Morris. Introduction. ii—basic terminology. *BMJ*, 324(7335):470–473, 2002.

[303] Dmytro Iatsenko, Peter V E McClintock, and Aneta Stefanovska. Nonlinear mode decomposition: a noise-robust, adaptive decomposition method. *Phys. Rev. E.*, 92:032916, 2015.

[304] Marek Malik, J Thomas Bigger, A John Camm, Robert E Kleiger, Alberto Malliani, Arthur J Moss, and Peter J Schwartz. Heart rate variability: Standards of measurement, physiological interpretation, and clinical use. *Eur. Heart J.*, 17:354–381, 1996.

[305] Dmytro Iatsenko, Alan Bernjak, Tomislav Stankovski, Yuri Shiogai, P Jane Owen-Lynch, Peter B M Clarkson, Peter V E McClintock, and Aneta Stefanovska. Evolution of cardiorespiratory interactions with age. *Phil. Trans. R. Soc. A*, 371:20110622, 2013.

[306] Marek Malik, T Farrell, T Cripps, and AJ Camm. Heart rate variability in relation to prognosis after myocardial infarction: selection of optimal processing techniques. *Eur. Heart J.*, 10(12):1060–1074, 1989.

[307] Peter G Katona and FELIX Jih. Respiratory sinus arrhythmia: noninvasive measure of parasympathetic cardiac control. *J. Appl. Physiol.*, 39(5):801–805, 1975.

[308] Vinayakrishnan Rajan, Babu Varghese, Ton G van Leeuwen, and Wiendelt Steenbergen. Review of methodological developments in laser Doppler flowmetry. *Lasers Med. Sci.*, 24(2):269–283, 2009.

[309] SJ Matcher, CE Elwell, CE Cooper, M Cope, and DT Delpy. Performance comparison of several published tissue near-infrared spectroscopy algorithms. *Anal. Biochem.*, 227(1):54–68, 1995.

[310] Susumu Suzuki, Sumio Takasaki, Takeo Ozaki, and Yukio Kobayashi. Tissue oxygenation monitor using nir spatially resolved spectroscopy. In *Optical Tomography and Spectroscopy of Tissue III*, volume 3597, pages 582–593. International Society for Optics and Photonics, 1999.

[311] Steven J Matcher, Peter J Kirkpatrick, K Nahid, Mark Cope, and David T Delpy. Absolute quantification methods in tissue near-infrared spectroscopy. In *Optical Tomography, Photon Migration, and Spectroscopy of Tissue and Model Media: Theory, Human Studies, and Instrumentation*, volume 2389, pages 486–496. International Society for Optics and Photonics, 1995.

[312] Hongyuan Liu, Matthias Kohl-Bareis, and Xiabing Huang. Design of a tissue oxygenation monitor and verification on human skin. In *European Conference on Biomedical Optics*, page 80871Y. Optical Society of America, 2011.

[313] Steven H Strogatz. Exploring complex networks. *nature*, 410(6825):268, 2001.

[314] Philip T Clemson and Aneta Stefanovska. Discerning non-autonomous dynamics. *Phys. Rep.*, 542(4):297–368, 2014.

[315] Peter E Kloeden and Christian Pötzsche. Nonautonomous dynamical systems in the life sciences. In *Nonautonomous dynamical systems in the life sciences*, pages 3–39. Springer, 2013.

[316] Philip Clemson, Gemma Lancaster, and Aneta Stefanovska. Reconstructing time-dependent dynamics. *Proc. IEEE*, 104(2):223–241, 2016.

[317] Ronald Newbold Bracewell and Ronald N Bracewell. *The Fourier transform and its applications*, volume 31999. McGraw-Hill New York, 1986.

[318] DV Anosov and AA Bolibruch. The riemann-hilbert problem, aspects of mathematics, e22, friedr. *Vieweg & Sohn, Braunschweig*, 1994.

[319] Gemma Lancaster. *Oscillations in microvascular flow: their relationship to tissue oxygenation, cellular metabolic function and their diagnostic potential for detecting skin melanoma.* PhD thesis, Lancaster University, Lancaster, UK, september 2015.

[320] Norden E Huang, Zheng Shen, Steven R Long, Manli C Wu, Hsing H Shih, Quanan Zheng, Nai-Chyuan Yen, Chi Chao Tung, and Henry H Liu. The empirical mode decomposition and the hilbert spectrum for nonlinear and non-stationary time series analysis. *Proc. R. Soc. Lond. A. Math Phys. Sci.*, 454(1971):903–995, 1998.

[321] J Harold Ahlberg, Edwin Norman Nilson, and Joseph Leonard Walsh. The theory of splines and their applications. *Mathematics in Science and Engineering, New York: Academic Press, 1967*, 1967.

[322] Zhaohua Wu and Norden E Huang. Ensemble empirical mode decomposition: a noise-assisted data analysis method. *Adv. Adapt. Data Anal.*, 1(01):1–41, 2009.

[323] Ingrid Daubechies. Ten lectures on wavelets, cbms-nsf regional conf. *Series in Appl. Math*, 61, 1992.

[324] Stéphane Mallat. *A wavelet tour of signal processing.* Elsevier, 1999.

[325] Leon Cohen. *Time-frequency analysis*, volume 778. Prentice hall, 1995.

[326] Paul S Addison. *The illustrated wavelet transform handbook: introductory theory and applications in science, engineering, medicine and finance.* CRC press, 2017.

[327] LW Sheppard, A Stefanovska, and PVE McClintock. Detecting the harmonics of oscillations with time-variable frequencies. *Phys. Rev. E*, 83(1):016206, 2011.

[328] Dmytro Iatsenko, Peter VE McClintock, and Aneta Stefanovska. Extraction of instantaneous frequencies from ridges in time–frequency representations of signals. *Signal Processing*, 125:290–303, 2016.

[329] Nathalie Delprat, Bernard Escudié, Philippe Guillemain, Richard Kronland-Martinet, Philippe Tchamitchian, and Bruno Torresani. Asymptotic wavelet and gabor analysis: Extraction of instantaneous frequencies. *IEEE Trans. Inf. Theory*, 38(2):644–664, 1992.

[330] Dmytro Iatsenko, Peter McClintock, and Aneta Stefanovska. Linear and synchrosqueezed time-frequency representations revisited: Overview, standards of use, resolution, reconstruction, concentration, and algorithms. *Digital Signal Processing*, 42, 04 2015.

[331] Yu-Chun Chen, Ming-Yen Cheng, and Hau-Tieng Wu. Non-parametric and adaptive modelling of dynamic periodicity and trend with heteroscedastic and dependent errors. *J R Stat Soc Series B Stat Methodol*, 76(3):651–682, 10 2014.

[332] Thomas Schreiber and Andreas Schmitz. Surrogate time series. *Physica D*, 142(3):346 – 382, 2000.

[333] James Theiler, Stephen Eubank, André Longtin, Bryan Galdrikian, and J Doyne Farmer. Testing for nonlinearity in time series: the method of surrogate data. *Physica D*, 58(1-4):77–94, 1992.

[334] R. Quian Quiroga, A. Kraskov, T. Kreuz, and P. Grassberger. Performance of different synchronization measures in real data: A case study on electroencephalographic signals. *Phys. Rev. E*, 65:041903, 2002.

[335] Gemma Lancaster, Dmytro Iatsenko, Aleksandra Pidde, Valentina Ticcinelli, and Aneta Stefanovska. Surrogate data for hypothesis testing of physical systems. *Phys. Rep.*, 748:1–60, 2018.

[336] Björn Kralemann, Matthias Frühwirth, Arkady Pikovsky, Michael Rosenblum, Thomas Kenner, Jochen Schaefer, and Maximilian Moser. In vivo cardiac phase response curve elucidates human respiratory heart rate variability. *Nat. Commun.*, 4, 2013.

[337] Tomislav Stankovski, Andrea Duggento, Peter VE McClintock, and Aneta Stefanovska. Inference of time-evolving coupled dynamical systems in the presence of noise. *Phys. Rev. Lett.*, 109(2):024101, 2012.

[338] Tomislav Stankovski, Valentina Ticcinelli, Peter VE McClintock, and Aneta Stefanovska. Coupling functions in networks of oscillators. *New J. Phys.*, 17 (3):035002, 2015.

[339] Udo Von Toussaint. Bayesian inference in physics. *Rev. Mod. Phys.*, 83(3): 943, 2011.

[340] Y. Kuramoto. *Chemical Oscillations, Waves, and Turbulence*. Dover Books on Chemistry Series. 2003.

[341] Michael G Rosenblum, Laura Cimponeriu, Anastasios Bezerianos, Andreas Patzak, and Ralf Mrowka. Identification of coupling direction: application to cardiorespiratory interaction. *Phys. Rev. E*, 65(4):041909, 2002.

[342] Tomislav Stankovski, Andrea Duggento, Peter VE McClintock, and Aneta Stefanovska. A tutorial on time-evolving dynamical bayesian inference. *Eur. Phys. J. Spec. Top.*, 223(13):2685–2703, 2014.

[343] Matlab toolbox for the dynamical bayesian inference and the calculation of coupling functions is publicly available at. `http://py-biomedical.lancaster.ac.uk`.

[344] Björn Kralemann, Arkady Pikovsky, and Michael Rosenblum. Reconstructing effective phase connectivity of oscillator networks from observations. *New J. Phys.*, 16(8):085013, 2014.

[345] Qian Peng, Asta Juzeniene, Jiyao Chen, Lars O Svaasand, Trond Warloe, Karl-Erik Giercksky, and Johan Moan. Lasers in medicine. *Rep. Prog. Phys.*, 71:056701, 2008.

[346] Nikiforos Kollias and Ali Baqer. Spectroscopic characteristics of human melanin in vivo. *J. Invest. Dermatol.*, 85:38– 42, 1985.

[347] N Kollias and Ali Baqer. On the assessment of melanin in human skin in vivo. *Photochem. Photobiol.*, 43:49–54, 1986.

[348] Nikiforos Kollias. The spectroscopy of human melanin pigmentation. *J. Invest. Dermatol.*, 102:268–268, 1994.

[349] Tom Lister, Philip A Wright, and Paul H Chappell. Optical properties of human skin. *J. Biomed. Opt.*, 17:090901, 2012.

[350] W E Pauli and I Ivancevic. Absorptive property of the skin for the long-waved rays of the spectrum. *Strahlenther Onkol*, 25:532–45, 1927.

[351] C Hawley Cartwright. Infra-red transmission of the flesh. *J. Opt. Soc. Am.*, 20:81–84, 1930.

[352] Aldrich Loyal Blaine. Supplementary notes on body radiation. *Smithson. Misc. Collect.*, 85:1–12, 1932.

[353] James D Hardy and Carl Muschenheim. The radiation of heat from the human body. IV. The emission, reflection, and transmission of infra-red radiation by the human skin. *J. Clin. Invest.*, 13:817–831, 1934.

[354] VV Dremin and AV Dunaev. How the melanin concentration in the skin affects the fluorescence-spectroscopy signal formation. *J. Opt. Technol.*, 83: 43–48, 2016.

[355] AK Murray, AL Herrick, and TA King. Laser Doppler imaging: a developing technique for application in the rheumatic diseases. *J. Rheumatol.*, 43:1210–1218, 2004.

[356] Torbjörn Söderström, Aneta Stefanovska, Mitja Veber, and Henry Svensson. Involvement of sympathetic nerve activity in skin blood flow oscillations in humans. *Am. J. Physiol. Heart Circ. Physiol.*, 284(5):H1638–H1646, 2003.

[357] H. Lilliefors. On the Kolmogorov-Smirnov test for normality with mean and variance unknown. *J. Amer. Stat. Assoc.*, 62:399–402, 1967.

[358] W. H. Kruskal and W. A. Wallis. Use of ranks in one-criterion variance analysis. *J. Amer. Stat. Assoc.*, 47:583–621, 1952.

[359] Frank Wilcoxon. Individual comparisons by ranking methods. *Biometrics*, 1:80–83, 1945.

[360] Michael R Esco, Michele S Olson, and Henry N Williford. Racial differences exist in cardiovascular parasympathetic modulation following maximal exercise. *J. Appl. Res. Technol.*, 10:24–32, 2010.

[361] Alan L Hinderliter, Andrew R Sager, Andrew Sherwood, Kathleen C Light, Susan S Girdler, and Park W Willis. Ethnic differences in forearm vasodilator capacity. *Am. J. Cardiol.*, 78(2):208–211, 1996.

[362] Peng Wei, LC Milbauer, J Enenstein, J Nguyen, W Pan, and RP Hebbel. Differential endothelial cell gene expression by african americans versus caucasian americans: a possible contribution to health disparity in vascular disease and cancer. *BMC Med.*, 9(1):2, 2011.

[363] Muhiddin A Ozkor, Ayaz M Rahman, Jonathan R Murrow, Nino Kavtaradze, Ji Lin, Amita Manatunga, Salim Hayek, and Arshed A Quyyumi. Differences in vascular nitric oxide and endothelium-derived hyperpolarizing factor bioavailability in blacks and whites. *Arterioscler. Thromb. Vasc. Biol.*, 34:1320–1327, 2014.

[364] Kiyoung Kim, Chansol Hurr, Jordan C Patik, and R Matthew Brothers. Attenuated cutaneous microvascular function in healthy young African Ameri-

cans: Role of intradermal l-arginine supplementation. *Microvasc. Res.*, 118: 1–6, 2018.

[365] Douglas F Dluzen, Nicole Noren Hooten, Yongqing Zhang, Yoonseo Kim, Frank E Glover, Salman M Tajuddin, Kimberly D Jacob, Alan B Zonderman, and Michele K Evans. Racial differences in microrna and gene expression in hypertensive women. *Sci. Rep.*, 6:35815, 2016.

[366] Akos Koller and Gabor Kaley. Endothelial regulation of wall shear stress and blood flow in skeletal muscle microcirculation. *Am. J. Physiol. Heart Circ. Physiol.*, 260(3):H862–H868, 1991.

[367] Michael Heideman, Don Johnson, and C Burrus. Gauss and the history of the fast fourier transform. *IEEE ASSP Mag.*, 1(4):14–21, 1984.

[368] Jean-Philippe Lachaux, Antoine Lutz, David Rudrauf, Diego Cosmelli, Michel Le Van Quyen, Jacques Martinerie, and Francisco Varela. Estimating the time-course of coherence between single-trial brain signals: an introduction to wavelet coherence. *Neurophysiol. Clin.*, 32(3):157–174, 2002.

[369] L. W. Sheppard, A. Stefanovska, and P. V. E. McClintock. Testing for time-localised coherence in bivariate data. *Phys. Rev. E*, 85:046205, 2012.

[370] Silvia Bertuglia, Antonio Colantuoni, Giuseppe Coppini, and Marcos Intaglietta. Hypoxia-or hyperoxia-induced changes in arteriolar vasomotion in skeletal muscle microcirculation. *Am. J. Physiol. Heart Circ. Physiol.*, 260 (2):H362–H372, 1991.

[371] Rod D Braun, Jennifer L Lanzen, and Mark W Dewhirst. Fourier analysis of fluctuations of oxygen tension and blood flow in r3230ac tumors and muscle in rats. *Am. J. Physiol. Heart Circ. Physiol.*, 277(2):H551–H568, 1999.

[372] Aneta Stefanovska. Dynamics of blood oxygenation gives better insight into tissue hypoxia than averaged values. *Am. J. Physiol. Heart Circ. Physiol.*, 296(5):H1224–H1226, 2009.

[373] August Krogh. The rate of diffusion of gases through animal tissues, with some remarks on the coefficient of invasion. *J. Physiol.*, 52(6):391–408, 1919.

[374] August Krogh. The number and distribution of capillaries in muscles with calculations of the oxygen pressure head necessary for supplying the tissue. *J. Physiol.*, 52(6):409–415, 1919.

[375] Deepti S Vikram, Jay L Zweier, and Periannan Kuppusamy. Methods for noninvasive imaging of tissue hypoxia. *Antioxid. Redox Signal.*, 9(10):1745–1756, 2007.

[376] Tokuo Yano, Chang-Shun Lian, Roghayyeh Afroundeh, Kazuki Shirakawa, and Takahiro Yunoki. Comparison of oscillations of skin blood flow and deoxygenation in vastus lateralis in light exercise. *Biol. Sport*, 31(1):15–20, 2014.

[377] Robert M Cohen, Harold Snieder, Christopher J Lindsell, Huriya Beyan, Mohammed I Hawa, Stuart Blinko, Raymond Edwards, Timothy D Spector, and R David G Leslie. Evidence for independent heritability of the glycation gap (glycosylation gap) fraction of hba1c in nondiabetic twins. *Diabetes Care*, 29(8):1739–1743, 2006.

[378] Richard M Bergenstal, Robin L Gal, Crystal G Connor, Rose Gubitosi-Klug, Davida Kruger, Beth A Olson, Steven M Willi, Grazia Aleppo, Ruth S Weinstock, Jamie Wood, and M Rickels. Racial differences in the relationship of glucose concentrations and hemoglobin a1c levels. *Ann. Intern. Med.*, 167 (2):95–102, 2017.

[379] John M Boltri, Ike S Okosun, Monique Davis-Smith, and Robert L Vogel. Hemoglobin a˜ 1˜ c levels in diagnosed and undiagnosed black, hispanic, and white persons with diabetes: Results from nhanes 1999-2000. *Ethn. Dis.*, 15 (4):562–567, 2005.

[380] Julienne K Kirk, Ralph B D'Agostino, Ronny A Bell, Leah V Passmore, Denise E Bonds, Andrew J Karter, and KM Venkat Narayan. Disparities in hba1c levels between african-american and non-hispanic white adults with diabetes: a meta-analysis. *Diabetes care*, 29(9):2130–2136, 2006.

[381] David C Ziemer, Paul Kolm, William S Weintraub, Viola Vaccarino, Mary K Rhee, Jennifer G Twombly, KM Venkat Narayan, David D Koch, and Lawrence S Phillips. Glucose-independent, black–white differences in hemoglobin a1c levels: a cross-sectional analysis of 2 studies. *Ann. Intern. Med.*, 152(12):770–777, 2010.

[382] Elizabeth Selvin, Michael W Steffes, Christie M Ballantyne, Ron C Hoogeveen, Josef Coresh, and Frederick L Brancati. Racial differences in glycemic markers: a cross-sectional analysis of community-based data. *Ann. Intern. Med.*, 154(5):303–309, 2011.

[383] William H Herman and Robert M Cohen. Racial and ethnic differences in the relationship between HbA_{1c} and blood glucose: implications for the diagnosis of diabetes. *J. Clin. Endocrinol. Metab.*, 97(4):1067–1072, 2012.

[384] William H Herman. Are there clinical implications of racial differences in HbA_{1c}? yes, to not consider can do great harm! *Diabetes Care*, 39(8): 1458–1461, 2016.

[385] Elizabeth Selvin. Are there clinical implications of racial differences in hba1c? a difference, to be a difference, must make a difference. *Diabetes Care*, 39 (8):1462–1467, 2016.

[386] Frans F Jobsis. Noninvasive, infrared monitoring of cerebral and myocardial oxygen sufficiency and circulatory parameters. *Science*, 198(4323):1264–1267, 1977.

[387] Mark Cope. *The development of a near infrared spectroscopy system and its*

application for non invasive monitoring of cerebral blood and tissue oxygenation in the newborn infants. PhD thesis, University of London, 1991.

[388] Marjola Thanaj, Andrew J Chipperfield, and Geraldine F Clough. Analysis of microvascular blood flow and oxygenation: Discrimination between two haemodynamic steady states using nonlinear measures and multiscale analysis. *Comput. Biol. Med.*, 102:157–167, 2018.

[389] Marjola Thanaj, Andrew J Chipperfield, and Geraldine F Clough. Multiscale analysis of microvascular blood flow and oxygenation. In *World Congress on Medical Physics and Biomedical Engineering 2018*, pages 195–200. Springer, 2019.

[390] Michael D Stern. Laser Doppler velocimetry in blood and multiply scattering fluids: theory. *Appl. Opt.*, 24(13):1968–1986, 1985.

[391] Viktor Dremin, Igor Kozlov, Mikhail Volkov, Nikita Margaryants, Andrey Potemkin, Evgeny Zherebtsov, Andrey Dunaev, and Igor Gurov. Dynamic evaluation of blood flow microcirculation by combined use of the laser Doppler flowmetry and high-speed videocapillaroscopy methods. *J. Biophotonics*, 12(6):e201800317, 2019.

[392] Maria Angela Franceschini, David A Boas, Anna Zourabian, Solomon G Diamond, Shalini Nadgir, David W Lin, John B Moore, and Sergio Fantini. Near-infrared spiroximetry: noninvasive measurements of venous saturation in piglets and human subjects. *J. Appl. Physiol.*, 92(1):372–384, 2002.

[393] Victor V Kislukhin. Regulation of oxygen consumption by vasomotion. *Math. Biosci.*, 191(1):101–108, 2004.

[394] Tzong-Luen Wang and Chi-Ren Hung. Role of tissue oxygen saturation monitoring in diagnosing necrotizing fasciitis of the lower limbs. *Ann. Emerg. Med.*, 44(3):222–228, 2004.

[395] Francisco C Ramirez, Sukhdeep Padda, Susan Medlin, Helen Tarbell, and Felix W Leung. Reflectance spectrophotometry in the gastrointestinal tract: limitations and new applications. *Am. J. Gastroenterol.*, 97(11):2780–2784, 2002.

[396] Louis H Miller, Dror I Baruch, Kevin Marsh, and Ogobara K Doumbo. The pathogenic basis of malaria. *Nature*, 415(6872):673, 2002.

[397] Alessandro Bartoloni and Lorenzo Zammarchi. Clinical aspects of uncomplicated and severe malaria. *Mediterr J Hematol Infect Dis*, 4(1), 2012.

[398] Kirk W Deitsch and Ron Dzikowski. Variant gene expression and antigenic variation by malaria parasites. *Annu. Rev. Microbiol.*, 71:625–641, 2017.

[399] M Roustit, S Blaise, C Millet, and JL Cracowski. Reproducibility and methodological issues of skin post-occlusive and thermal hyperemia assessed by single-point laser Doppler flowmetry. *Microvasc. Res.*, 79(2):102–108, 2010.

[400] Adebola Onanuga, Oluwatoyin A Igbeneghu, Adebayo Lamikanra, et al. A study of the relationship between the observation of fever symptoms and parasitemia among children in the federal capital territory, nigeria. *Ann Trop Med PH*, 8(1):1, 2015.

[401] Salwa ME A-elgayoum, El-Amin El-Rayah, and Hayder A Giha. Towards a noninvasive approach to malaria diagnosis: detection of parasite dna in body secretions and surface mucosa. *J. Mol. Microbiol. Biotechnol.*, 18(3): 148–155, 2010.

[402] Francis Krampa, Yaw Aniweh, Gordon Awandare, and Prosper Kanyong. Recent progress in the development of diagnostic tests for malaria. *Diagnostics*, 7(3):54, 2017.

[403] M Ciuca, L Ballif, M Chelarescu-Vieru, et al. Immunity in malaria. *Trans. R. Soc. Trop. Med. Hyg.*, 27(6), 1934.

[404] Gordon Covell. Relationship between malarial parasitaemia and symptoms of the disease: a review of the literature. *Bull. World Health Organ.*, 22(6): 605, 1960.

[405] Jacques Verdrager. Observations on the longevity of plasmodium falciparum: with special reference to findings in mauritius. *Bull. World Health Organ.*, 31(5):747, 1964.

[406] WC Earle. The course of naturally acquired malaria. geneva: World health organization. document who/mal/333, 1962.

[407] Wilson Sama, Gerry Killeen, and Tom Smith. Estimating the duration of plasmodium falciparum infection from trials of indoor residual spraying. *Am. J. Trop. Med. Hyg.*, 70(6):625–634, 2004.

[408] AA Hamad, IM El Hassan, AA El Khalifa, GI Ahmed, SA Abdelrahim, TG Theander, and DE Arnot. Chronic plasmodium falciparum infections in an area of low intensity malaria transmission in the sudan. *Parasitology*, 120 (05):447–456, 2000.

[409] Fusheng Yang and Wangcai Liao. Modeling and decomposition of hrv signals with wavelet transforms. *IEEE Eng. Med. Biol.*, 16(4):17–22, 1997.

[410] Maja Bracic Lotric, Aneta Stefanovska, Dusan Stajer, and Vilma Urbancic-Rovan. Spectral components of heart rate variability determined by wavelet analysis. *Physiol. Meas.*, 21(4):441, 2000.

[411] Stefan Thurner, Markus C Feurstein, and Malvin C Teich. Multiresolution wavelet analysis of heartbeat intervals discriminates healthy patients from those with cardiac pathology. *Phys. Rev. Lett.*, 80(7):1544, 1998.

[412] Arndt Effern, Klaus Lehnertz, Thomas Grunwald, Guillén Fernández, Peter David, and Christian E Elger. Time adaptive denoising of single trial event-related potentials in the wavelet domain. *Psychophysiology*, 37(6):859–865, 2000.

[413] Vilma Urbančič-Rovan, Alan Bernjak, Aneta Stefanovska, Katja Ažman-Juvan, and Andreja Kocijančič. Macro-and microcirculation in the lower extremities—possible relationship. *Res. Clin. Pract.*, 73(2):166–173, 2006.

[414] Katja Ažman-Juvan, Alan Bernjak, Vilma Urbančič-Rovan, Aneta Stefanovska, and Dušan Štajer. Skin blood flow and its oscillatory components in patients with acute myocardial infarction. *J. Vasc. Res.*, 45(2):164–172, 2008.

[415] Ingrid Daubechies, Jianfeng Lu, and Hau-Tieng Wu. Synchrosqueezed wavelet transforms: An empirical mode decomposition-like tool. *Appl. Comput. Harmon. A.*, 30(2):243–261, 2011.

[416] Milan Paluš and Martin Vejmelka. Directionality of coupling from bivariate time series: How to avoid false causalities and missed connections. *Phys Rev E*, 75(5):056211, 2007.

[417] L. W. Sheppard, V. Vuksanović, P. V. E. McClintock, and A. Stefanovska. Oscillatory dynamics of vasoconstriction and vasodilation identified by time-localized phase coherence. *Phys. Med. Biol.*, 56:3583–3601, 2011.

[418] Yunus A Abdulhameed, Peter VE McClintock, and Aneta Stefanovska. Race-specific differences in the phase coherence between blood flow and oxygenation: A simultaneous NIRS, white light spectroscopy and LDF study. *J. Biophotonics*, 2019.

[419] Björn Kralemann, Laura Cimponeriu, Michael Rosenblum, Arkady Pikovsky, and Ralf Mrowka. Phase dynamics of coupled oscillators reconstructed from data. *Phys. Rev. E*, 77(6):066205, 2008.

[420] MJ Leahy, FFM De Mul, GE Nilsson, and R Maniewski. Principles and practice of the laser-Doppler perfusion technique. *Technol. Health Care*, 7 (2-3):143–162, 1999.

[421] Leon Goldman, Donald J Blaney, DJ Kindel, and Ernst K Franke. Effect of the laser beam on the skin. *J. Invest. Dermatol.*, 40:2, 1963.

[422] Ingemar Fredriksson, Marcus Larsson, and Tomas Stromberg. Measurement depth and volume in laser Doppler flowmetry. *Microvasc. Res.*, 78(1):4–13, 2009.

[423] Z Q Zhao and P W Fairchild. Dependence of light transmission through human skin on incident beam diameter at different wavelengths. In *Laser-Tissue Interaction IX*, volume 3254, pages 354–361, Bellingham, 1998. SPIE.

[424] Caerwyn Ash, Michael Dubec, Kelvin Donne, and Tim Bashford. Effect of wavelength and beam width on penetration in light-tissue interaction using computational methods. *Lasers Med. Sci.*, 32:1909–1918, 2017.

[425] Claudia N Keilhauer and François C Delori. Near-infrared autofluorescence imaging of the fundus: visualization of ocular melanin. *Invest. Ophthal. Vis. Sci.*, 47:3556–3564, 2006.

[426] Irwin M Braverman. The cutaneous microcirculation: ultrastructure and microanatomical organization. *Microcirculation*, 4:329–340, 1997.

[427] Irwin M Braverman. The cutaneous microcirculation. *J. Invest. Dermatol. Symp. Proc.*, 5:3–9, 2000.

[428] Aletta E Karsten and Jacoba E Smit. Modeling and verification of melanin concentration on human skin type. *Photochem. Photobiol.*, 88:469–474, 2012.

[429] Irwin M Braverman, Jeffrey S Schechner, David G Silverman, and Agnes Keh-Yen. Topographic mapping of the cutaneous microcirculation using two outputs of laser-Doppler flowmetry: flux and the concentration of moving blood cells. *Microvasc. Res.*, 44:33–48, 1992.

[430] R. F. Bonner and R Nossal. Principles of laser-Doppler flowmetry. In A. P.

Shepherd and P. Å. Öberg, editors, *Laser-Doppler Blood Flowmetry*, pages 17–45. Springer, Berlin, 1990.

[431] S Alaluf, D Atkins, K Barrett, M Blount, N Carter, and A Heath. Ethnic variation in melanin content and composition in photoexposed and photoprotected human skin. *Pigment Cell Res.*, 15(2):112–118, 2002.

[432] E Berardesca, J De Rigal, JL Leveque, and HI Maibach. In vivo biophysical characterization of skin physiological differences in races. *J. Invest. Dermatol.*, 182:89–93, 1991.

[433] LaBarron K Hill, Dixie D Hu, Julian Koenig, John J Sollers III, Gaston Kapuku, Xiaoling Wang, Harold Snieder, and Julian F Thayer. Ethnic differences in resting heart rate variability: a systematic review and meta-analysis. *Psychosom. Med.*, 77:16, 2015.

[434] Agnes Mbonyiryivuze, Isaiah Omollo, Balla Diop Ngom, Bonex Mwakikunga, Simon Mokhotjwa Dhlamini, E Park, and Malik Maaza. Natural dye sensitizer for Grätzel cells: Sepia melanin. *Sci. Educ.*, 3(1):1–6, 2015.

[435] M Magarelli. *Purification, characterization and photodegradation studies of modified sepia melanin Sepia (Sepia officinalis). Determination of Eumelanin content in fibers from Alpaca (Vicugna pacos).* PhD thesis, Doctoral Thesis., Macerata: University of Camerino, 2011.

[436] Zhiwei Huang, Harvey Lui, Michael XK Chen, Abdulmajeed Alajlan, David I McLean, and Haishan Zeng. Raman spectroscopy of in vivo cutaneous melanin. *J. Biomed. Opt.*, 9(6):1198–1206, 2004.

[437] Giuseppe Perna, Maria Lasalvia, Crescenzio Gallo, Giuseppe Quartucci, and Vito Capozzi. Vibrational characterization of synthetic eumelanin by means of raman and surface enhanced raman scattering. *Open Surf Sci J*, 5(1), 2013.

[438] Tianyi Wu, Xiaoqin Wang, Chunyin Wei, Huawei Cheng, Xiaozhen Wang, Yan Li, Haining Zhao, Ping Young, Guilan Li, Zhigang Wang, et al. Hemoglobin levels in qinghai-tibet: different effects of gender for tibetans vs. han. *J. Appl. Physiol.*, 98(2):598–604, 2005.

[439] Hiroaki Kosaka. Nitric oxide and hemoglobin interactions in the vasculature. *Biochim. Biophys. Acta. Bioenerg.*, 1411(2):370 – 377, 1999.

[440] BRUCE Klitzman and BRIAN R Duling. Microvascular hematocrit and red cell flow in resting and contracting striated muscle. *Am. J. Physiol. Heart Circ. Physiol.*, 237(4):H481–H490, 1979.

[441] Walter H Reinhart, Nathaniel Z Piety, and Sergey S Shevkoplyas. Influence of feeding hematocrit and perfusion pressure on hematocrit reduction (fåhraeus effect) in an artificial microvascular network. *Microcirculation*, 24(8):e12396, 2017.

[442] K Lossius and M Eriksen. Spontaneous flow waves detected by laser Doppler in human skin. *Microvasc. Res.*, 50(1):94–104, 1995.

[443] Angelo Sassaroli and Sergio Fantini. Comment on the modified beer–lambert law for scattering media. *Phys. Med. Biol.*, 49(14):N255, 2004.

[444] Evgeny Zherebtsov, Viktor Dremin, Alexey Popov, Alexander Doronin, Daria Kurakina, Mikhail Kirillin, Igor Meglinski, and Alexander Bykov. Hyperspectral imaging of human skin aided by artificial neural networks. *Biomed. Opt. Express*, 10(7):3545–3559, 2019.

[445] Yunus A Abdulhameed, Gemma Lancaster, Peter V E McClintock, and Aneta Stefanovska. On the suitability of laser-Doppler flowmetry for capturing microvascular blood flow dynamics from darkly pigmented skin. *Physiol. Meas.*, 40:074005, 2019.

[446] Tsin W Yeo, Daniel A Lampah, Enny Kenangalem, Emiliana Tjitra, J Brice

Weinberg, Donald L Granger, Ric N Price, and Nicholas M Anstey. Decreased endothelial nitric oxide bioavailability, impaired microvascular function, and increased tissue oxygen consumption in children with falciparum malaria. *J. Infect. Dis.*, 210(10):1627–1632, 2014.

[447] Patrick Davies and I Maconochie. The relationship between body temperature, heart rate and respiratory rate in children. *Emerg. Med. J.*, 26(9): 641–643, 2009.

[448] David J Weatherall, Louis H Miller, Dror I Baruch, Kevin Marsh, Ogobara K Doumbo, Climent Casals-Pascual, and David J Roberts. Malaria and the red cell. *ASH Education Program Book*, 2002(1):35–57, 2002.

[449] Oluwagbemiga O Aina, Chimere O Agomo, Yetunde A Olukosi, Hilary I Okoh, Bamidele A Iwalokun, Kathleen N Egbuna, Akwaowo B Orok, Olusola Ajibaye, Veronica NV Enya, Samuel K Akindele, et al. Malariometric survey of ibeshe community in ikorodu, lagos state: dry season. *Malar. Res. Treat.*, 2013, 2013.

[450] SC Beards, GM Joynt, and J Lipman. Haemodynamic and oxygen transport response during exchange transfusion for severe falciparum malaria. *Postgrad. Med. J.l*, 70(829):801–804, 1994.

[451] Damian Bruce-Hickman. Oxygen therapy for cerebral malaria. *Travel Med. Infect. Di.*, 9(5):223 – 230, 2011.

[452] M English, R Sauerwein, C Waruiru, M Mosobo, J Obiero, B Lowe, and K Marsh. Acidosis in severe childhood malaria. *QJM: monthly journal of the Association of Physicians*, 90(4):263–270, 1997.

[453] TE Taylor, A Borgstein, and ME Molyneux. Acid-base status in paediatric plasmodium falciparum malaria. *QJM: An International Journal of Medicine*, 86(2):99–109, 1993.

[454] Michael English, Jeanine Punt, Isaiah Mwangi, Kieran McHugh, and Kevin Marsh. Clinical overlap between malaria and severe pneumonia in african children in hospital. *Trans. R. Soc. Trop. Med. Hyg.*, 90(6):658–662, 1996.

[455] Sonja Junge, Ayo Palmer, Brian M Greenwood, E Kim Mulholland, and Martin W Weber. The spectrum of hypoxaemia in children admitted to hospital in the gambia, west africa. *Trop. Med. Int. Health*, 11(3):367–372, 2006.

[456] M Ciuca, G Lupasco, E Ballif-Negulici, P Constantinesco, A Cristesco, I Sandesco, World Health Organization, et al. Experimental research on the infectivity for a. atroparvus of p. vivax or p. falciparum asymptomatic parasitaemias in relation to acquired immunity in countries where malaria is endemic. 1963.

[457] Thibaut Brugat, Adam James Reid, Jing-wen Lin, Deirdre Cunningham, Irene Tumwine, Garikai Kushinga, Sarah McLaughlin, Philip Spence, Ulrike Böhme, Mandy Sanders, et al. Antibody-independent mechanisms regulate the establishment of chronic plasmodium infection. *Nat. Microbiol.*, 2:16276, 2017.

[458] Nicholas M Anstey, Donald L Granger, Mushtaq Y Hassanali, Esther D Mwaikambo, Patrick E Duffy, and J Brice Weinberg. Nitric oxide, malaria, and anemia: inverse relationship between nitric oxide production and hemoglobin concentration in asymptomatic, malaria-exposed children. *Am. J. Trop. Med. Hyg.*, 61(2):249–252, 1999.

[459] Xin-zhuan Su, Virginia M Heatwole, Samuel P Wertheimer, Frangoise Guinet, Jacqueline A Herrfeldt, David S Peterson, Jeffrey A Ravetch, and Thomas E Wellems. The large diverse gene family var encodes proteins involved in cytoadherence and antigenic variation of plasmodium falciparum-infected erythrocytes. *Cell*, 82(1):89–100, 1995.

[460] KN Brown, IN Brown, World Health Organization, et al. Immunity to malaria: antigenic variation in chronic infections of plasmodium knowlesi. *Nature*, 208:1286–1288, 1966.

[461] Elizabeth A Ashley and Nicholas J White. The duration of plasmodium falciparum infections. *Malar. J.*, 13(1):500, 2014.

[462] Richard A Armstrong. When to use the b onferroni correction. *Ophthal and Physl Opt*, 34(5):502–508, 2014.

[463] CN Anigbogu and OA Olubowale. Effects of malaria on blood pressure, heart rate, electrocardiogram and cardiovascular response to change in posture. *Nig. Q. J. Hosp. Med.*, 12(1):17–20, 2002.

[464] Susan Jean Hall. *Basic biomechanics*. McGraw-Hill Boston, MA:, 2007.

[465] Sonnenblick EH Robinson TF, Factor SM. The heart as a suction pump. *Sci. Am.*, 6:62–69, 1986.